Università
Ca'Foscari
Venezia

Master's Degree

in Environmental Science

Final Thesis

Climate Anomalies in the Southeast Asian Region surrounding Typhoon Haiyan's landfall in the Philippines

Supervisor
Prof. Angelo Rubino

Co-supervisor
Prof. Davide Zanchettin

Graduand
Maria Florentina Magistrado
Matriculation number 888328

Academic Year
2021 / 2022

TABLE OF CONTENTS

LIST OF TABLES

LIST OF FIGURES

ABBREVIATIONS, ACRONYMS, AND SYMBOLS

^{0}C	Degree Celsius
AR5	IPCC's Fifth Assessment Report
AR6	IPCC's Sixth Assessment Report
AVHRR	Advanced Very High Resolution Radiometer
CCKP	Climate Change Knowledge Portal
CIDA	Canadian International Development Agency
CMIP5	Coupled Model Intercomparison Project Phase 5
CO2	Carbon Dioxide
CPES	Compendium of Philippine Environment Statistics
CRU	Climatic Research Unit
DINCAE	Data INterpolating Convolutional Auto-Encoder method
ECDF	Empirical Cumulative Distribution Function
ECMWF	European Centre for Medium-Range Weather Forecasts
ECV	Essential Climate Variable
EEPSEA	Economy and Environment Program for Southeast Asia
EM-DAT	Emergency Events Database
ENSO	El Niño–Southern Oscillation
ERA5	ECMWF Reanalysis version 5
GFDL	Geophysical Fluid Dynamics Laboratory
GHG	Greenhouse Gas
GCOS	Global Climate Observing System
GODAE	Global Ocean Data Assimilation Experiment
GPCP	Global Precipitation Climatology Project
GPM	Global Precipitation Measurement
HadISST	The Hadley Centre Global Sea Ice and Sea Surface Temperature
HiFLOR	High-Resolution Forecast-Oriented Low Ocean Resolution
HiRAM	High-Resolution Atmospheric Model
HYCOM	HYbrid Coordinate Ocean Model

IAPSO	International Association for the Physical Sciences of the Oceans
IMERG	Integrated Multi-satellitE Retrievals for GPM
IPCC	Intergovernmental Panel for Climate Change
IDRC	International Development Research Centre
JASON	July, August, September, October, November period
JTWC	Joint Typhoon Warning Center
kph	Kilometer per hour
LC	Loop Currents
MJO	Madden–Julian Oscillation
MM5	Fifth-generation Penn State / National Center for Atmospheric Research mesoscale Model
MODIS	Moderate Resolution Imaging Spectroradiometer
mph	miles per hour
NASA	National Aeronautics and Space Administration
NCEI	National Centers for Environmental Information
NCEP	National Centers for Environmental Prediction
NCEP-FNL	Final Operational Global Analysis data of the NCEP
NDRRMC	National Disaster Risk Reduction and Management Council
NetCDF	Network Common Data Form
NHC	National Hurricane Center
NOAA	National Oceanic Atmospheric Administration
NOPP	National Ocean Partnership Program
ONI	Oceanic Niño Index
PAGASA	Philippine Atmospheric Geophysical Astronomical Services Administration
PDI	Power Dissipation Index
PSA	Philippine Statistics Authority
PSL	Physical Sciences Laboratory of NOAA
PSML	Permanent Service for Mean Sea Level
RCP	Representative Concentration Pathways

SAT	Surface Air Temperature
SIDA	Swedish International Development Cooperation Agency
SST	Sea Surface Temperature
TAO	Tropical Atmosphere Ocean
TC	Tropical Cyclone
TRMM	Tropical Rainfall Measurement Mission
TS	Tropical Storm
W/m^2	Watt per square meter
WBG	World Bank Group
WMO	World Meteorological Organization
WRF	Weather Research and Forecast

EXECUTIVE SUMMARY

The link between climate and typhoons are well studied, particularly in determining if changes in typhoon characteristics are forced by certain climate anomalies / trends. However, only few assessed the impact of a typhoon event to the weather / climate anomalies surrounding the typhoon period. In Southeast Asia, no study investigated the effects of Super Typhoon Haiyan that devastated the Philippines, to the weather / climate variables before and after its landfall. Hence, the motivation of this thesis study is drawn from this gap.

In this study, the spatio-temporal anomalies using observational and reanalysis datasets i.e., GPCP, CRU, HadISST and ERA5 are analyzed, exploring temperature and precipitation, to determine how anomalies surrounding the Haiyan period compare with meteo-climatic variability between the non-typhoon and typhoon months / years. From the results, the anomalies are evident within the focal region (SE Asia) in as far as the annual, seasonal, and monthly values are concerned. For these periods, results revealed that the precipitation are wetter-than-average and temperature are warmer-than-average during the year, season and month when Typhoon Haiyan occurred (Y2013, SON 2013, November 2013), providing a background of the possible impacts of the typhoon Haiyan occurrence during these periods. Between precipitation and temperature anomalies, the temperature is notoriously higher (that is apparently illustrated by the red-dominated anomaly maps), as compared to precipitation with blue and red colors distributed across different geographic locations across the SE Asian map. This is likewise supported by the result of the ECDF plots showing the percentage of positive (negative) values demonstrating wet (dry) anomalies for precipitation and hot (cold) anomalies for temperature.

The effects of seasonal phases and inter-annual variations (dry/wet, monsoon, ENSO) on precipitation and temperature patterns were also assessed. The analysis revealed that ENSO and monsoon significantly impacts the precipitation patterns in the region. However, ENSO does not significantly impact the temperature. Although it must be emphasized that Typhoon Haiyan occurred on an ENSO-Neutral year, therefore, it may have not necessarily influenced the variability of the studied variables. Albeit, the regression analysis with precipitation and temperature against Nino 3.4 Index shows that these variables are negatively correlated to the SST anomaly with high significance.

Using wind, pressure, precipitation and runoff data, the daily spatio-temporal evolution of abnormal weather patterns surrounding the landfall period (before, during, and after) is determined. The results revealed that during the typhoon period, the highest anomalies with respect to all variables (precipitation, runoff, windspeed and pressure) are recorded when typhoon Haiyan made landfall (November 7 & 8) predominantly in the Philippines where there is a large disparity of the calculated anomalies during these days, as compared to the rest of the days during the typhoon period. November 7 and 8 also topped the rank when compared with the same days of the non-typhoon years, especially with the windspeed and precipitation values.

With respect to the inter-variable relationship, the result of the multiple linear regressions revealed that precipitation and runoff are positively correlated with windspeed, while negatively related with pressure, meaning, the cyclonic (low pressure) Typhoon Haiyan event increased the precipitation and runoff in as far as the Philippines is concerned.

Building from these results, it can be deduced that an extreme event such as Typhoon Haiyan can profoundly influence the climate variables surrounding its occurrence. In addition, non-TC-induced activities/events like ENSO and monsoon can further enhance the effects, especially on the precipitation patterns in the region.

It must also be emphasized that results vary from one dataset to another, demonstrating that there are inconsistencies with the datasets, in as far as the analyzing these anomalies for its amplitude and geographical locations are considered. It can be noted that both GPCP and CRU data are constructed using rain gauge data and inhomogeneity with the recorded values can be a factor that affects the results. On the other hand, ERA5 is based on model results that also have its own estimation uncertainties.

From this study, further research can be conducted investigating the differences of the analyzed datasets. A deeper understanding on the effects of EN/LN can also be performed especially on years when maxima/minima values of the studied variables were recorded. Other extreme typhoon events can also be explored not just in the Philippines but in other countries of the region.

STRUCTURE OF THE THESIS

This thesis paper is organized into the following chapters:

Chapter 1 introduces the technical definition and description of cyclones/hurricanes/storms/typhoons and their interrelation with climate change, as documented in pertinent literature. A short information about typhoons in Southeast Asia (particularly the Philippines) is also discussed. The highlights of the selected key papers that studied typhoons and climate anomalies are summarized according to the focus of their studies and the models, methods, and data used for analysis – characterizing the influence of changes in climatological variables on cyclone/typhoon variabilities. The papers are grouped and presented according to the investigated area, i.e., outside and within the Southeast Asian region. This chapter also explains the rationale behind the chosen topic based on the research gaps identified from the literature review, specifically on papers studying typhoon-induced impacts on climatic variables surrounding its occurrence and the use of observational (GPCP, CRU, HadISST) and reanalyzed (ERA5) datasets. Moreover, the thesis study's objectives, scope, and limitations are illustrated.

Chapter 2 defines the spatial coverage of the study, predominantly focusing on the geographical location of the target region (Southeast Asia) and its climate characteristics. This characterization is then associated with the region's vulnerability to multiple climate hazards – one of which is constituted by cyclones, where "Typhoon Haiyan" that caused severe damage to some parts of the Philippines in November 2013, is highlighted. This chapter also describes the datasets used and the methodologies and tools adopted to collect, pre-process, and analyze them regarding the Typhoon Haiyan event and the climatological responses to it (e.g., trends and cycles).

Chapter 3 illustrates the main results of the analysis, discusses the findings revealed by the results, and shows how the results and interpretations relate to previously published studies.

Chapter 4 states the conclusions drawn and provides and outline of the theoretical implications, significance, and any possible future applications of the thesis work.

CHAPTER 1: BACKGROUND OF THE STUDY

1.1 Understanding Typhoons and Climate Change

The Philippine Atmospheric Geophysical Astronomical Services Administration (PAGASA) describes "Tropical Cyclone (TC)" as a "warm-core low-pressure system with a spiral inflow of mass at the bottom and spiral outflow at the top". Its formation always occurs over oceans where sea surface and air temperatures are greater than 26°C. In the process, the air receives heat from the sea, and large amounts of sensible and latent heat are accumulated, spiraling towards the center. This heat exchange occurs rapidly due to a large amount of spray thrown by the wind into the air, liberating a massive latent heat of condensation, thus giving TC its required energy[1].

PAGASA further defines TC as "a non-frontal, synoptic-scale phenomenon that develops at any level over tropical and sub-tropical water, with an organized circulation"[2]. Depending on the region, its nomenclature varies in different parts of the world. It is referred to as *"hurricanes"* in the North Atlantic, Eastern North Pacific, and South Pacific Ocean, *"cyclonic"* in the Bay of Bengal, Arabian Sea, and Western South Indian Ocean, *"willy-willy"* in the eastern part of the Southern Indian Ocean, and *"typhoons"* in the Western North Pacific Ocean[3]. For guidance on the locations of these major global oceans, see ***Figure 1*** below.

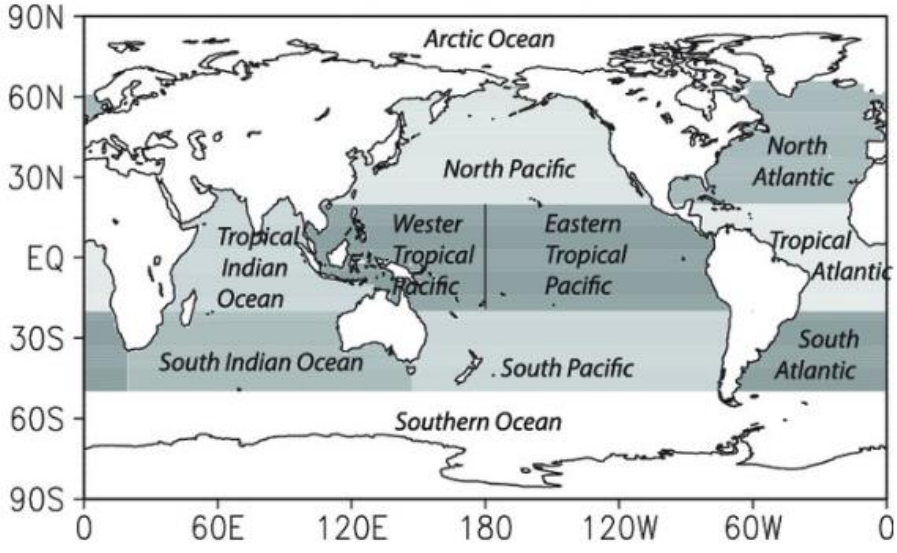

Figure 1. Map of the Ocean Regions (Luo, Leung, Zhou, & Zhang, 2015)

[1] Sourced from "*About Tropical Cyclones*" at the PAGASA website, https://www.pagasa.dost.gov.ph/information/about-tropical-cyclone

[2, 3] Ibid

Although TC forms over oceans, it can never develop in the South Atlantic and the Southeastern Pacific due to the cooler sea surface temperature (SST) and higher vertical wind shears. TC occurrences are usually situated at latitudes greater than 5° from the equator. Typically, they reach their greatest intensity while over warm tropical water. Albeit weakening as they move inland (landfall), they often leave damages to properties or human casualties[4].

The Philippines is one of the Countries mostly impacted by typhoons. It is located along the typhoon belt in the Pacific and is visited by about twenty typhoons every year – five of which are destructive[5]. It was observed that there was an increase in the number of intense typhoons over the Philippine Sea after the mid-2000s (He et al., 2017). Based on meteorological records from National Hurricane Center (NHC) and Joint Typhoon Warning Center (JTWC), five (5) out of the eleven (11) strongest TC that made landfall in world history hit the Country -- with Typhoon Goni that recently occurred in 2020 topping the list [see **Table 1**][6]. Typhoon Haiyan on the other hand, despite landing on the second spot per wind strength, remained to be the topmost destructive typhoon in the Country, based on cost of damage[7]. These estimates of economic losses consist of damages to buildings and transportation networks, loss of revenue for businesses, and loss of crops, per an article by Uy & Pilar (2018)[8].

Table 1. World's Top Eleven (11) Strongest Tropical Cyclone at Landfall

Rank	Name	Year	Wind speed	Affected location
	Local *(International)*		**[miles per hour (mph)]**	**Province / Country**
1	Super Typhoon Rolly *(Goni)*	2020	195	Catanduanes, Philippines
2	Super Typhoon Yolanda *(Haiyan)*	2013	190	Leyte, Philippines
3	Super Typhoon Ferdie *(Meranti)*	2016	190	Itbayat, Philippines
4	Hurricane Dorian	2019	185	Bahama Islands
5	Great Labor Day Hurricane	1935	185	Florida, U.S.A

[4] Ibid
[5] According to the "*Information on Disaster Risk Reduction of the Member Countries [the Philippines]*" by Asia Disaster Reduction Center (ADRC), https://www.adrc.asia/nationinformation.php?NationCode=608&Lang=en
[6] List taken from the paper by Santos (2020)
[7]The ranking is based on cost of damages per the typhoon assessment report of del Rosario (2014) through the Philippine National Disaster Risk Reduction and Management Council (NDRRMC)
[8] Written in the Business World, based on data reported in the Compendium of Philippine Environment Statistics (CPES) of the Philippine Statistics Authority (PSA)

6	Super Typhoon Joan	1959	185	Eastern Taiwan
7	Hurricane Irma	2017	180	Leeward Islands
8	Cyclone Winston	2016	180	Fiji
9	Super Typhoon Juan *(Megi)*	2010	180	Luzon, Philippines
10	Super Typhoon Iliang *(Zeb)*	1998	180	Luzon, Philippines
11	Cyclone Monica	2006	180	Northern Territory, Australia

There is a scientific consensus that climate change contributes to stronger typhoons due to the higher sea surface and subsurface temperatures, which remove the natural buffer on typhoon strength when cold water upwells below the ocean's surface (Holden & Marshall, 2018). These intensity changes largely concern the Countries in East and Southeast Asia (Mei & Xie, 2016). According to the Sixth Assessment Report (AR6)[9] of the Intergovernmental Panel for Climate Change (IPCC), fewer but more extreme typhoons (with stronger wind speeds) have affected the Southeast Asian region in the 21st century. However, there is no significant trend in the overall number recorded. IPCC further reports that rainfall will increase in northern latitude but will decrease in the Maritime Continent where the Philippines belongs. Analyzing the typhoon data from 1951 to 2013, Cinco et al. (2016) revealed that during this period there was a decreasing trend in the number of landfalling typhoons in the Country, with fewer typhoons having wind speeds above 118 kilometers per hour (kph) but more extreme typhoons with wind speeds above 150 kph. A more recent study by Tran, Ritchie, & Perkins-Kirkpatrick (2022) supports this observation showing that over the 50-yr period (1970 to 2019), the TC exposure in Southeast Asia relative to the Western North Pacific climatology has consistently shifted northward; hence, decreasing the landfall events in the Philippines and Vietnam while increasing in some South China areas. Correspondingly, Chen et al. (2021) found that the TC mean inland landfall intensity will increase by 2 m/s (6%) in the Western North Pacific the by the end of the 21st century, based on model projections.

Studies covering other regions showed varying responses of Tropical Cyclones / Hurricanes / Tropical Storms (TS) to external forcings. Bhatia et al. (2019) and Knutson et al. (2020) showed that more intense TCs are consistent with the expected impacts of global warming due to anthropogenic forcings. Trenberth et al. (2018) concurred with this by demonstrating that there

[9] Sourced from *"Regional Fact Sheet-Asia",* IPCC AR6, Working Group I: The Physical Science Basis, https://www.ipcc.ch/report/ar6/wg1/downloads/factsheets/IPCC_AR6_WGI_Regional_Fact_Sheet_Asia.pdf

is a link between climate change and the above-normal activities of the recent Atlantic hurricanes in 2017 (i.e., Harvey, Irma, and Maria), wherein the ocean heat content due to global warming has "supercharged and exacerbated" them. Using hurricane Harvey as an isolated case study, they observed that the ocean heat content was highest on record globally and in the Gulf of Mexico before the northern summer of 2017. These record-high values fueled and intensified hurricane Harvey bringing flood rains on land. In the context of global distribution, Murakami et al. (2020) demonstrate that the individual effect of external forcings like greenhouse gases (GHG), aerosols, and volcanic activities on TC from 1980 to 2018 can be distinguished in terms of the spatial pattern of occurrence (varying per region) rather than their frequency, with the global spatial distribution being attributed to the increase in GHG emissions. Another study by Villarini & Vecchi (2012) explored projections of North Atlantic TS, revealing that over the first half of the twenty-first century, an increase in TS frequency arises from radiative forcings other than increasing atmospheric concentration of CO_2 . However, projected TS trends over the entire 21st century do not show consistent dependence on the Coupled Model Intercomparison Project Phase 5 (CMIP5) scenarios [Representative Concentration Pathways (RCP) 2.6, 4.5, and 8.5][10]. Besides sea-surface temperature (SST), most of the uncertainties in the North Atlantic TS frequency are influenced by the complex nature of the climate system and its response to radiative forcing.

1.2 Review of Pertinent Studies on Typhoons and Climate Variables

Building on the knowledge of "typhoons" and "climate", a more extensive literature review of scholarly articles and scientific journals is carried out using these keywords to deepen the understanding of their interconnection. The search resulted in some key papers that provide various models, methods, and datasets, showing how cyclone/hurricane/typhoon behaviors and climate variables are related. Many of these studies are done outside of the Southeast Asian region, as presented in **Table 2.**

[10] Four RCP scenarios [2.6, 4.5, 6 and 8.5] are adopted by IPCC for its Fifth Assessment Report (AR5). RCPs are named after a possible range of radiative forcing values [cumulative measure of human emissions of GHGs from all sources (expressed in Watts per square meter) in the year 2100, relative to pre-industrial values +2.6, +4.5, +6.0 and +8.5 W/m^2 respectively]. In the above-cited paper however, only the three RCPs [2.6, 4.5 and 8.5] were considered.

Table 2. Studies on the relationship between climate variables and typhoons conducted outside Southeast Asia

Author/s	Study focus	Methods / Models / Data Used
Wang & Wang (2019)	Explain inter-annual variability of TC activity over the **Western North Pacific** using SST anomalies in the **Pacific, Indian and Atlantic oceans**	Observed two modes of variability: 1) forced by SST anomalies in the eastern-central Pacific and tropical Atlantic; 2) a coupled ocean-atmosphere mode and a dipole SST anomaly in the Indo-Pacific warm pool[11]
	Predict the two **Western North Pacific** Subtropical High modes and TC activity [genesis number, tropical storm days, and power dissipation index] in the peak TC season (July–September) together with trans-basin SST predictors of the preceding season	Built a set of physics-based empirical models
Bhatia et al. (2018)	Provide insight on how the distribution of TC intensification can be transformed due to climate change, by "nudging" SST with different climatological targets and a specific radiative forcing	Used three 70-yr High-Resolution Forecast-Oriented Low Ocean Resolution (HiFLOR) model at the Geophysical Fluid Dynamics Laboratory (GFDL)
Mei, Xie, Zhao & Wang (2015)	Study TC tracks from observations and simulations forced by SSTs, using interannual-to-decadal variability of annual TC track	Used a 25-km-resolution version of the GFDL High-Resolution Atmospheric Model (HiRAM) and a regional atmospheric model,

[11] The tropical warm pool, otherwise known as Indo-Pacific Warm Pool, is a mass of ocean water, spanning almost half the globe -- from the western waters of the equatorial Pacific to the eastern Indian Ocean. This body of water holds the warmest seawaters in the world, driving heat and moisture high into the atmosphere thereby affecting the climate of the surrounding land (NASA, 2001; De Deckker, 2016)

	density in the **Western North Pacific**	considering two modes of decadal variability: 1) a nearly basin-wide mode (which links to variations in TC number and is forced by SST variations over the <u>off-equatorial tropical central North Pacific</u>); 2) a dipole mode between the <u>subtropics</u> and <u>lower latitudes</u> (associated with the **Atlantic** multidecadal oscillation)
Jin et al. (2013)	Demonstrate the effect of **Central Pacific** warming on the observed atmospheric and TC variability over ***East Asia*** during the Central Pacific - El Niño period	Used Weather Research and Forecast (WRF) - based regional climate model
Kiliç & Raible (2013)	Investigate the influence of SST anomalies on the hurricane characteristics	Performed a set of sensitivity experiments on the case of Hurricane Katrina in 2005, using the WRF model
Choi, Kim & Byun (2010)	Seasonal prediction of summer TC frequency in the mid-latitudes of ***East Asia*** relative to SST anomalies	Constructed a multiple linear regression model
Tu, Chou & Chu (2009)	Understand the seasonal time series changes of typhoons in the vicinity of ***Taiwan*** concerning SST anomalies	Applied Bayesian analysis

NOTE: **Boldface** texts indicate major ocean regions, ***italics*** indicate the study area /country, and biogeographical subdivision (as depicted in ***Figure 2***) are <u>underlined</u>

In the study by Wang & Wang (2019), the first mode of interannual TC variability [i.e., forced by SST anomalies in the eastern-central Pacific and tropical Atlantic] showed a shift in TC formation locations southeastward/northwestward but had an insignificant influence on the total number

of TC genesis. However, it affects the track of TC, the number of tropical storm days, and power dissipation index. The second mode [i.e., a coupled ocean-atmosphere mode and a dipole SST anomaly in the Indo-Pacific warm pool] significantly impacted the total number of TC genesis. Moreover, the built models' predictions revealed inter-annual variabilities of the Western North Pacific Subtropical High and variability of Western North Pacific TC activity.

The climate model experiment Bhatia et al. (2018) performed using prescribed climatological ocean and radiative forcing based on observations from 1986–2005, shows similarities with the observations in the simulated intensification distributions and the percentage of TCs that become major hurricanes under warmer conditions. Comparing the control experiment perturbed by climatological SSTs to multi-models projecting SST anomalies and atmospheric radiative forcing from either 2016–35 or 2081–2100 (RCP 4.5 scenario), the frequency, intensity, and intensification distribution of TCs all shift to higher values as the 21st century progresses.

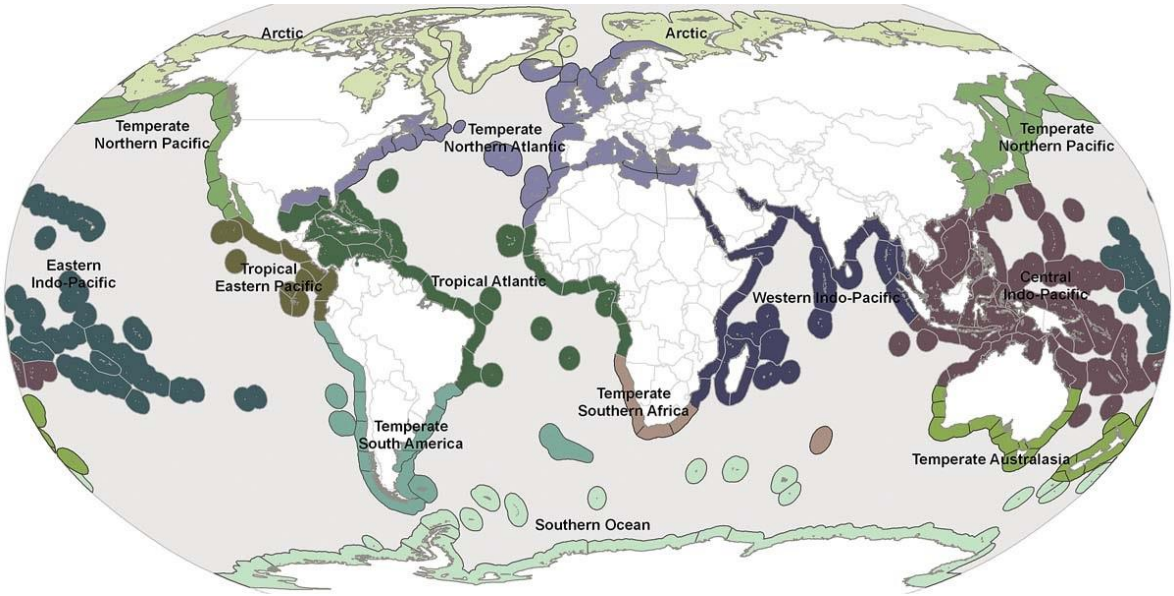

Figure 2. Biogeographic realms and marine ecoregional boundaries of the world[12]
(Spalding et al., 2007)

The internal variability in TC track density between 1979 and 2008, as examined using ensemble atmospheric model simulations by Mei et al. (2015), shows prominent spatial and seasonal patterns, particularly strong in the South China Sea and along the East Asia coast.

The first set of sensitivity experiments by Kiliç & Raible (2013), using basin-wide changes of the

[12] For a more detailed description of the ocean regions and their jurisdiction, please refer to ANNEX 1 as appended.

SST magnitude, revealed that the hurricane intensity goes along with the SST changes, such that SST increase leads to hurricane intensification. Moreover, the trajectory shifted to the west with increasing SSTs, and to the east while SST decreased due to the strengthening of the background flow. On the other hand, the influence of idealized Loop Current eddies[13] generated by localized SST anomalies showed that the hurricane's intensity is enhanced with increasing SST close to the core of a tropical cyclone. Negative nearby SST anomalies reduce the intensity, while positive SST anomalies (located west or north of the hurricane centre) change its trajectory. The SST anomaly attracts the hurricane, causing additional moisture sources and increased vertical winds.

Based on the analysis and model simulations by Tu et al. (2009), warm SST anomalies over the equatorial Western and Central Pacific is a major contributing factor to a northward-shifted typhoon track.

The study of Choi et al. (2010) revealed an interesting result, wherein the presence of large amounts of sea ice during the preceding spring that continued into the summer prevented Western Pacific Subtropical High from advancing toward mid-latitudes of East Asia, thus, reducing summer TC frequency. Relative to this, the study by Jin et al. (2013) shows that the number of TCs approaching East Asia in July–October is positively correlated with SSTs in the equatorial and northern off-equatorial Central Pacific oceans. The study showed that northern off-equatorial Central Pacific warming, rather than equatorial Central Pacific warming, effectively induces local irregular steering flows relative to the observed increase in TC activity over East Asia during Central Pacific - El Niño period. Furthermore, a sensitivity analysis was performed where the prescribed Central Pacific - El Niño related SST anomaly is confined near the equator. This did not capture the observed TC increase over East Asia. On the other hand, those including the off-equatorial region showed atmospheric and TC variabilities. The off-equatorial Central Pacific SST anomaly influences the expansion of "anomalous cyclonic response" farther northward to the Philippine Sea, creating a tunnel effect in the East China Sea where more TCs move to East Asian coastal regions, affecting China, Taiwan, Korea, and Japan.

Common to these papers are the Oceanic Region (Western North Pacific) and the use of SST as a climatological variable of study. Although the results did not yield a consistent or predictable pattern, it was evident that SST anomalies can influence the TC formation and its activity.

[13] The circulation of the Gulf of Mexico is dominated by a warm ocean current called Loop Currents (LC). At random intervals, a part of the warm water separates as a Loop Current ring (known as "eddy"). The warm LC water and the associated eddy, supply energy and allow hurricanes to intensify, as with the case of Hurricane Rita in 2005 that passed over an LC and converted the ocean's heat into storm energy (University of Colorado- Boulder, 2005)

Despite most of the above-reviewed papers being conducted outside of Southeast Asia, a few articles were found covering this region, as summarized below.

Table 3. Studies on the relationship between climate variables and typhoons conducted within Southeast Asia

Author/s	Study focus	Methods / Models / Data Used
Comiso, Perez & Stock (2015)	Investigated the correlation of historically strong typhoons in the ***Philippines*** to the SST, water vapor, clouds, winds, sea level pressure, and precipitation	The role of SST in the formation of Typhoon Haiyan in 2013 was evaluated considering two study areas - the Warm Pool Region and the West Pacific Region, using an enhanced version of Reynold's dataset incorporating Advanced Very High Resolution Radiometer (AVHRR) SST, Moderate Resolution Imaging Spectroradiometer (MODIS) and National Centers for Environmental Prediction (NCEP) reanalysis data.
Wang, Zhao, Qiao & Zhao (2018)	Analyze the impact of warm core ocean eddy combined with climate-change-induced SST on Typhoon Haiyan's intensification process	Conducted numerical simulations using observational data from AVHRR-only V2 SST; and Tropical Atmosphere Ocean (TAO) and Argo buoy datasets
Kang & Kimura (2003)	Investigate the areas around ***East Asia*** subtropical anticyclone to analyze the influence of the regional climate of ***Japan*** and ***Korea*** in the summer, relative to the SST increase around the ***Philippine Islands***	Use a regional atmospheric fifth-generation Penn State / National Center for Atmospheric Research mesoscale model (MM5) ver. 3.5 with realistic lateral and surface boundary forcing

NOTE: ***Italicized*** texts indicate the study area /country, while underlined texts represent regional oceanic subdivision

The three papers alike used SST as the common climate variable for analysis. Similarly, they revealed that this variable could influence the variations in typhoon/cyclone behavior, as described in detail below:

Results of the study by Comiso et al. (2015) showed that the SST is well-correlated with wind strength, and the observed trends in SST suggest that extremely destructive typhoons like Haiyan are more likely to occur in the future. Further analysis indicated that water vapor, clouds, winds, and sea level pressure for the same period did not reveal strong signals associated with the typhoon event.

Per Wang et al. (2018), the observed data showed that Typhoon Haiyan intensified, and the maximum sustained winds increased after encountering a double warm-core ocean eddy. The study reveals that the presence of the warm-core eddy and climate-change-induced SST increase resulted in the rapid intensification of Typhoon Haiyan. Between the two factors, the warm-core ocean eddy that significantly brought more heat into the upper ocean played the leading role in the intensification, while climate warming made a lesser contribution. Moreover, with the increased thickness of the mixed layer associated with the warm-core ocean eddy, Typhoon Haiyan did not significantly decrease the SST to the east of the Philippines, as is typical of typhoons.

Kang & Kimura (2003) used climate model simulations to reveal that the uniform increase of SST around the Philippine Islands propagated a Rossby wave[14], resulting in an anomalous subtropical anticyclone around Japan/Korea. The Rossby wave propagation is linear, where the model response to negative SST anomalies reverses polarity. This suggests that the response to the SST forcing around the Philippine Islands is a deterministic problem since its magnitude depends on the size of the SST anomaly. Conversely, nonlinearity increases if there is a tropical depression or typhoon in the model domain. There is also a zonally weakened upper-level jet, and a meridionally intensified low-level jet, when the Rossby wave is excited by SST changes, where a

[14] As described by the National Oceanic Atmospheric Administration (NOAA), National Weather Service, Rossby waves are planetary waves that form naturally in rotating fluids. Due to the rotation of the Earth, these waves develop within the ocean and atmosphere. Since these waves are large and massive movements spanning horizontally across the planet, they can influence the weather and climate conditions as they transfer heat from the tropics to the poles and return the cold air toward the tropics. The horizontal movements (especially its speed) are dependent on the latitude of the wave, such that at lower latitudes (close to the equator), it takes months to a year for it to travel across the ocean, while those that form away from the equator (i.e., mid-latitudes) may take about 10 to 20 years. Vertically, the waves move small along the surface and large along the deeper portion where there is thermocline, or the transition point between upper warm and colder depth of the ocean. Rossby Waves also help locate jet streams and can mark out surface low pressure systems.

positive SST anomaly intensifies the meandering of the upper-level jet, taking about five days for the atmospheric circulation to respond to such an SST forcing. On the vertical, the model showed barotropic and baroclinic responses over 40°N∼55°N, 100°E∼160°E, and over 10°N∼40°N, 100°E∼140°E, respectively. Moreover, the effect of SST forcing is approximately four times stronger than the internal model variability. For Japan and Korea, positive SST forcing affects the precipitation pattern, causing rainfall to decrease in Japan and increase in Korea, contrastingly. Meanwhile, positive and negative SST forcing affect the precipitation around the Philippine Islands – wherein a positive SST forcing increases precipitation, and vice versa. Lastly, the response to the Rossby wave is sensitive to the geographical location of SST forcing, reaching a maximum in 110°E∼140°E, 10°N∼20°N, where the experiments are carried out.

1.3 Research Gaps

From the literature review in the preceding section, we can deduce that the link between anomalies in climate variables and the intensification, track formation, density, trajectory, genesis number, strength, and duration of typhoons/storms/hurricanes/cyclones are well studied. However, they vary with respect to their scope (location and period). Most of these studies aim to determine if changes in typhoon characteristics are forced by specific climate anomalies/trends, but there are only a few studies on the impact of a typhoon event to the weather/climate anomalies surrounding the typhoon period. One of these is Ji et al. (2021), who investigated SST and chlorophyll concentration responses to typhoons over the East China Sea. They combined multi-source satellite data using the weighted average method and reconstructed them through the Data INterpolating Convolutional Auto-Encoder method (DINCAE). Guzman & Jiang (2012), on the other hand, explored the general trends of TC rainfall rates based on a time series of a nineteen-year [1998–2016] observational data from the Tropical Rainfall Measurement Mission (TRMM) and the Global Precipitation Measurement mission, to analyze how they are associated with increases in SST and total precipitable water around the TC environment. Meanwhile, Deo et al. (2020) investigated TC-induced extreme rainfall events over the past few decades for the Southwest Pacific nations in the context of climate variability and change. Their study developed Bayesian regression models for individual island nations to understand better the relationships between TC-induced extreme rainfall and the combinations of various climatic drivers modulating the relationship. Comparatively, Lao, Zhou, and Wu (2008) used the Global Precipitation Climatology Project (GPCP), TRMM, and storm track data to explain

the relationship between TC and extreme rain events for July to November period (JASON)[15] in the North Atlantic and Western North Pacific.

In addition, only minimal literature focuses on Southeast Asia and Philippine typhoons. Benchmarking from the previously cited papers in *Section 1.2* that investigate the relationship between climate variables and the intensification of Typhoon Haiyan, no studies were exploring the effects of the typhoon on the weather or climate variables before and after its landfall. Along with this, the expanded literature search using the keywords "Haiyan" and "ERA5" found only one related paper [e.g., Oggini et al., 2021], which partly discusses these subjects. Here, Oggini et al. (2021) studied the surface response [i.e., surface wind and sea surface temperature] to super-typhoon Haiyan based on satellite and Argo float data and evaluated atmospheric and oceanic analysis or reanalysis datasets (i.e., NCEP-FNL, ERA5, and HYCOM)[16]. However, one paper by Bhatia et al. (2020) used ERA5 to calculate the trends in TC intensification in response to climate change, but this only redirects to the premise that several studies were already undertaken on that topic and not the contrary.

On the use of observational datasets to evaluate the effects of cyclones/typhoons on precipitation, papers like Lao et al. (2020) and Trenberth et al. (2018) *[as already cited]* applied their analyses to GPCP data. However, these did not concern Haiyan nor the target area of study (Southeast Asian region). A paper investigating weather-related catastrophes [e.g., Miller, Muir-Wood & Boissonnade, 2008] used temperature data from the Climatic Research Unit (CRU) of the University of East Anglia to evaluate the climate trend from 1950-2005. Nevertheless, the study aims to survey the losses caused by the catastrophe – not to link the TC activity to the temperature trends. Other non-TC-related studies use CRU to demonstrate the trends in either temperature or precipitation.

Regarding papers that utilize the datasets in one study vis-à-vis cyclone/hurricane/storm occurrence, Nogueira (2020) and Watters & Battaglia (2021) have performed an inter-comparison between these datasets. Nogueira (2020) compared the differences among GPCP,

[15] JASON is an acronym for the months of July, August, September, October, November

[16] NCEP-FNL stands for the Final Operational Global Analysis data of the National Centers for Environmental Prediction (NCEP), ERA5 is the fifth-generation atmospheric reanalysis of the European Centre for Medium-Range Weather Forecasts (ECMWF), while HYCOM is an acronym for HYbrid Coordinate Ocean Model, a data-assimilative hybrid isopycnal-sigma-pressure (generalized) coordinate ocean model, developed and evaluated by multi-institutions through the sponsorship of the National Ocean Partnership Program (NOPP), as part of the U.S. Global Ocean Data Assimilation Experiment (GODAE).

ERA5-Interim, and ERA, to understand the global rainfall flux trends over a 40-yr period [1979–2018], but it barely delved into storms [i.e., storm track regions] as the study focus. On the other hand Watters & Battaglia (2021) compared the GPCP and ERA5 datasets to the Integrated Multi-satellitE Retrievals for GPM[17] (IMERG) to understand the precipitation systems in the case of Hurricane Irma in 2017. Regardless of these two papers, the minimal number of relevant studies gives an opportunity to extend this research subject.

Lastly, the interrelationship among anomalies in the studied variables induced by the typhoon event can be examined. For instance, Jiang et al. (2008) investigated whether the storms with higher wind/intensity during the Atlantic Ocean hurricane season in 2005 signify a strong rainfall potential before and during the landfall. Correspondingly, Jiang et al. (2008) compared the same parameters in a different study for two North Atlantic Hurricanes [Isidore and Lili] in 2002. Besides primarily attributing the probability of extreme rainfall to the increased TC activity, Deo et al. (2021) *[who likewise studied TC-induced rainfall response as previously cited]* also demonstrated that other underlying climatic conditions that are non-TC induced [e.g., La Niña or El Nino period, intra-seasonal variability like Madden–Julian Oscillation (MJO)[18], monsoon, etc.] can also have an implication on the rainfall pattern. This is supported by studies of Lyon & Camargo (2009), that observed the influence of seasonally varying ENSO on the rainfall and TC activity in the Philippines, and Kumar et al. (2007), which examined the variations in the relationship between ENSO and monsoon rainfall over South Asia. These two papers both used precipitation data from CRU for their analyses.

Considering the above findings, an assessment of the effects of Typhoon Haiyan on the climate variables/drivers surrounding its occurrence with the use of ERA5, GPCP, and CRU datasets, particularly on the Southeast Asia region where the Philippines belongs (and where the extreme typhoon “Haiyan” wreaked havoc), will be a valuable contribution to scientific research. Furthermore, the papers that investigate inter-variable relationships before and during the typhoon event and the probable effects of non-typhoon climatic conditions happening simultaneously or beyond the typhoon duration give supplementary insight on how the analysis

[17] GPM stands for Global Precipitation Measurement

[18] MJO is an atmospheric [i.e. clouds, rainfall, winds, and pressure] disturbance throughout the planet, moving eastward in the tropics and returning to its starting point at an average of about 30 to 60 days. MJO is distinct from El Niño–Southern Oscillation (ENSO) which is stationary and is associated with persistent features over the Pacific Ocean basin, lasting for several seasons or longer. MJO events can occur multiple times within a season (i.e. week-to-week basis), and so it is best described as intra-seasonal tropical climate variability (Gottschalck, 2014).

can be expounded. These reasons, thereby, befit the motivation of this thesis.

1.4 Objectives, Scope, and Limitations

The overarching scope of this study is to analyze the spatio-temporal anomalies using observational and reanalysis datasets, i.e., GPCP, CRU, HadISST, and ERA5, to determine how anomalies surrounding the Haiyan period compare with meteo-climatic variability between the non-typhoon and typhoon months/years. Using wind, pressure, precipitation, and runoff data, the daily spatio-temporal evolution of abnormal weather patterns surrounding the landfall period (before, during, and after) will be determined, and their inter-variable correlation will be measured. Regression and other statistical treatments will also be carried out to understand which environmental signal is likely impacted by the typhoon event - whether it corresponds to changes in temperature, pressure, wind, precipitation, or runoff values. The effects of seasonal phases and inter-annual variations (dry/wet, monsoon, ENSO) on precipitation and temperature patterns will also be assessed.

Global data will be calculated for comparison, but the assessment will concentrate on the Southeast Asian region to highlight this area's major spatial trends and climatological structures and any anomalous behaviors relative to the selected climate variables. Due to the volume of datasets that need to be analyzed, especially on the daily values, only 5 of the 54 essential climate variables[19] were considered for the analysis. Nonetheless, these parameters are adequate to achieve the central aim of this study.

As to the availability of observational data that is crucial in reconstructing long-term climate patterns and analyses of extreme weather events, there has been a challenge in the Southeast Asian region in keeping, preserving, and archiving observational data over time. Since this has not been a priority by government agencies, data availability only reaches back a few decades. This can be complemented, however, by comparing already-processed maps or graphs from sites or institutions that analyze climate data within the region. These will be beneficial to match the results obtained from this thesis' data analysis.

[19] Per the Global Climate Observing System (GCOS) of the World Meteorological Organization (WMO), an Essential Climate Variable (ECV) is a physical, chemical, or biological variable or group of linked variables that are critical to the characterization of Earth' s climate. Currently, there are 54 ECVs specified by GCOS

CHAPTER 2: STUDY AREA, DATA, AND METHODOLOGY

2.1 Description and Climate Characterization of the Study Area

The focal region of interest in this study is Southeast Asia. This region is between the continental part of the rest of Asia to the North, and the oceanic part (Indian and Pacific Oceans) to the South and East, with its latitudinal position lying approximately within 30^0N and 10^0S *[see **Figure 3**].* These geographical factors profoundly influence the region giving it a distinct climate. Southeast Asian countries are divided into continental (Myanmar, Thailand, Laos, Cambodia, and Vietnam) and insular (Malaysia, Singapore, Indonesia, the Philippines, Brunei, and East Timor]. The continental sub-area experiences more seasonality, extreme temperature and rainfall, and more pronounced dry spells, while the insular [otherwise known as the "maritime continent" due to the greater expanse of the sea than land] have a more equable climate (Chuan, 2005; Frederick & Leinbach, 2022). Rainfall in the region, nonetheless, is more associated with the change in seasons rather than the temperature variations.

Southeast Asia falls within the warm and humid tropics and a generally monsoonal climate. It is subject to regular monsoon systems – the northeast (dry monsoon) and the southwest (wet monsoon), in which the prevailing winds reverse direction every six months, producing wet and dry periods for most of the region. The northeast monsoon occurs from November to March, bringing relatively dry, cool air, and a small amount of precipitation to the mainland. In this period, the southwestward air passes over the sea where it warms and gathers moisture, causing heavy precipitation when the air rises over mountains and encounters landmass (Frederick & Leinbach, 2022). The onset of this monsoon varies from one area to another, characterized by increased rainfall. It arrives in mid-November along the east coast of Malaysia and in early December towards the south. In the eastern side of the Philippines, it arrives in November for the northern part, December for the central, and January for the southern. In Indonesia, the onset is felt in November and December. A critical feature of this monsoon is the cold surge from Siberia, affecting the South China Sea. The extent of this effect is observed from diffused cloud covers in the northern part of the South China Sea, the northern and central Philippines, and the West Pacific for most of the period. These extreme cold surges can reduce the air temperature in the northern side of Southeast Asia, particularly in places located at 17^0N and beyond. Nearer to the equatorial South China Sea, heavy rains and severe flooding may occur due to enhanced convection that causes pre-existing disturbances, e.g., southern Thailand, Malaysia, and Singapore. While the cold surges enhance convective activity, the middle and late cold surges

bring about dry conditions. For this reason, Malaysia and Indonesia seldom experience heavy rainfalls after mid-January and early March, respectively. In the eastern part of the Philippines, heavy rains seldom occur after January in the northern part, after February in the central, and after March in the southern part (Chuan, 2005).

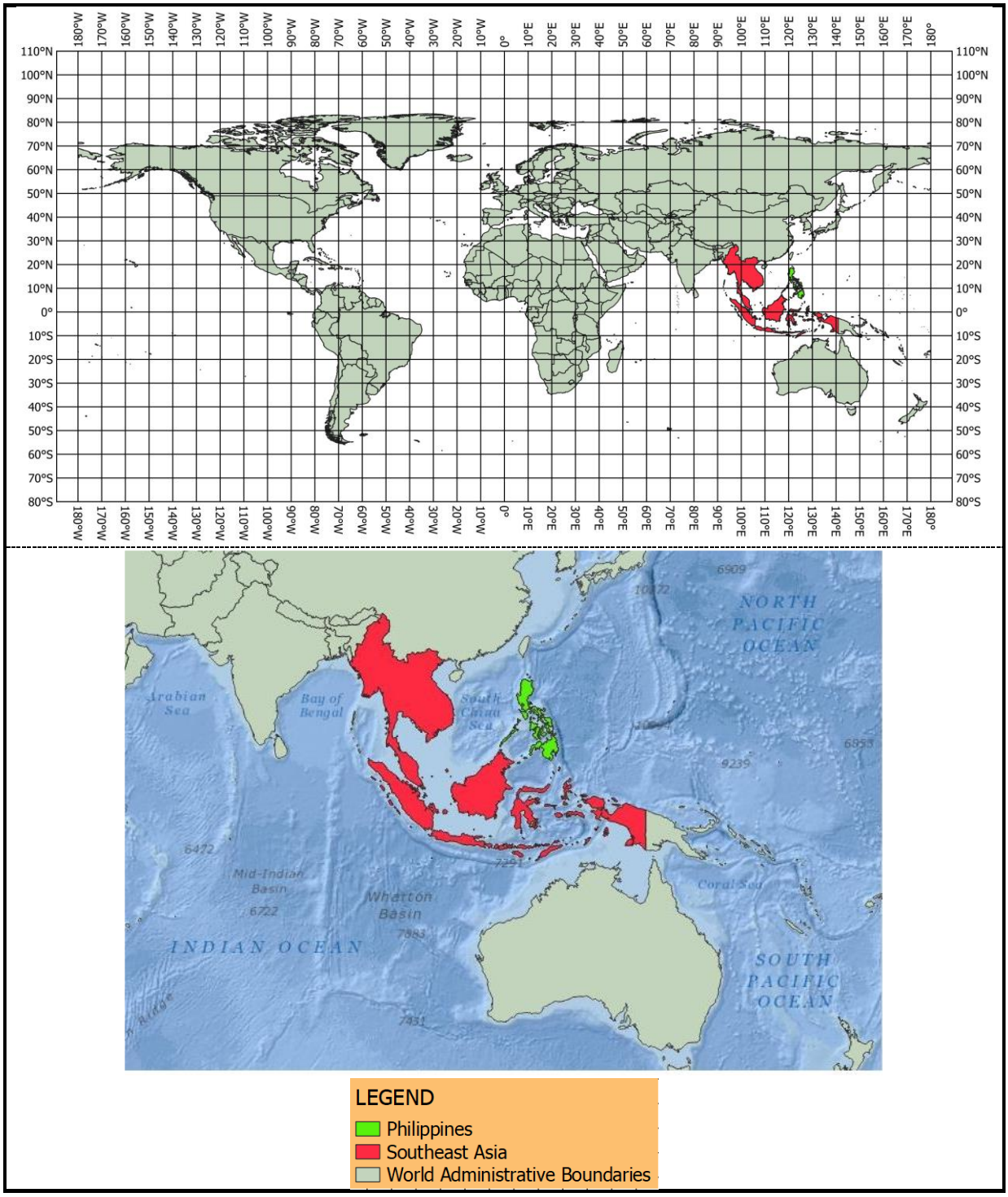

Figure 3. Geographical location of the Southeast Asian Region and the Philippines[20]

[20] Map is produced through the QGIS software. Sources of shapefiles are cited in *Section 2.2*

On the other hand, the southwest monsoon prevails from May to September when the air reverses and dominantly flows to the northeast. The bulk of the rainfall during this period goes to the mainland, affecting southern Malaysia and the insular part of Southeast Asia, hence, there is a little or non-prolonged dry season in this part of the region. This is mainly observed along the equatorial side, and the east coast of the Philippines (Frederick & Leinbach, 2022). A crucial feature of this monsoon is the trough. This is a low-pressure region and a heat source characterizing wet and windy weather closely linked to the monsoonal disturbances that produce considerable rainfall over Southeast Asia. Southwest monsoon also shows oscillations in rainfall, causing wave disturbances, which develop into tropical storms and typhoons under favorable conditions. Most heavy rains during this monsoon period are attributed to tropical waves, mid-tropospheric cyclones, and the convergence zone (Chuan, 2005).

Many cyclonic disturbances produce only moderate rainfall, but in certain cases, they mature into tropical storms *[called cyclones in the Indian Ocean or typhoons in the Pacific].* These events bring heavy rains and devastation to the areas where they hit (Frederick & Leinbach, 2022). In fact, there has been significant growth in the number of extreme weather-related events in the region, such as increase in flooding, storms, and landslides, since the start of the last century (Beirne, Renzhi & Volz, 2021). This is depicted in the figure below.

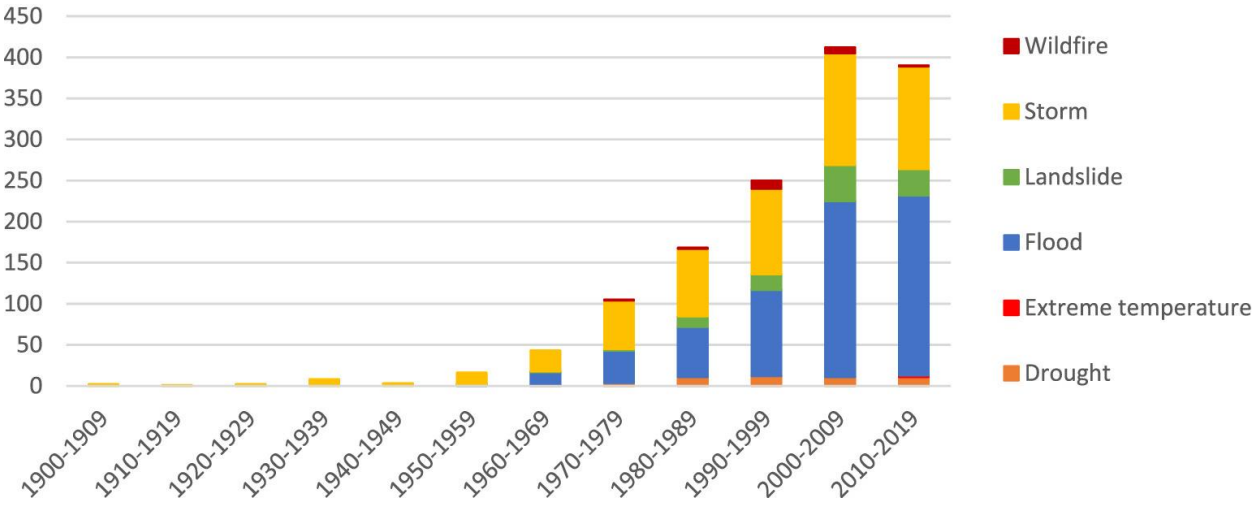

Figure 4. Historical trend of extreme weather occurrences in Southeast Asia[21]

The same paper by Beirne et al. (2021) further states that four Southeast Asian countries are

[21] Original figure, sourced from Beirne et al. (2021), as compiled using data from EM-DAT (2020). EM-DAT stands for Emergency Events Database (https://www.emdat.be/), that contains essential data on the occurrence of global mass disasters from 1900 to the present.

among the top ten most affected by climate-related disasters from 1999-2018, based on global record of fatalities and economic losses[22]. These are Myanmar, the Philippines, Vietnam, and Thailand *[ranked 2nd, 4th, 6th, and 8th, respectively].* Regarding multi-climate hazard vulnerability, ***Figure 5*** shows the hazard map of the countries in Southeast Asia[23], per the paper by Yusuf & Francisco (2009).

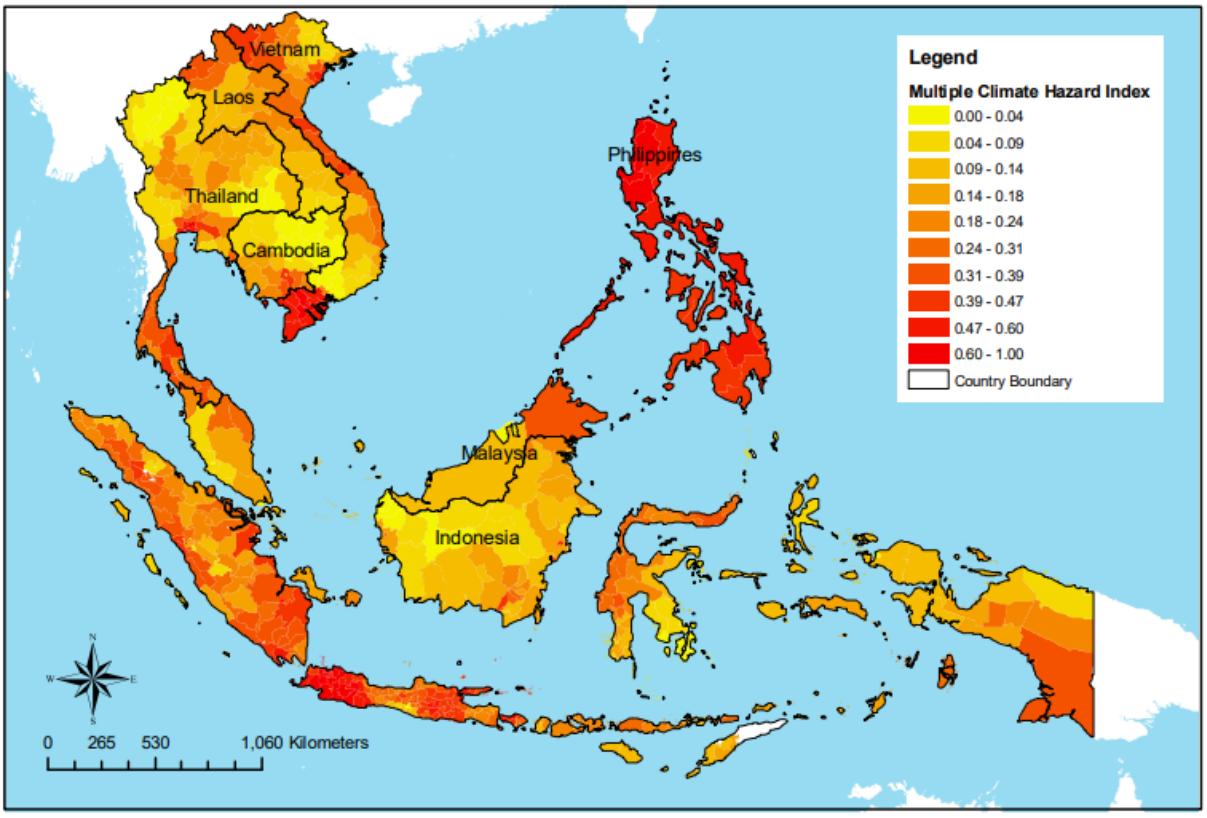

NOTE: *For the scale levels in the legend, zero (0) indicates the lowest vulnerability, and one (1) means the highest*

Figure 5. Multi-climate hazard map of Southeast Asia

From the figure above, the hotspots *[dark-orange to red colored areas]* include the north-western and Mekong region of Vietnam, the coastal regions of Vietnam (facing the South China Sea),

[22] According to the ranking by Germanwatch using Climate Risk Index (Eckstein, Künzel, Schäfer, & Winges, 2019).

[23] For this cited paper, only seven [Thailand, Vietnam, Laos, Cambodia, Indonesia, Malaysia, and the Philippines] were assessed out of the eleven Southeast Asian countries. These countries belong to the Economy and Environment Program for Southeast Asia (EEPSEA) (https://eepsea.org/), a networking initiative founded in 1993 by the International Development Research Centre (IDRC), the Swedish International Development Cooperation Agency (SIDA) and the Canadian International Development Agency (CIDA), to support research and give training in environmental and resource economics among its members, that previously included China and Papua New Guinea *[non-Southeast-Asian countries].* In 2015, the EEPSEA has evolved into Economy and Environment Partnership for Southeast Asia (EEPSEA Partnership), a regional platform for transdisciplinary research to address global environmental challenges among the countries in the region. This partnership now includes Myanmar as an additional member.

Bangkok and its surrounding areas in Thailand, almost all the regions of the Philippines, and the western and eastern parts of Java Island in Indonesia. Dominant hazards are then identified from these climate hotspots, as listed in the following table.

Table 4. Hotspots and dominant climate hazards among Southeast Asian countries[24]

HAZARD HOTSPOT	DOMINANT HAZARDS
Northwestern Vietnam	Droughts
Eastern coastal areas of Vietnam	Cyclones, droughts
Mekong region of Vietnam	Sea level rise
Bangkok and its surrounding area in Thailand	Sea level rise, floods
Southern regions of Thailand	Droughts, floods
The Philippines	Cyclones, landslides, floods, droughts
Sabah state in Malaysia	Droughts
The western and eastern area of Java Island, Indonesia	Droughts, floods, landslides, sea level rise

As reflected in the Figure and Table above, the Philippines is highly vulnerable to multi-climate hazards, especially in cyclone and rainfall-induced hazards [flooding and landslides] or the lack of it [droughts]. This is supported by statistics from Climate Change Knowledge Portal[25] that gave an overview of the country's frequent natural disasters. As presented in ***Figure 6*****,** storms [276 *(46.94%)*] comprise the biggest percentage of natural hazard incidents in the Philippines, followed by floods [136 *(23.13%)*]. Whereas the rain-induced landslides [29 *(4.93%)*] ranked 4th, and droughts [8 *(1.36%)*] ranked 8th out of 10 recorded hazard occurrences in the country from 1980 to 2020.

For cyclones/typhoons in particular, the Visayan Islands in the Philippines were devastated by Super Typhoon Haiyan on 8th November 2013. Following its landfall, it has been recorded as the strongest-ever typhoon during that period based on satellite data (Comiso et al., 2015), until Typhoon Goni surpassed its strength in 2020 *[see* **Table 1** *on page 13]*. However, another paper

[24] Table sourced from the same paper by Yusuf & Francisco (2009)

[25] The Climate Change Knowledge Portal (CCKP) by the World Bank Group (WBG) is a climate-related information hub with global data on historical and future climate, vulnerabilities, and impacts. Aggregated data are also accessible on a national, sub-national, and watershed scale.

by Lagmay et al. (2015) and information from NOAA[26] specify that Typhoon Haiyan has maximum sustained winds reaching 315 kph (~195 mph), which could tie it to the recorded wind speed of Goni. Nevertheless, the Typhoon Haiyan event draws the basis for the scope and area of study in this thesis paper.

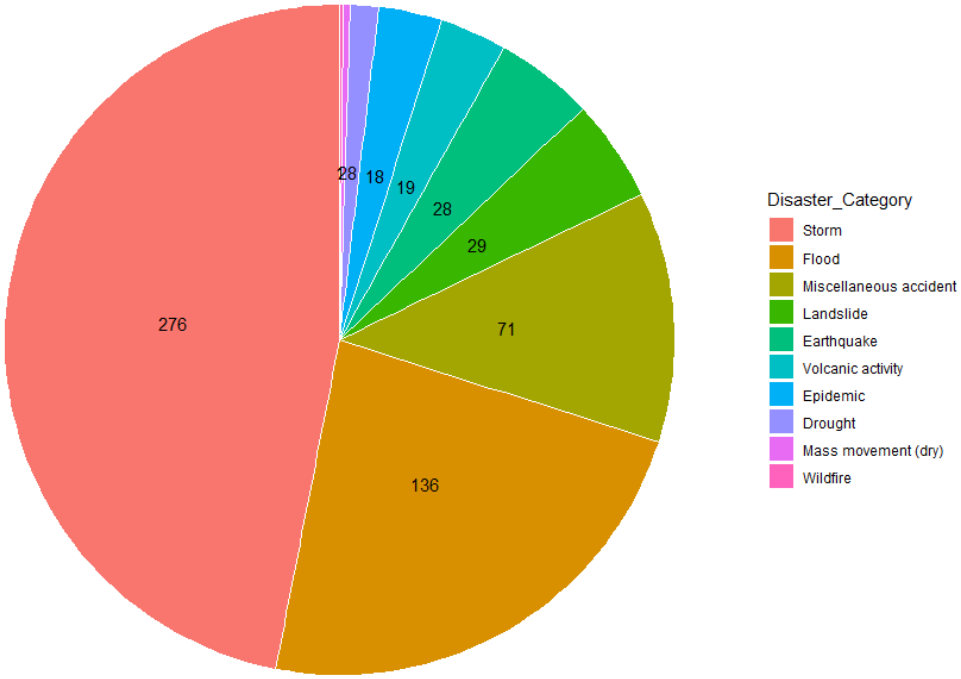

Figure 6. Average Annual Natural Hazard Occurrences in the Philippines [1980-2020][27]

2.2 Datasets Used

A significant volume of data was collected for this study, essentially on the climate variables for analysis. Four (4) climate datasets are downloaded and analyzed for this study namely GPCP, CRU, ERA5 and Hadley Centre Global Sea Ice and Sea Surface Temperature (HadISST). They range from daily, monthly, seasonal, and annual values.

GPCP provides precipitation analysis from surface and satellite measurements spanning from 1979 to the present for monthly, and from 1996 to the present for daily data. CRU is a gridded historical dataset derived from observational data (land-based, except Antarctica) recorded from 1901 to present. It provides temperature and rainfall values from weather stations worldwide

[26] Sourced from: https://scijinks.gov/haiyan/, a site produced by the NASA Space Place team at NASA's Jet Propulsion Laboratory for NOAA National Environmental Satellite, Data, and Information Service (NESDIS), with funds from the Geostationary Operational Environmental Satellite – R Series program and the Joint Polar Satellite System program.
[27] Chart is produced by the R program, but data used for charting is sourced from the CCKP site, https://climateknowledgeportal.worldbank.org/country/philippines/vulnerability

and derivative products, including monthly and long-term historical climatologies. ERA5 provides estimates of many atmospheric, land, and oceanic climate variables extending from 1950 to the present. ERA5 combines historical observations into global estimates using advanced modeling and data assimilation systems. HadISST provides globally complete fields of SST, with data available from 1871 to the present. This is used as a boundary for ERA5. The metadata of these datasets is summarized in **Table 5.**

Table 5. Metadata of Datasets used for Analyses

Dataset	Variable	Description	Format	Unit	Spatial domain[28]	Spatial resolution	Temporal range[29]	Source / Data access
GPCP Monthly	Precipitation	Monthly satellite-gauge and associated precipitation error estimate (Version 2.3)	NetCDF (Network Common Data Form)	mm/day	Global	2.5^0 lon x 2.5^0 lat	1981 to 2020	Adler et al., 2018; NCEI[30]
GPCP Daily	Precipitation	Daily precipitation estimates (Version 1.3)	NetCDF	mm/day	Global	1^0 lon x 1^0 lat	1996 to 2021	Adler et al., 2018; NCEI[31]
CRU Monthly timeseries	Precipitation	Timeseries of monthly mean values (Version 4.06)	NetCDF	mm/month	Global	0.5^0 lon x 0.5^0 lat	1981 to 2020	Osborn et al., 2020[32]; CCKP[33]
CRU Monthly timeseries	Surface Air Temperature	Timeseries of monthly mean values (Version 4.06)	NetCDF	^{0}C	Global	0.5^0 lon x 0.5^0 lat	1981 to 2020	-do-
CRU Annual timeseries	Precipitation	Timeseries of annual mean values (Version 4.06)	NetCDF	mm/year	Global	0.5^0 lon x 0.5^0 lat	1981 to 2020	-do-
CRU Annual timeseries	Surface Air Temperature	Timeseries of monthly mean values (Version 4.06)	NetCDF	^{0}C	Global	0.5^0 lon x 0.5^0 lat	1981 to 2020	-do-
ERA5 Monthly timeseries	Precipitation	Timeseries of monthly mean values	NetCDF	mm/month	Global	0.5^0 lon x 0.5^0 lat	1981 to 2020	CCKP

[28] The downloaded datasets cover global maps but coordinates for the focal region (SE Asia) are extracted from these.
[29] This column indicates only the years used for the analyses. Considering that GPCP covers data beginning from 1979, the temporal range selected for the analysis is 1981-2020 to have an exact 40-year period and to have uniform temporal comparison for all datasets. Only the daily GPCP data has an added year (2021) to compensate for the lacking number of years analyzed, since data is only available from 1996.
[30] NCEI direct download: https://www.ncei.noaa.gov/data/global-precipitation-climatology-project-gpcp-monthly/
[31] NCEI direct download: https://www.ncei.noaa.gov/data/global-precipitation-climatology-project-gpcp-daily/access/
[32] CRU site: https://crudata.uea.ac.uk/cru/data/hrg/
[33] Climate Change Knowledge Portal by the World Bank Group: https://climateknowledgeportal.worldbank.org/download-data

ERA5 Monthly timeseries	Surface Air Temperature	Timeseries of monthly mean values	NetCDF	^{0}C	Global	0.5^0 lon x 0.5^0 lat	1981 to 2020	-do-
ERA5 Annual timeseries	Precipitation	Timeseries of annual mean values	NetCDF	mm/year	Global	0.5^0 lon x 0.5^0 lat	1981 to 2020	-do-
ERA5 Annual timeseries	Surface Air Temperature	Timeseries of monthly mean values	NetCDF	^{0}C	Global	0.5^0 lon x 0.5^0 lat	1981 to 2020	-do-
ERA 5 Daily	Total precipitation (Var 228)	Total amount of water accumulated over a particular time period	NetCDF	m/day	Global	1^0 lon x 1^0 lat	1981 to 2020	C3S Climate Data Store, Copernicus[34]
ERA 5 Daily	10 m U wind component (Var 165)	Eastward component of wind at the height of 10m from Earth's surfrace	NetCDF	m/s	Global	0.5^0 lon x 0.5^0 lat	1981 to 2020	-do-
ERA 5 Daily	10 m V wind component (Var 166)	Northward component of the 10m wind	NetCDF	m/s	Global	0.5^0 lon x 0.5^0 lat	1981 to 2020	-do-
ERA 5 Daily	Mean sea level pressure (Var 151)	Pressure of the atmosphere adjusted to the height of mean sea level	NetCDF	Pa	Global	0.5^0 lon x 0.5^0 lat	1981 to 2020	-do-
ERA 5 Daily	Runoff (Var 205)	Total amount of water accumulated over a particular time period as a sum of surface + sub-surface runoff	NetCDF	depth in m	Global	0.25^0 lon x 0.25^0 lat	1981 to 2020	-do-
HadISST monthly	Sea surface temperature (SST Version 1.1)	Monthly SST for ocean only	NetCDF	^{0}C	Global	0.25^0 lon x 0.25^0 lat	1981 to 2020	Met Office Hadley Centre[35]

[34] https://climate.copernicus.eu/climate-data-store

[35] HadISST1 Data download: https://www.metoffice.gov.uk/hadobs/hadisst/data/download.html

To investigate the effects of ENSO on the studied climate variables, ENSO-related datasets were likewise downloaded for analysis. ENSO is monitored using several indices (i.e., Nino 1+2, 3, 3.4, 4, ONI, and TIN), and anomalies are computed for a 30-year baseline period. The Niño 3.4 index and the Oceanic Niño Index (ONI) are the commonly used indices in defining El Niño and La Niña events (Trenberth; NCAR, 2016). Therefore, these were used for the analysis. Commonly, El Niño (La Niña) or Warm (Cold) phases are characterized by a five consecutive 3-month running mean of SST anomalies (ERSST.v5) in the Niño 3.4 region *(as shown in **Figure 7).*** This phenomenon is observed in the equatorial Pacific Ocean, with a threshold of above (below) +0.5°C (-0.5°C).

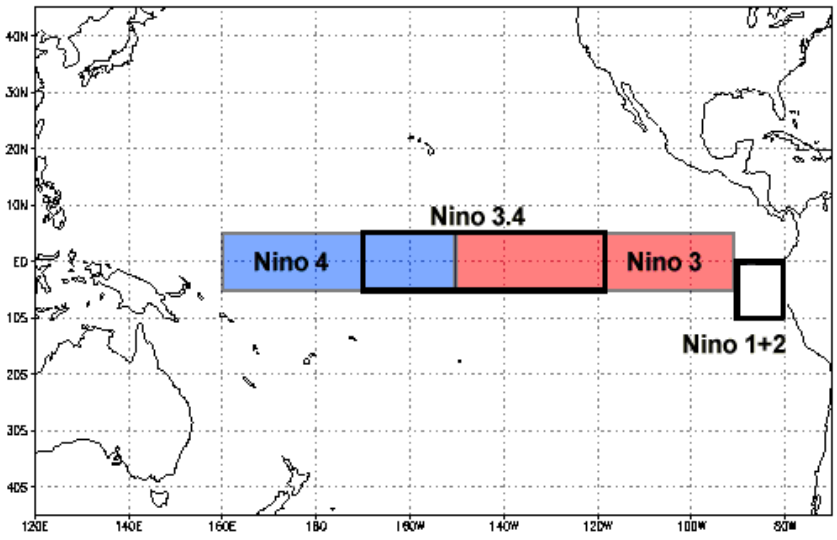

Figure 7. Nino Regions[36]

The ONI 3-month running mean values is taken from the Climate Prediction Center, National Weather Service of NOAA[37]. Data are available from 1950 to present, but for this analysis, only the values from 1981-2020 are used. For the monthly analysis, the Niño 3.4 SST Index was downloaded from Physical Sciences Laboratory of NOAA[38]. These values are calculated from HadISST1 spanning from 1870 to September 2021. Same as with ONI, only the 1981 to 2020 data were used for the analysis. Both time series are available in tabular format but were copied in CSV files for ease of use during data processing.

Some GIS shapefiles were also used to produce maps demonstrating the locations of the focal area and points of emphasis, that include the World Administrative Boundaries[39] and Marine Boundaries for SE Asia[40].

[36] Information and map are sourced from https://www.ncei.noaa.gov/access/monitoring/enso/sst
[37] Sourced from https://origin.cpc.ncep.noaa.gov/products/analysis_monitoring/ensostuff/ONI_v5.php
[38] Sourced from https://psl.noaa.gov/gcos_wgsp/Timeseries/Nino4/ credits to Rayner et al., 2003
[39] Sourced from https://international.ipums.org/international/gis.shtml
[40] Sourced from https://www.marineregions.org/gazetteer.php?p=details&id=18092

2.3 Methods & Tools in Data Analysis

PRE-PROCESSING OF DATA

Prior to the analysis of each dataset using the R software, the data are pre-processed with the aid of Climate Data Operator (CDO) to compute the daily, monthly, seasonal, and annual means. These were useful especially for computing the climatological means of data that involves multi-year values. Operators like ydaymean (computes climatology for the mean of same day for all years), yseasmean (computes climatology for same season of multiple years), ymonmean (computes climatology for same month of multiple years), monmean (computes for the monthly mean only), seasmean (computes for mean of the season only), and yearmean (computes for yearly mean only), were used for the calculations. Since the datasets vary, e.g., GPCP is for daily accumulated precipitation, while the CRU and ERA5 use monthly and annual accumulated values, CDO was also used to convert daily into monthly or yearly values through the muldpm (multiply with day per month) and muldpy (multiply with day per year).

For the analysis of SE Asian region, since the netCDF files cover the entire global coordinates, the values of the coordinates for SE Asia are extracted using the sellonlatbox (select longitude and latitude) operator. The maritime extent of SE Asia [with coordinates at longitude: 92.205 to 141.007 degrees and latitude: -10.930 to 28.547 degrees] is used for this operation. The decimal degrees are utilized because the netCDF files use this gridding format. During this process however, there were files that are not directly in lonlat grids but were in generic format, hence, these were formatted by selecting the appropriate grid, through the -selgrid operator.

For analysis that only requires a particular day, season, month, or year, the operators like selday (extract the values for the selected day/s), selmon (select the month/s), selseas (select the season/s) and selyear (select the year/s) were used. For the daily analysis, since the ERA5 datasets are large and take time to process in R due to its 0.25° lon x 0.25° lat resolution, the global data is re-gridded into 1° lon x 1° lat resolution, using the remapcon (conservative remapping) operator. This was done since the interest of the analysis is not necessarily focused on the global values but on SE Asia. The daily dataset for SE Asia, however, remained with the original grid resolution.

For data that requires the use of spatial mean, the fldmean operator was used to compute the

weighted mean of the values per grid point

DATA ANALYSIS

After all the required data are pre-processed and ready, further data analysis were performed through the R program.

Baseline (reference) period

The standard reference period for calculating climatologies was the 30-year period of 1981-2010, until the World Meteorological Organization recently recommended that the 30-year base period should be updated to 1991-2020 to better reflect the change in the climate. WMO's Services Commission recommends to its members the adoption of the new 30-year baseline, with the use of the 1981-2010 base year until the end of 2020.

Since the data utilized for this thesis are only until December 2020, the 1981-2010 baseline is used as a reference period all throughout the analyses.

Annual analysis

For precipitation, CRU, ERA5, and GPCP are analyzed individually both for the global and SE Asian region, but the three datasets are merged in one time series plot to determine trends and patterns for comparison. The maximum and minimum values were then identified to see the common years for all datasets. The same analysis is performed for the annual temperature using CRU, HadISST, and ERA5 datasets. From the absolute annual and baseline climatology values, the anomalies are computed and again plotted as bar and line chart, this time merging both the precipitation and temperature values in one plot. Maximum and minimum values are again identified and compared among the datasets for purposes of inspecting their commonalities. The values for Y2013 are then extracted and compared for both the precipitation and temperature datasets and the percentile and rank of these values are determined to demonstrate how extreme is Y2013 compared to other "non-typhoon" years.

Seasonal analysis

The standard global seasons are used for this study. These are DJF (winter) season, MAM (spring) season, JJA (summer) season, and SON (autumn) season. As with the annual analysis, the precipitation and temperature datasets are individually processed but are all incorporated into the same time series plot for comparison. Maximum and minimum global and SE Asian values are likewise identified to check the if the datasets have common maximum/minimum years/seasons . Since typhoon Haiyan occurred in November 2013, a separate yearly timeseries for the SON season is plotted, this time focusing on the SE Asia region only. Similarly, the maximum and minimum absolute values are inspected to identify the common year. From the absolute and baseline values, the SON anomalies are then computed and plotted into bar and line chart, and the values for the Year 2013 are again extracted and compared, to determine how extreme the SON 2013 values among the 40 years considered.

Another plot is created reflecting the seasonal values of the Asian region for Y2013 only. The plot is inspected to compare the common maximum or minimum seasons among the datasets, with the same year.

All plots used the "ggplot2" package, since it has features that are helpful in improving the plots' aesthetics.

Monthly analysis

The same sequence, as with the seasonal analysis, was performed for the monthly datasets to plot the time series and inspect the common maximum/minimum year for each month, among the datasets. A separate yearly time series using November month only is plotted to identify which are the maximum or minimum years and if there are commonalities among the datasets. Anomalies are likewise computed for all of November, and the values for Y2013 are again extracted and plotted for comparison with respect to its rank and percentile.

Another plot is created, this reflecting the monthly absolute values and anomalies (from January to December) for Y2013. The same comparison for maximum and minimum is made.

Investigating the ENSO and monsoonal influence

For the annual analysis, the influence of ENSO (El Niño, La Niña, or Neutral) on the precipitation

and temperature anomalies are investigated. To determine which is the classification of each year, the colors used by the Climate Prediction Center for ONI served as a reference where periods of below and above normal SSTs are colored in blue and red when the threshold of a minimum of 5 consecutive overlapping 3-month mean is met. As these are overlapping months, there are years, however, that both El Niño and La Niña can be seen. For these cases, the prevailing phenomenon will be based on what is observed toward the end of the year – the period when ENSO normally matures (Rasmusson & Carpenter, 1982). For the seasonal analysis however, the Niño 3.4 Index values anomalies are used, with the 3-month mean computed from the monthly SST values. The same 3-month mean as with the seasonal months (DJF, MAM, JJA, and SON) are picked, for a uniform temporal comparison.

For the monthly analysis, the Niño 3.4 Index values are likewise used since these are computed on a monthly timescale, and the same months are picked (e.g., November only or January to December), depending on the analysis performed.

To investigate the effect of monsoonal variations on the monthly precipitation values, the months are classified into Northeast (denoting Northeast monsoon month), Southwest (denoting Southwest monsoon month), and None (or not a monsoon month). Northeast months include November to March, Southwest months include May to September, while None months are only April and October. This classification is consistent with the region's climate characterization, as discussed in *Section 2.1.*

Daily analysis

Similarly, the time series of the daily values are plotted for the global and SE Asian region. For this analysis, the datasets used are only GPCP and ERA5 for precipitation and ERA5 for winds, pressure, and runoff.

Similarly, the maximum and minimum day, month, and year are identified from the time series plot. Additionally, the highest absolute and precipitation anomaly (per grid point) is identified to check if it falls within the typhoon days *(Haiyan was formed on November 3 and dissipated on November 11, 2013)* and within the affected area. This was done by picking the coordinates of the longitude and latitude of the point with the highest value. This point is then mapped using QGIS to visualize its location.

Likewise, the anomalies are computed, plotted, and inspected for the maximum and minimum

day, month, and year. For GPCP, considering that the temporal range is from 1996 to 2021, the climatology value is the mean of all 26-year period rather than the baseline periods 1981-2010 and 1991-2020 used for the analysis of ERA5 data. The grid point and day with the highest precipitation anomaly are then identified to investigate again if these coincide with the days and points of interest.

Separate plots were created, showing absolute, baseline, and computed anomalies for the typhoon days. The days are also colored according to before (Nov. 3-6; denoting before landfall), during (Nov. 7 & 8; landfall days), and after (Nov. 9-11; after landfall days). Since the official date of landfall is November 8, in the morning of Philippine time, November 7 and 8 are classified as "during" days in this study since the dataset used the UTC time zone. Technically, however, the official landfall date is 20:40 UTC on November 7, but records indicated that there were several other succeeding landfalls in other parts of the country until late November 8.

Mapping

Climatological maps are generated from annual, seasonal, monthly, and daily values to visualize the spatial coverage and location of major anomalous areas. Individual maps show the climatology and absolute values for the study year (2013), study season (SON 2013), and study month (November 2013) using a rainbow color scale. To guarantee uniform color scales among the datasets, the same z-limit values were set, ensuring that most of the values and their corresponding colors were properly displayed on the map. For precipitation, the colors range from red, orange, yellow, green, blue, and magenta (low or dry to high or wet). The reverse colors were used for temperature, where magenta denotes cold and red denotes warm. However, some extreme values beyond the set z-limit cannot be displayed; thereby, blank white spots can be seen.

For the anomaly maps, only blue and red color scales are used for better visualization. For precipitation, blue signifies a wetter (positive) anomaly, and red is for a drier (negative) anomaly. For temperature, blue means colder (negative) anomaly, and red means hotter (positive) anomaly. For the daily maps, the corresponding pressure and runoff values are indicated by contours using viridis gradient, while windspeed used the same rainbow color gradient as precipitation.

The anomaly points that are beyond the local 5-95 percentile among the values within the SE Asian map (per grid point) are also determined and plotted. For precipitation, values that are

higher than the 95th percentile are colored dark blue to signify extreme wet anomaly, and red to signify extreme dry anomaly. For temperature, the reverse colors are used where red signifies extreme warm anomaly and dark blue denotes extreme cold anomaly.

For plotting these maps, the "raster" and "lattice" packages in R, are used.

2.4 Statistical Treatment

Percentile

To compute for the local 5-95 percentile range to determine anomaly points that are beyond this threshold, quantiles are computed using the *quantile ()* function in R. For the ranking on how extreme are the Y2013, SON 2013 and November 2013 anomalies compared to the rest of the 40 years considered, the *ecdf ()* is used since it returns the percentile values.

Analysis of variance & Wilcoxon Rank Sum Test

Analysis of variance (ANOVA) is performed to determine whether the monsoonal phases and ENSO variations have affected the precipitation and temperature patterns. The significant influence is measured based on the p and F values of the results. Taking into account two parameters only (excluding ENSO-Neutral year, and non-monsoon month), another test is performed this time using Wilcoxon rank sum.

Prior to testing, all datasets are detrended using the *detrend ()* function from the "pracma" package in R.

For these analyses, the *aov ()* and *wilcox.test ()* functions in R are used to compute the p and F values.

Correlation

To better understand the strength and direction of association among the variables (precipitation, temperature, and SST anomalies), a Pearson's correlation analysis [i.e., precipitation vs. temperature, precipitation vs. SST, temperature vs. SST] is performed for each of the datasets. The pairing is done for similar datasets i.e., CRU precipitation vs. CRU temperature, ERA5 precipitation vs. ERA5 temperature. The correlation is then supported by regressing the variables against each other, to compute for the p-values, where significant

correlations are only considered when the p-value is lower than 0.05, even if the correlation coefficient that indicates their relationships are high.

All datasets are likewise detrended before subjecting them into the correlation and regression analyses.

Serial correlations are also inspected using the *acf ()* function in R, as autocorrelation can affect the results.

Density plot, scatterplot and boxplot

To visualize how the above-analyzed values are clustered or dispersed and to to better understand the result of the correlation analysis, density plots were used to show the data distribution, with particular attention to skewness (to the right or left), kurtosis (if there are sharp peaks in the graph), and boxplot are used to show the shape of the distribution, dispersion/spread of the values and to identify outliers. The scatterplot is also used to check if the relationship of the correlated values is reflected in the plot.

For these analyses, probability density are plotted using *hist ()* function, while *skewness ()* and *kurtosis ()* functions are used from the "moments" package in R. For the boxplot, the *geom_boxplot()* function in the "ggplot2" package is used. For plotting the pairwise comparison, correlation and density plots together in one frame, the *pairs ()* function from the "GGally" package is used.

Empirical cumulative distribution function

To understand the differences of the anomaly maps (why it is more colored red or blue or even), the ECDF is used to show the percentage of values equal to or above zero (positive). This is because the median of the z-limit for the color is intentionally set at zero for easier visualization as to whether the points have positive or negative anomalies. For this, the *ecdf ()* function is used.

To confirm this percentage, the count of the positive or negative values are also computed by sub-setting first the anomaly values greater than or equal to zero and counting the False (negative) and True (zero or positive) using the table () function in R.

Welch t-test analysis

Apart from distinguishing the differences of the anomaly values among the datasets through the

ECDF and count, they are also subjected to a Welch Two-Sample t-test to further examine if, indeed, datasets are significantly different among each other. Significant differences are based on the p-values and evidence of the most robust significant difference are based on the highest t-value among the t-test comparison, i.e., CRU vs. ERA5, CRU vs. GPCP, ERA5 vs. GPCP. HadISST was not tested, since no other dataset that measures SST can be compared to it. For this test, the t.test () function is used.

Regression analysis

Simple linear and multiple regression analyses are conducted for the daily variables to assess the effect of the winds or winds + pressure (regressor) to the precipitation and runoff values (response variables). For precipitation, different regression models are tried [regressed with: 1) winds only; 2) winds + time; 3) winds + pressure; 4) winds + pressure + time; 5) pressure only; 6) pressure + time] to check which model results to high R^2, and whether changing the regressors will result to improvement in adjusted R^2 and AIC. Better models should have high R^2 with a minimum AIC. The mean of residuals and the correlation of residuals and fitted values are also inspected since a zero mean and a negative correlation indicates a good model. Another indication of good fitting is that the plot of the residuals vs. the fitted values do not show any visible pattern among the points.

To see the linear relationship between the regressor and response variables, the summary of coefficients are inspected whether they are negatively related (and with a steep negative slope) or positively related (and with a steep positive slope). The significance of this relationship is determined based on the p values.

The same analysis was done for runoff, including testing of an additional model [regressed with 1) wind + pressure + precipitation; and 2) wind + pressure + precipitation + time]. Here, precipitation is added as one of the regressors. For all the analysis, the *lm()* function is used for the computation.

Lastly, regression plots are created for each variable to present their individual relationships. To plot the regression lines, the *ggscatter ()* function from "ggpubr" package is used.

CHAPTER 3: RESULTS AND DISCUSSION

3.1 Annual Analysis

Results

The absolute annual cumulative mean precipitation and temperature values are plotted in ***Figure 8*** for the global mean (left panels) and for the south-east-asian region (sea, right panels). In terms of maximum and minimum values, ERA5 and GPCP have a common global maximum year (2016) for precipitation, while CRU and HadISST have a common global maximum year (2020) for temperature. In SE Asia, CRU and ERA5 have a common maximum year (2017), while ERA5 and GPCP have a common minimum year (1997) for precipitation. CRU and ERA5, on the other hand share a common minimum year (1984) for temperature.

For the "typhoon year", i.e., the year when Typhoon Haiyan occurred, the absolute mean, baseline climatology, and anomaly values of the SE Asian region for the year 2013 are extracted for all the datasets used, as summarized in **Table 6.**

Table 6. Year 2013 Absolute Annual Mean, Baseline Climatology and Anomaly Values for Precipitation & Temperature [SE Asia]

Var.	CRU			ERA5			GPCP | HadISST		
	Absolute	*Baseline*	*Anomaly*	*Absolute*	*Baseline*	*Anomaly*	*Absolute*	*Baseline*	*Anomaly*
Precip.	2297.626	2171.179	126.448	**2492.249**	**2236.699**	**255.551**	2259.561	2041.359	218.202
Temp.	24.257	24.064	0.193	25.779	25.510	**0.269**	**28.387**	**28.172**	0.215

NOTE: Precipitation units: ***mm;*** Temperature units: ^{0}C
For the third dataset/s, **GPCP** is used for precipitation while **HadISST** is used for SST analyses
Highest values among the datasets are emphasized in **boldface colored fonts**

As reflected in the above table, ERA5 has the highest precipitation anomaly for Y2013 among CRU, ERA5, and GPCP datasets, and ERA5 likewise resulted in the highest temperature anomaly. For temperature however, HadISST measures a different variable than CRU and ERA5, hence, this cannot be compared with the two. Looking at how extreme the Y2013 is compared to the non-typhoon years, the following **Tables 7 and 8** summarize the percentile of Y2013 for each dataset, both for precipitation and temperature.

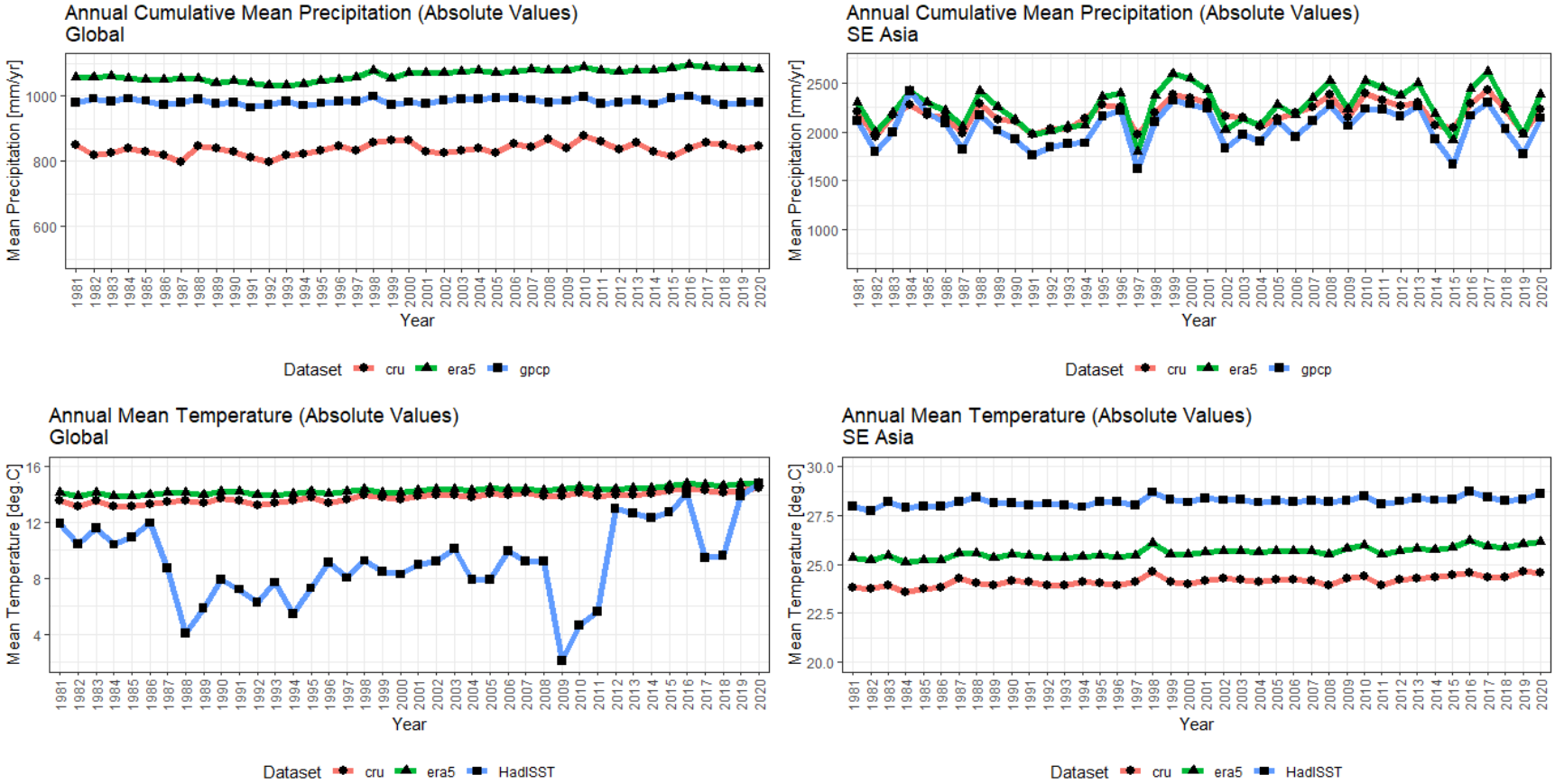

PRECIPITATION

Max. Global Mean (CRU): 876.545 (mm/year) in 2010; Max. SEA Mean (CRU): 2431.398 (mm/year) in 2017
Min. Global Mean (CRU): 796.527 (mm/year) in 1987; Min. SEA Mean (CRU): 1944.03 (mm/year) in 1982
Max. Global Mean (ERA5): 1095.453 (mm/year) in 2016; Max. SEA Mean (ERA5): 2615.704 (mm/year) in 2017
Min. Global Mean (ERA5): 1031.623 (mm/year) in 1992; Min. SEA Mean (ERA5): 1800.307 (mm/year) in 1997
Max. Global Mean (GPCP): 999.026 (mm/year) in 2016; Max. SEA Mean (GPCP): 2412.65 (mm/year) in 1984
Min. Global Mean (GPCP): 963.791 (mm/year) in 1991; Min. SEA Mean (GPCP): 1618.595 (mm/year) in 1997

TEMPERATURE/ SST

Max. Global Mean (CRU): 14.435 (^{0}C) in 2020; Max. SEA Mean (CRU): 24.63 (^{0}C) in 2019
Min. Global Mean (CRU): 13.109 (^{0}C) in 1984; Min. SEA Mean (CRU): 23.586 (^{0}C) in 1984
Max. Global Mean (ERA5): 14.81 (^{0}C) in 2016; Max. SEA Mean (ERA5): 26.185 (^{0}C) in 2016
Min. Global Mean (ERA5): 13.849 (^{0}C) in 1985; Min. SEA Mean (ERA5): 25.096 (^{0}C) in 1984
Max. Global Mean (HadISST): 14.767 (^{0}C) in 2020; Max. SEA Mean (HadISST): 28.705 (^{0}C) in 2016
Min. Global Mean (HadISST): 2.093 (^{0}C) in 2009; Min. SEA Mean (HadISST): 27.738 (^{0}C) in 1982

Figure 8. Annual Mean Precipitation and Temperature (Absolute Values) for Global and SE Asian Region

Table 7. Rank and Percentile of Y2013 Precipitation Anomalies [SE Asia]

Dataset	Precipitation
CRU	> Fn1.A<-ecdf(df1.1$Precip.Anomaly[1:40]) > Fn1.A(df1.1$Precip.Anomaly[1:40][df1.1$Year[1:40]==2013]) [1] 0.85 > summary(Fn1.A) Empirical CDF: 40 unique values with summary Min. 1st Qu. Median Mean 3rd Qu. Max. -227.15 -74.26 10.75 11.25 106.50 260.22 Rank: 7
ERA5	> Fn2.A<-ecdf(df1.1$Precip.Anomaly[41:80]) > Fn2.A(df1.1$Precip.Anomaly[41:80][df1.1$Year[41:80]==2013]) [1] 0.875 > summary(Fn2.A) Empirical CDF: 40 unique values with summary Min. 1st Qu. Median Mean 3rd Qu. Max. -436.39 -168.97 45.91 18.21 176.39 379.01 Rank: 6
GPCP	> Fn3.A<-ecdf(df1.1$Precip.Anomaly[81:120]) > Fn3.A(df1.1$Precip.Anomaly[81:120][df1.1$Year[81:120]==2013]) [1] 0.875 > summary(Fn3.A) Empirical CDF: 40 unique values with summary Min. 1st Qu. Median Mean 3rd Qu. Max. -422.764 -145.157 52.270 5.711 154.613 371.292 Rank: 6

Table 8. Percentile of Y2013 Temperature Anomalies [SE Asia]

Dataset	Temperature
CRU	> Fn1.B<-ecdf(df1.2$Temp.Anomaly[1:40]) > Fn1.B(df1.2$Temp.Anomaly[1:40][df1.2$Year[1:40]==2013]) [1] 0.7 > summary(Fn1.B) Empirical CDF: 40 unique values with summary Min. 1st Qu. Median Mean 3rd Qu. Max. -0.47800 -0.11675 0.08000 0.07675 0.21850 0.57100 Rank: 13
ERA5	> Fn2.B<-ecdf(df1.2$Temp.Anomaly[41:80]) > Fn2.B(df1.2$Temp.Anomaly[41:80][df1.2$Year[41:80]==2013]) [1] 0.775 > summary(Fn2.B) Empirical CDF: 39 unique values with summary Min. 1st Qu. Median Mean 3rd Qu. Max. -0.41500 -0.09350 0.08200 0.09297 0.25950 0.67400 Rank: 10
HadISST	> Fn3.B<-ecdf(df1.1$SST.Anomaly[1:40]) > Fn3.B(df1.1$SST.Anomaly[1:40][df1.1$Year[1:40]==2013]) [1] 0.85 > summary(Fn3.B) Empirical CDF: 40 unique values with summary Min. 1st Qu. Median Mean 3rd Qu. Max. -0.43400 -0.06500 0.04000 0.04752 0.14050 0.53300 Rank: 7

As shown, ERA5 and GPCP are the highest for the three precipitation datasets – with both having the Y2013 on the 87.5th percentile and ranking 6th out of the 40 years, while HadISST is the highest for the temperature datasets, with Y2013 on the 85th percentile and ranking 7th among all years

For spatial comparison, the maps of the 30-yr climatology, absolute and anomaly values for Y2013 are depicted in ***ANNEX 3*** for precipitation and temperature. Globally and in SE Asia, the temperature anomaly maps showed more dominant red than blue spots, demonstrating a prevalence of positive (warm) anomalies as background climatic conditions for Haiyan occurrence. For precipitation, the global anomaly maps show wet anomaly (blue colors) and dry anomaly (red colors) distributed all over the map, at different locations in the considered datasets. In SE Asia, CRU and ERA5 visually showed more blue points (wetter) compared to GPCP for precipitation, with the largest anomalies (dark-blue spots) in ERA5. The Empirical Cumulative Distribution Function (ECDF) plots for precipitation anomalies **[*Figure 9*]** and the count of positive or negative values in **Table 9** show that about 70% of the values are equal to or above 0 (positive) for CRU, while ERA5 and GPCP have about 80%.

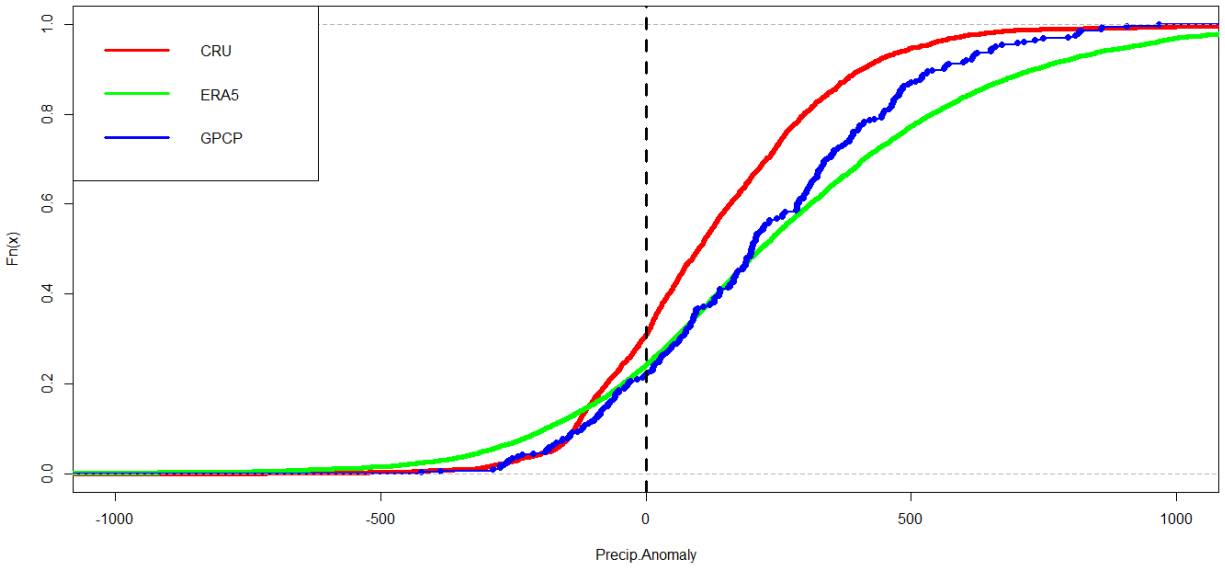

Figure 9. Empirical Cumulative Distribution Plots of Y2013 Precipitation Anomalies for SE Asia

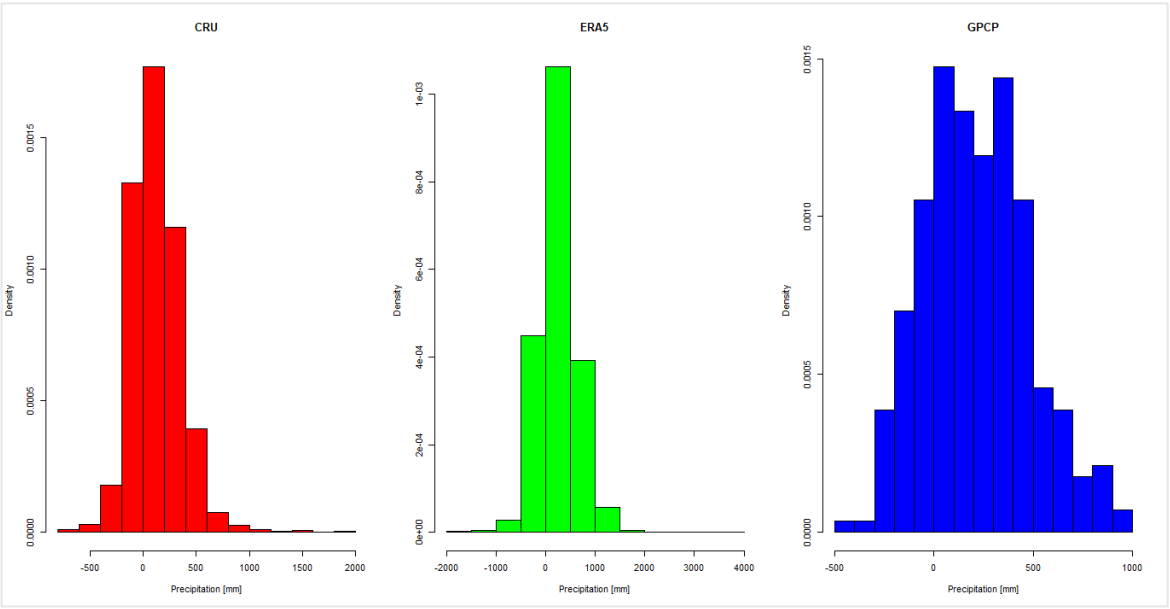

Figure 10. Probability Distribution Plots of Y2013 Precipitation Anomalies for SE Asia

With respect to the distribution of precipitation anomaly values, the skewness [*CRU = 1.064, ERA5 = 0.380, GPCP =0.254*] indicates that all datasets are positively skewed or more concentrated to the left of the graph as shown in the density plot in ***Figure 10*** -- with GPCP being more symmetric having skewness closer to zero. The kurtosis *[CRU =7.819, ERA5 = 5.510, GPCP = 2.766]* also reveals that the GPCP value is closer to 3 hence more normally distributed than CRU and ERA5 with both having sharp peaks on the graph.

For temperature anomalies, the ECDF plots in ***Figure 11*** show that CRU has the least percentage (about 90%) among the three datasets, while ERA5 and HadISST have almost 100% of the values above 0. This is likewise confirmed by the count of positive and negative values in **Table 9.**

With respect to the distribution of anomaly values, the skewness [*CRU = -0.628, ERA5 = 1.202, HadISST = -0.298*] indicates that ERA5 is positively skewed or concentrated to the left, while CRU and HadISST are negatively skewed or more concentrated to the right of the graph as shown in the density plot in ***Figure 12***. Among the datasets, HadISST is more symmetric with skewness closer to zero. The kurtosis *[CRU = 3.280, ERA5 = 7.828, HadISST = 3.054]* also reveals that HadISST value is closer to 3 hence more normally distributed than CRU and ERA5, with ERA5 having sharp peaks on the graph.

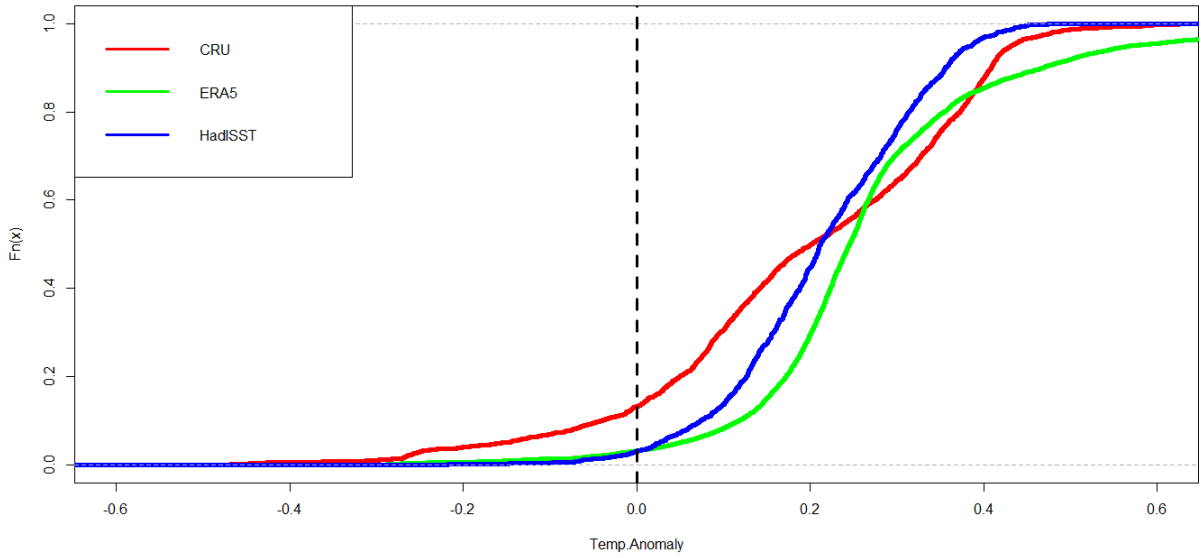

Figure 11. Empirical Cumulative Distribution Plots of Y2013 Temperature Anomalies for SE Asia

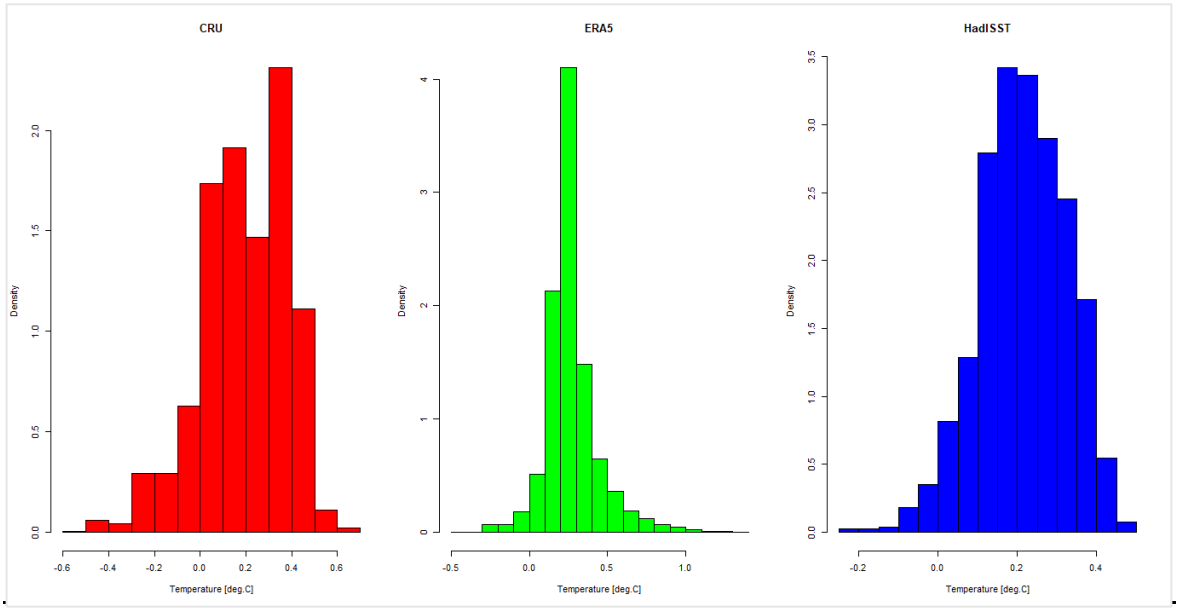

Figure 12. Probability Distribution Plots of Y2013 Temperature Anomalies for SE Asia

Table 9. Count of Negative vs. Zero/Positive Annual Precipitation and Temperature Anomalies for Y2013

	PRECIPITATION	TEMPERATURE
CRU	> pos_cru<-prcp_2013_cru$anomaly>=0 > table(pos_cru) pos_cru FALSE TRUE 828 1855 > table(pos_cru)[2]/(table(pos_cru)[2]+table(pos_cru)[1])	> pos_cru<-tmp_annual_cru_2013$anomaly>=0 > table(pos_cru) pos_cru FALSE TRUE 356 2327

	TRUE 0.6913902	> table(pos_cru)[2]/(table(pos_cru)[2]+table(pos_cru)[1]) TRUE 0.8673127
ERA5	> pos_era5<-prcp_2013_era5$anomaly>=0 > table(pos_era5) pos_era5 FALSE TRUE 1868 5874 > table(pos_era5)[2]/(table(pos_era5)[2]+table(pos_era5)[1]) TRUE 0.7587187	> pos_era5<-tmp_annual_era5_2013$anomaly>=0 > table(pos_era5) pos_era5 FALSE TRUE 246 7496 > table(pos_era5)[2]/(table(pos_era5)[2]+table(pos_era5)[1]) TRUE 0.9682253
GPCP | HadISST	> pos_gpcp<-prcp_2013_gpcp$anomaly>=0 > table(pos_gpcp) pos_gpcp FALSE TRUE 63 222 > table(pos_gpcp)[2]/(table(pos_gpcp)[2]+table(pos_gpcp)[1]) TRUE 0.7789474	> pos_HadISST<-tmp_annual_HadISST_2013$anomaly>=0 > table(pos_HadISST) pos_HadISST FALSE TRUE 48 1491 > table(pos_HadISST)[2]/(table(pos_HadISST)[2]+table(pos_HadISST)[1]) TRUE 0.9688109

The 5-95 percentiles of the anomaly values for all the grid points were also calculated to show the points that are beyond the threshold. Shown in ***Figures 13 & 14*** are the points with anomaly values exceeding the local 5 -95 range denoted by red (blue) for dry (wet) anomalies, while the reverse colors were used for temperature, where the points below the 5th percentile are marked with blue (or cold) and the points above 95th percentile are marked with red (or hot). It is seen that there are clear differences in the locations of these marked red (or blue) points, demonstrating that there are inconsistencies in the locations of high (or low) precipitation and temperature anomalies in terms of its geographic location in as far as the year when typhoon Haiyan occurred, is considered.

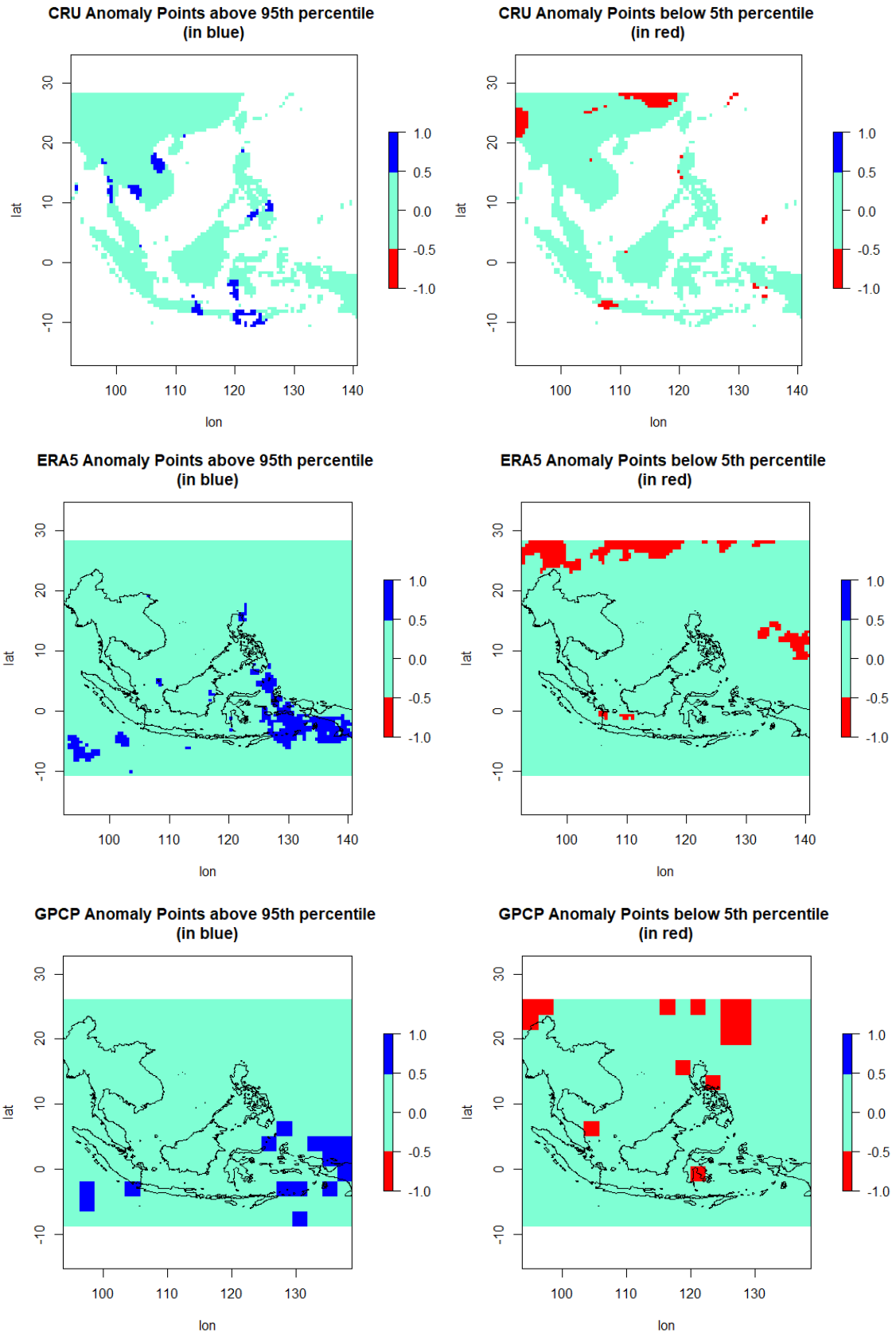

Figure 13. Maps Showing Anomaly Points Beyond 5-95 Percentile for Y2013 Precipitation [SE Asia]

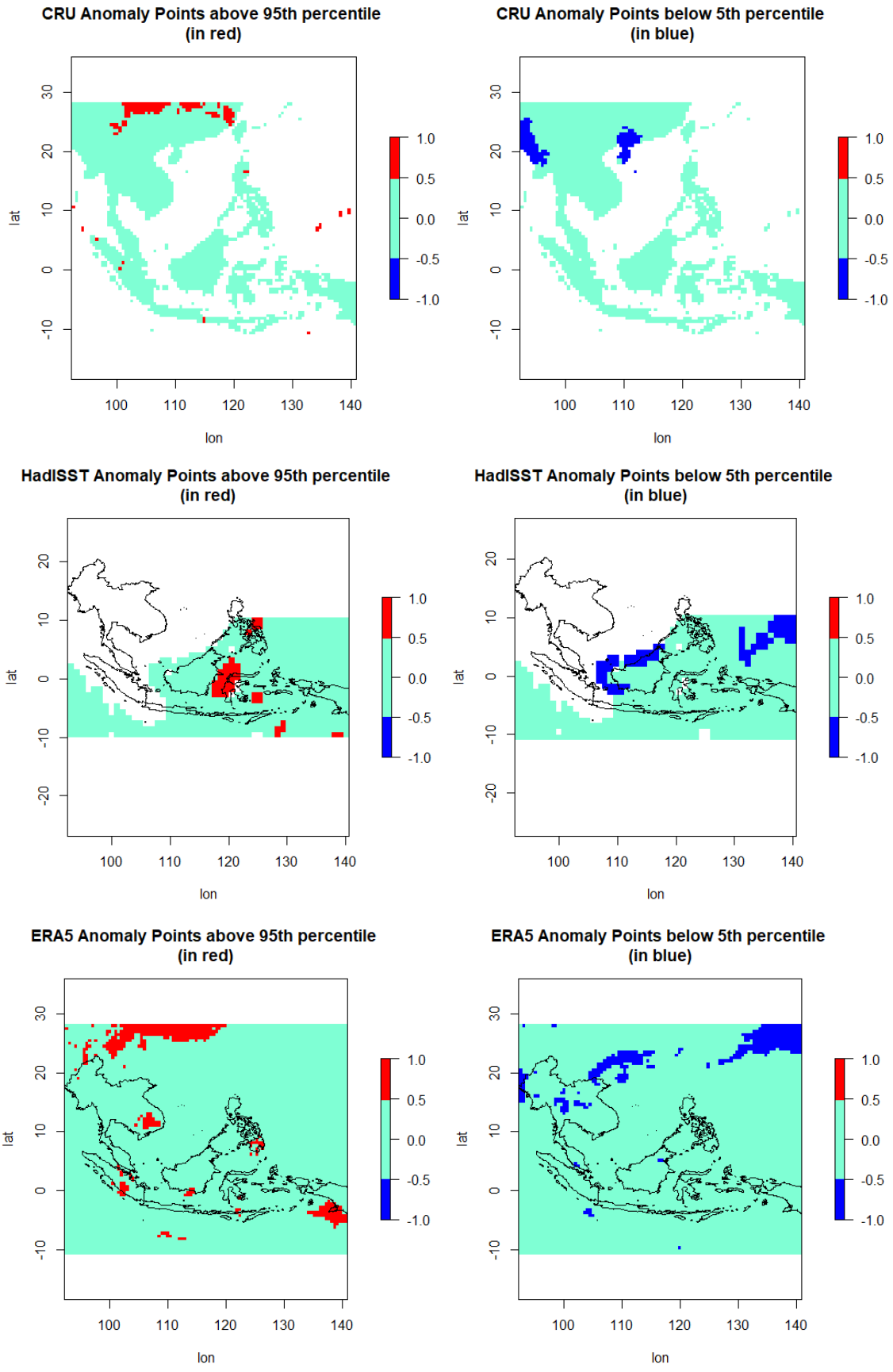

Figure 14. Maps Showing Anomaly Points Beyond 5-95 Percentile for Y2013 Temperature [SE Asia]

To further compare the differences in the values, the summary of the t-test for each dataset [as

summarized in **Table 10**] shows that CRU, ERA5, and GPCP are significantly different in terms of precipitation anomalies -- having relatively low p-values for CRU vs. ERA5 and CRU vs. GPCP, and just a little lower than 0.05 for ERA5 vs. GPCP. Based on the highest t-value, the strongest evidence of difference is between CRU & ERA5. For temperature, CRU and ERA5 are likewise significantly different. HadISST was excluded from this analysis since only CRU and ERA5 measure surface air temperatures among the three.

Table 10. Results of Welch Two-Sample t-test for Y2013 Precipitation and Temperature Anomalies

	PRECIPITATION	TEMPERATURE
CRU vs. ERA5	data: prcp_2013_cru$anomaly and prcp_2013_era5$anomaly t = -19.878, df = 7469.9, p-value < 2.2e-16 alternative hypothesis: true difference in means is not equal to 0 95 percent confidence interval: -137.2749 -112.6301 sample estimates: mean of x mean of y 122.7846 247.7371	data: tmp_annual_cru_2013$anomaly and tmp_annual_era5_2013$anomaly t = -18.586, df = 4260.5, p-value < 2.2e-16 alternative hypothesis: true difference in means is not equal to 0 95 percent confidence interval: -0.08435525 -0.06825695 sample estimates: mean of x mean of y 0.1929929 0.2692990
CRU vs. GPCP	data: prcp_2013_cru$anomaly and prcp_2013_gpcp$anomaly t = -5.556, df = 334.37, p-value = 5.643e-08 alternative hypothesis: true difference in means is not equal to 0 95 percent confidence interval: -122.93596 -58.64702 sample estimates: mean of x mean of y 122.7846 213.5761	N/A
ERA5 vs. GPCP	data: prcp_2013_era5$anomaly and prcp_2013_gpcp$anomaly t = 2.1005, df = 328.22, p-value = 0.03645 alternative hypothesis: true difference in means is not equal to 0 95 percent confidence interval: 2.167778 66.154240 sample estimates: mean of x mean of y 247.7371 213.5761	N/A

The SE Asian precipitation and temperature anomalies are plotted against the ENSO variations, as presented in ***Figure 15,*** to investigate whether the El Niño/Southern Oscillation (ENSO) phenomenon impacts the yearly precipitation and temperature in the region. For the plot, the years are categorized into El Niño (EN), La Niña (LN), and Neutral (N), based on the 3-month running mean values of the

Oceanic Nino Index (ONI), as described in detail in *Chapter 2, Section 2.3.*

As seen, most of the precipitation anomalies are positive for LN years (green bars) and negative for EN years (red bars). However, a few green bars fall along negative anomalies, and a few red bars fall along positive precipitation anomalies at different years. For the N years (blue bars), they fall either along positive or negative precipitation anomalies, but exhibit a common pattern where both years 1981 and 2013 have positive precipitation anomalies, while years 1990 and 1993 have negative precipitation anomalies – for all three datasets.

Comparing the anomaly years in the same plot, CRU and ERA5 have a common maximum year (2017) for precipitation and minimum year (1984) for temperature. ERA5 and GPCP, otherwise, have a common minimum year (1997) for precipitation anomaly, and ERA5 and HadISST have a common maximum year (2016) for temperature anomaly. With respect to the typhoon year (2013), the precipitation and temperature anomaly values differ among the datasets, yet ERA5 has the highest precipitation and temperature anomalies, as previously presented in **Table 6.** Being an ENSO Neutral year, the plot and the values in the same table show that both precipitation and temperature anomalies are positive.

To statistically characterize the influence of ENSO variations (EN, LN and N) on the precipitation and temperature anomalies, an Analysis of Variance (ANOVA) is performed for each dataset as detailed in **Table 11.** The results showed that the precipitation anomalies for all datasets are significantly influenced by ENSO variations with very low p-values (marked with a green rectangle). The large F values likewise confirm this result. For temperature anomalies (marked with a red rectangle), only HadISST is influenced by the ENSO variation, although the p-value indicates lower significance being slightly higher than 0.05. It is important to stress that Haiyan occurred in a neutral year, as anomalies of ENSO would have otherwise likely significantly affected its occurrence and evolution.

A Wilcoxon rank sum test is also performed, accounting only the EN and LN years as presented in **Table 12.** Like the ANOVA results, only precipitation anomalies showed significant p-values.

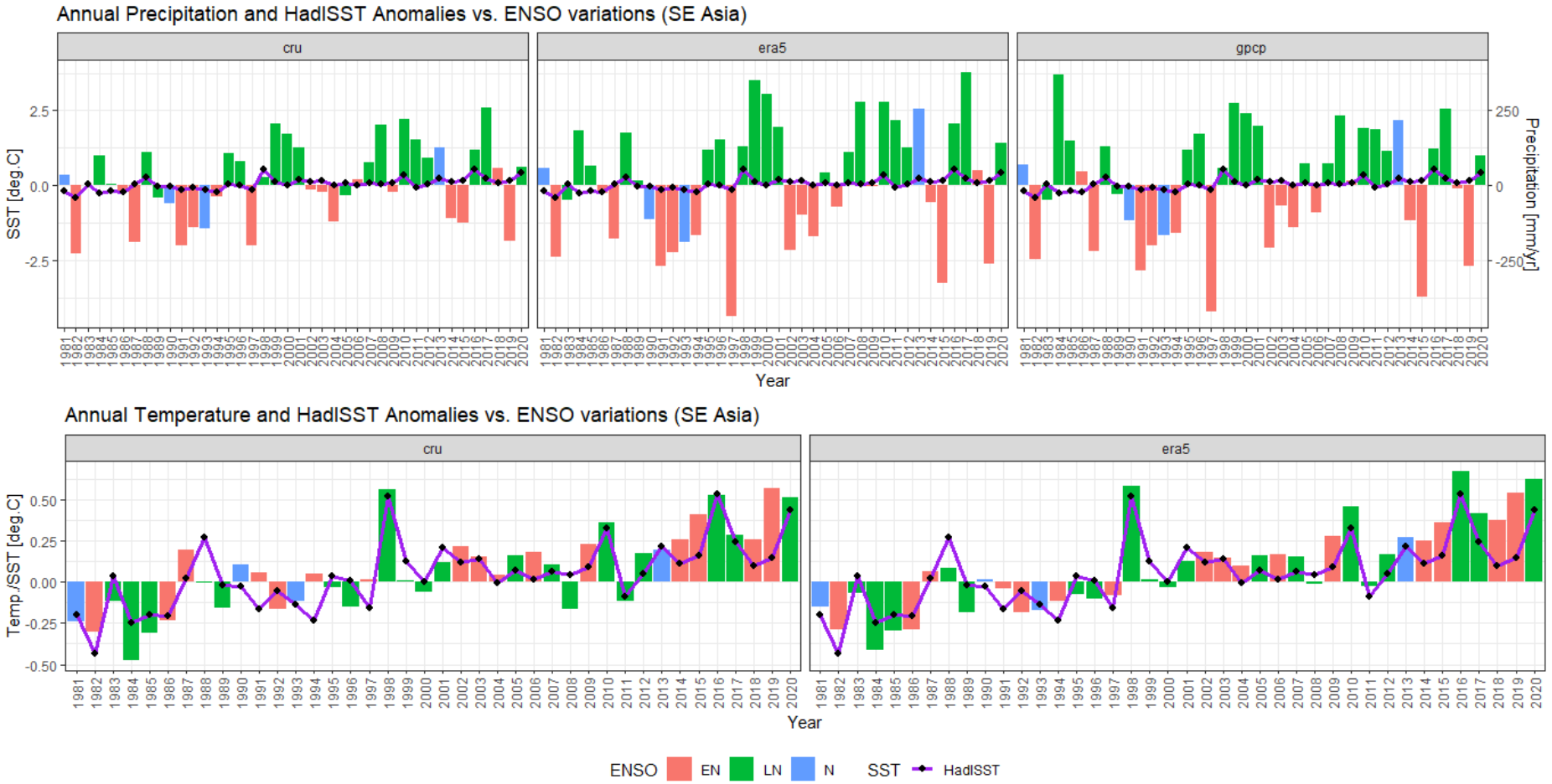

CRU

Max. **Precip.** Anomaly: 260.22 (mm) in 2017
Min. **Precip.** Anomaly: -227.149 (mm) in 1982
Max. **Temp.** Anomaly: 0.571 (^{0}C) in 2019
Min.**Temp.** Anomaly: -0.478 (^{0}C) in 1984

ERA5

Max. **Precip**. Anomaly: 379.006 (mm) in 2017
Min. **Precip.** Anomaly: -436.392 (mm) in 1997
Max. **Temp**. Anomaly: 0 0.674 (^{0}C) in 2016
Min.**Temp.** Anomaly: -0.415 (^{0}C) in 1984

GPCP | HadISST

Max. **Precip.** Anomaly: 371.292 (mm) in 1984
Min. **Precip**. Anomaly: -422.764 (mm) in 1997
Max. **SST**. Anomaly: 0.533 (^{0}C) in 2016
Min.**SST.** Anomaly -0.434 (^{0}C) in 1982

Figure 15. Annual Precipitation and Temperature/SST Anomalies vs. ENSO variations (SE Asia)

Table 11. Results of Analysis of Variance for Annual Precipitation & Temperature Anomalies against ENSO [SE Asia]

Dataset	ANOVA results

CRU	`> summary(aov(df1.1$Precip.DT[1:40]~df1.1$ENSO[1:40]))`
	`Df Sum Sq Mean Sq F value Pr(>F)`
	`df1.1$ENSO[1:40] 2 353779 176889 22.37 4.28e-07 ***`
	`Residuals 37 292551 7907`
	`---`
	`Signif. codes: 0 '***' 0.001 '**' 0.01 '*' 0.05 '.' 0.1 ' ' 1`
	`> summary(aov(df1.2$Temp.DT[1:40]~df1.2$ENSO[1:40]))`
	`Df Sum Sq Mean Sq F value Pr(>F)`
	`df1.2$ENSO[1:40] 2 0.0492 0.02461 0.523 0.597`
	`Residuals 37 1.7419 0.04708`

ERA5	`> summary(aov(df1.1$Precip.DT[41:80]~df1.1$ENSO[41:80]))`
	`Df Sum Sq Mean Sq F value Pr(>F)`
	`df1.1$ENSO[41:80] 2 1030105 515052 32.51 7.09e-09 ***`
	`Residuals 37 586108 15841`
	`---`
	`Signif. codes: 0 '***' 0.001 '**' 0.01 '*' 0.05 '.' 0.1 ' ' 1`
	`> summary(aov(df1.2$Temp.DT[41:80]~df1.2$ENSO[41:80]))`
	`Df Sum Sq Mean Sq F value Pr(>F)`
	`df1.2$ENSO[41:80] 2 0.0276 0.01381 0.26 0.772`
	`Residuals 37 1.9652 0.05311`

GPCP / HadISST	`> summary(aov(df1.1$Precip.DT[81:120]~df1.1$ENSO[81:120]))`
	`Df Sum Sq Mean Sq F value Pr(>F)`
	`df1.1$ENSO[81:120] 2 914200 457100 30.75 1.36e-08 ***`
	`Residuals 37 550055 14866`
	`---`
	`Signif. codes: 0 '***' 0.001 '**' 0.01 '*' 0.05 '.' 0.1 ' ' 1`
	`> summary(aov(df1.2$SST.DT[1:40]~df1.2$ENSO[1:40]))`
	`Df Sum Sq Mean Sq F value Pr(>F)`
	`df1.2$ENSO[1:40] 2 0.2006 0.10030 3.219 0.0514 .`
	`Residuals 37 1.1530 0.03116`
	`---`
	`Signif. codes: 0 '***' 0.001 '**' 0.01 '*' 0.05 '.' 0.1 ' ' 1`

Table 12. Results of Wilcoxon Rank Sum Test on Annual Precipitation and Temperature Anomalies for EN and LN years

Dataset	Wilcoxon Test Results

CRU Precip.	`> wilcox.test(Precip.DT[1:40] ~ ENSO[1:40], data = df1.1, conf.int = TRUE)`
	
	`data: Precip.DT[1:40] by ENSO[1:40]`
	`W = 18, p-value = 4.362e-07`
	`alternative hypothesis: true location shift is not equal to 0`
	`95 percent confidence interval:`
	`-264.2979 -132.7509`
	`sample estimates:`
	`difference in location`
	`-204.0518`

CRU Temp.	`> wilcox.test(Temp.DT[1:40] ~ ENSO[1:40], data = df1.2, conf.int = TRUE)`
	
	`data: Temp.DT[1:40] by ENSO[1:40]`
	`W = 195, p-value = 0.2758`

	alternative hypothesis: true location shift is not equal to 0 95 percent confidence interval: -0.08565767 0.22234233 sample estimates: difference in location 0.07507208
ERA5 Precip.	> wilcox.test(Precip.DT[41:80] ~ ENSO[41:80], data = df1.1, conf.int = TRUE) data: Precip.DT[41:80] by ENSO[41:80] W = 5, **p-value = 5.2e-09** alternative hypothesis: true location shift is not equal to 0 95 percent confidence interval: -420.6027 -253.6029 sample estimates: difference in location -344.2017
ERA5 Temp.	> wilcox.test(Temp.DT[41:80] ~ ENSO[41:80], data = df1.2, conf.int = TRUE) data: Temp.DT[41:80] by ENSO[41:80] W = 165, **p-value = 0.8875** alternative hypothesis: true location shift is not equal to 0 95 percent confidence interval: -0.1761172 0.1683153 sample estimates: difference in location 0.007378376
GPCP Precip.	> wilcox.test(Precip.DT[81:120] ~ ENSO[81:120], data = df1.1, conf.int = TRUE) data: Precip.DT[81:120] by ENSO[81:120] W = 6, **p-value = 8.21e-09** alternative hypothesis: true location shift is not equal to 0 95 percent confidence interval: -395.2323 -234.9853 sample estimates: difference in location -324.7317
HadISST	> wilcox.test(SST.DT[1:40] ~ ENSO[1:40], data = df1.2, conf.int = TRUE) data: SST.DT[1:40] by ENSO[1:40] W = 105, **p-value = 0.08271** alternative hypothesis: true location shift is not equal to 0 95 percent confidence interval: -0.24021371 0.01385485 sample estimates: difference in location -0.1182621

Discussion

On the percentile and ranking of Y2013 as well as the ECDF plots that displayed the percentage of positive anomalies, it is evident that Haiyan occurred in a warmer-than-average and much wetter-than-average year in SE Asia, according to all inspected datasets.

For the precipitation anomaly maps, the GPCP has higher percentage of positive values than CRU, but there appears to have more blue-dominated anomaly map for CRU. This can be due to CRU having more grid points with finer grid resolution (0.5^0 x 0.5^0) than GPCP (2.5^0 x 2.5^0). For

temperature anomalies, the high percentage of positive values confirm the red-dominated anomaly maps for SE Asia for all three datasets. Checking information from other institutions to compare the generated anomaly maps, the Annual 2013 Global Climate Report[41] by the National Centers for Environmental Information (NCEI) NOAA states that 2013 was the fourth warmest year globally since 1880 records, supporting the red-dominated global anomaly maps. For precipitation, the report specifies that global land-based stations measured near-average on balance for this year but varied greatly from region to region. This explains the not-so-evenly distributed blue and red colors at different points in the continents. by the National Centers for Environmental Information (NCEI) NOAA states that 2013 was the fourth warmest year globally since 1880 records, supporting the red-dominated global anomaly maps. For precipitation, the report specifies that global land-based stations measured near-average on balance for this year but varied greatly from region to region. This explains the not-so-evenly distributed blue and red colors at different points in the continents.

The differences across the maps that depict the points beyond the 5-95 local range also manifest that there are general inconsistencies across datasets regarding not only the amplitude of large precipitation and temperature anomalies around the Haiyan typhoon but also their geographical position. The inconsistencies are most apparent for precipitation – a notoriously more difficult variable to monitor and simulate than temperature. Overall, as far as the SE Asian region and annual-mean values are considered, the empirical distributions demonstrate that for both precipitation and temperature, different datasets provide a clearly different description of the Y2013 anomalies, pointing to a lack of consistency about the background climatic conditions upon which Haiyan occurred. It must be noted, however, that the points analyzed are individual grid points in the map, but their spatial relevance differs since they are at varying latitudes. Hence the empirical distributions are not comparable – from one to the other.

On the effect of ENSO, SE Asian countries have historically experienced significant climate-related issues with El Niños causing deficient rainfall or drought that impacts the crop production, particularly in Indonesia and Philippines (Shean, 2014). This supports the result of the analysis where most red bars (EN years) fall on negative precipitation anomalies. For green bars (LN years) falling on positive precipitation anomalies, a previously cited paper by Deo et al. (2021) studying Southwest Pacific nations confirms this observation, where non-TC-induced LN years enhance

[41] Sourced from https://www.ncei.noaa.gov/access/monitoring/monthly-report/global/201313

rainfall. However, it has a lower probability than combined TC and LN to induce extreme rainfall. In SE Asia, a study by Wang, Luo & Liu (2020) used a 31-yr running mean from 1901–2017 to calculate the correlation coefficient (CC) between rainfall variations and ENSO, indicating that tropical subregions of Asia (including SE Asia) show a robust and stable relationship with ENSO, with persistent CCs that are significantly above the 99% (95%) confidence level. In their study, strong correlations denote drier anomalies during EN and wetter anomalies on LN. However, they also noted that the response to EN and LN is asymmetric and differs between major or minor ENSO events. On the contrary, the same paper by Deo et al. (2021) also states that an EN year can influence intense/extreme rainfall when combined with a TC activity. This could explain why a few green bars in the plot fall along negative anomalies, and a few red bars fall along positive precipitation anomalies at different years. While on Neutral years, TC-combined contributions to rainfall vary (increasing or decreasing) from one area to another. Consistent with this, the plot shows that some N years (blue bars) fall either along positive or negative precipitation anomalies. Looking further at other literature, the previously cited paper by Tran, Ritchie, & Perkins-Kirkpatrick (2022) mentioned that fewer TC landfalls occur in SE Asia in EN years, with locations shifting northwestward over mainland Asia, while landfalls are higher and more distributed in LN and highest in N years. However, it is beyond this thesis's scope to investigate whether the N years other than 2013 have experienced strong TC activities that contributed to the rainfall variations.

On the temperature, the plot did not necessarily show that EN years have positive while LN years have negative anomalies but a related paper by Thirumalai, DiNezio, Okumura & Deser (2017) observed that there is a robust relationship between ENSO and SE Asian surface air temperatures (SATs) with all April extremes occurring during EN years. Upon quantifying the relative contributions of long-term warming and 2015-2016 EN year to the extreme SAT in April 2016, the study found that global warming increases the likelihood of record-breaking April extremes, estimating that 29% of the 2016 anomaly was caused by warming and 49% by El Niño.

Taking into consideration the result of the statistical treatments, the ANOVA and Wilcoxon tests deduced that ENSO has significantly affected the precipitation patterns, but there is no significant effect on the temperature anomalies vis-a-vis the EN/LN/N year variations.

3.2 Seasonal Analysis

Results

The yearly SON values for precipitation and temperature (Global and SE Asia) are plotted in ***Figure 16.*** Looking at the maximum and minimum values, CRU and ERA5 share a common minimum year (1991) with respect to global precipitation values. For SE Asia, ERA5 and GPCP both share a common maximum year (2010) and minimum year (1997). For temperature, CRU and ERA5 share a common maximum year (2020), while only CRU and ERA5 share a common minimum year (1992) globally. In SE Asia, only CRU and HadISST have a common maximum year (1998). It is again apparent that the various datasets provide different information on the recorded maxima/minima years, an indication of the differences among them.

Like the annual analysis, the yearly SON absolute, baseline, and anomaly values for the year 2013 are extracted and summarized in **Table 13.**

Table 13. SON 2013 Absolute Mean, Baseline and Anomaly Values for Precipitation & Temperature

Var.	CRU			ERA5			GPCP | HadISST		
	Absolute	*Baseline*	*Anomaly*	*Absolute*	*Baseline*	*Anomaly*	*Absolute*	*Baseline*	*Anomaly*
Precip.	573.771	536.644	**37.127**	**614.463**	**588.446**	26.017	589.989	555.982	34.007
Temp.	24.347	24.341	0.006	25.751	25.693	**0.138**	**28.595**	**28.481**	0.114

NOTE: Precipitation units: ***mm;*** Temperature units: ^{0}C
For the third datasets, **GPCP** is used for precipitation while **HadISST** is used for temperature analyses
Highest values among the datasets are emphasized in **boldface colored fonts**

As reflected in the above table, CRU has the highest precipitation anomaly for Y2013 among the CRU, ERA5, and GPCP datasets, while ERA5 has the highest anomaly among the datasets measuring temperature. However, as previously mentioned in the annual analysis, HadISST measures a different variable than CRU and ERA5, hence, this can't be compared with the two.

On how extreme the Y2013 is compared to the non-typhoon years, **Tables 14 and 15** summarize the percentile and ranking of SON for Y2013, for all the years considered, among all the datasets.

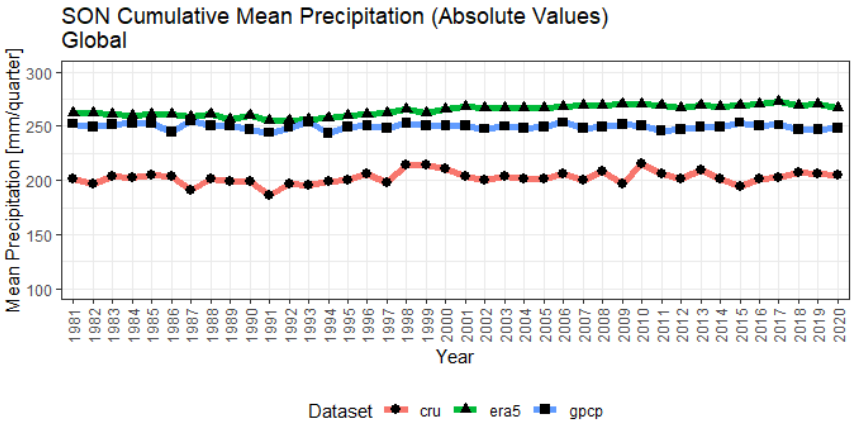

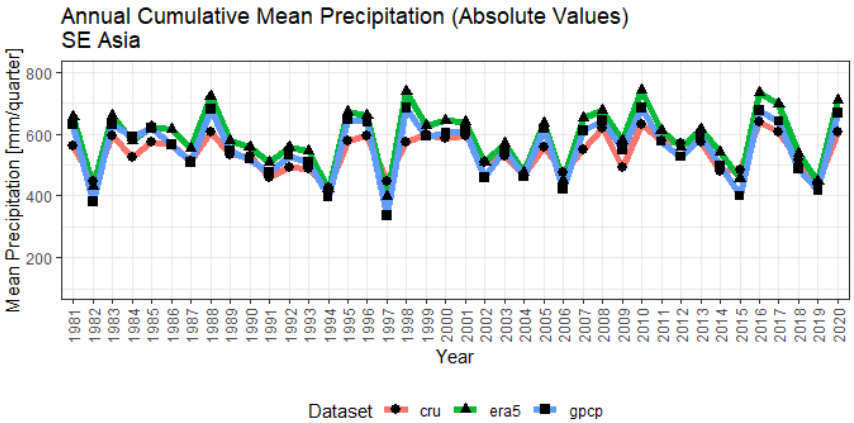

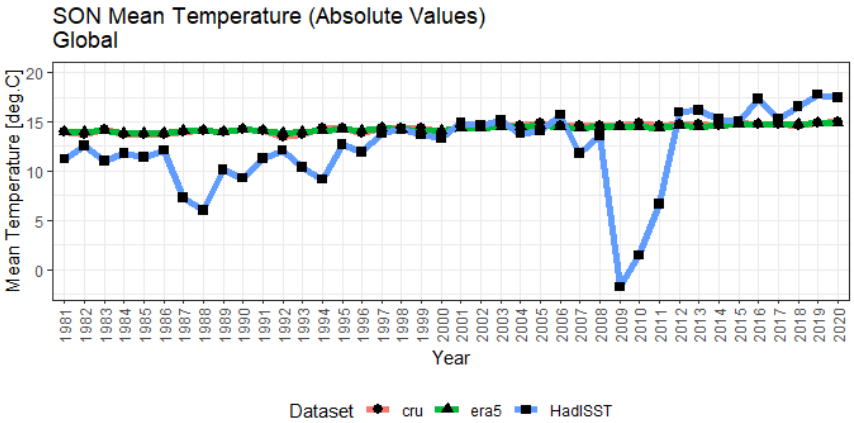

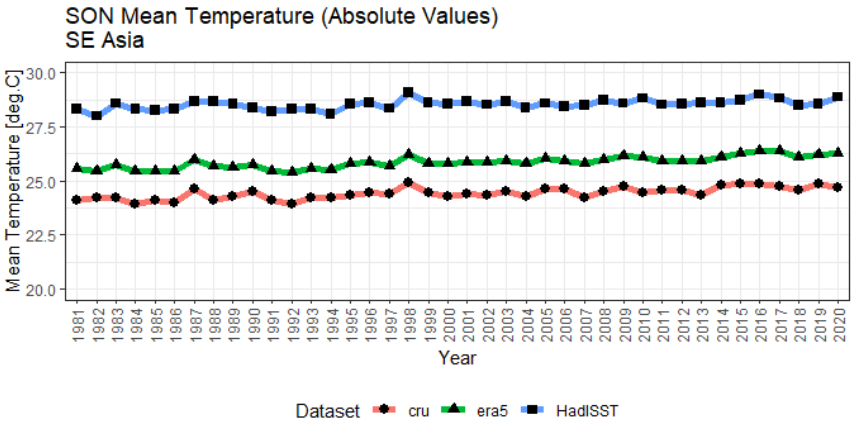

PRECIPITATION

Max. Global Mean (CRU): 215.676 (mm/quarter) in 2010; Max. SEA Mean (CRU): 638.781 (mm/quarter) in 2016
Min. Global Mean (CRU): 185.718 (mm/quarter) in 1991; Min. SEA Mean (CRU): 424.791 (mm/quarter) in 1994
Max. Global Mean (ERA5): 272.394 (mm/quarter) in 2017; Max. SEA Mean (ERA5): 741.867 (mm/quarter) in 2010
Min. Global Mean (ERA5): 254.874 (mm/ quarter) in 1991; Min. SEA Mean (ERA5): 395.616 (mm/quarter) in 1997
Max. Global Mean (GPCP): 255.066 (mm/ quarter) in 1987; Max. SEA Mean (GPCP): 683.304 (mm/ quarter) in 2010
Min. Global Mean (GPCP): 243.18 (mm/ quarter) in 1994; Min. SEA Mean (GPCP): 336.582 (mm/ quarter) in 1997

TEMPERATURE/ SST

Max. Global Mean (CRU): 15 (^{0}C) in 2020; Max. SEA Mean (CRU): 24.9 (^{0}C) in 1998
Min. Global Mean (CRU): 13.521 (^{0}C) in 1992; Min. SEA Mean (CRU): 23.917 (^{0}C) in 1984
Max. Global Mean (ERA5): 14.87 (^{0}C) in 2020; Max. SEA Mean (ERA5): 26.364 (^{0}C) in 2016
Min. Global Mean (ERA5): 13.812 (^{0}C) in 1992; Min. SEA Mean (ERA5): 25.403 (^{0}C) in 1992
Max. Global Mean (HadISST): 17.767 (^{0}C) in 2019; Max. SEA Mean (HadISST): 29.069 (^{0}C) in 1998
Min. Global Mean (HadISST): -1.786 (^{0}C) in 2009; Min. SEA Mean (HadISST): 27.984 (^{0}C) in 1982

Figure 16. Yearly SON Precipitation and Temperature Absolute Values (Global & SE Asia)

Table 14. Percentile of SON 2013 Precipitation Anomalies [SE Asia]

Dataset	Precipitation
CRU	> Fn1.A(df1.1$Precip.Anomaly[1:40][df1.1$Year[1:40]==2013]) [1] 0.675 > summary(Fn1.A) Empirical CDF: 40 unique values with summary Min. 1st Qu. Median Mean 3rd Qu. Max. -111.853 -46.492 17.002 3.117 51.800 102.137 Rank: 14
ERA5	> Fn2.A<-ecdf(df1.1$Precip.Anomaly[41:80]) > Fn2.A(df1.1$Precip.Anomaly[41:80][df1.1$Year[41:80]==2013]) [1] 0.575 > summary(Fn2.A) Empirical CDF: 40 unique values with summary Min. 1st Qu. Median Mean 3rd Qu. Max. -192.8290 -49.6178 6.5840 0.3222 66.5757 153.4200 Rank: 18
GPCP	> Fn3.A<-ecdf(df1.1$Precip.Anomaly[81:120]) > Fn3.A(df1.1$Precip.Anomaly[81:120][df1.1$Year[81:120]==2013]) [1] 0.575 > summary(Fn3.A) Empirical CDF: 40 unique values with summary Min. 1st Qu. Median Mean 3rd Qu. Max. -219.399 -60.210 14.221 -1.987 73.050 127.323 Rank: 18

Table 15. Percentile of SON 2013 Temperature Anomalies [SE Asia]

Dataset	Temperature
CRU	> Fn1.B<-ecdf(df1.1$Temp.Anomaly[1:40]) > Fn1.B(df1.1$Temp.Anomaly[1:40][df1.1$Year[1:40]==2013]) [1] 0.4 > summary(Fn1.B) Empirical CDF: 39 unique values with summary Min. 1st Qu. Median Mean 3rd Qu. Max. -0.4240 -0.1010 0.0660 0.0760 0.2455 0.5590 Rank: 24
ERA5	> Fn2.B<-ecdf(df1.1$Temp.Anomaly[41:80]) > Fn2.B(df1.1$Temp.Anomaly[41:80][df1.1$Year[41:80]==2013]) [1] 0.575 > summary(Fn2.B) Empirical CDF: 39 unique values with summary Min. 1st Qu. Median Mean 3rd Qu. Max. -0.34900 -0.09750 0.09400 0.09985 0.29300 0.61200 Rank: 18
HadISST	> Fn3.B<-ecdf(df1.1$SST.Anomaly[1:40]) > Fn3.B(df1.1$SST.Anomaly[1:40][df1.1$Year[1:40]==2013]) [1] 0.65 > summary(Fn3.B) Empirical CDF: 39 unique values with summary Min. 1st Qu. Median Mean 3rd Qu. Max. -0.49700 -0.11700 0.07300 0.05228 0.17500 0.58700 Rank: 15

As shown, CRU is the highest among the three precipitation datasets – with the SON 2013 on the 67.5th percentile and ranking 14th out of 40 years, while HadISST is the highest for the temperature datasets, with SON 2013 on the 65th percentile and ranking 15th among all years. Compared to Y2013, the SON 2013 anomalies are not as high, with just above the average precipitation and temperature anomalies, in as far as all SON seasons from 1980 to 2020 are considered.

For spatial comparison, the maps of the 30-yr climatology, absolute and anomaly values for SON 2013 are depicted in ***ANNEX 4*** for both precipitation and temperature. Globally and in SE Asia, the temperature anomaly maps showed some blue spots although there is still prevalent red, demonstrating positive (hotter) anomalies. For precipitation, anomaly maps again show blue and red colors distributed at various locations. Statistically, the Empirical Cumulative Distribution Function (ECDF) plots for precipitation anomalies **[*Figure 17*]** and the count of positive or negative values in **Table 16** show that about 70% of the anomaly values are equal to or above 0 (positive) for CRU, while ERA5 and GPCP have about 60%. These values show that SON 2013 is just slightly wetter-than-average with respect to the baseline climatology, despite Haiyan's occurrence.

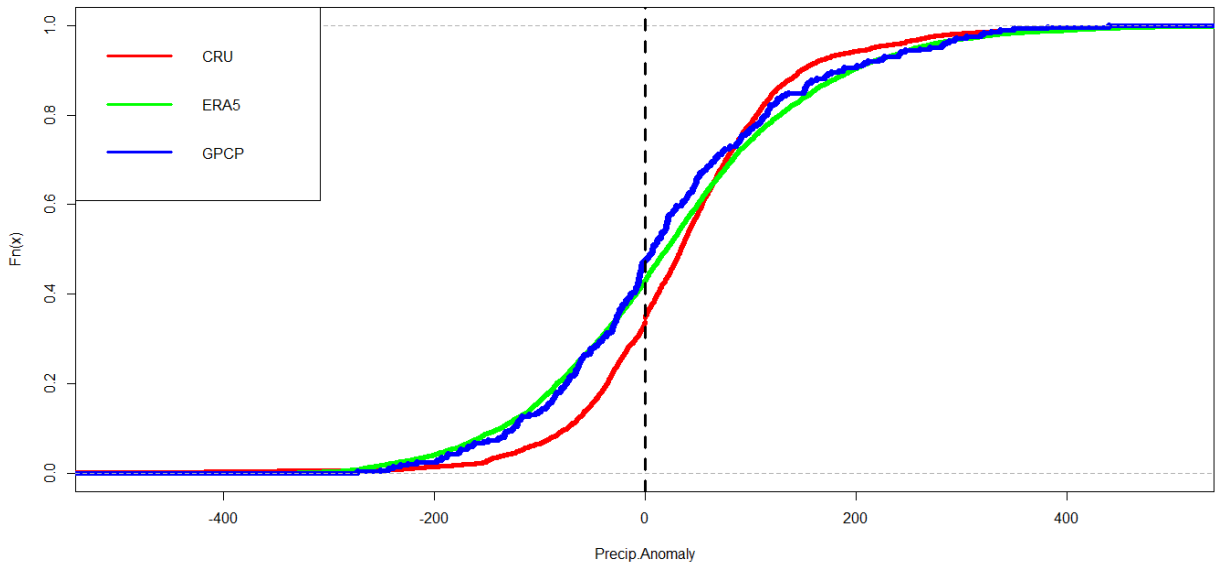

Figure 17. Empirical Cumulative Distribution Plots of SON 2013 Precipitation Anomalies [SE Asia]

With respect to the distribution of anomaly values, the skewness [*CRU = 0.082, ERA5 = 0.410, GPCP = 0.503*] indicates that all datasets are positively skewed or more concentrated to the left of the graph as shown in density plot in ***Figure 18*** -- with CRU having more symmetry as the

skewness is closer to zero. The kurtosis *[CRU = 7.797, ERA5 = 3.814, GPCP = 3.446]* also reveals that GPCP have a more normal distribution with kurtosis closer to 3 than CRU and ERA5. Among the three, CRU has sharp peaks on the graph.

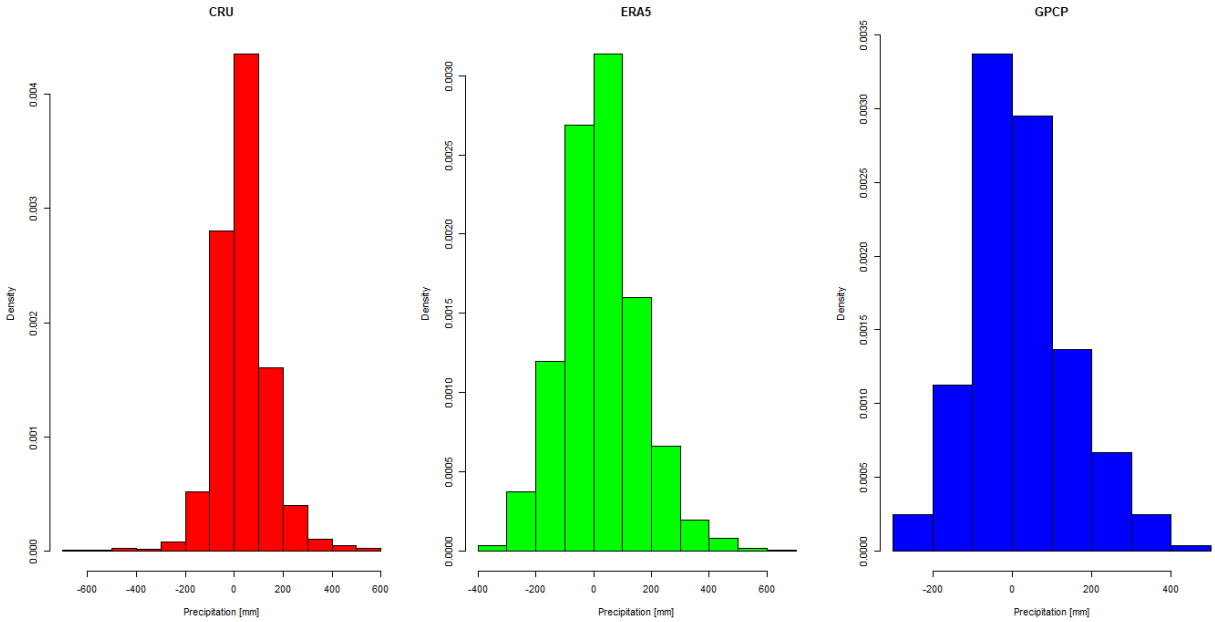

Figure 18. Probability Distribution Plots of SON 2013 Precipitation Anomalies for SE Asia

The ECDF plots in ***Figure 19*** are more apparent for temperature anomalies, showing a higher percentage of positive anomalies for both ERA5 and HadISST (about 80%), compared to CRU (about 50%). This is confirmed by the summary of counts in **Table 16.** As with precipitation, these values also show that SON 2013 is hotter-than-average, with respect to the baseline climatology, across all datasets.

With respect to the distribution of anomaly values, the skewness [*CRU = -0.664, ERA5 = 0.070, HadISST = -0.200*] indicates that CRU and HadISST are negatively skewed or more concentrated to the right of the graph, while ERA5 is positively skewed or more concentrated to the left as shown in the density plot in ***Figure 23***. ERA5 is more symmetric among the three having skewness closer to zero. The kurtosis *[CRU = 3.240, ERA5 = 4.178, HadISST = 3.882]* also reveals that CRU value have a more normal distribution being closer to 3 than ERA5 and HadISST, with ERA5 and HadISST having more sharp peaks on the graph.

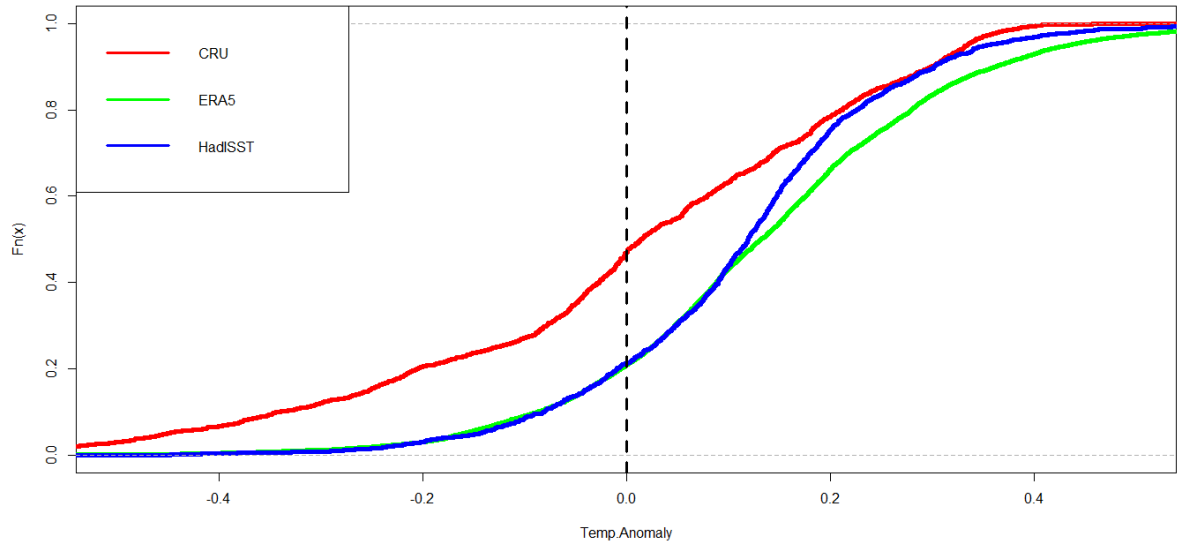

Figure 19. Empirical Cumulative Distribution Plots of SON 2013 Temperature Anomalies [SE Asia]

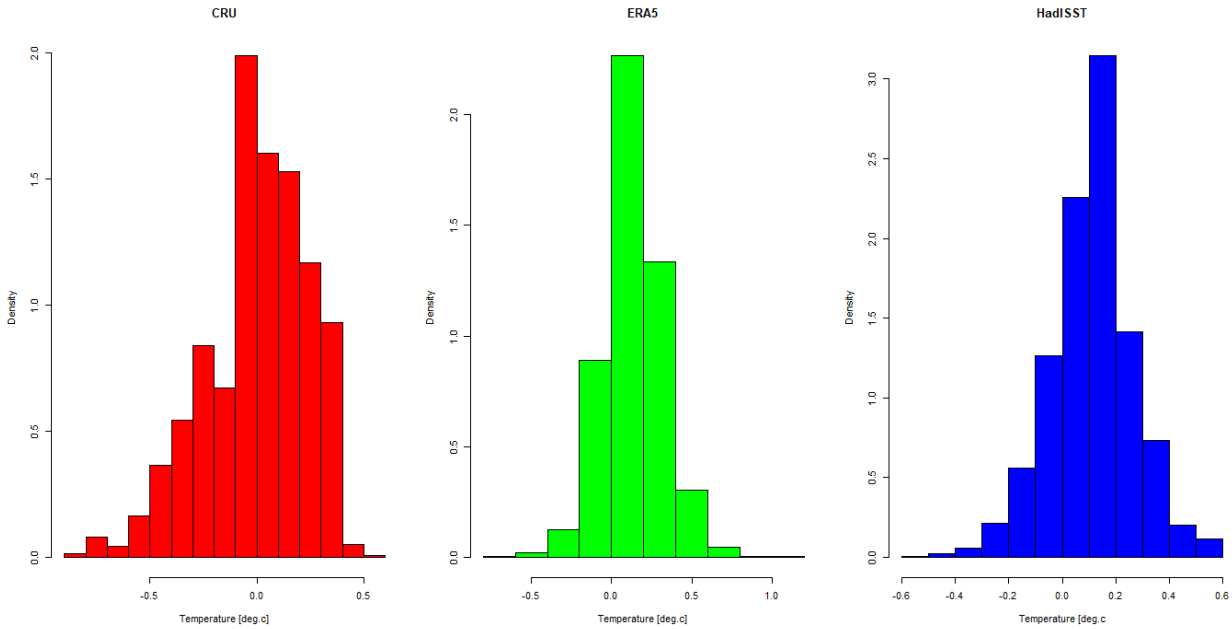

Figure 20. Probability Distribution Plots of SON 2013 Temperature Anomalies for SE Asia

Table 16. Count of Negative vs. Zero/Positive SON 2013 Precipitation and Temperature Anomalies

	PRECIPITATION	TEMPERATURE
CRU	> pos_cru<-prcp_SON_cru_2013$anomaly >=0 > table(pos_cru) pos_cru FALSE TRUE 906 1777 > table(pos_cru)[2]/(table(pos_cru)[2]+table(pos_cru)[1]) TRUE	> pos_cru<-tmp_SON_cru_2013$anomaly>=0 > table(pos_cru) pos_cru FALSE TRUE 1255 1428 > table(pos_cru)[2]/(table(pos_cru)[2]+table(pos_cru)[1]) TRUE

	0.6623183	0.53224

ERA5	`> pos_era5<-prcp_SON_era5_2013$anomaly>=0`
	`> table(pos_era5)`
	`pos_era5`
	`FALSE TRUE`
	`3328 4414`
	
	`> table(pos_era5)[2]/(table(pos_era5)[2]+table(pos_era5)[1])`
	`TRUE`
	`0.5701369`
		`> pos_era5<-tmp_SON_era5_2013$anomaly>=0`
		`> table(pos_era5)`
		`pos_era5`
		`FALSE TRUE`
		`1612 6130`
		
		`> table(pos_era5)[2]/(table(pos_era5)[2]+table(pos_era5)[1])`
		`TRUE`
		`0.7917851`

GPCP | HadISST	`> pos_gpcp<-prcp_SON_gpcp_2013$anomaly>=0`
	`> table(pos_gpcp)`
	`pos_gpcp`
	`FALSE TRUE`
	`135 150`
	
	`> table(pos_gpcp)[2]/(table(pos_gpcp)[2]+table(pos_gpcp)[1])`
	`TRUE`
	`0.5263158`
		`> pos_HadISST<-tmp_SON_HadISST_2013$anomaly>=0`
		`> table(pos_HadISST)`
		`pos_HadISST`
		`FALSE TRUE`
		`328 1211`
		
		`> table(pos_HadISST)[2]/(table(pos_HadISST)[2]+table(pos_HadISST)[1])`
		`TRUE`
		`0.7868746`

The 5-95 percentiles of the anomaly values for all the grid points were also calculated to show the anomalies for SON 2013 that are beyond the threshold. Shown in ***Figures 21 & 22*** are the points with anomaly values exceeding the local 5 (red or dry) and 95 (blue or wet) range for precipitation, and the reverse with points below 5 marked with blue (or cold) and above 95 marked with red (or hot) for temperature anomalies. As with the annual analysis, there are clear differences across the maps, again demonstrating the general inconsistency among the datasets regarding the amplitude and locations of the anomalies throughout the entire SE Asian region. Inconsistencies are both apparent for precipitation and temperature.

Further comparing the anomaly values among the datasets, the summary of the t-test results in **Table 17** shows that CRU vs. ERA5 and CRU vs. GPCP are significantly different in terms of precipitation. CRU vs. ERA5 have relatively low p-value, while CRU vs. GPCP has a p-value just a little lower than 0.05. ERA5 and GPCP on the other hand did not show significant difference between them. Basing on the highest t-value, the strongest evidence of difference is between CRU & ERA5 for precipitation. With respect to temperature anomalies, CRU & ERA5 are significantly different with a relatively low p-value. HadISST is excluded from the t-test.

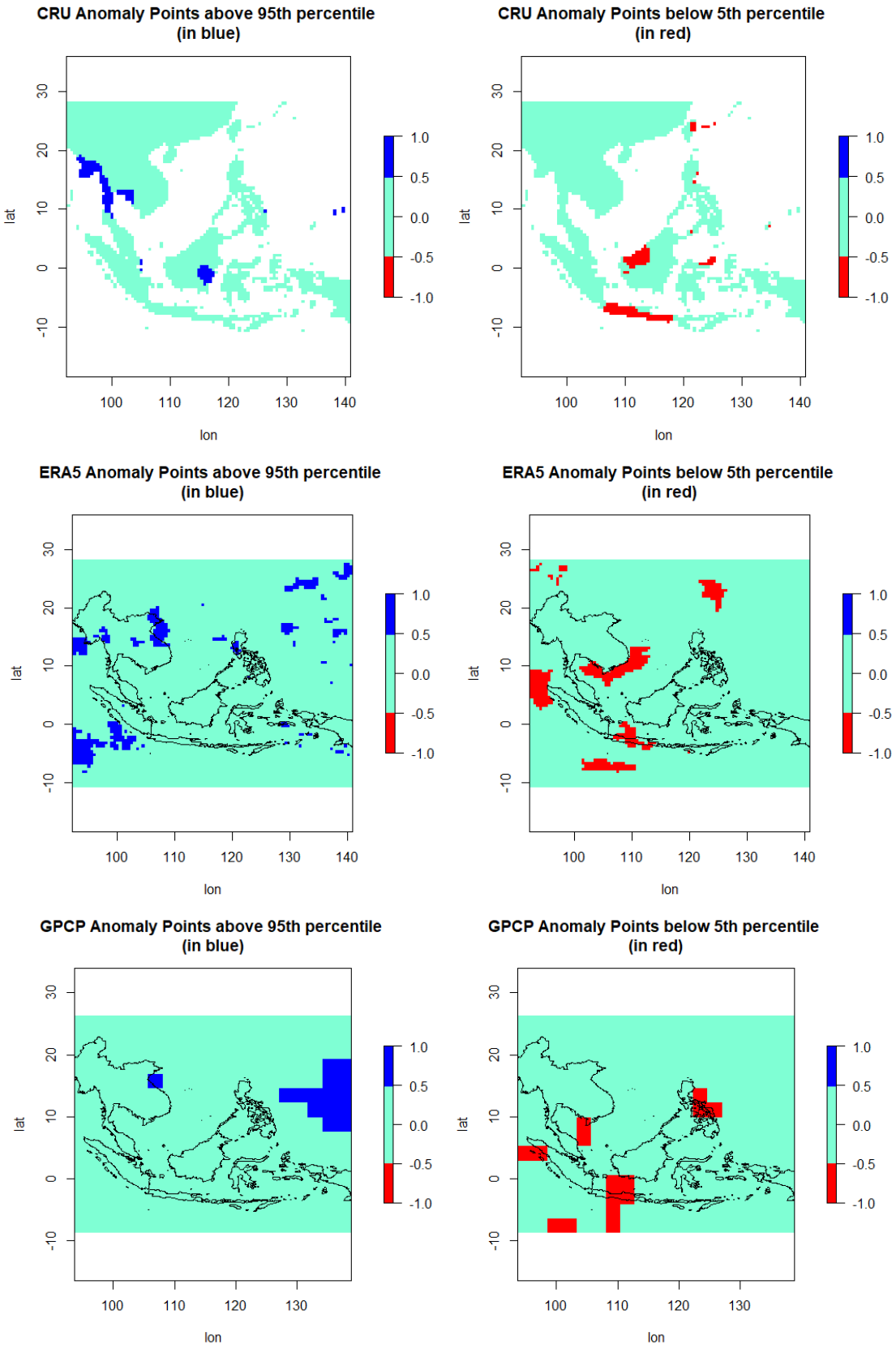

Figure 21. Maps Showing Anomaly Points Beyond 5-95 Percentile for SON 2013 Precipitation [SE Asia]

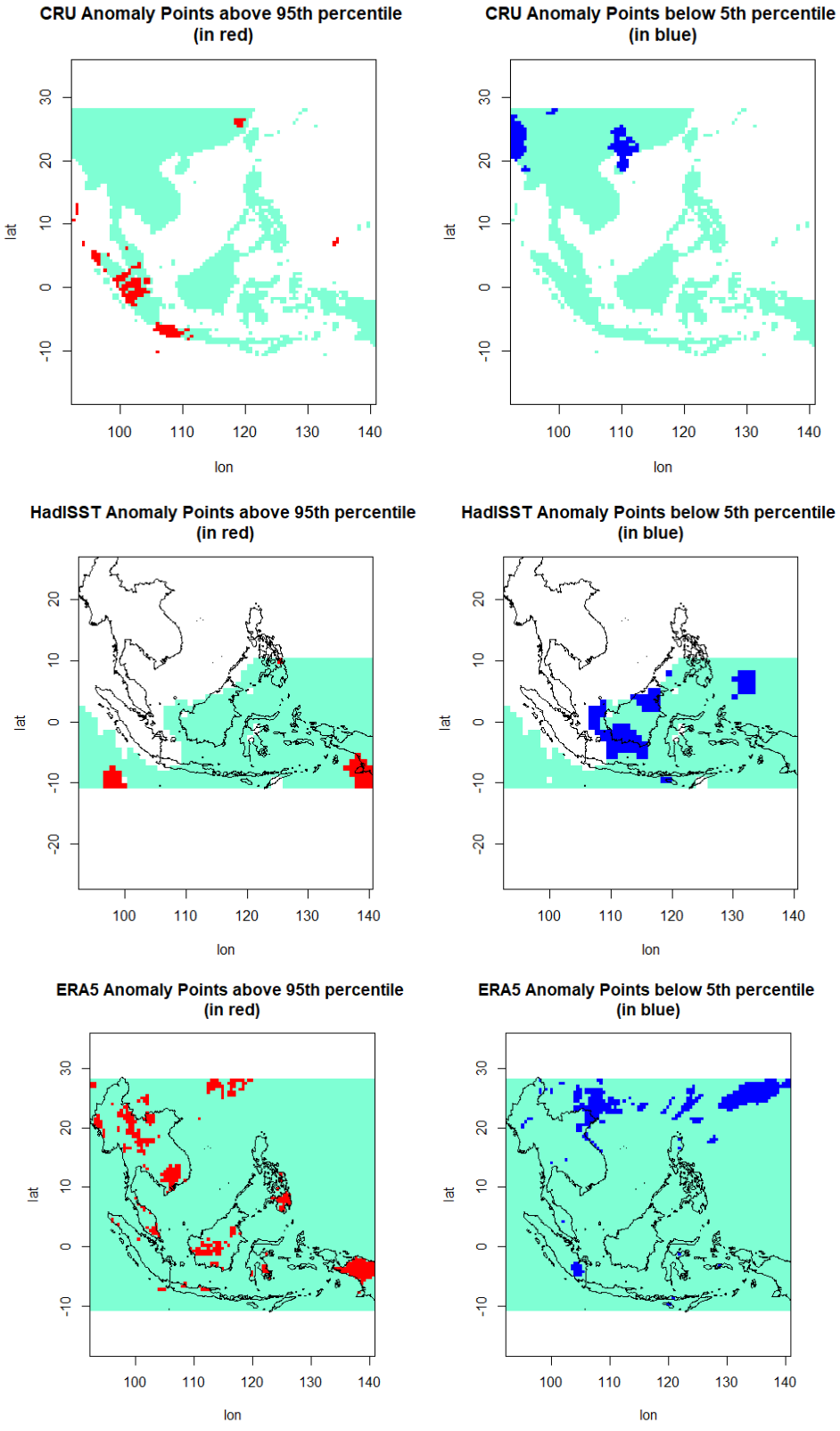

Figure 22. Maps Showing Anomaly Points Beyond 5-95 Percentile for SON 2013 Temperature [SE Asia]

Table 17. Results of Welch Two-Sample t-test for SON 2013 Precipitation and Temperature Anomalies

	PRECIPITATION	TEMPERATURE
CRU vs. ERA5	data: prcp_SON_cru_2013$anomaly and prcp_SON_era5_2013$anomaly t = 4.2247, df = 5799.4, p-value = 2.429e-05 alternative hypothesis: true difference in means is not equal to 0 95 percent confidence interval: 5.854015 15.990371 sample estimates: mean of x mean of y 36.71606 25.79387	data: tmp_SON_cru_2013$anomaly and tmp_SON_era5_2013$anomaly t = -26.714, df = 3852.3, p-value < 2.2e-16 alternative hypothesis: true difference in means is not equal to 0 95 percent confidence interval: -0.1445941 -0.1248210 sample estimates: mean of x mean of y 0.0004153987 0.1351229766
CRU vs. GPCP	data: prcp_SON_cru_2013$anomaly and prcp_SON_gpcp_2013$anomaly t = 1.9872, df = 330.79, p-value = 0.04773 alternative hypothesis: true difference in means is not equal to 0 95 percent confidence interval: 0.1532826 30.2989706 sample estimates: mean of x mean of y 36.71606 21.48994	N/A
ERA5 vs. GPCP	data: prcp_SON_era5_2013$anomaly and prcp_SON_gpcp_2013$anomaly t = 0.57139, df = 309.11, p-value = 0.5681 alternative hypothesis: true difference in means is not equal to 0 95 percent confidence interval: -10.51721 19.12508 sample estimates: mean of x mean of y 25.79387 21.48994	N/A

The yearly SON precipitation, temperature and SST anomalies are then plotted to inspect the maximum and minimum years for each variable. As shown in ***Figure 23,*** ERA5 and GPCP share common maximum (2010) and minimum (1997) years for precipitation anomalies. On temperature, no common maximum or minimum year is observed for all datasets. Notable from this plot however is the year 1997 which registered the maximum for both Nino 3.4 and CRU temperature anomalies. Contrastingly, 1997 is the minimum year for precipitation anomaly in ERA5 and GPCP. This year was also the minimum year recorded for GPCP and ERA5 in terms of annual mean.

Figure 24 to 26 presents the plots of the linear regression between Precipitation, Temperature, HadISST and Nino 3.4 SST anomalies, for the yearly SON season, among all datasets. For CRU, regressions for precipitation vs. HadISST, precipitation vs. Nino 3.4 SST, temperature vs. HadISST,

and temperature vs. Nino 3.4 SST all resulted to a significant p-value, with both precipitation and temperature being positively correlated with HadISST, and precipitation and temperature and being negatively correlated to Nino 3.4. For ERA5, the regression of precipitation against temperature, HadISST, and Nino 3.4 all resulted to significant p-values, with precipitation positively correlated with temperature and HadISST and negatively correlated with Nino 3.4. ERA5 temperature likewise resulted to a significant p-value when regressed with HadISST, and both variables are positively correlated. GPCP on the other hand, showed a positive correlation with HadISST and Nino3.4 SST, all with significant p-values. Lastly, HadISST also resulted in a significant p-value with negative correlation to Nino 3.4. These relationships are likewise reflected in the scatterplots in ***Figure 27*** where the red, green or blue circles incline toward the left if negatively correlated and toward the right if positively correlated. The rest of the correlations without a corresponding significant p-value (i.e., CRU precipitation vs. temperature, CRU temperature vs. Nino 3.4 and ERA5 temperature vs. Nino 3.4) otherwise show that the circles are more distributed across different parts of the plot, than displaying an inclining left or right pattern. Although the values are more or less evenly spread and clustered as shown in the density plot and boxplot in ***Figures 27 and 28,*** there are outliers for CRU and ERA5 temperature as well as HadISST which may have partly affected the regression analysis. Nevertheless, almost all the regressions still produced significant p-values.

Focusing on the seasonal changes in SE Asia for the whole Y2013, the absolute precipitation and temperature values are plotted in ***Figure 29.*** All three datasets have the same maximum season (JJA), while ERA5 and GPCP share a common minimum season (MAM) for precipitation. For temperature, all datasets have the same maximum (JJA) and minimum (DJF) seasons.

The seasonal anomalies for Y2013 are then computed using the baseline reference and are plotted in ***Figure 30***. To check if the highest or lowest anomaly season for precipitation and temperature also corresponds to the highest or lowest SST anomaly for ENSO, the Nino3.4 seasonal SSTs are likewise presented in the same plot. As seen, ERA5 and GPCP share common maximum (JJA) and minimum (SON) seasons for precipitation anomalies. For temperature, CRU and ERA5 have a common maximum season (DJF), while all CRU, ERA5 and HadISST have the same minimum season (SON). The Nino3.4 SST anomaly on the other hand has the same maximum season (SON) as the CRU precipitation anomaly, among others. From these observations, the precipitation and temperature for the SON season of the Y2013 is comparatively low than the rest of the seasons despite Haiyan occurring in November of this year. It is also noteworthy that September belongs to

the Southwest monsoon season when it is expected that large volume of rain goes to the mainland, however, only CRU registered SON as the maximum precipitation season among the datasets. It is also notable that the Nino 3.4 SST anomaly is highest for this season. When ENSO is supposed to peak on DJF, for the Y2013, it showed otherwise. This can be a manifestation that ENSO may have a background effect on the changes of the precipitation and temperature variables. The interpretation of this observation, however, is not delved further and is beyond the scope of this thesis paper.

Discussion

Relating the results to literature information, papers by Diffenbaugh & Scherer (2011), Hawkins & Sutton (2012), Lehner, Deser, & Sanderson (2018), and Herring et al. (2015) found that there are significant temporal shifts in warmer temperatures in the summer season, particularly at lower latitudes, with one study [e.g., Mahlstein, Hegerl, & Solomon, 2012] indicating that Mainland SE Asia has likely experienced distinctly higher peak seasonal surface air temperature (SAT) since the year 2000 due to global warming. These observations coincide with the plots for seasonal absolute values in Y2013 where the maximum temperatures are in the JJA (summer) season. Correspondingly, the JJA season also registered the highest precipitation, although for SE Asia the JJA months belong to the northeast monsoon season, where bulk of the rain is in the mainland. The effect of monsoons on precipitation in SE Asia will be discussed further in the section for monthly analysis.

It is also interesting to link the result of this analysis to the study by Wang, Luo & Liu (2020) *[as previously cited in the preceding Section],* where the relationship of DJF ENSO anomaly and precipitation reverses from SO-ND (meaning a shift to a positive relationship from the persistent negative correlation for ten months) over a large region of Asia except for SE Asia. In the plot of seasonal anomalies for Y2013, DJF is the minimum season for Nino3.4 while SON is the minimum season for precipitation (although with ERA5 and GPCP only). This indicates that there is a positive relationship with ENSO DJF and precipitation SON, contrary to what the paper found where SE Asia is exempted from this shift. Only with the CRU dataset that the opposite is noted – wherein SON is the maximum season, thereby showing that ENSO DJF and SON precipitation for this dataset are negatively related.

Checking maps produced by other institutions, a global map by NCEI NOAA[42] shows that the 2013 SON in Alaska is the third wettest SON since 1918 records, while Australia experienced the warmest period on record for SON 2013 *[please refer to **ANNEX 2** to view the full map].* This is likewise shown in the blue-dominated (wetter or positive anomaly) for Alaska and the red-dominated (hotter or positive anomaly) for Australia in the precipitation and temperature anomaly maps generated for this study. Russia also observed the warmest November record in Y2013, thereby showing a dark-red color for this area.

On the difference of colors displayed between the ERA5 and GPCP precipitation anomaly maps despite having relatively similar percentage of positive anomaly values, this may be due to ERA5 having a finer resolution (more grid points) than GPCP.

[42] Sourced from: https://www.ncei.noaa.gov/access/monitoring/monthly-report/service/global/extremes/201311.gif

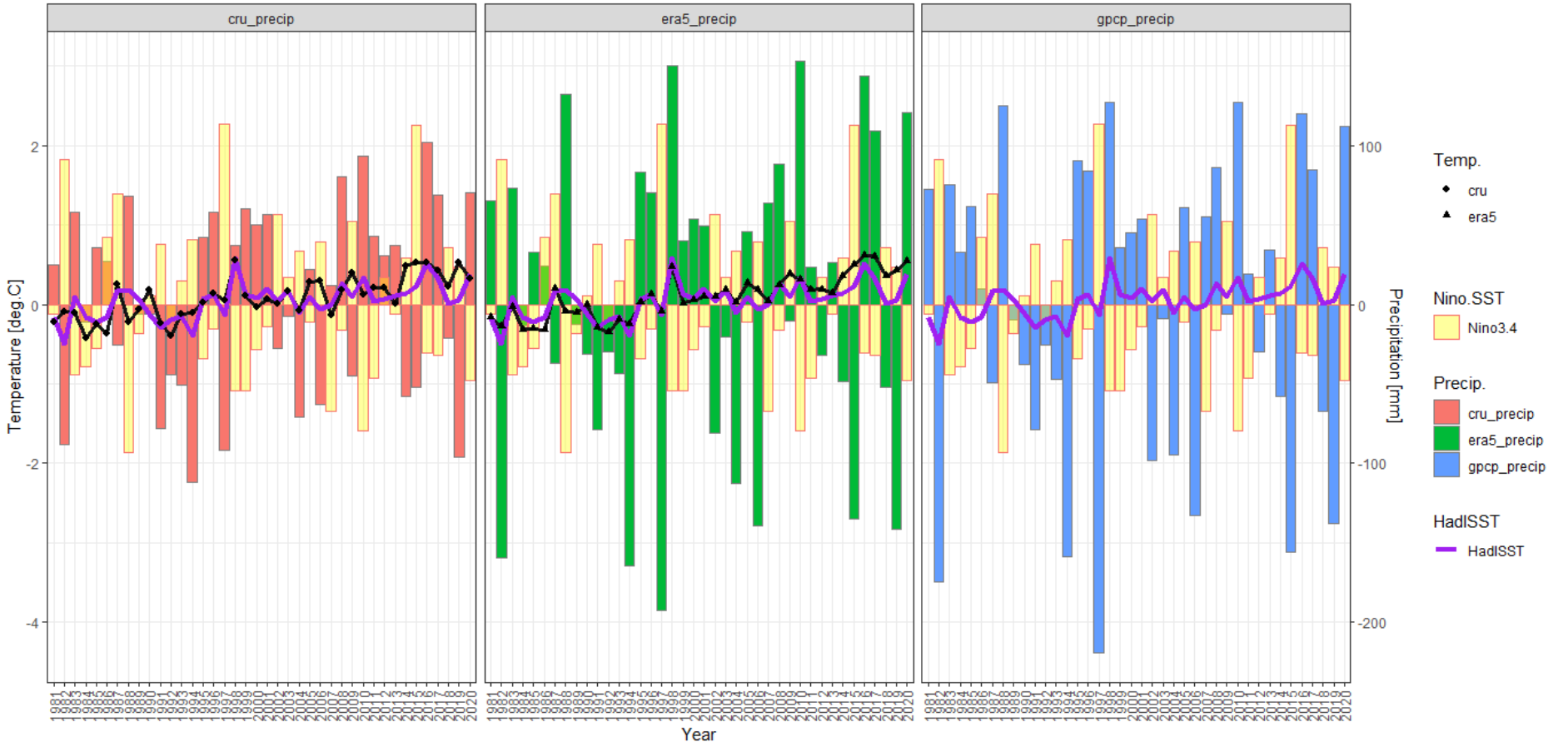

CRU

Max. **Precip.** Anomaly: 102.137 (mm) in 2016
Min. **Precip.** Anomaly: -111.853 (mm) in 1994
Max. **Temp.** Anomaly: 0.559 (^{0}C) in 1997
Min. **Temp.** Anomaly: -0.424 (^{0}C) in 1984

ERA5

Max. **Precip**. Anomaly: 153.42 (mm) in 2010
Min. **Precip.** Anomaly: -192.829 (mm) in 1997
Max. **Temp**. Anomaly: 0.612 (^{0}C) in 2016
Min. **Temp.** Anomaly: -0.349 (^{0}C) in 1992

GPCP / HadISST

Max. **Precip.** Anomaly: 127.323 (mm) in 2010
Min. **Precip**. Anomaly: -219.399 (mm) in 1997
Max. **SST**. Anomaly: 0.587 (^{0}C) in 1998
Min. **SST.** Anomaly: -0.497 (^{0}C) in 1982

Nino 3.4

Max. **SST**. Anomaly: 2.27 (^{0}C) in 1997
Min. **SST.** Anomaly: -1.867 (^{0}C) in 1988

Figure 23. Yearly SON Precipitation and Temperature/SST Anomalies (SE Asia)

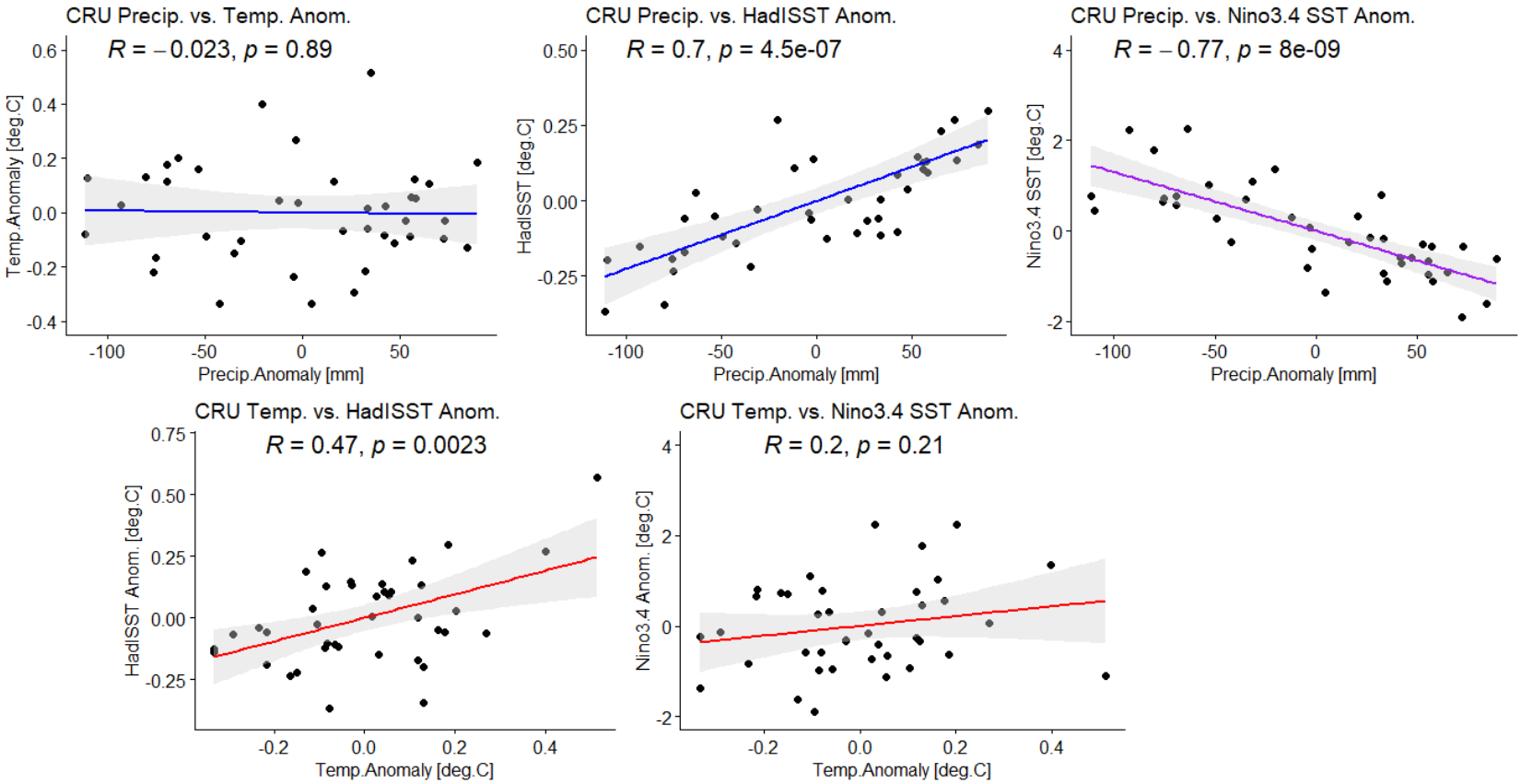

Figure 24. Linear Regression of CRU dataset for Yearly SON anomalies

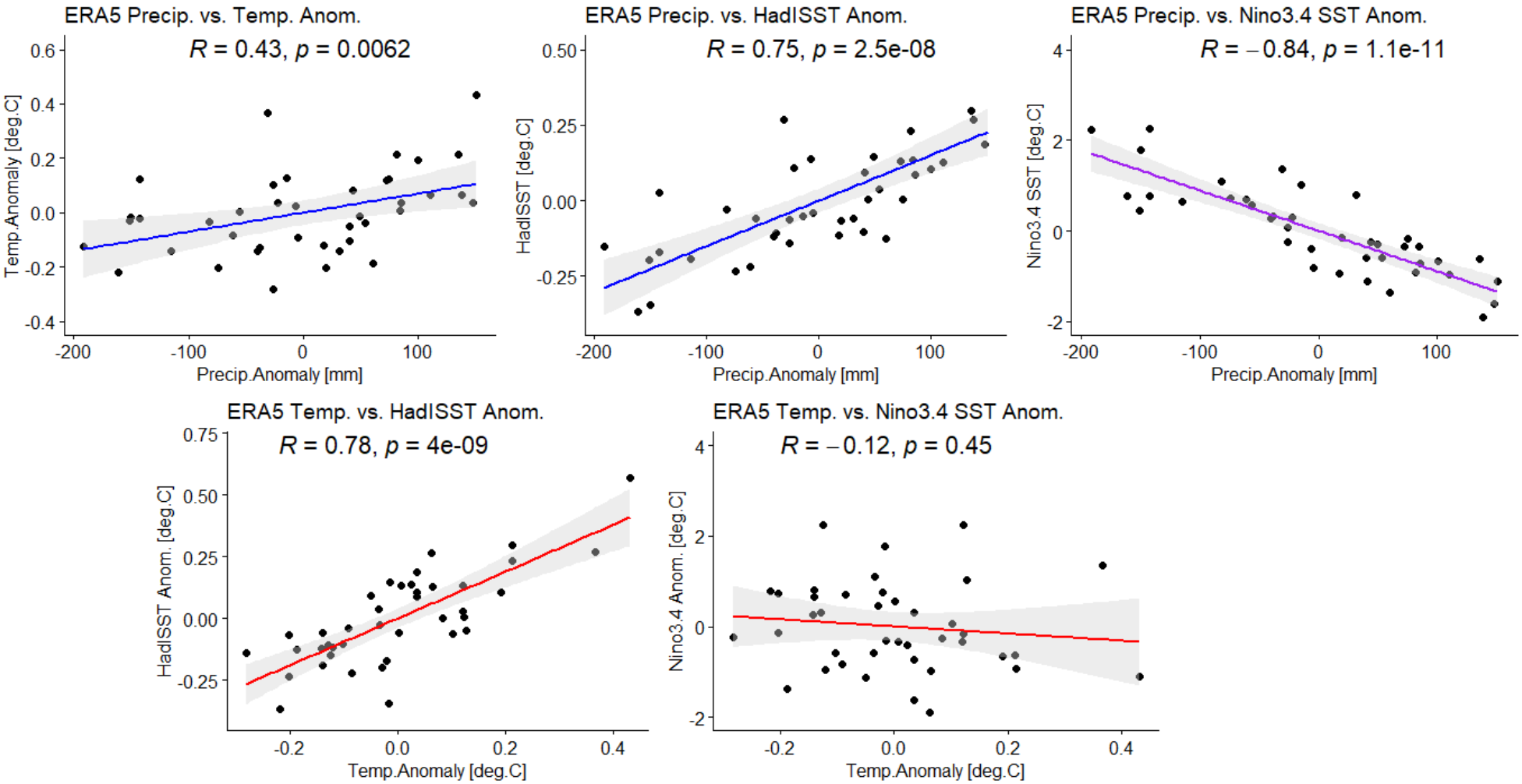

Figure 25. Linear Regression of ERA5 dataset for Yearly SON anomalies

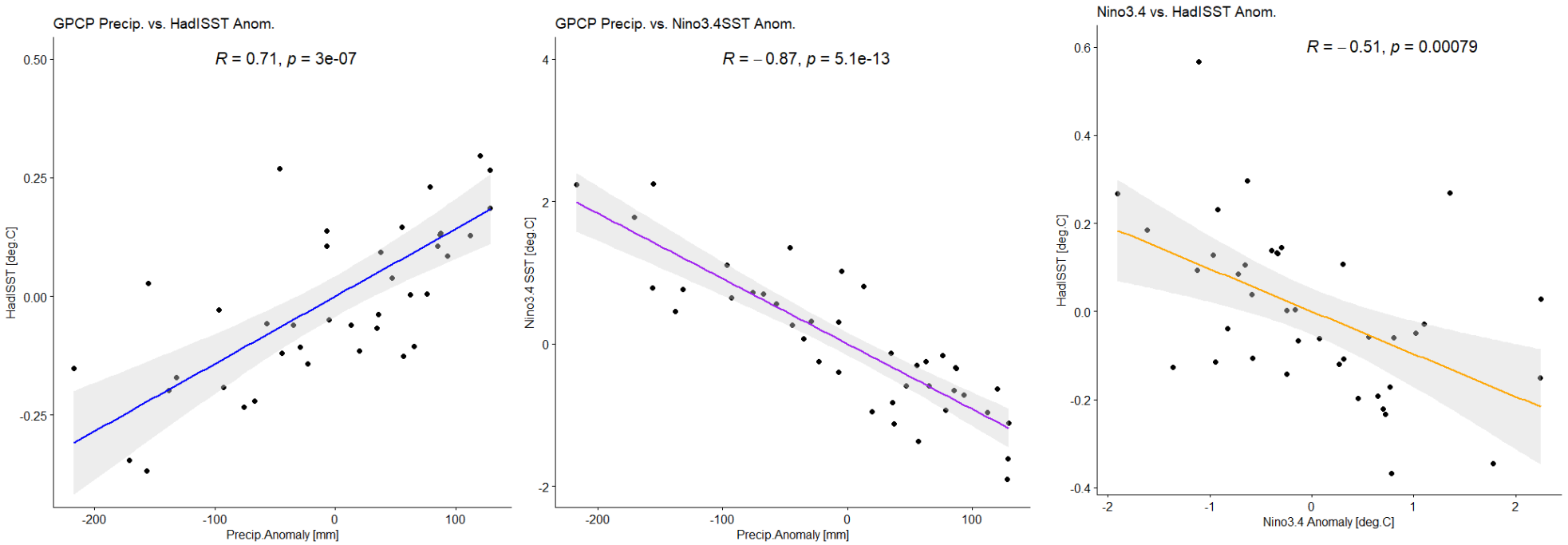

Figure 26. Linear Regression of GPCP and HadISST datasets for Yearly SON anomalies

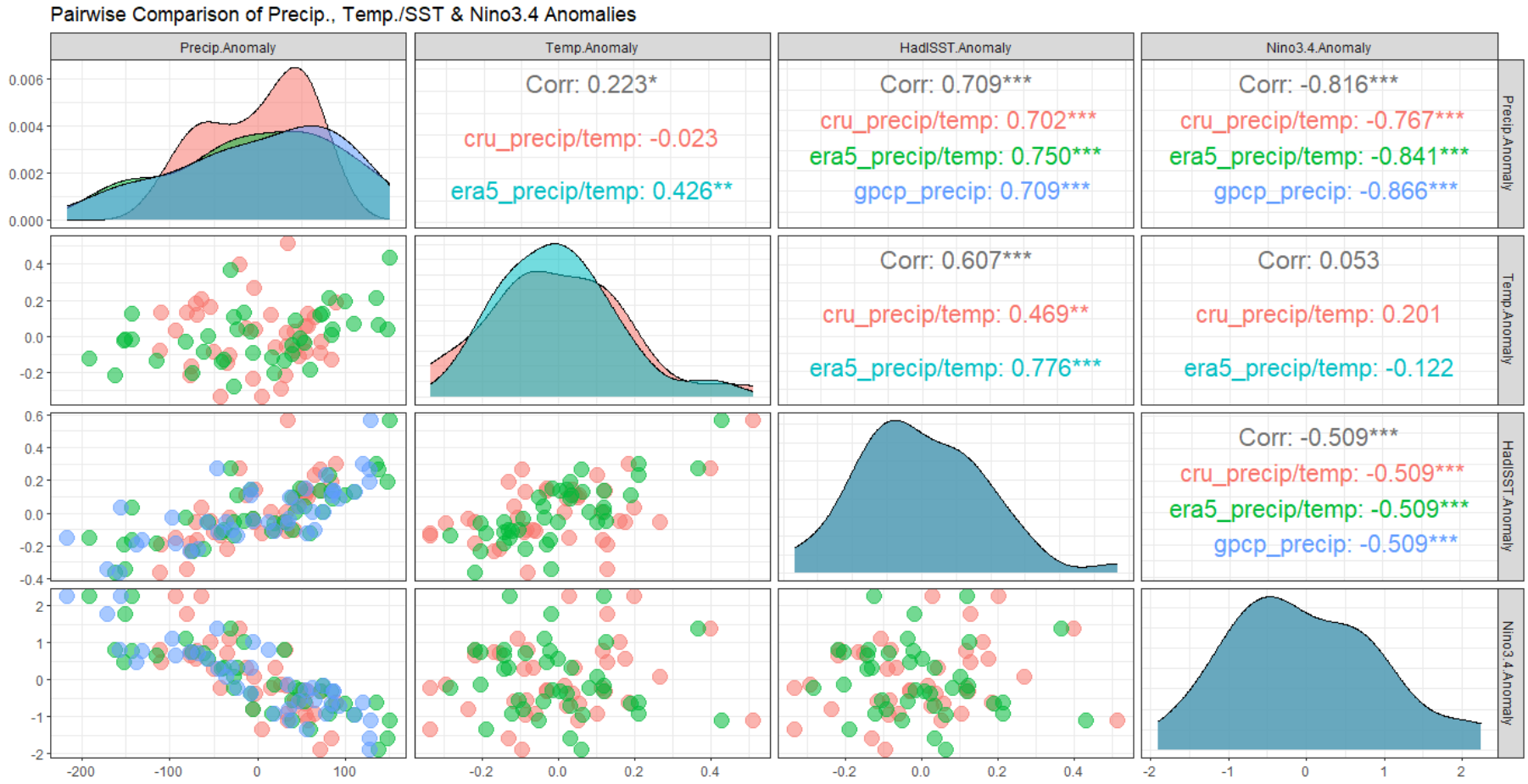

Figure 27. Scatterplots, Density Plots and Correlation Coefficients of Yearly SON Precip., Temp., HadISST and Nino3.4 Anomalies

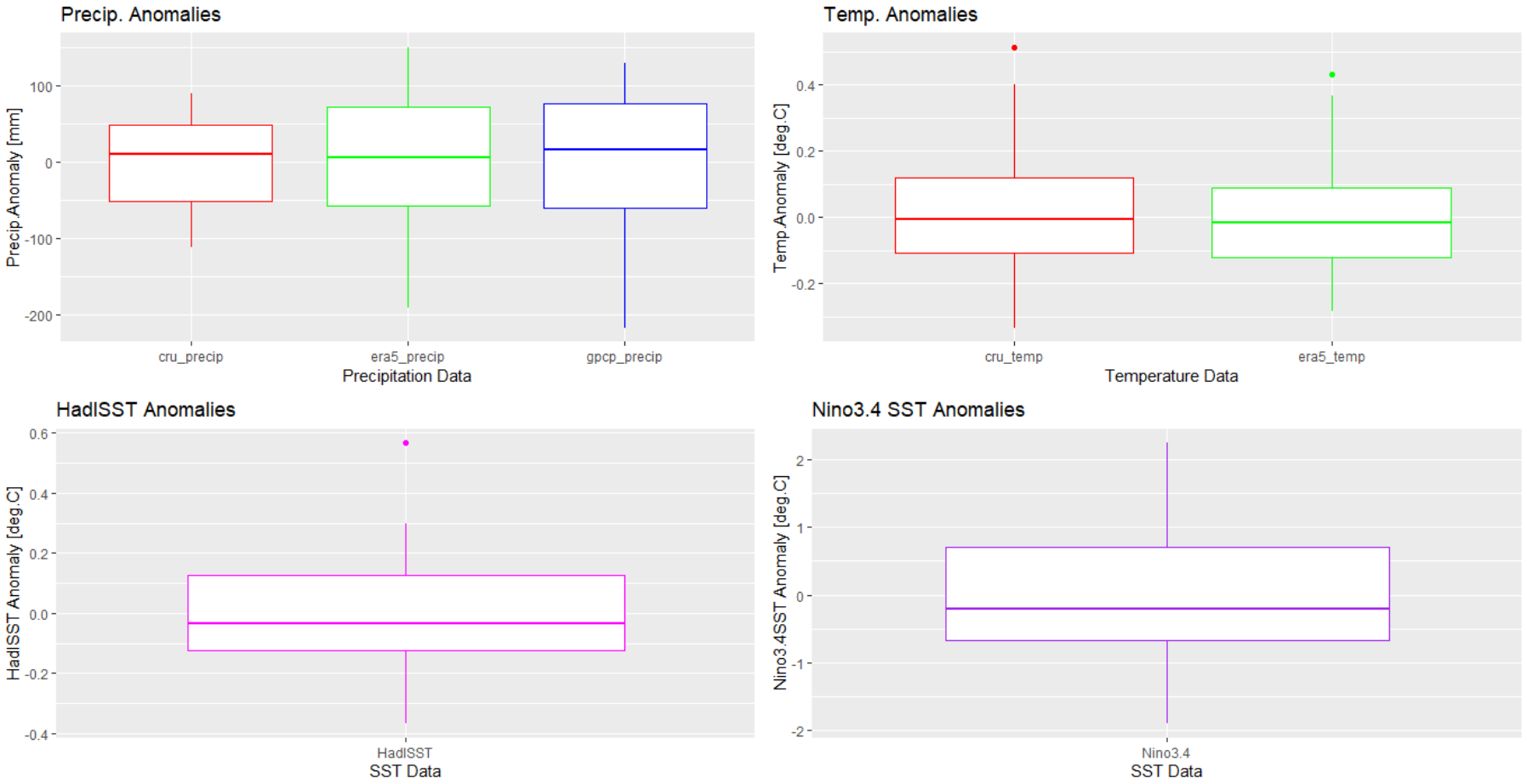

Figure 28. Boxplots of Yearly SON Precip., Temp./SST and Nino3.4 Anomalies

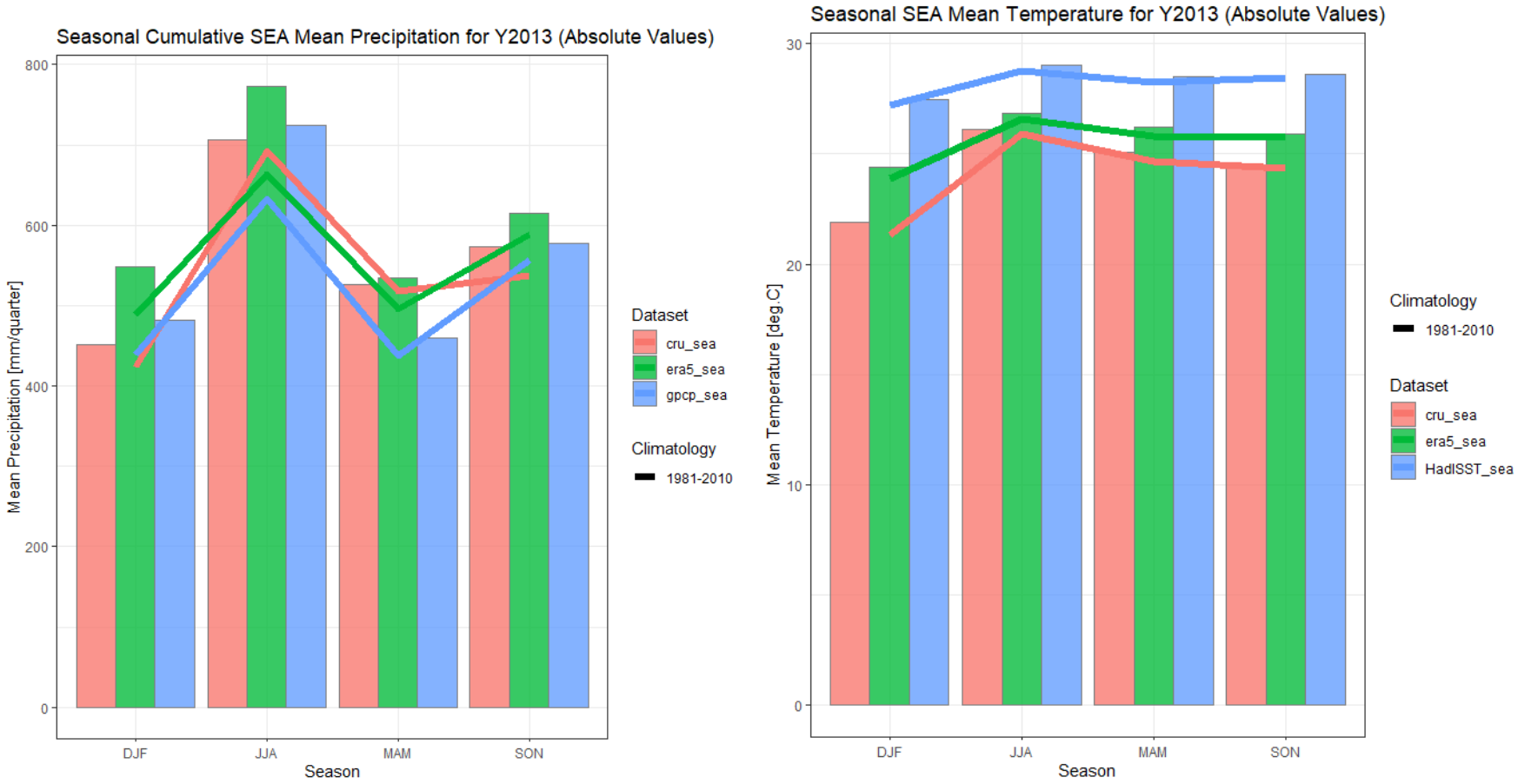

Max. SEA Mean **(CRU):** 706.3934 (mm/quarter) in Season JJA
Min. SEA Mean **(CRU):** 451.984 (mm/quarter) in Season DJF
Max. SEA Mean **(ERA5):** 772.336 (mm/quarter) in Season JJA
Min. SEA Mean **(ERA5):** 534.195 (mm/quarter) in Season MAM
Max. SEA Mean **(GPCP):** 724.807 (mm/quarter) in Season JJA
Min. SEA Mean **(GPCP):** 459.124 (mm/quarter) in Season MAM

Max. SEA Mean **(CRU):** 26.116 (^{0}C) in Season JJA
Min. SEA Mean **(CRU):** 21.879 (^{0}C) in Season DJF
Max. SEA Mean **(ERA5):** 26.825 (^{0}C) in Season JJA
Min. SEA Mean **(ERA5):** 24.384 (^{0}C) in Season DJF
Max. SEA Mean **(HadISST):** 29.016 (^{0}C) in Season JJA
Min. SEA Mean **(HadISST):** 27.469 (^{0}C) in Season DJF

Figure 29. Seasonal Precipitation and Temperature Values for Y2013 (SE Asia)

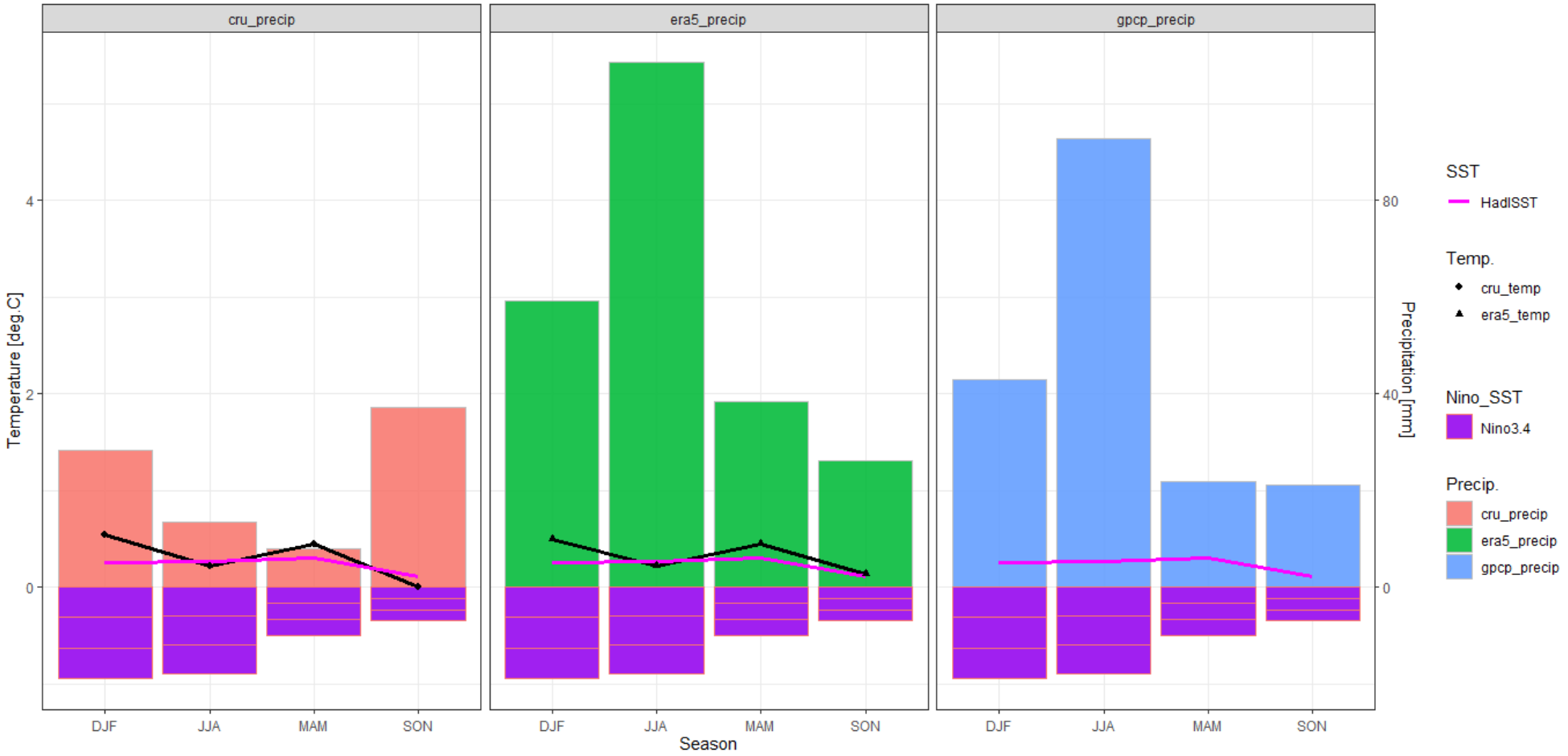

CRU
Max. **Precip.** Anomaly: 37.126 (mm) in Season SON
Min. **Precip.** Anomaly: 8.034 (mm) in Season MAM
Max. **Temp.** Anomaly: 0.544 (^{0}C) in Season DJF
Min. **Temp.** Anomaly: 0.006 (^{0}C) in Season SON

ERA5
Max. **Precip.** Anomaly: 108.419 (mm) in Season JJA
Min. **Precip.** Anomaly: 26.016 (mm) in Season SON
Max. **Temp.** Anomaly: 0.494 (^{0}C) in Season DJF
Min. **Temp.** Anomaly: 0.138 (^{0}C) in Season SON

GPCP / HadISST
Max. **Precip.** Anomaly: 92.672 (mm) in Season JJA
Min. **Precip.** Anomaly: 21.024 (mm) in Season SON
Max. **SST** Anomaly: 0.303 (^{0}C) in Season MAM
Min. **SST** Anomaly 0.114 (^{0}C) in Season SON

Nino 3.4 SST
Max. **SST** Anomaly: -0.117 (^{0}C) in Season SON
Min. **SST** Anomaly: -0.317 (^{0}C) in Season DJF

Figure 30. Y2013 Seasonal Anomalies for Precipitation and Temperature against Nino3.4 SST (SE Asia)

3.3 Monthly Analysis

Results

The yearly November absolute mean precipitation and temperature values are plotted in ***Figure 31***. In terms of maximum and minimum, CRU and ERA5 have a common global minimum year (1991) for precipitation, while CRU and ERA5 have a common global maximum year (2020) for temperature. In SE Asia, ERA5 and GPCP both have common maximum (1988) and minimum year (2006) years for precipitation. For temperature, CRU and ERA5 share a common maximum year (2016) and all three datasets have the same minimum year (1992). Again, the information provided according to the maxima/minima values present differences among the datasets, like the annual and seasonal analysis.

The absolute mean, baseline, and anomaly values of the SE Asian region for November 2013 are extracted for all the datasets, as summarized below.

Table 18. November 2013 Absolute Annual Mean, Baseline and Anomaly Values for Precipitation & Temperature [SE Asia]

Var.	CRU			ERA5			GPCP | HadISST		
	Absolute	*Baseline*	*Anomaly*	*Absolute*	*Baseline*	*Anomaly*	*Absolute*	*Baseline*	*Anomaly*
Precip.	172.753	156.188	**16.565**	**197.198**	**188.919**	8.279	173.089	169.585	3.5043
Temp.	23.230	23.039	**0.191**	25.256	25.116	0.140	**28.421**	**28.330**	0.091

NOTE: Precipitation units: ***mm;*** Temperature units: ^{0}C
For the third dataset/s, **GPCP** is used for precipitation while **HadISST** is used for SST analyses
Highest values among the datasets are emphasized in **boldface colored fonts**

As reflected above, CRU has the highest anomaly for both precipitation and temperature, different from what the annual and seasonal analysis observed when ERA5 was consistently highest in as far as annual and seasonal means are concerned. On the significance of November 2013 values compared to Novembers of other years, the percentiles are summarized in the following **Tables 19 and 20.**

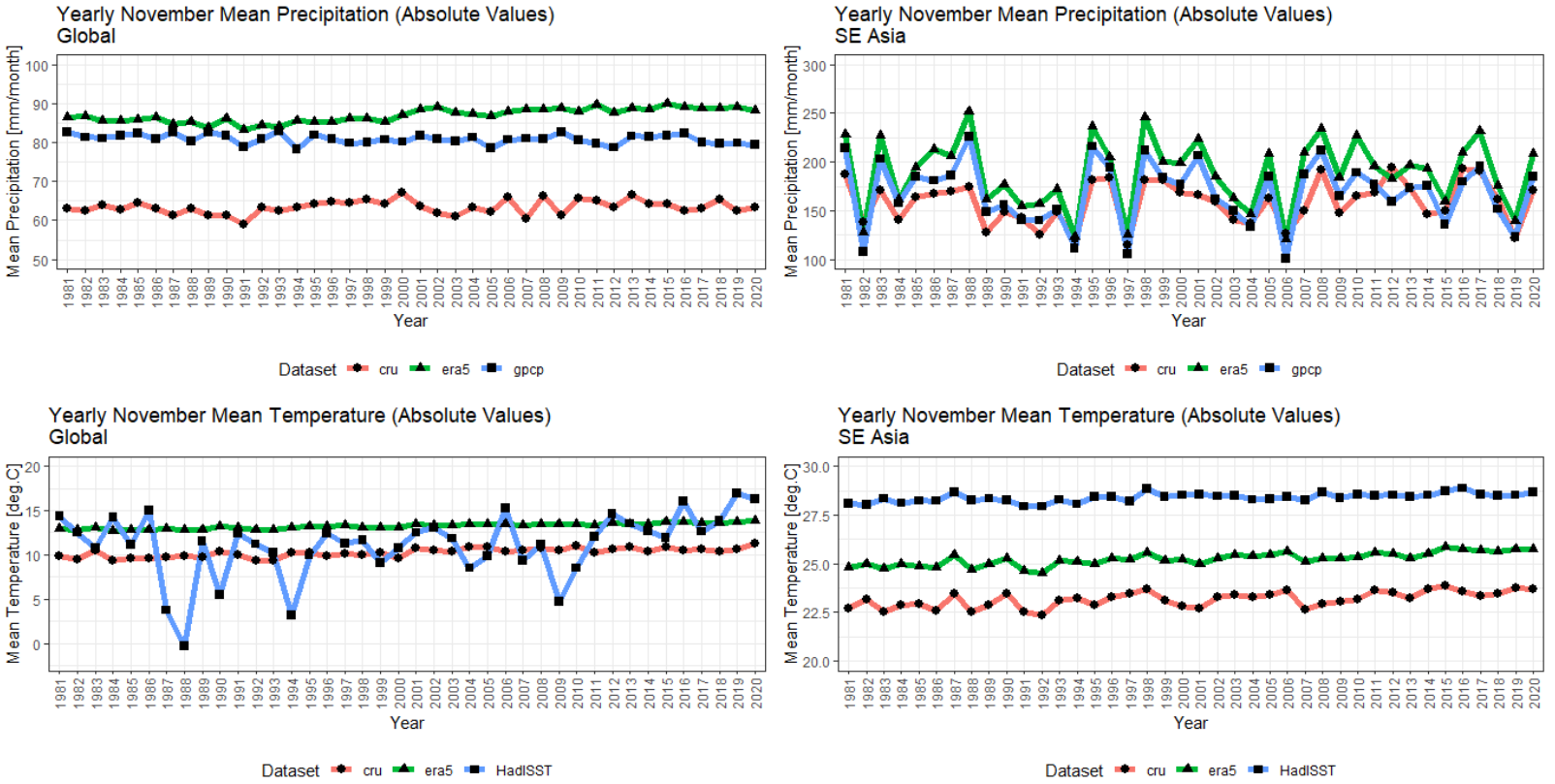

PRECIPITATION

Max. Global Mean (CRU): 67.212 (mm/month) in 2000; Max. SEA Mean (CRU): 194.508 (mm/month) in 2012
Min. Global Mean (CRU): 59.063 (mm/month) in 1991; Min. SEA Mean (CRU): 115.01 (mm/month) in 1997
Max. Global Mean (ERA5): 89.82 (mm/month) in 2015; Max. SEA Mean (ERA5): 251.242 (mm/month) in 1988
Min. Global Mean (ERA5): 83.293 (mm/month) in 1991; Min. SEA Mean (ERA5): 121.121 (mm/month) in 2006
Max. Global Mean (GPCP): 83.002 (mm/month) in 1993; Max. SEA Mean (GPCP): 226.264 (mm/month) in 1988
Min. Global Mean (GPCP): 78.239 (mm/month) in 1994; Min. SEA Mean (GPCP): 101.009 (mm/month) in 2006

TEMPERATURE/SST

Max. Global Mean (CRU): 11.223 (^{0}C) in 2020; Max. SEA Mean (CRU): 23.886 (^{0}C) in 2015
Min. Global Mean (CRU): 9.358 (^{0}C) in 1993; Min. SEA Mean (CRU): 22.347 (^{0}C) in 1992
Max. Global Mean (ERA5): 13.907 (^{0}C) in 2020; Max. SEA Mean (ERA5): 25.852 (^{0}C) in 2015
Min. Global Mean (ERA5): 12.717 (^{0}C in 1984; Min. SEA Mean (ERA5): 24.523 (^{0}C) in 1992
Max. Global Mean (HadISST): 16.921 (^{0}C) in 2019; Max. SEA Mean (HadISST): 28.874 (^{0}C) in 2016
Min. Global Mean (HadISST): -0.324 (^{0}C) in 1988; Min. SEA Mean (HadISST): 27.936 (^{0}C) in 1992

Figure 31. Yearly November Precipitation and Temperature Absolute Values (Global & SE Asia)

Table 19. Percentile of November 2013 Precipitation Anomalies [SE Asia]

Dataset	Precipitation
CRU	> Fn1.A<-ecdf(df1.1$Precip.Anomaly[1:40]) > Fn1.A(df1.1$Precip.Anomaly[1:40][df1.1$Year[1:40]==2013]) [1] 0.75 > summary(Fn1.A) Empirical CDF: 40 unique values with summary Min. 1st Qu. Median Mean 3rd Qu. Max. -41.178 -13.799 7.521 2.747 16.953 38.320 Rank: 11
ERA5	> Fn2.A<-ecdf(df1.1$Precip.Anomaly[41:80]) > Fn2.A(df1.1$Precip.Anomaly[41:80][df1.1$Year[41:80]==2013]) [1] 0.55 > summary(Fn2.A) Empirical CDF: 40 unique values with summary Min. 1st Qu. Median Mean 3rd Qu. Max. -67.79800 -26.89850 5.90600 0.08252 21.75050 62.32300 Rank: 19
GPCP	> Fn3.A<-ecdf(df1.1$Precip.Anomaly[81:120]) > Fn3.A(df1.1$Precip.Anomaly[81:120][df1.1$Year[81:120]==2013]) [1] 0.475 > summary(Fn3.A) Empirical CDF: 40 unique values with summary Min. 1st Qu. Median Mean 3rd Qu. Max. -68.576 -20.134 6.279 -1.015 18.054 56.679 Rank:22

Table 20. Percentile of November 2013 Temperature Anomalies [SE Asia]

Dataset	Temperature
CRU	> Fn1.B<-ecdf(df1.1$Temp.Anomaly[1:40]) > Fn1.B(df1.1$Temp.Anomaly[1:40][df1.1$Year[1:40]==2013]) [1] 0.5 > summary(Fn1.B) Empirical CDF: 40 unique values with summary Min. 1st Qu. Median Mean 3rd Qu. Max. -0.6910 -0.1645 0.1955 0.1342 0.4365 0.8480 Rank: 21
ERA5	> Fn2.B<-ecdf(df1.1$Temp.Anomaly[41:80]) > Fn2.B(df1.1$Temp.Anomaly[41:80][df1.1$Year[41:80]==2013]) [1] 0.475 > summary(Fn2.B) Empirical CDF: 40 unique values with summary Min. 1st Qu. Median Mean 3rd Qu. Max. -0.5930 -0.1237 0.1535 0.1261 0.3688 0.7350 Rank:22

HadISST	> Fn3.B<-ecdf(df1.1$SST.Anomaly[1:40]) > Fn3.B(df1.1$SST.Anomaly[1:40][df1.1$Year[1:40]==2013]) [1] 0.525 > summary(Fn3.B) Empirical CDF: 39 unique values with summary Min. 1st Qu. Median Mean 3rd Qu. Max. -0.39300 -0.07950 0.08400 0.05659 0.18900 0.54400 **Rank: 19**

As shown, CRU is the highest for precipitation, being on the 75th percentile, ranking on the 11th among the 40 years, while HadISST is the highest for temperature, being on the 52.5th percentile, ranking on the 19th. From the above table, it can also be construed that November 2013 is not comparatively wetter and warmer than the rest of the years, despite the occurrence of Haiyan on this same month.

To visualize, the maps of the 30-yr climatology, absolute and anomaly values for November 2013 are presented in ***ANNEX 5*** for precipitation and temperature. Globally and in SE Asia, the temperature anomaly maps showed more dominant red (and dark-red) spots, demonstrating positive (hotter) anomalies. For precipitation, the anomaly maps show blue (and dark blue) spots, indicating a positive (wetter) month, but some red (drier) areas are also depicted. Statistically, the Empirical Cumulative Distribution Function (ECDF) plots for precipitation anomalies **[*Figure 32*]** and the count of positive or negative values in **Table 21** show that CRU has the highest percentage of values equal to or above 0 (at 56%). ERA5 followed, still with more than 50% of positive values. GPCP on other hand has roughly 50% of positive values, meaning, there are drier than wetter points. This demonstrates that indeed, November 2013 is just slightly wetter-than-average month, as regards the baseline climatology.

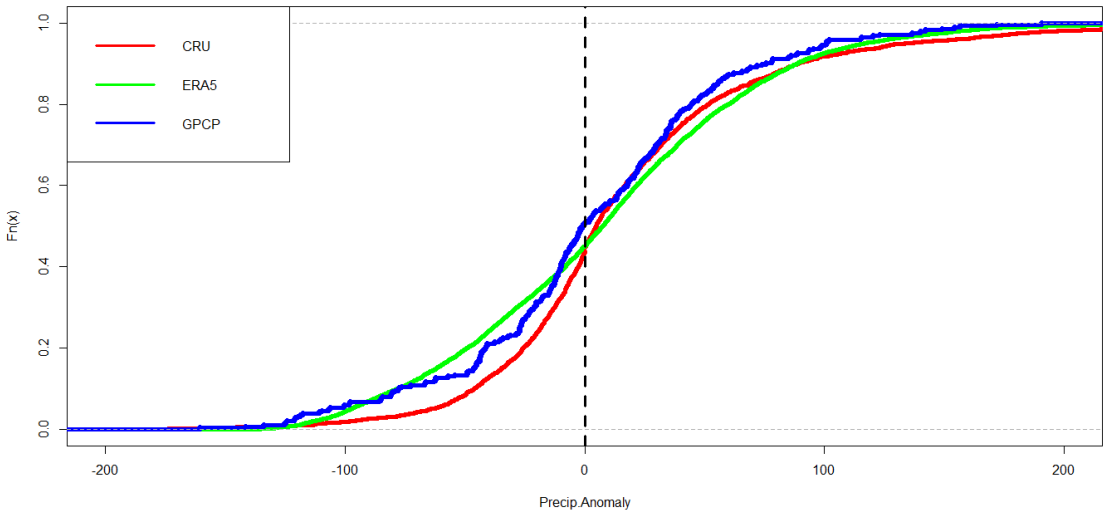

Figure 32. Empirical Cumulative Distribution Plots of November 2013 Precipitation Anomalies for SE Asia

With respect to the distribution of anomaly values, the skewness [*CRU = 1.166, ERA5 = 0.475, GPCP = 0.089*] indicates that all datasets are positively skewed or concentrated to the left as shown in the figure below. Among the datasets, GPCP is more symmetric with skewness closer to zero. The kurtosis *[CRU = 6.261, ERA5 = 4.061, GPCP = 3.566]* also reveals that GPCP value is closer to 3 hence more normally distributed than CRU and ERA5, with CRU having sharp peaks on the graph.

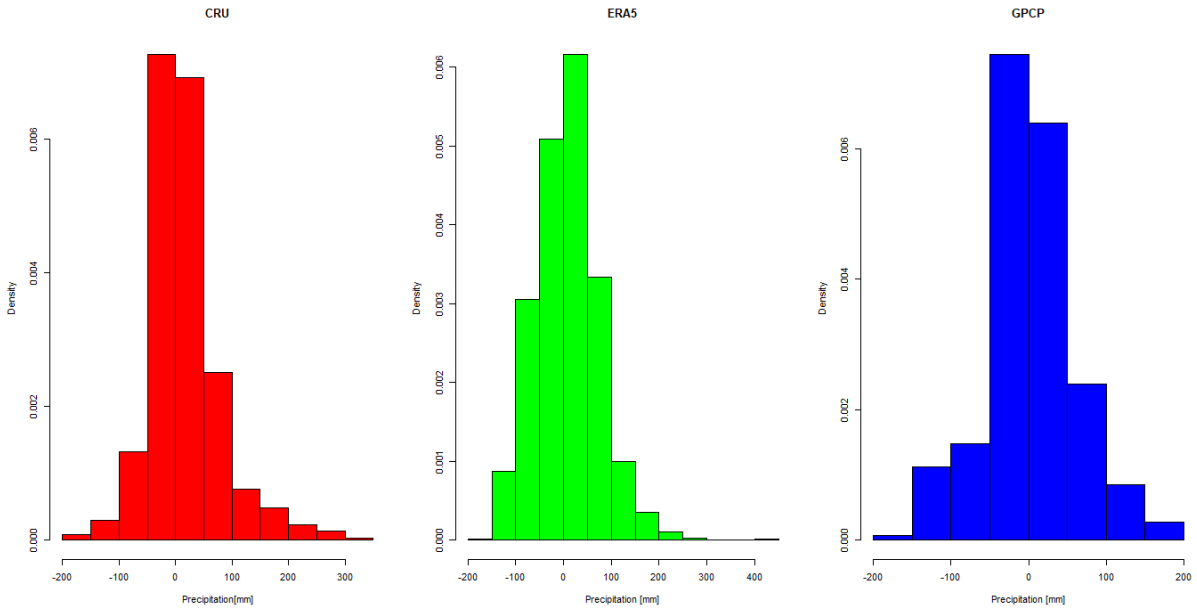

Figure 33. Probability Distribution Plots of November 2013 Precipitation Anomalies for SE Asia

For temperature anomalies, the ECDF plots in ***Figure 34*** and the summary of counts in **Table 21** show that CRU likewise has the highest percentage (70%) among the three datasets, while ERA5 and HadISST have almost 70% of the values above 0. This indicates that November 2013 is a little hotter than average, compared to the baseline climatology, in as far as the three datasets are concerned.

With respect to the distribution of anomaly values, the skewness [*CRU = -0.597, ERA5 = 0.222, HadISST = 0.158]* indicates that CRU is negatively skewed or more concentrated on the right, while ERA5 and HadISST are positively skewed or concentrated to the left. Among the datasets, HadISST is more symmetric with skewness closer to zero. The kurtosis *[CRU = 5.048, ERA5 = 5.519, HadISST = 4.3689]* also reveals that HadISST value is closer to 3 hence more normally distributed than CRU and ERA5, with ERA5 having sharp peaks on the graph, as shown in ***Figure 35.***

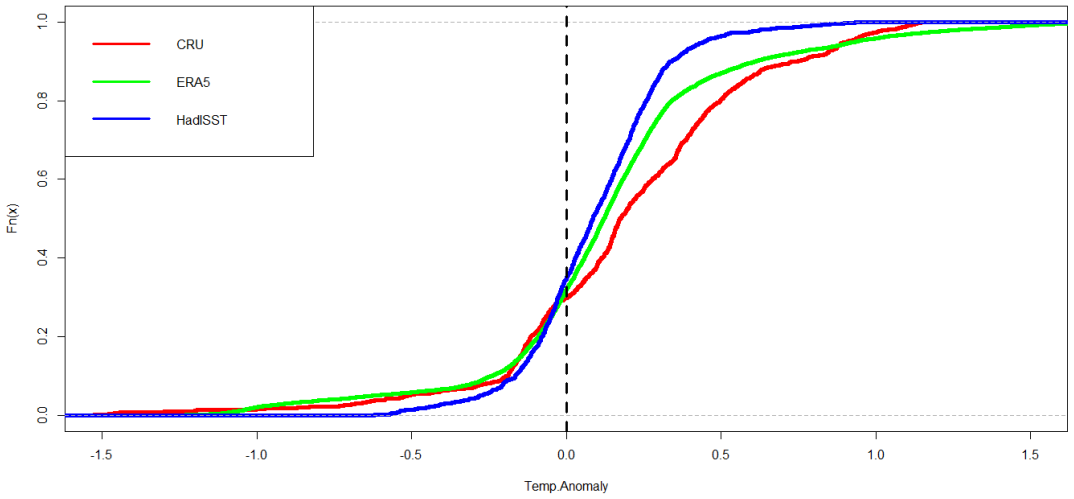

Figure 34. Empirical Cumulative Distribution Plots of November 2013 Temperature Anomalies for SE Asia

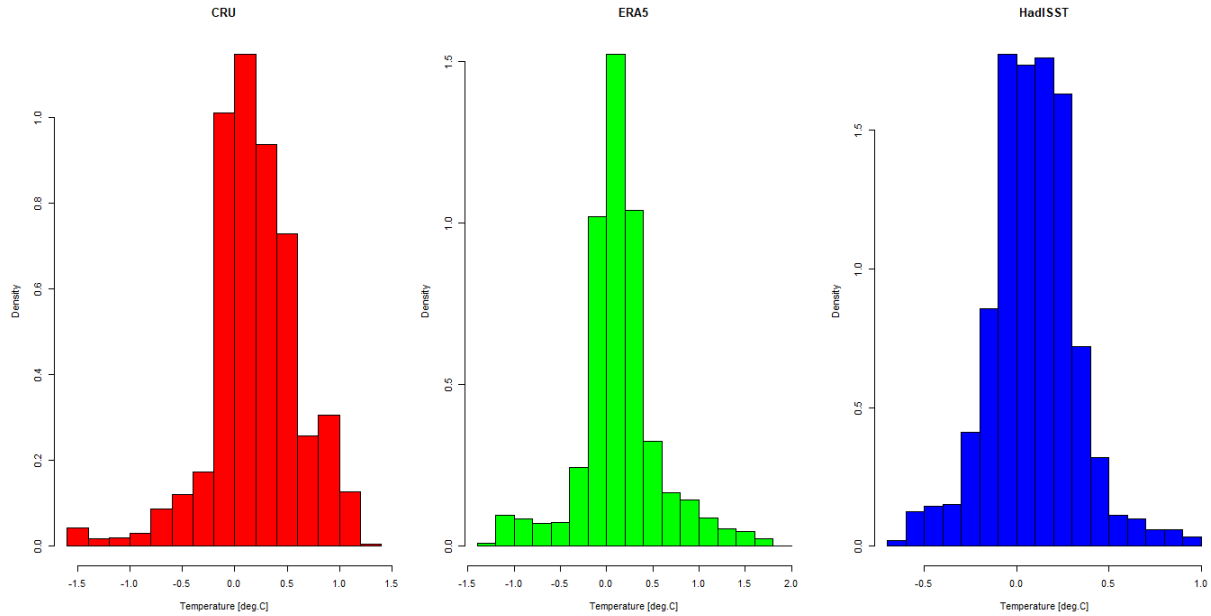

Figure 35. Probability Distribution Plots of November 2013 Temperature Anomalies for SE Asia

Table 21. Count of Negative vs. Zero/Positive Annual Precipitation and Temperature Anomalies for November 2013

	PRECIPITATION	TEMPERATURE
CRU	> pos_cru<-prcp_nov2013_cru$anomaly>=0 > table(pos_cru) pos_cru FALSE TRUE 1175 1508 > table(pos_cru)[2]/(table(pos_cru)[2]+table(pos_cru)[1])	> pos_cru<-tmp_nov2013_cru$anomaly>=0 > table(pos_cru) pos_cru FALSE TRUE 803 1880 > table(pos_cru)[2]/(table(pos_cru)[2]+table(pos_cru)[1]) TRUE

	TRUE 0.5620574	0.7007082
ERA5	> pos_era5<-prcp_nov2013_era5$anomaly>=0 > table(pos_era5) pos_era5 FALSE TRUE 3490 4252 > table(pos_era5)[2]/(table(pos_era5)[2]+table(pos_era5)[1]) TRUE 0.5492121	> pos_era5<-tmp_nov2013_era5$anomaly>=0 > table(pos_era5) pos_era5 FALSE TRUE 2475 5267 > table(pos_era5)[2]/(table(pos_era5)[2]+table(pos_era5)[1]) TRUE 0.6803152
GPCP | HadISST	> pos_gpcp<-prcp_nov2013_gpcp$anomaly>=0 > table(pos_gpcp) pos_gpcp FALSE TRUE 144 141 > table(pos_gpcp)[2]/(table(pos_gpcp)[2]+table(pos_gpcp)[1]) TRUE 0.4947368	> pos_HadISST<-tmp_nov2013_HadISST$anomaly>=0 > table(pos_HadISST) pos_HadISST FALSE TRUE 535 1004 > table(pos_HadISST)[2]/(table(pos_HadISST)[2]+table(pos_HadISST)[1]) TRUE 0.6523717

The 5-95 percentiles of the grid points were also calculated to show the significance of the anomaly values. These significant points are shown in ***Figures 36 & 37***. The same difference between the datasets is observed as with the annual and seasonal analysis, showing lack of consistency among the datasets in terms of amplitude and location of these points.

To further compare the differences in the values, the summary of the t-test for each dataset [as summarized in **Table 22**] shows that CRU vs. ERA5, and CRU vs. GPCP are significantly different in terms of precipitation anomalies, having relatively low p-values for all the t-test analyses. ERA5 & GPCP otherwise did not show significant difference. Based on the highest t-value, the strongest evidence of difference is still between CRU & ERA5. For temperature, CRU and ERA5 are likewise significantly different. HadISST was excluded from the t-test, like the annual and seasonal analysis. The non-significant difference of ERA5 and GPCP demonstrates that the mean of the anomaly values for both datasets does not vary -- an indication that the values of the anomalies for November 2013 as computed from these datasets are comparable. It must be regarded however, that ERA5 has a larger number of grid points analyzed than GPCP.

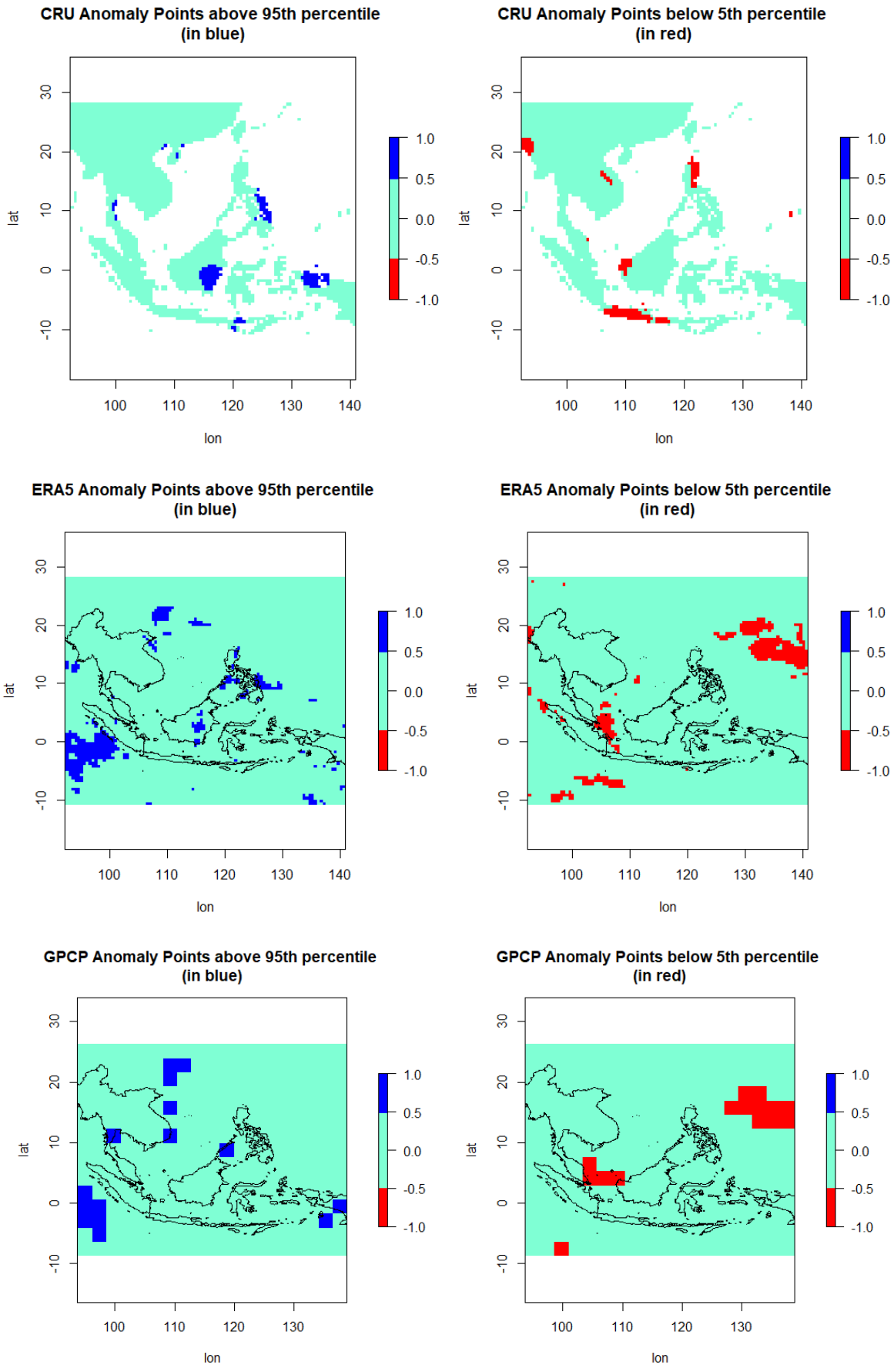

Figure 36. Maps Showing Anomaly Points Beyond 5-95 Percentile for November 2013 Precipitation [SE Asia]

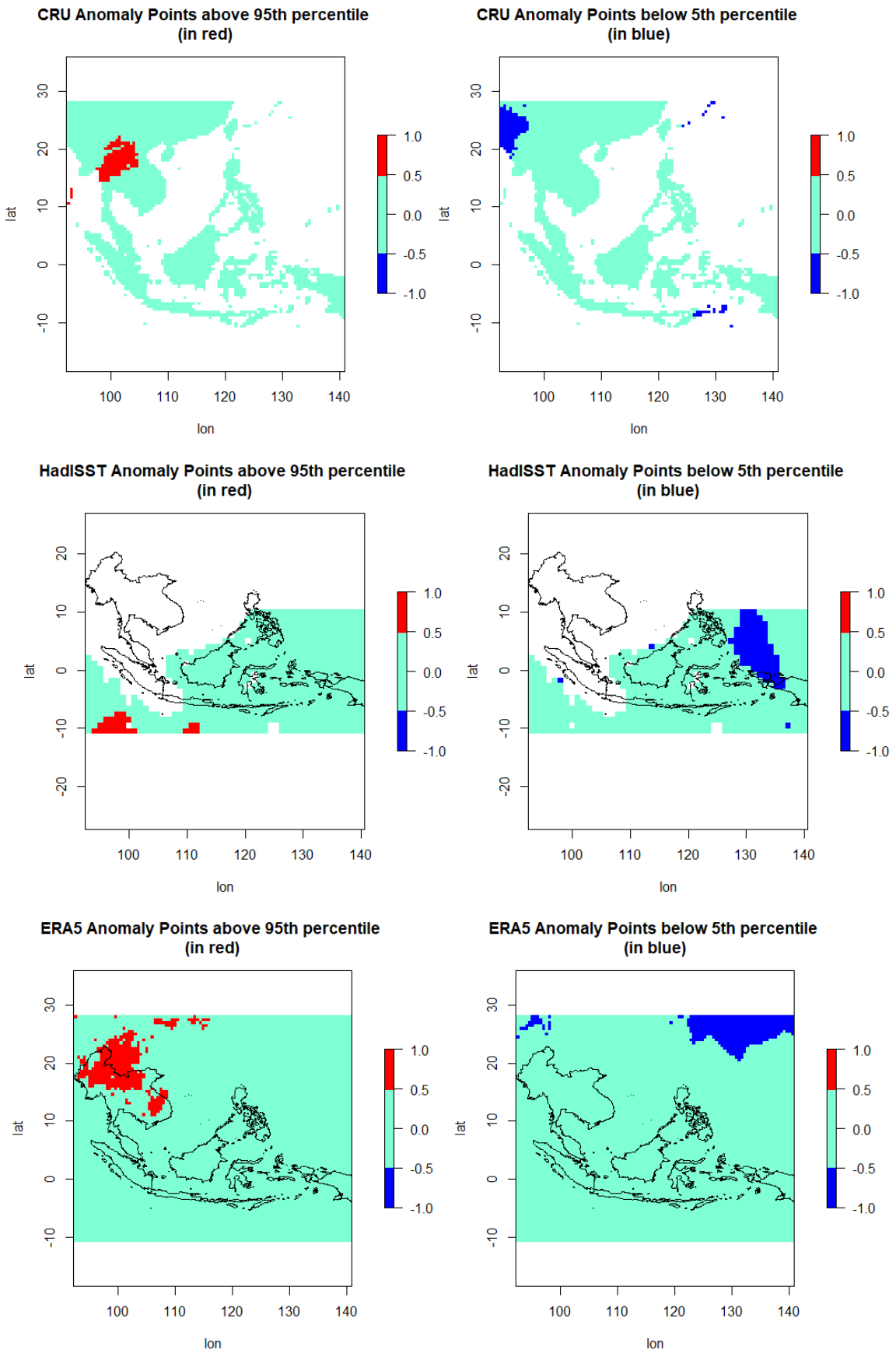

Figure 37. Maps Showing Anomaly Points Beyond 5-95 Percentile for November 2013 Temperature [SE Asia]

Table 22. Results of Welch Two-Sample t-test for Y2013 Precipitation and Temperature Anomalies

	PRECIPITATION	TEMPERATURE
CRU vs. ERA5	data: prcp_nov2013_cru$anomaly and prcp_nov2013_era5$anomaly t = 5.8121, df = 4867.6, p-value = 6.562e-09 alternative hypothesis: true difference in means is not equal to 0 95 percent confidence interval: 5.487889 11.074443 sample estimates: mean of x mean of y 15.995053 7.713887	data: tmp_nov2013_cru$anomaly and tmp_nov2013_era5$anomaly t = 5.6106, df = 4733.2, p-value = 2.131e-08 alternative hypothesis: true difference in means is not equal to 0 95 percent confidence interval: 0.03463220 0.07183357 sample estimates: mean of x mean of y 0.1909865 0.1377536
CRU vs. GPCP	data: prcp_nov2013_cru$anomaly and prcp_nov2013_gpcp$anomaly t = 3.4661, df = 356.43, p-value = 0.0005925 alternative hypothesis: true difference in means is not equal to 0 95 percent confidence interval: 5.531305 20.040467 sample estimates: mean of x mean of y 15.995053 3.209167	N/A
ERA5 vs. GPCP	data: prcp_nov2013_era5$anomaly and prcp_nov2013_gpcp$anomaly t = 1.2642, df = 310.77, p-value = 0.2071 alternative hypothesis: true difference in means is not equal to 0 95 percent confidence interval: -2.506364 11.515805 sample estimates: mean of x mean of y 7.713887 3.209167	N/A

The SE Asian absolute monthly precipitation and temperature values for Y2013 are plotted in ***Figure 38***. As seen ERA5 and GPCP show a common maximum month (July), while all three datasets have common minimum month (March) for precipitation. For temperature, all three datasets share a common maximum month (June), while CRU and ERA5 have a common minimum month (December).

The precipitation values are then plotted against the monsoonal variations, as presented in ***Figure 39,*** to investigate whether the monsoonal changes impact the monthly precipitation. For the plot, the months are categorized into Northeast (for Northeast monsoon month), Southwest (for Southwest monsoon), and None (or not a monsoon month). This is likewise discussed in *Chapter 2, Section 2.3.* As shown, high precipitation values are observed in the months of May to September or the Southwest monsoon months (blue bars), compared to the Northeast (green) and non-monsoon (red) months.

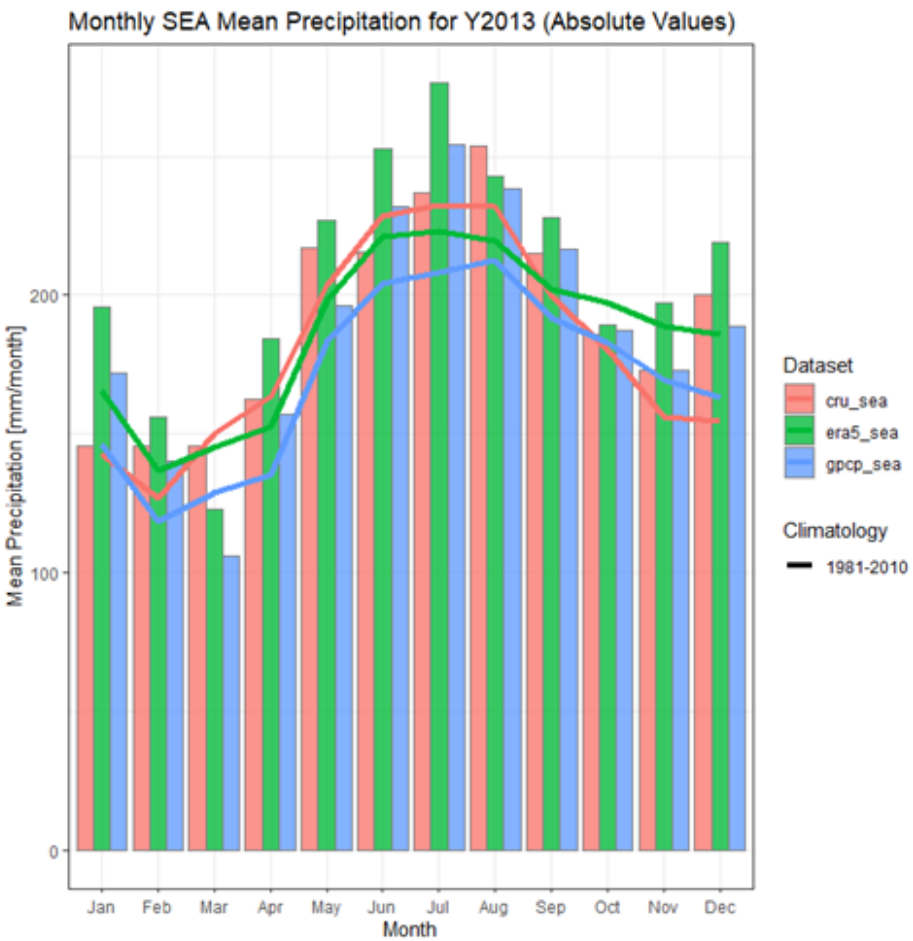

Max. SEA Mean **(CRU):** 253.906 (mm/month) in August;
Min. SEA Mean **(CRU):** 145.691 (mm/month) in March
Max. SEA Mean **(ERA5):** 276.446 (mm/month) in July;
Min. SEA Mean **(ERA5):** 122.663 (mm/month) in March
Max. SEA Mean **(GPCP):** 254.152 (mm/month) in July;
Min. SEA Mean **(GPCP):** 105.973 (mm/month) in March

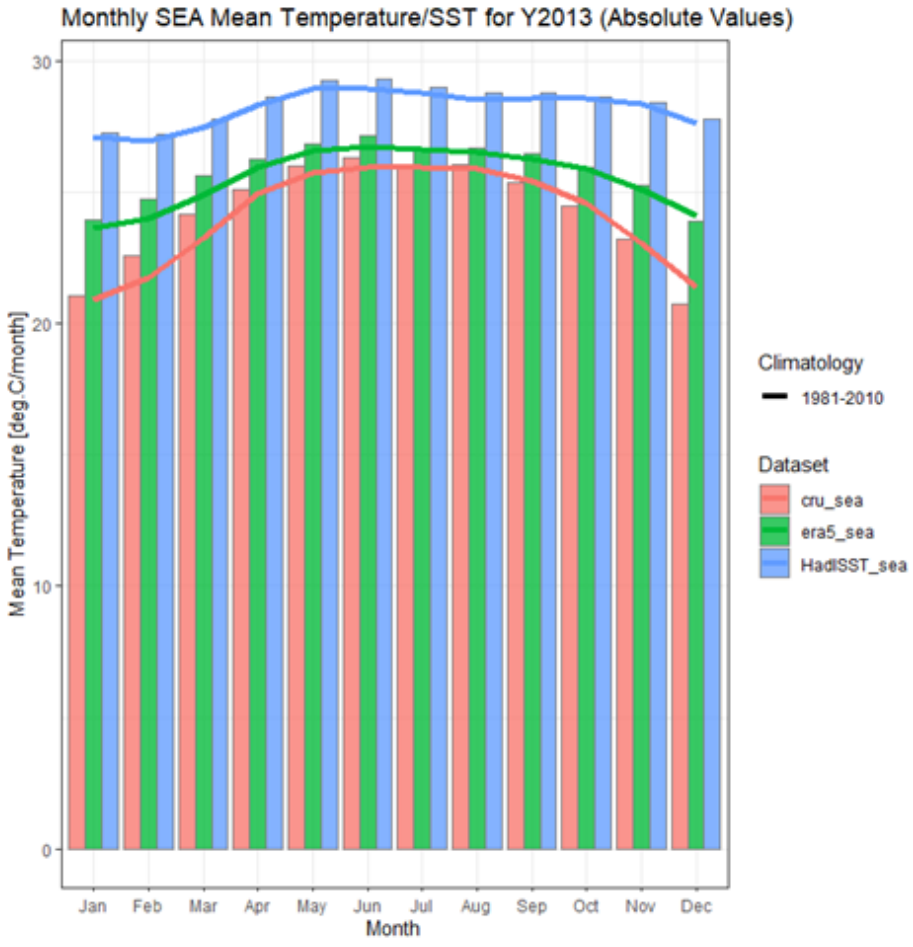

Max. SEA Mean **(CRU):** 26.299 (^{0}C) in June;
Min. SEA Mean **(CRU):** 20.747 (^{0}C) in December
Max. SEA Mean **(ERA5):** 27.127 (^{0}C) in June;
Min. SEA Mean **(ERA5):** 23.889 (^{0}C) in December
Max. SEA Mean **(HadISST):** 2 29.281 (^{0}C) in June;
Min. SEA Mean **(HadISST):** 27.187 (^{0}C) in February

Figure 38. Monthly Precipitation and Temperature Values for Y2013 (SE Asia)

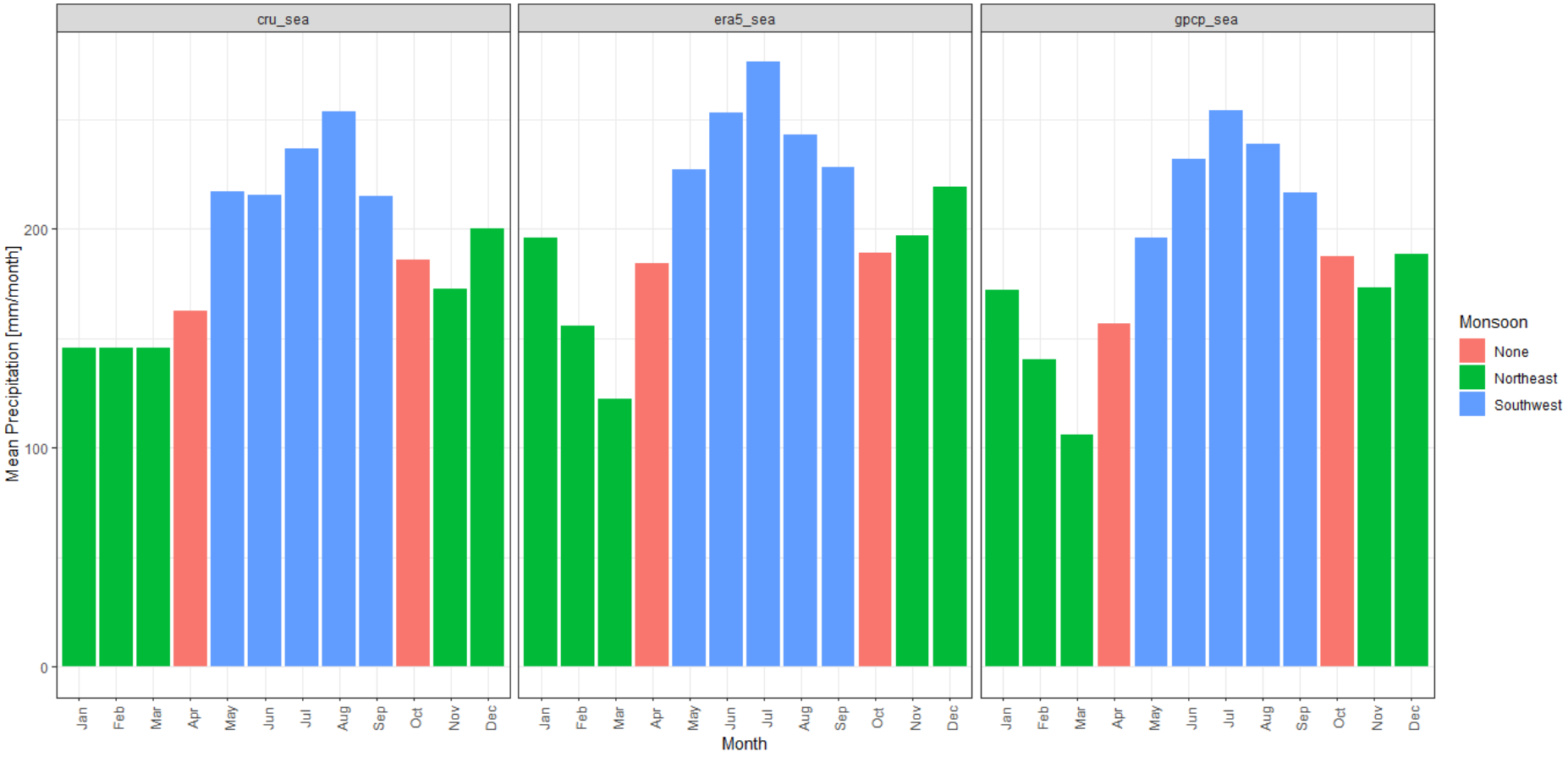

Figure 39. Monthly Precipitation Values for Y2013 against Monsoonal Variations (SE Asia)

To statistically understand the influence of these monsoonal variations on the regional precipitation, an Analysis of Variance (ANOVA) is performed for each dataset as detailed in **Table 23.** The results showed that the precipitation anomalies for all datasets are significantly influenced by ENSO variations with very low p-values (marked with a green rectangle). The large

F values likewise confirm this result. Among the three precipitation datasets, CRU has the least p-value, while ERA5 are higher than the two.

A Wilcoxon rank sum test is also performed, accounting only the Northeast and Southwest monsoon months as presented in **Table 24.** Like the ANOVA, the result showed significant p-values.

Table 23. Results of Analysis of Variance for Monthly Absolute Precipitation for Y2013 against Monsoonal Variations

Dataset	ANOVA results

CRU	`> summary(aov(prcp_df2$Precip.DT[1:12]~prcp_df2$Monsoon[1:12]))`
	`Df Sum Sq Mean Sq F value Pr(>F)`
	`prcp_df2$Monsoon[1:12] 2 11314 5657 15.36 0.00125 **`
	`Residuals 9 3314 368`
	`---`
	`Signif. codes: 0 '***' 0.001 '**' 0.01 '*' 0.05 '.' 0.1 ' ' 1`

ERA5	`> summary(aov(prcp_df2$Precip.DT[13:24]~prcp_df2$Monsoon[13:24]))`
	`Df Sum Sq Mean Sq F value Pr(>F)`
	`prcp_df2$Monsoon[13:24] 2 12205 6102 7.654 0.0114 *`
	`Residuals 9 7175 797`
	`---`
	`Signif. codes: 0 '***' 0.001 '**' 0.01 '*' 0.05 '.' 0.1 ' ' 1`

GPCP	`> summary(aov(prcp_df2$Precip.DT[25:36]~prcp_df2$Monsoon[25:36]))`
	`Df Sum Sq Mean Sq F value Pr(>F)`
	`prcp_df2$Monsoon[25:36] 2 13227 6613 9.424 0.0062 **`
	`Residuals 9 6316 702`
	`---`
	`Signif. codes: 0 '***' 0.001 '**' 0.01 '*' 0.05 '.' 0.1 ' ' 1`

Table 24. Results of Wilcoxon Rank Sum Test on Y2013 Monthly Absolute Precipitation for Northeast and Southwest Monsoon

Dataset	Wilcoxon Test Results

CRU Precip.	`> wilcox.test(Precip.DT[1:12] ~ Monsoon[1:12], data = prcp_df2, conf.int = TRUE)`
	
	`data: Precip.DT[1:12] by Monsoon[1:12]`
	`W = 0, p-value = 0.007937`
	`alternative hypothesis: true location shift is not equal to 0`
	`95 percent confidence interval:`
	`-104.81715 -20.23711`
	`sample estimates:`
	`difference in location`
	`-67.59499`

ERA5 Precip.	`> wilcox.test(Precip.DT[13:24] ~ Monsoon[13:24], data = prcp_df2, conf.int = TRUE)`
	
	`data:  Precip.DT[13:24] by Monsoon[13:24]`
	`W = 0, p-value = 0.007937`
	`alternative hypothesis: true location shift is not equal to 0`
	`95 percent confidence interval:`
	`-118.17368  -25.44986`
	`sample estimates:`
	`difference in location`
	`-59.46255`

GPCP Precip.	`> wilcox.test(Precip.DT[25:36] ~ Monsoon[25:36], data = prcp_df2, conf.int = TRUE)`
	
	`data:  Precip.DT[25:36] by Monsoon[25:36]`
	`W = 0, p-value = 0.007937`
	`alternative hypothesis: true location shift is not equal to 0`
	`95 percent confidence interval:`
	`-124.67852  -25.79639`
	`sample estimates:`
	`difference in location`
	`-66.91553`

The yearly November anomalies for precipitation and temperature are plotted in ***Figure 40***. To again understand if ENSO SST has an effect on the variables, Nino3.4 SST anomalies for all Novembers considered are likewise plotted. From this plot, ERA5 and GPCP share the same minimum year (2006) for precipitation, while CRU and ERA5 have common maximum (2015) and minimum years for temperature. Nino 3.4 also have the same maximum year (2015) as with the ERA5 and GPCP precipitation maximum. From these values, regression analysis are performed to understand their inter-variable relationships. ***Figures 41 to 43*** presents the plots of the linear regression among the monthly Precipitation, Temperature, HadISST and Nino 3.4 SST anomalies, for all datasets. As seen, almost the p-values are significant for the all the regressions, except for CRU precipitation vs. temperature, ERA5 precipitation vs. temperature and ERA5 Temperature vs. Nino3.4. The relationship of HadISST vs. Nino3.4 are likewise insignificant. Based on the results with significant p-values, the CRU precipitation and temperature are positively correlated with HadISST and Nino 3.4 respectively, while CRU precipitation and Nino3.4 are negatively correlated. For ERA5, positive correlations were also noted for both precipitation and temperature vs. HadISST, and negative correlation for precipitation and Nino 3.4. For GPCP, precipitation is positively correlated with HadISST while negatively correlated with Nino3.4. The significant relationships evidently showed that among all the datasets, the correlations of precipitation and temperature to HadISST and Nino3.4 are all uniform -- where precipitation and temperature increases with HadISST and vice versa, while precipitation decreases as Nino 3.4 increases (and v.v.) The scatterplots ***(Figure 44)*** also display these relationships where the circles

are inclined toward the right for positive correlations and toward the left for negative correlations. The rest of the correlations without a corresponding significant p-value otherwise show that the circles are more distributed across different parts of the plot, than displaying an inclining left or right pattern. It was also noted from the density plot in ***Figure 44,*** and boxplot in ***Figure 45*** that ERA5 temperature and HadISST have outliers and ERA5 temperature appears to have a peak in the curve, which could have affected the regression results.

The monthly anomalies for precipitation and temperature/SST in Y2013 are plotted in ***Figure 45*** against the monthly Nino3.4 SST anomalies***.*** Comparing the months, ERA5 and GPCP have a common maximum month (July) and minimum month (March) for precipitation. For temperature, CRU and ERA5 both share common maximum (March) and minimum (December) months. For Nino3.4, maximum and minimum months are November and January respectively, which are not common to all the precipitation or temperature datasets analyzed.

Discussion

From the ANOVA and Wilcoxon tests, it is apparent that the monsoonal variations (Northeast and Southwest) within the SE Asian region affected the precipitation patterns for the Y2013. The plots for Y2013 monthly absolute and anomaly values are also consistent with the seasonal analysis, wherein the monthly absolute and anomaly values have maximum temperature in June (summer season). Correspondingly, the months of July and August also registered the highest precipitation (absolute and anomaly values), which fall within the Northeast Monsoon season when the rain is concentrated in the mainland. March on the other hand is the minimum month, which falls within the Southwest monsoon season where only small amounts of rain goes to the mainland during this period. It should be noted however, that CRU slightly varied from the two precipitation datasets having different maximum and minimum precipitation anomaly months. For temperature, the minimum months recorded are December and February wherein in these months, dry and cool air is observed in the mainland for SE Asian region. One remarkable observation is that November 2013 has low precipitation anomaly values, despite the occurrence of Typhoon Haiyan during this month.

Checking maps produced by other institutions, the same global map in ***ANNEX 2,*** shows that California experienced record-low precipitation in November 2013, while Austria has the wettest November since 2002, that explains the red (dry) and blue (wet) colors in these parts of the map.

For temperature, Spain experienced the coolest November since 1985 records, while Russia has the warmest November since 1891 thereby showing blue and dark-red colors for these areas. For SE Asia, the percentage of negative and positive anomalies for precipitation is around 50-50 hence the blue and red spots are even. Albeit positive, the mean precipitation anomaly for November 2013 throughout the region is low.

From the regression analysis, it is also notable that Precipitation and Temperature are positively affected by the HadISST but the Nino3.4 has negative correlation to these variables, when both are measuring SST values. Following the observations of previously cited papers, SE Asia is expected to be excluded from the positive correlation with ENSO compared to the rest of Asia during the SO-ND months, hence the negative correlation with the precipitation and Nino 3.4 confirms this result.

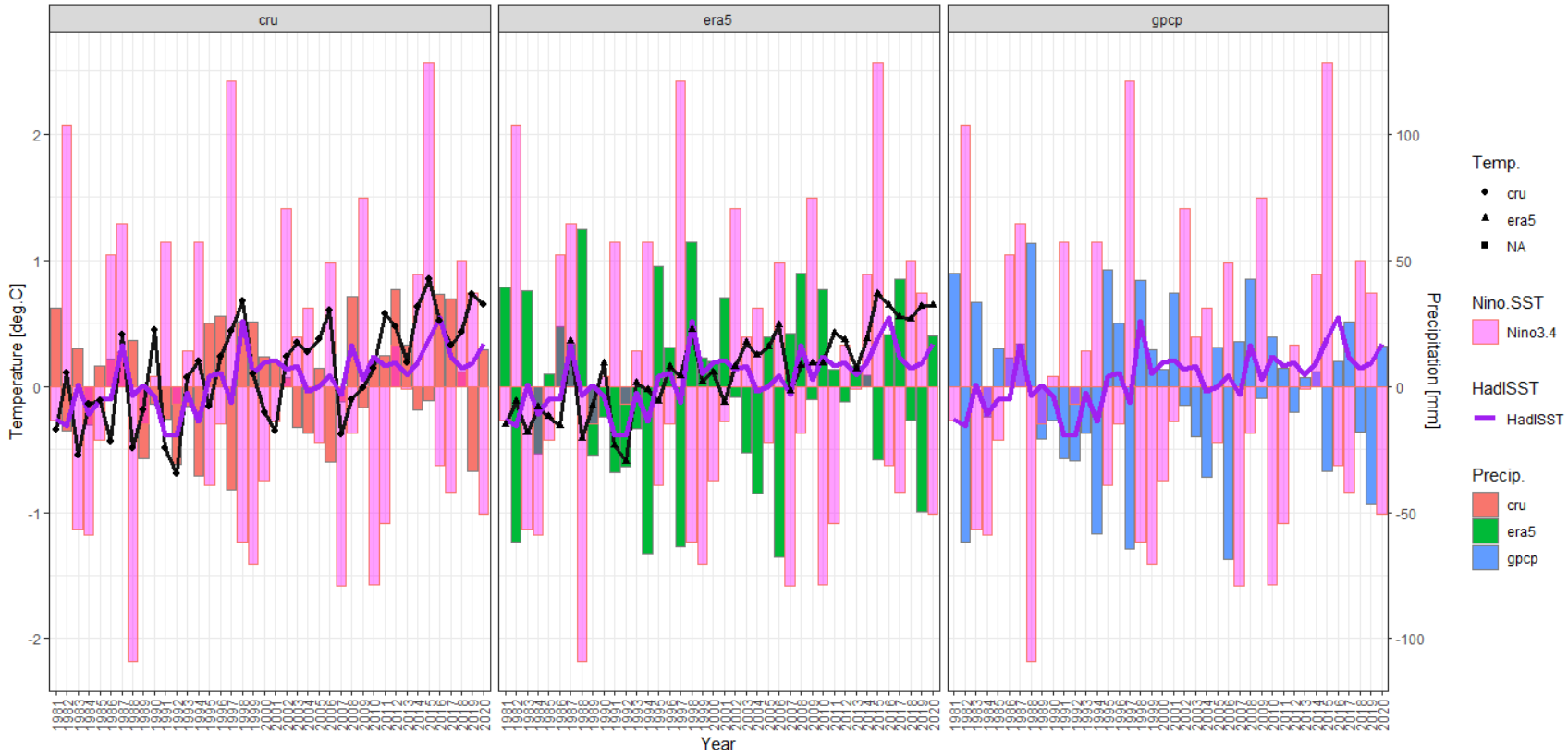

CRU

Max. **Precip.** Anomaly: 38.32 (mm) in 2012
Min. **Precip.** Anomaly: -41.178 (mm) in 1997
Max. **Temp.** Anomaly: 0.848 (^{0}C) in 2015
Min.**Temp.** Anomaly: -0.691 (^{0}C) in 1992

ERA5

Max. **Precip**. Anomaly: 62.323 (mm) in 1988
Min. **Precip.** Anomaly: -67.798 (mm) in 2006
Max. **Temp**. Anomaly: 0.735 (^{0}C) in 2015
Min.**Temp.** Anomaly: -0.593 (^{0}C) in 1992

GPCP / HadISST

Max. **Precip.** Anomaly: 56.679 (mm) in 1988
Min. **Precip**. Anomaly: -68.576 (mm) in 2006
Max. **SST**. Anomaly: 0.544 (^{0}C) in 2016
Min.**SST.** Anomaly: -0.393 (^{0}C) in 1992

Nino 3.4

Max. **SST**. Anomaly: 2.57 (^{0}C) in 2015
Min.**SST.** Anomaly: -2.18 (^{0}C) in 1998

Figure 40. Yearly November Precipitation and Temperature/SST Anomalies against Nino3.4 SST (SE Asia)

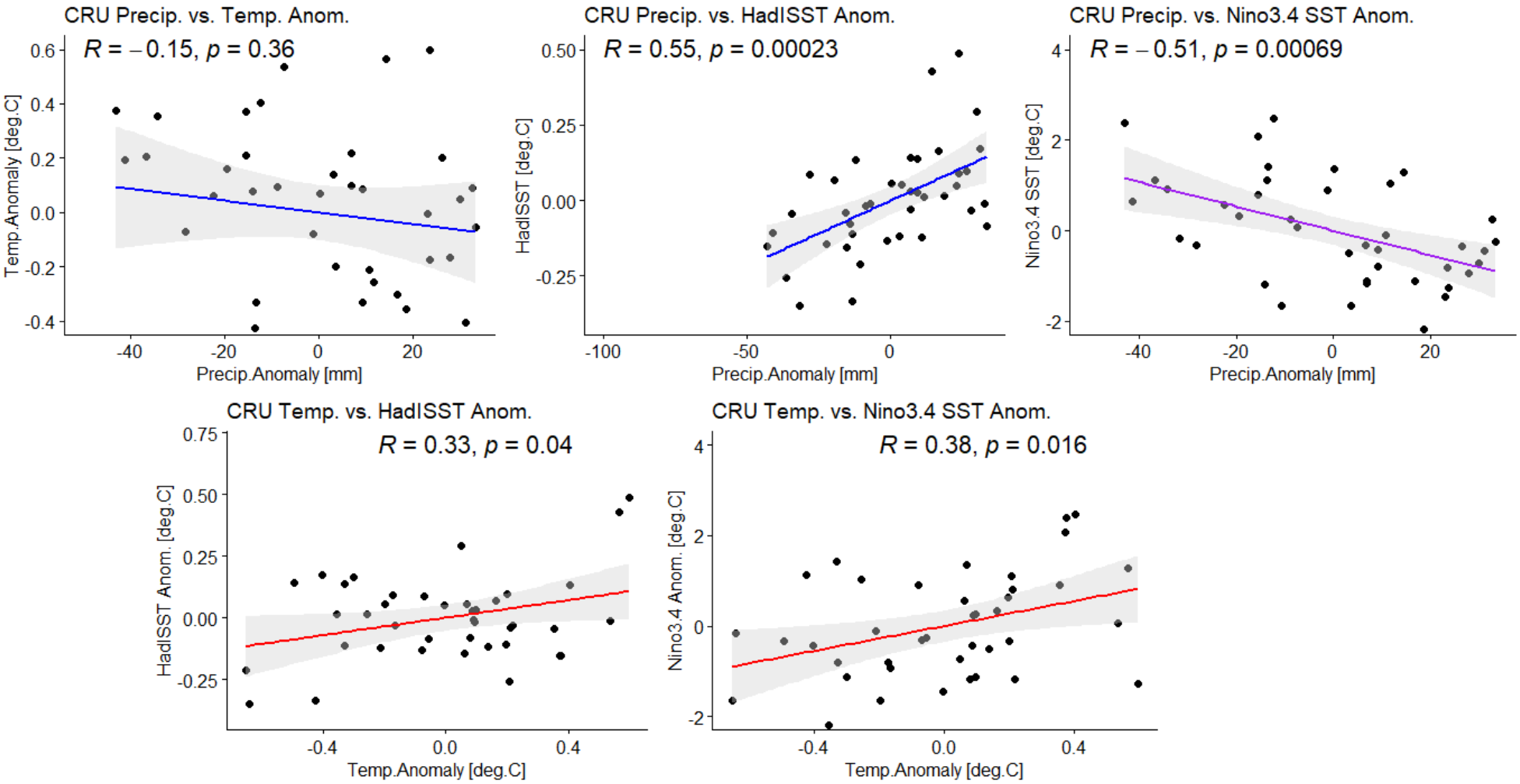

Figure 41. Linear Regression of CRU dataset for Yearly November Anomalies

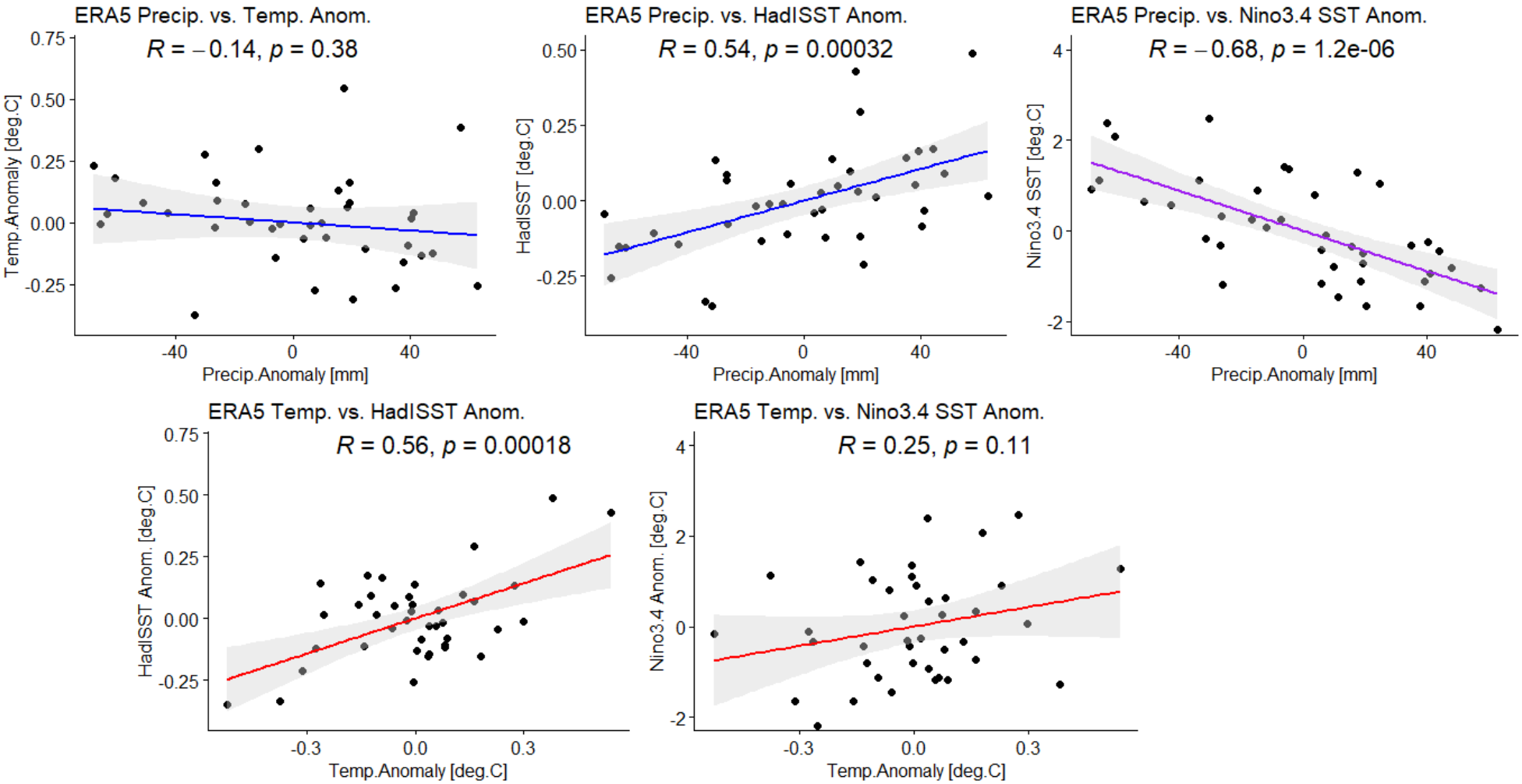

Figure 42. Linear Regression of ERA5 dataset for Yearly November Anomalies

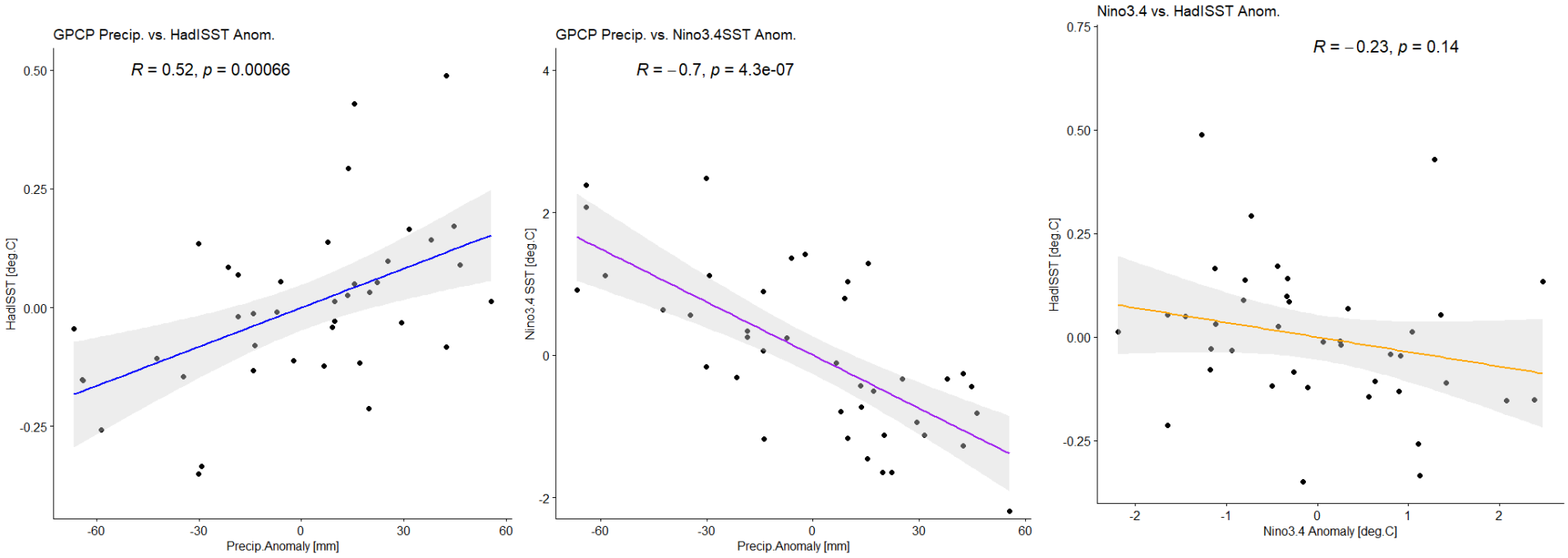

Figure 43. Linear Regression of GPCP and HadISST datasets for November 2013 anomalies

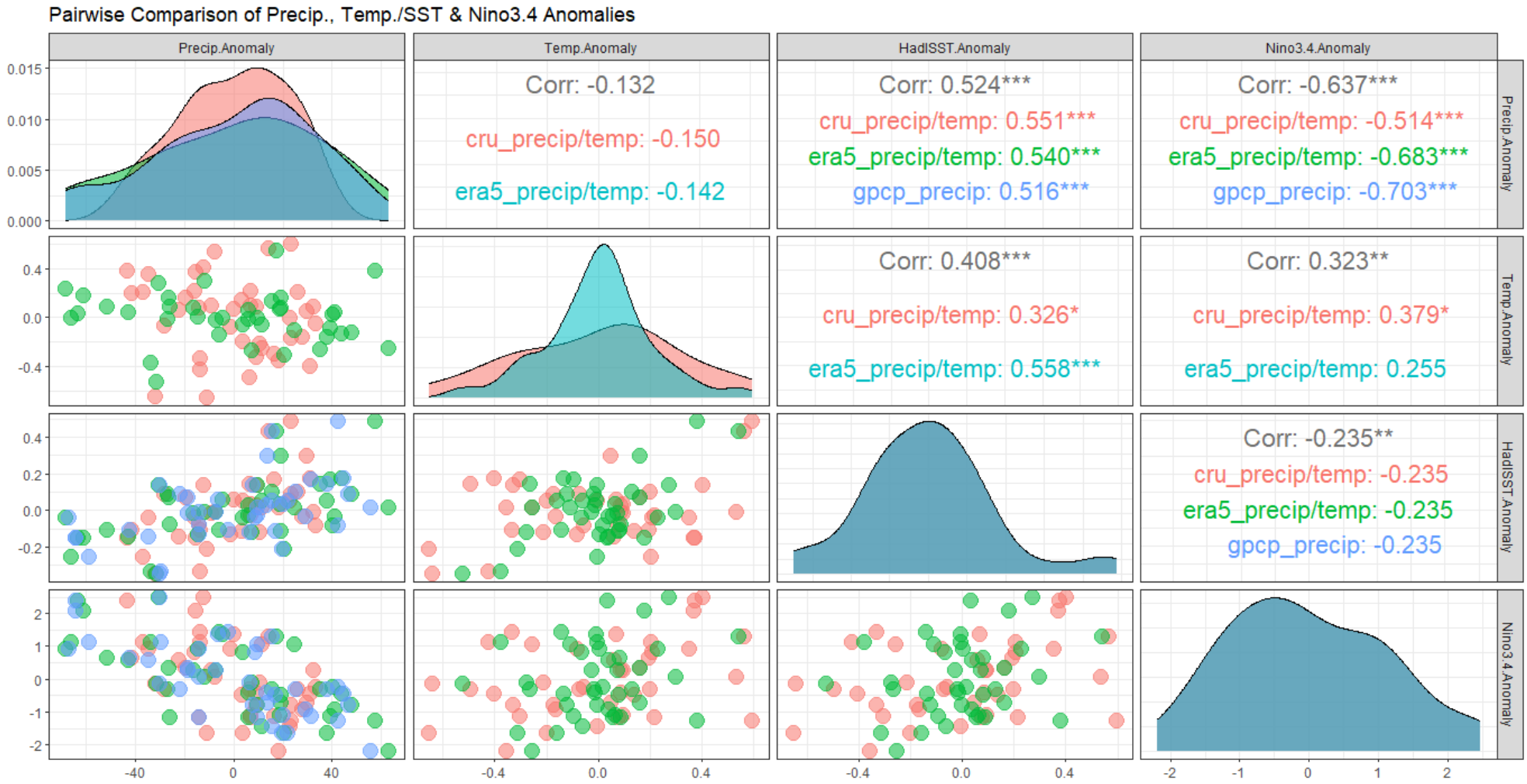

Figure 44. Scatterplots, Density Plots and Correlation Coefficients of Yearly November Precip., Temp., HadISST and Nino3.4 Anomalies

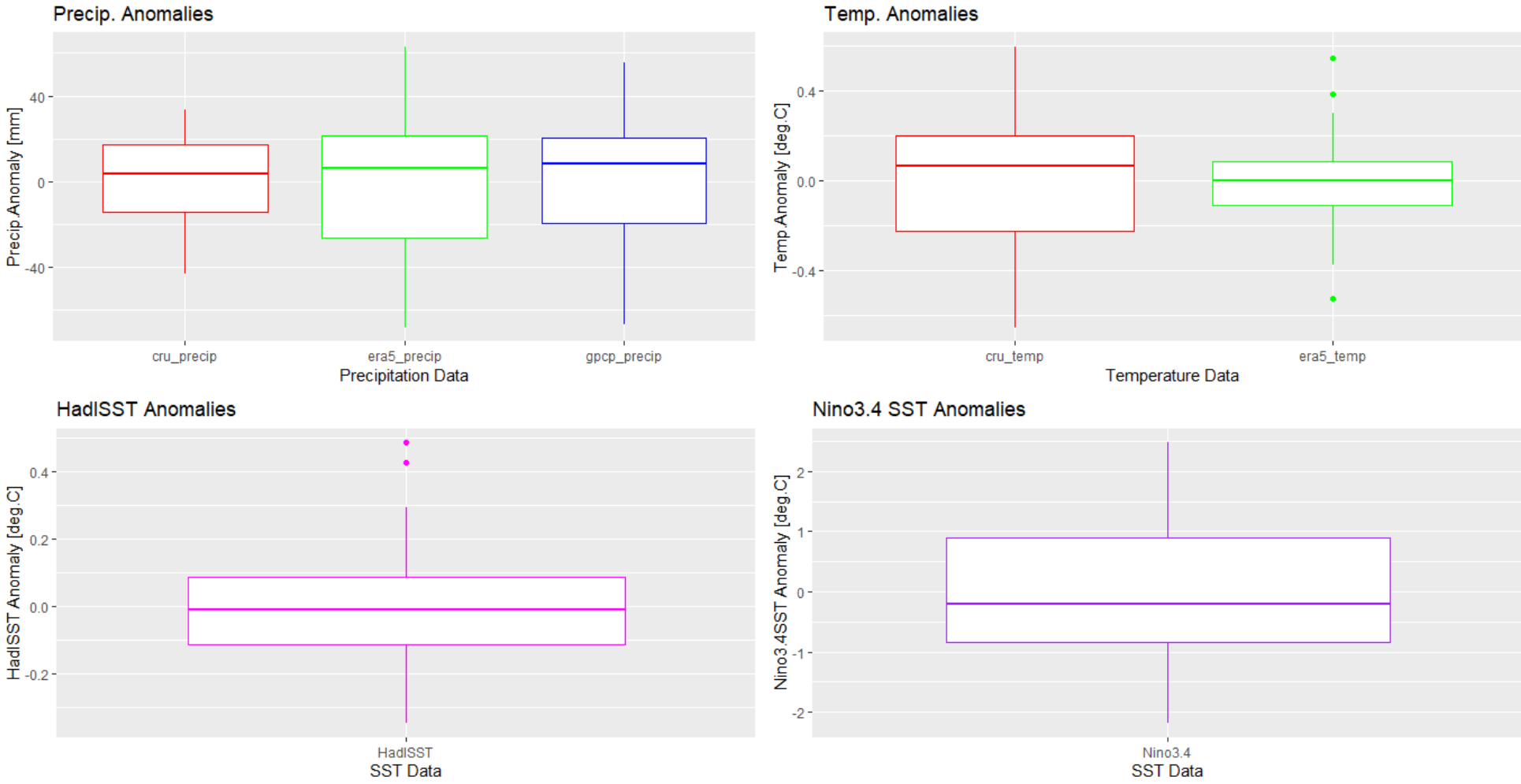

Figure 45. Boxplots of Yearly November Precip., Temp./SST and Nino3.4 Anomalies

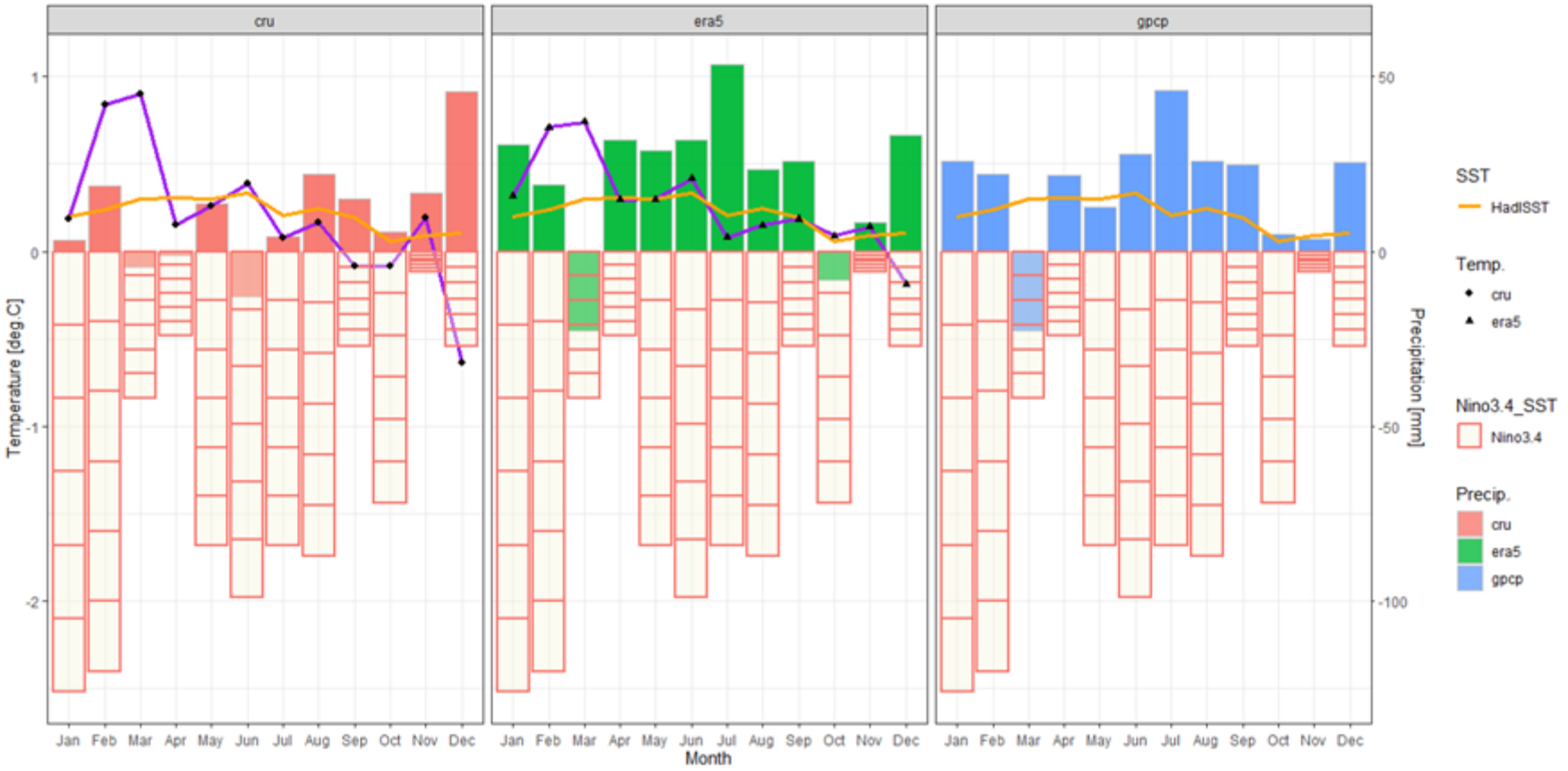

CRU
Max. **Precip.** Anomaly: 45.757 (mm) in December
Min. **Precip.** Anomaly: -12.828 (mm) in June
Max. **Temp.** Anomaly: 0.900 (^{0}C) in March
Min. **Temp.** Anomaly: -0.637 (^{0}C) in December

ERA5
Max. **Precip.** Anomaly: 53.319 (mm) in July
Min. **Precip.** Anomaly: -22.561 (mm) in March
Max. **Temp.** Anomaly: 0.741 (^{0}C) in March
Min. **Temp.** Anomaly: -0.187 (^{0}C) in December

GPCP I HadISST
Max. **Precip.** Anomaly: 45.954 (mm) in July
Min. **Precip.** Anomaly: -22.693 (mm) in March
Max. **SST** Anomaly: 0.333 (^{0}C) in June
Min. **SST** Anomaly: 0.057 (^{0}C) in October

Nino3.4 SST
Max. **SST** Anomaly: -0.02 (^{0}C) in November
Min. **SST** Anomaly: -0.42 (^{0}C) in January

Figure 46. Y2013 Monthly Anomalies for Precipitation and Temperature against Nino3.4 SST (SE Asia)

3.4. Daily Analysis

Results

For the daily analysis, the focus is on the days when the Typhoon Haiyan formed, made landfall and dissipated (Nov. 3 to 11, 2013). From these days it is apparent that spatially (***Figure 47),*** there is a concentration of low pressure forming around the Philippine Area of Responsibility -- evidence of the cyclonic activity over the country linked with the passage of the typhoon.

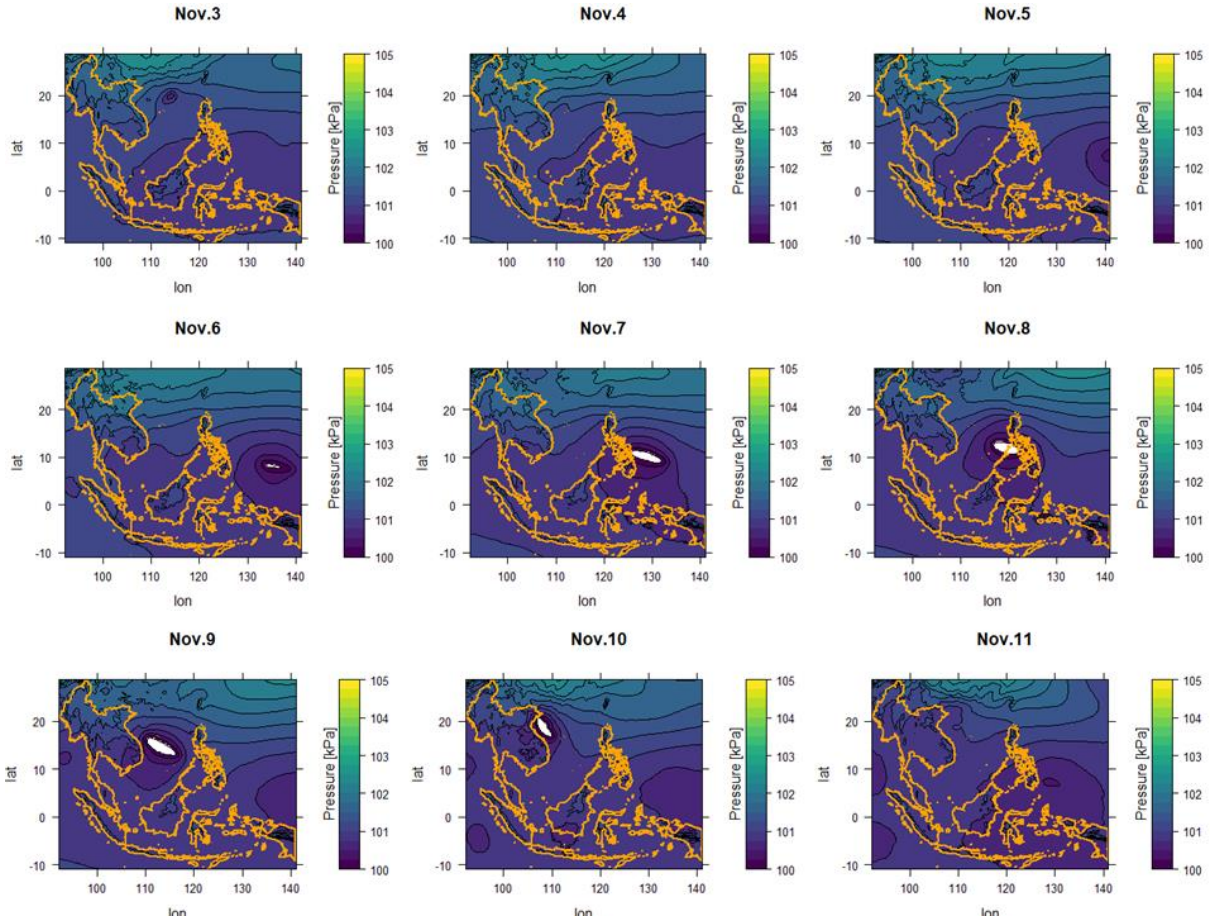

Figure 47. Cyclonic Formation of Low Pressure in SE Asia from ERA5 Absolute Pressure Values [Nov.3-11]

Building from this, the annual timeseries of the spatial mean for SE Asia and the Philippines, are plotted for each day (from 3 to 11 November) with various atmospheric variables, to inspect any temporal trends or notable maxima/minima. The timeseries for windspeed, as plotted in ***Figure 48*** show that neither of the typhoon days registered as the maximum or minimum among all the years considered (1981-2020). However, for the daily mean anomalies during the typhoon period

itself, there is a large disparity of windspeed anomaly observed in the Philippines during the landfall days [Nov. 7 & 8], as shown in ***Figure 49*** [right plot, left panel], compared to the mean values in SE Asia. From the maps of absolute and anomaly values ***[Figure 50]*** the concentration of high windspeed is also evident in the Philippines for these days. It can also be noted from the timeseries plot that Philippines has a higher mean windspeed values than SE Asia.

The same is true for the timeseries of Pressure in ***Figure 51*** where neither of the typhoon days registered as the maximum or minimum among all the years considered. For Nov. 7 & 8, pressure registered a negative anomaly for both locations ***[Figure 52],*** although a dip in pressure anomaly is more observed toward the last day of the typhoon in the whole SE Asian region than in the Philippines. The concentration of low-pressure values is also evident in the Philippines as visually shown in the map in ***Figure 53.*** From the timeseries plot, but both locations follow a more uniform range for mean pressure values.

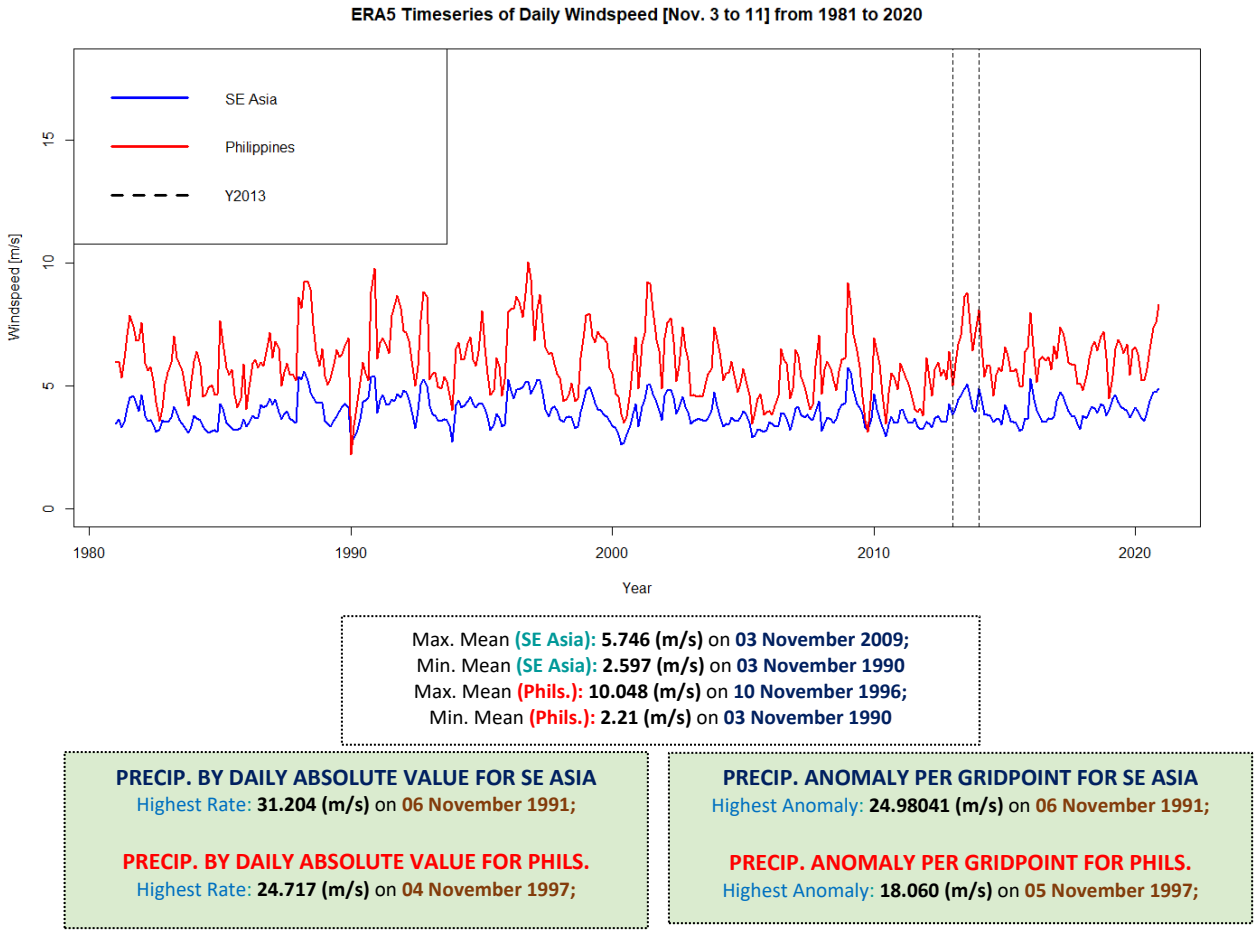

Figure 48. ERA5 Timeseries of Daily Mean Windspeed (Absolute Values) [Nov.3-11]

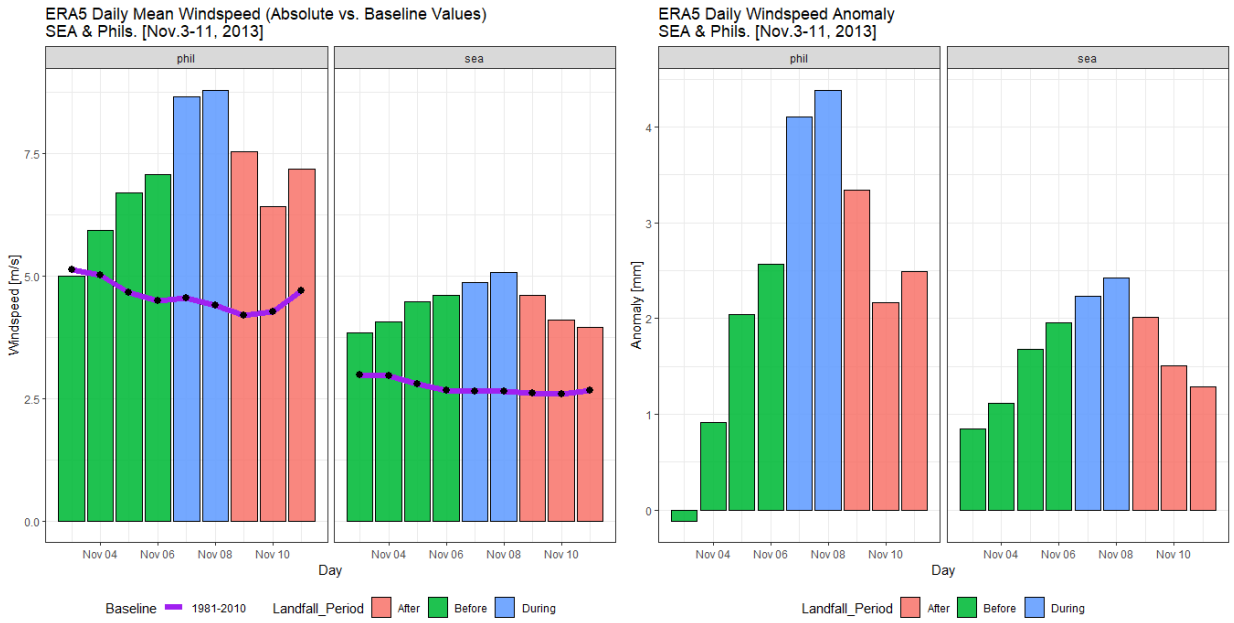

Figure 49. ERA5 Plot of Daily Windspeed (Absolute Values &Anomalies) during the Typhoon Period

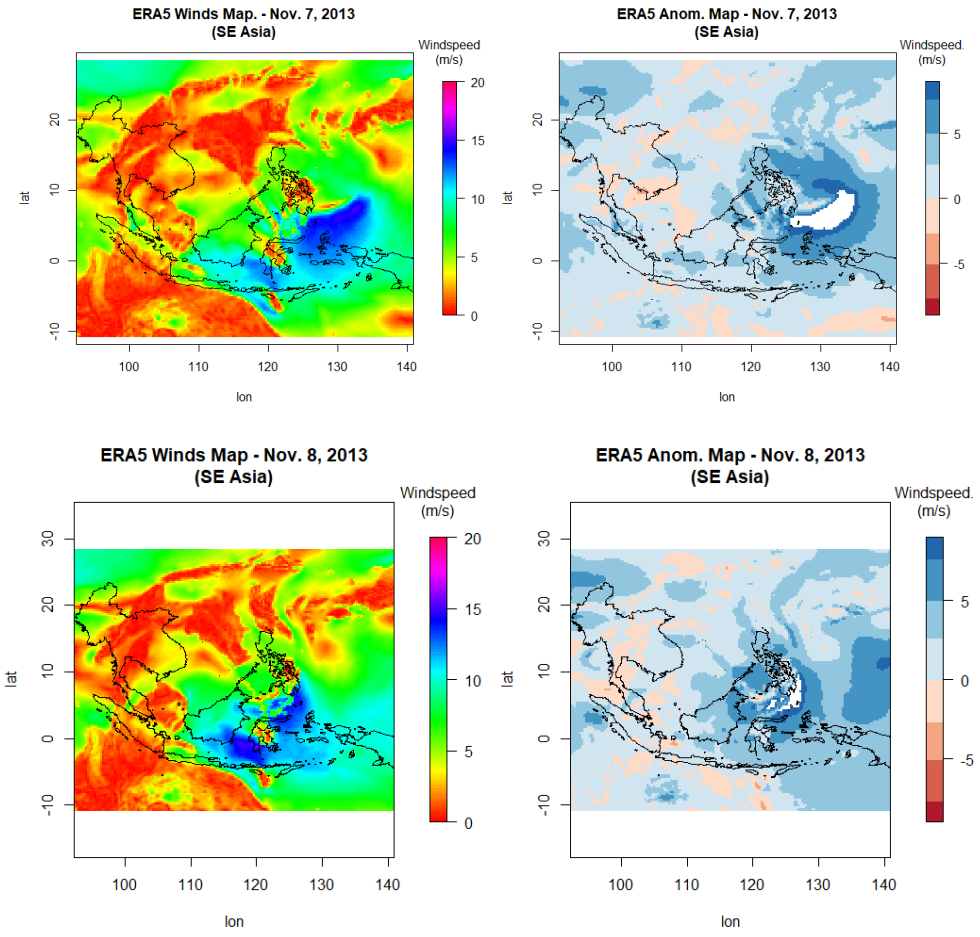

Figure 50. SE Asian Maps of Daily Windspeed (Absolute & Anomalies) for ERA5 on Nov. 7 & 8

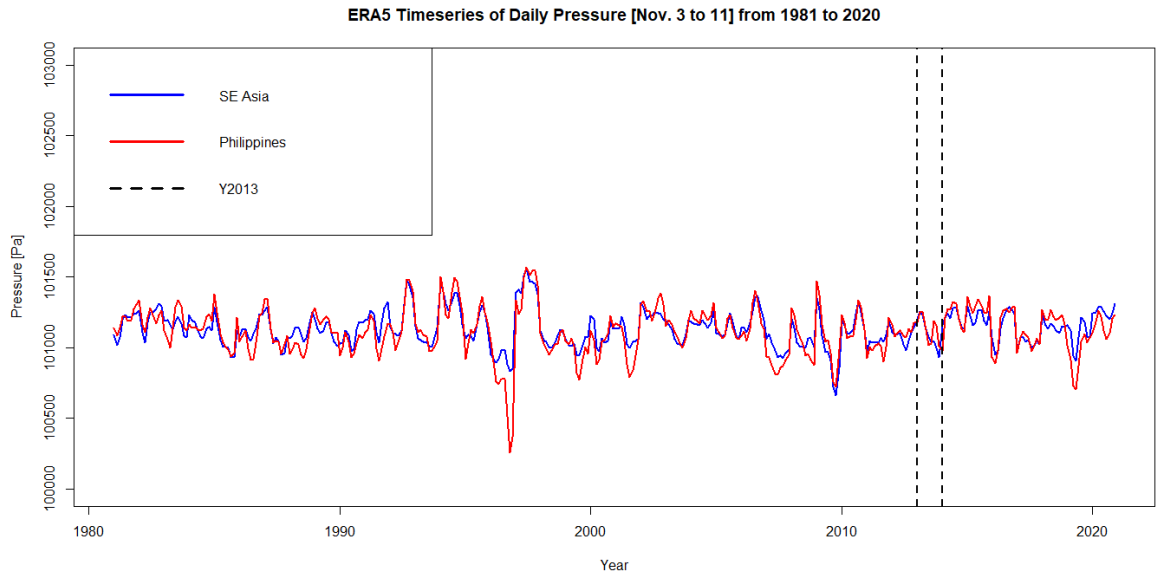

Max. Mean (SE Asia): **101561 (Pa)** on **07 November 1997**
Min. Mean (SE Asia): **100663 (Pa)** on **10 November 2009**
Max. Mean (Phils.): **101568 (Pa)** on **07 November 1997**
Min. Mean (Phils.): **100258 (Pa)** on **10 November 1996**

PRECIP. BY DAILY ABSOLUTE VALUE FOR SE ASIA
Highest Rate: **104099.4 (Pa)** on **08 November 2002**

PRECIP. BY DAILY ABSOLUTE VALUE FOR PHILS.
Highest Rate: **103276.5 (Pa)** on **09 November 2002**

PRECIP. ANOMALY PER GRIDPOINT FOR SE ASIA
Highest Anomaly: **2022.023 (Pa)** on **09 November 2002**

PRECIP. ANOMALY PER GRIDPOINT FOR PHIL.
Highest Anomaly: **1343.148 (Pa)** on **09 November 2002**

Figure 51. ERA5 Timeseries of Daily Mean Pressure (Absolute Values) [Nov.3-11]

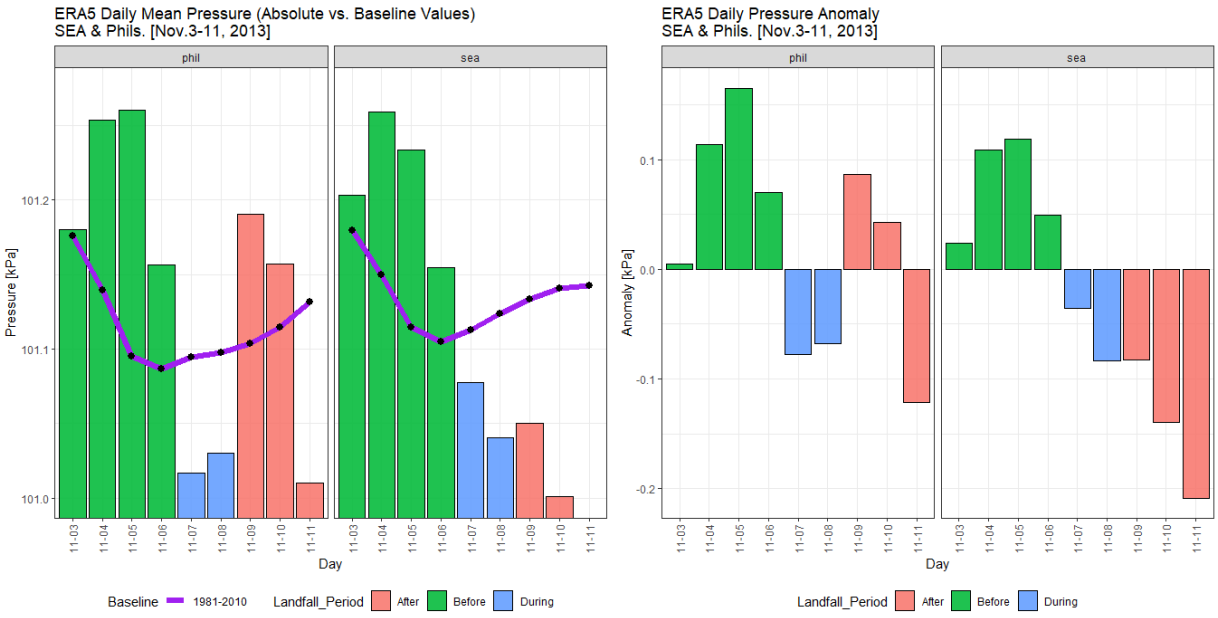

Figure 52. ERA5 Plots of Daily Mean Pressure (Absolute & Anomalies) during the Typhoon Period

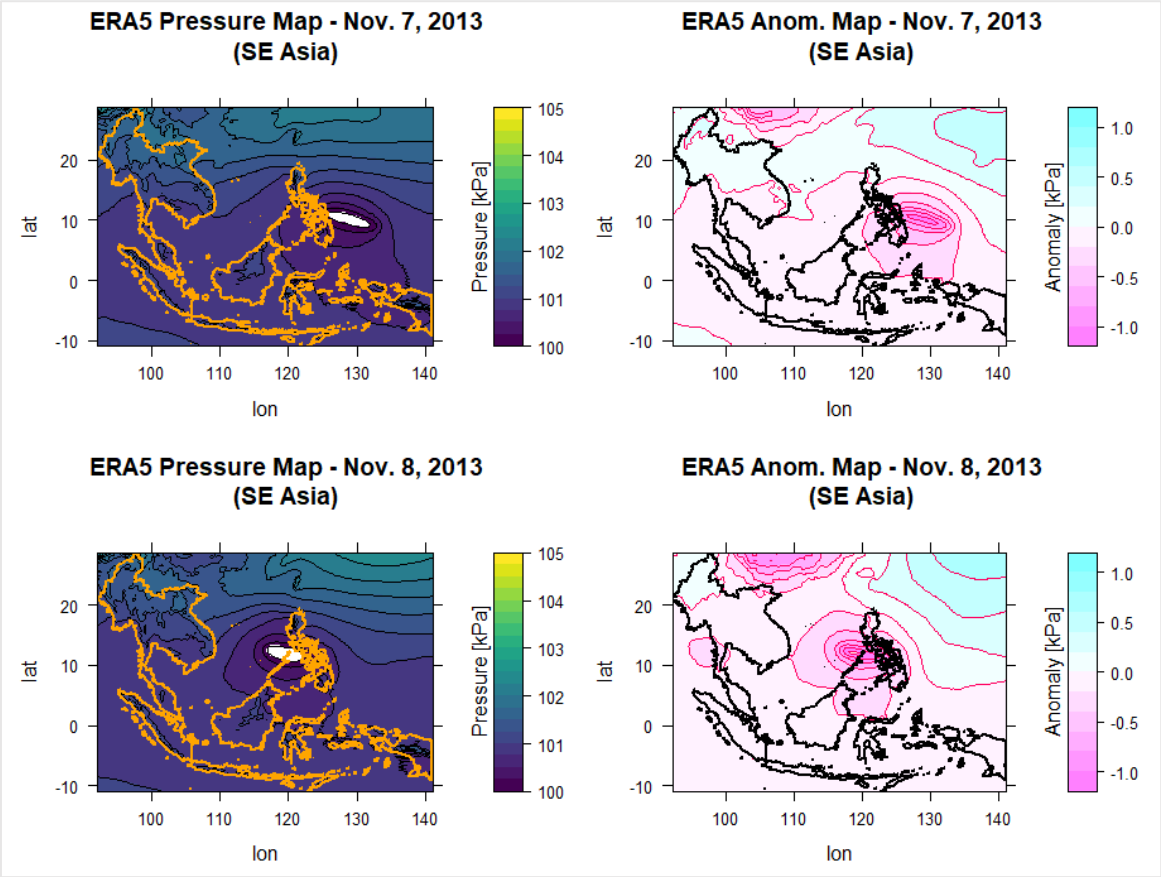

Figure 53. SE Asian Maps of Daily Mean Pressure (Absolute & Anomalies) for ERA5 on Nov. 7 & 8

For precipitation, two datasets are plotted and compared [GPCP and ERA5]. As discussed in the *Methods Section*, GPCP only has available daily data from 1996 hence the timeseries is from 1996 to 2021, and climatology reference value is likewise computed directly from this 26-yr period. As seen from the timeseries plots ***Figure 54*** for GPCP and ***Figure 55*** for ERA5, neither of the typhoon days registered as the maximum or maximum considering the mean daily absolute and anomaly values. However, upon investigation of the local values (analysis at grid point level), it was found that for GPCP the highest absolute precipitation for Philippines and the highest anomaly for SE Asia falls on the same day when Typhoon Haiyan made landfall (November 8, 2013). Extracting the coordinates where these values are observed, the map (see ***Figure 56***) shows that the point falls within the Philippines. ERA5 otherwise recorded it on a different day and year (17 November 2019), but the location of highest absolute value and highest anomaly are on the same spot, as shown in ***Figure 57.***

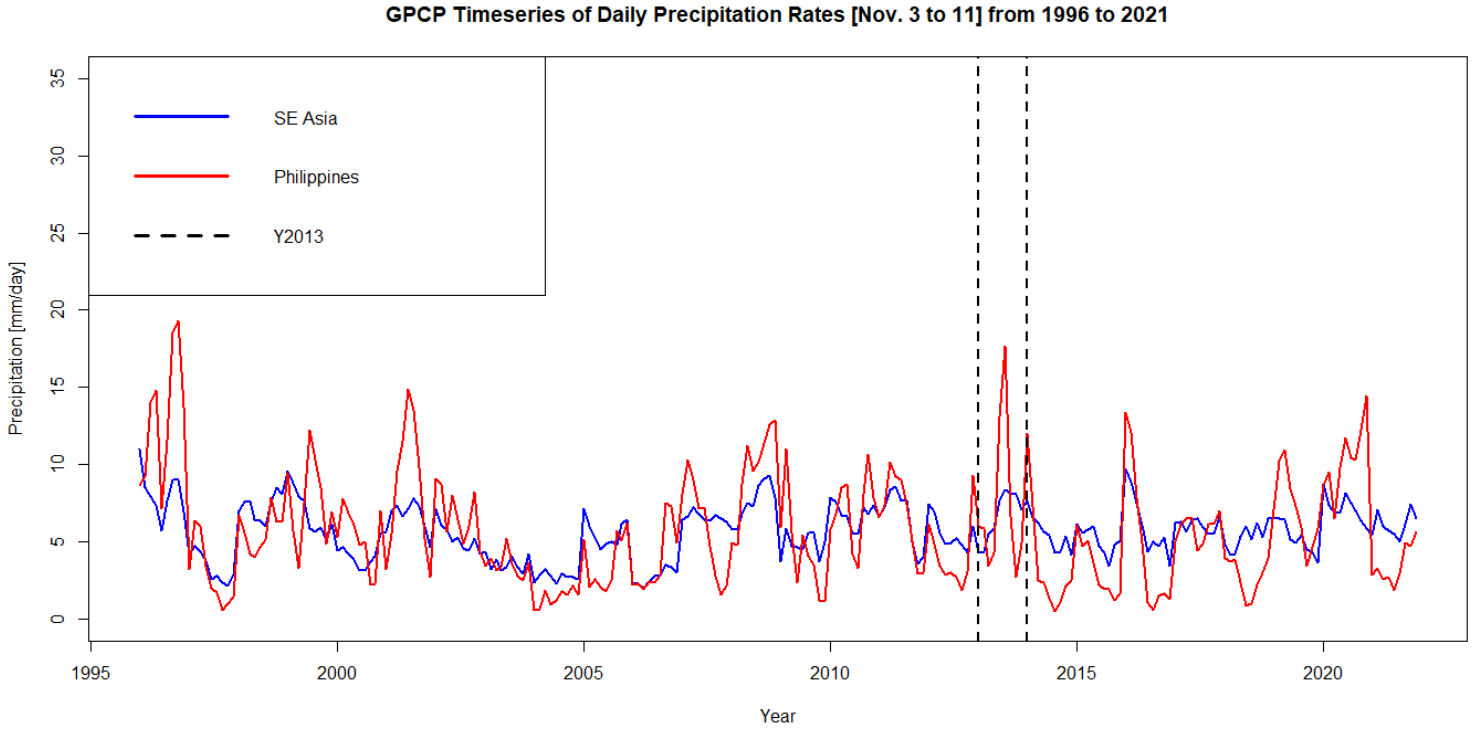

Max. Mean (SE Asia): **10.989 (mm/day)** on **03 November 1996**
Min. Mean (SE Asia): **2.005 (mm/day)** on **05 November 2006**
Max. Mean (Phils.): **19.332 (mm/day)** on **10 November 1996**
Min. Mean (Phils.): **0.501 (mm/day)** on **08 November 2014**

PRECIP. BY DAILY ABSOLUTE VALUE FOR SE ASIA / PHILS.

Highest Rate: **99.978 (mm/day)** on **08 November 2013**
at ***latitude 12^0, longitude 120^0***

PRECIP. ANOMALY PER GRIDPOINT FOR SE ASIA
Highest Anomaly: **93.40 (mm)** on **10 November 1996**

PRECIP. ANOMALY PER GRIDPOINT FOR PHIL.
Highest Anomaly: **90.216 (mm)** on **08 November 2013**
at ***latitude 13^0, longitude 133^0***

Figure 54. GPCP Timeseries of Daily Mean Precip. (Absolute & Values) [Nov.3-11]

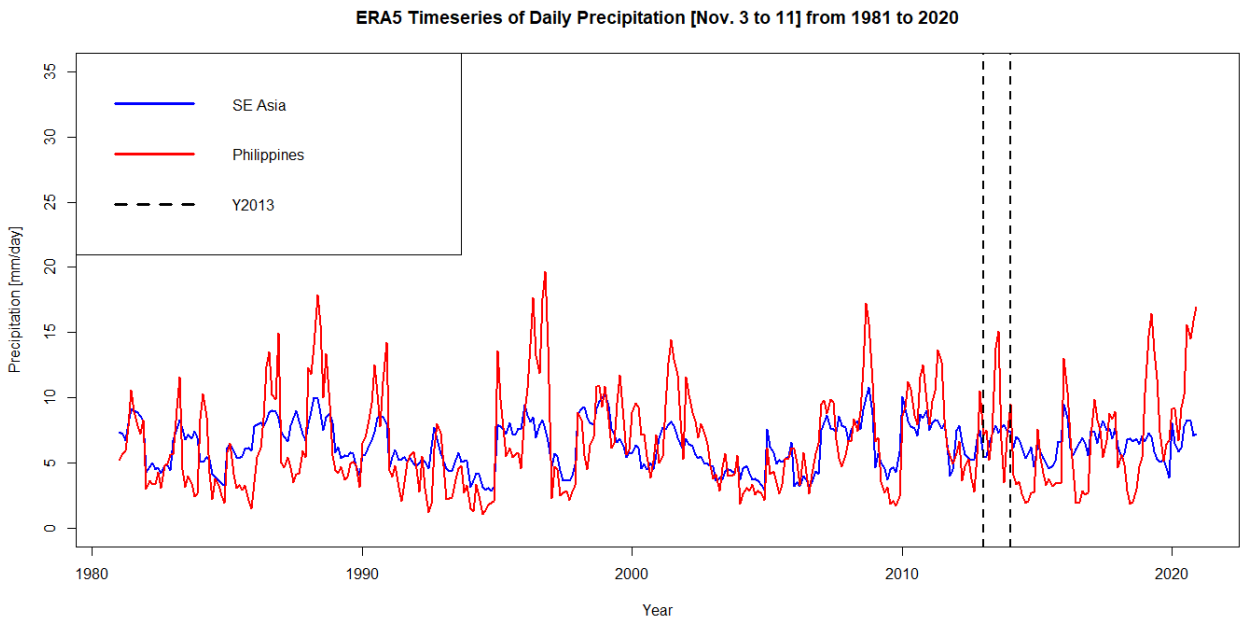

Max. Mean (SE Asia): **10.835 (mm/day)** on **10 November 2008**
Min. Mean (SE Asia): **2.843 (mm/day)** on **10 November 1994**
Max. Mean (Phils.): **19.641 (mm/day)** on **10 November 1996**
Min. Mean (Phils.): **1.056 (mm/day)** on **07 November 1994**

PRECIP. BY DAILY ABSOLUTE VALUE FOR SE ASIA / PHILS.

Highest Rate: **470.490 (mm/day)** on **07 November 2019**
at ***latitude 12.787^0, longitude 116.156^0***

PRECIP. ANOMALY PER GRIDPOINT FOR SE ASIA /PHIL.
Highest Anomaly: **462 (mm)** on **07 November 2019**
at ***latitude 12.787^0, longitude 116.156^0***

Figure 55. ERA5 Timeseries of Daily Mean Precip. (Absolute Values) [Nov.3-11]

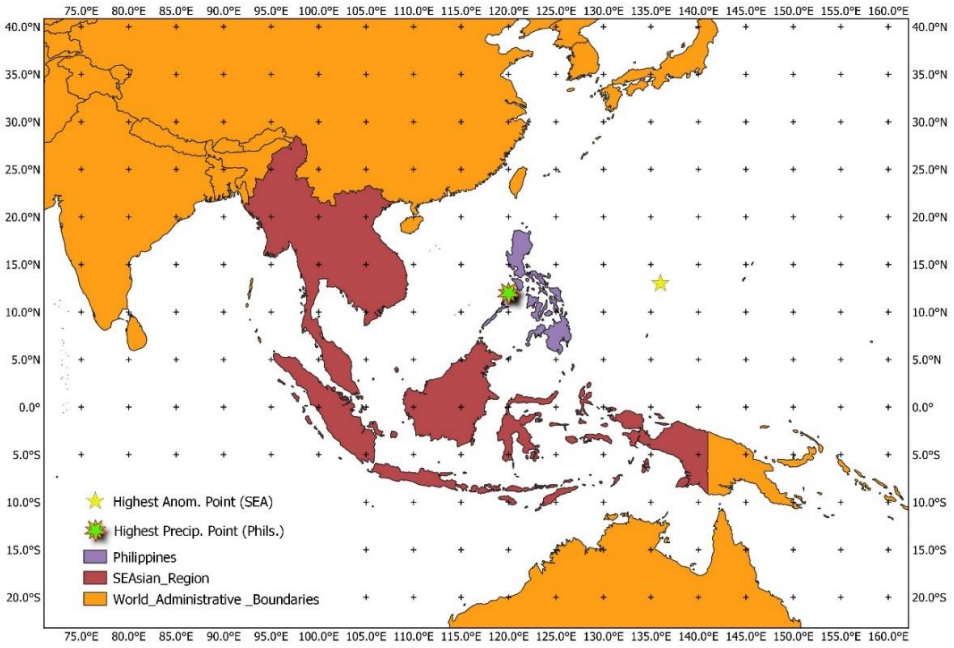

Figure 56. Map Showing the Grid point with Highest Absolute Precipitation & Precipitation Anomaly for GPCP

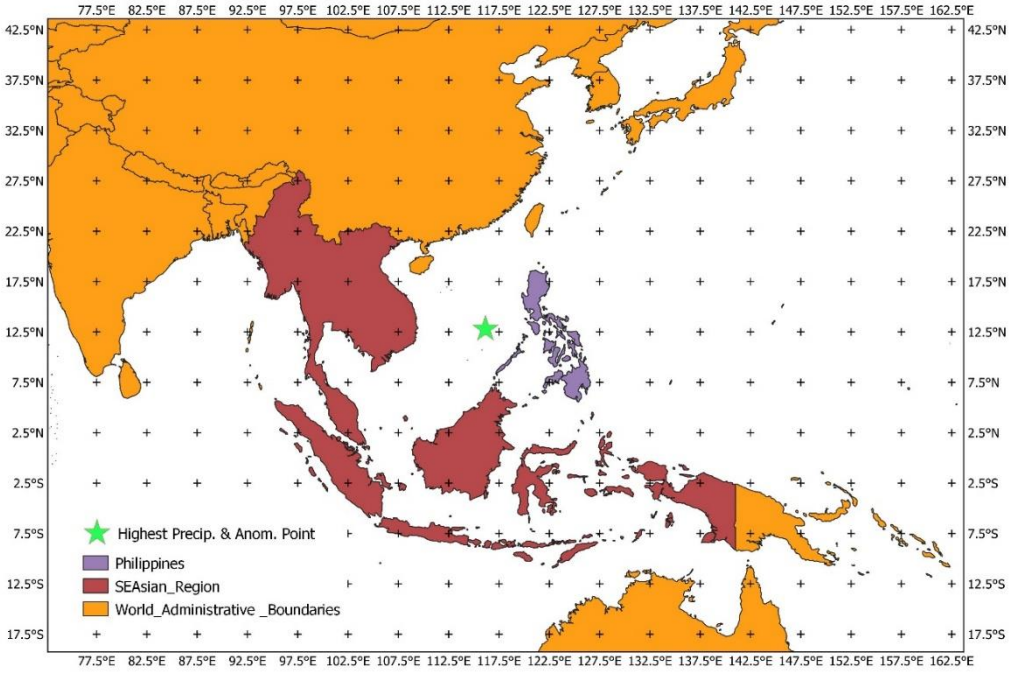

Figure 57. Map Showing the Grid point with Highest Absolute Precipitation & Anomaly for ERA5

For the spatially-averaged mean anomalies of the days when Typhoon Haiyan occurred, the highest positive precipitation anomaly is observed during the landfall days (November 7 & 8) for both GPCP

and ERA5, as shown in ***Figure 58.*** Again, the disparity of anomalies for these days is large, comparing Philippines and SE Asia.

Based on the timeseries plots, the daily mean values for Philippine precipitation are again higher than the spatial mean for the whole SE Asian region. From the maps, it is also clear that large precipitation anomalies for these two days are concentrated within the Philippines, as seen in ***Figure 59.*** Between GPCP and ERA5 the location of the major spatial structures varied – as GPCP is more concentrated on the central part of the country (Visayas Islands) where the Typhoon made several landfalls, while ERA5 is more concentrated on the southern part.

Figure 58. GPCP and ERA5 Plots of Daily Mean Precip. (Absolute & Anomalies) during the Typhoon Period

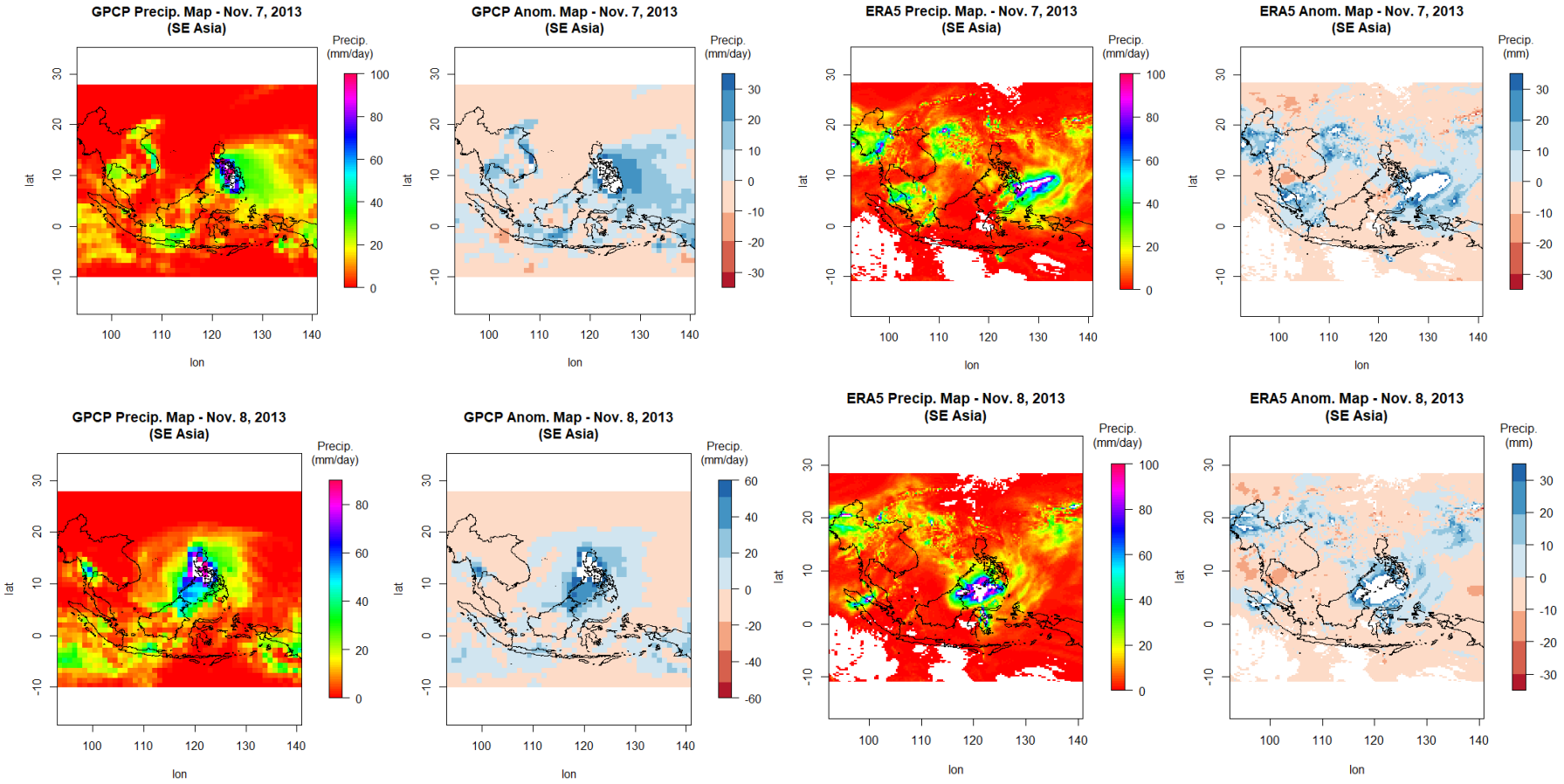

Figure 59. SE Asian Maps of Daily Mean Pressure (Absolute & Anomalies) for GPCP and ERA5 on Nov. 7 & 8

For the runoff, there is a very high anomaly on the 8th November for the Philippines, while SE Asia registered the highest positive anomaly on the last day of the typhoon period, as shown in the plots and Figures that follow. The runoff anomalies for Nov. 7 and 8, however, is not evident in the maps due to trivial differences across each grid point.

Based on the timeseries plot, the Philippines again has higher runoff mean values compared to the spatial mean of the entire SE Asia region.

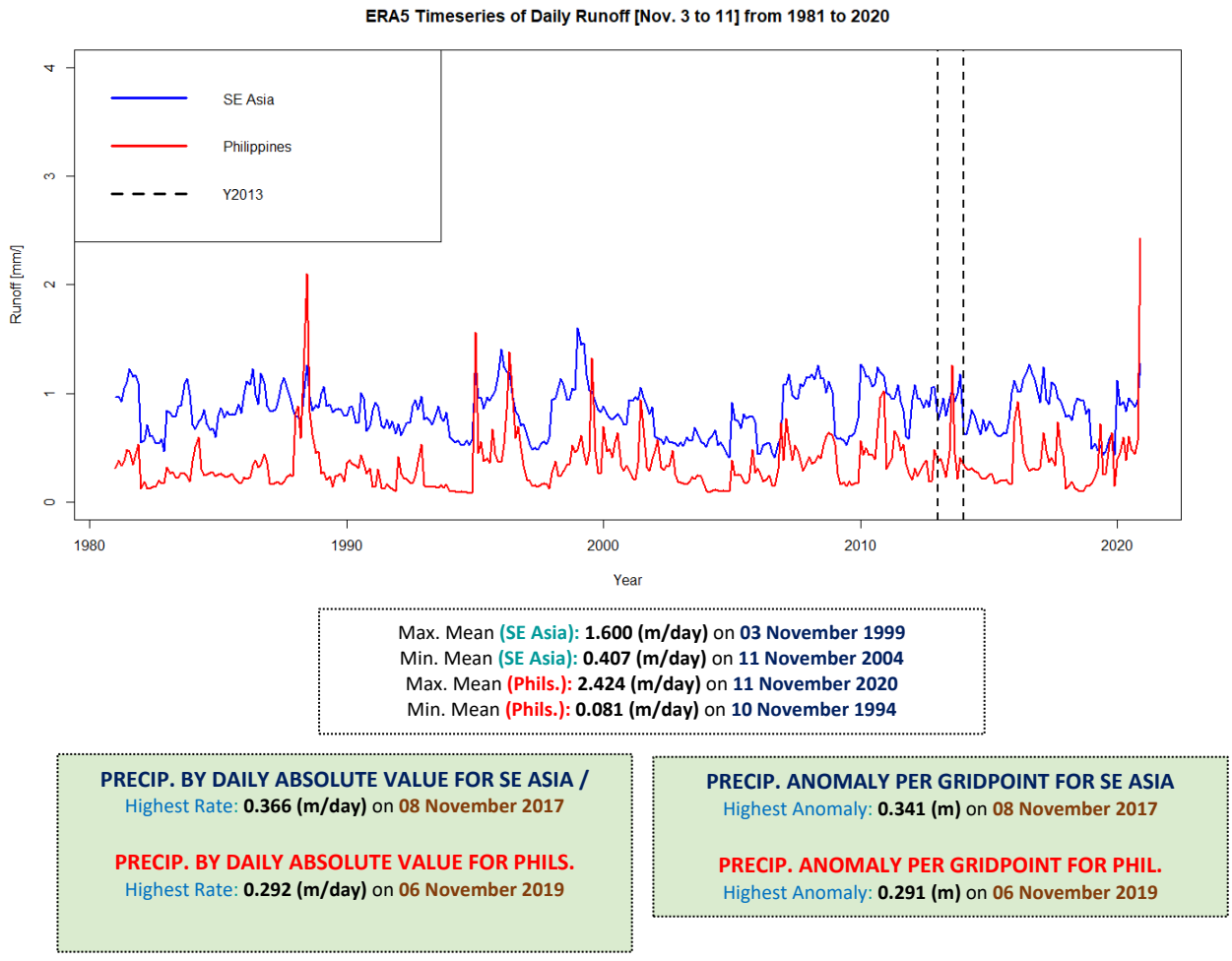

Figure 60. ERA5 Timeseries of Daily Mean Runoff (Absolute Values) [Nov.3-11]

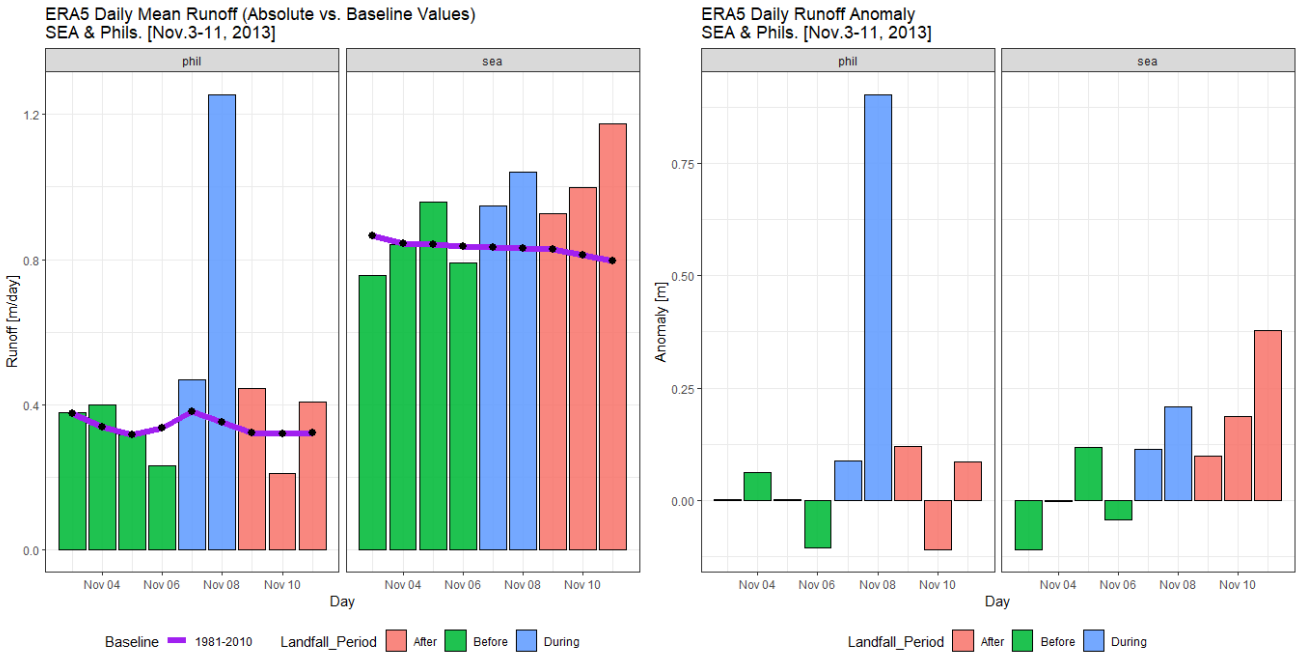

Figure 61. ERA5 Plots of Daily Mean Runoff (Absolute & Anomalies) during the Typhoon Period

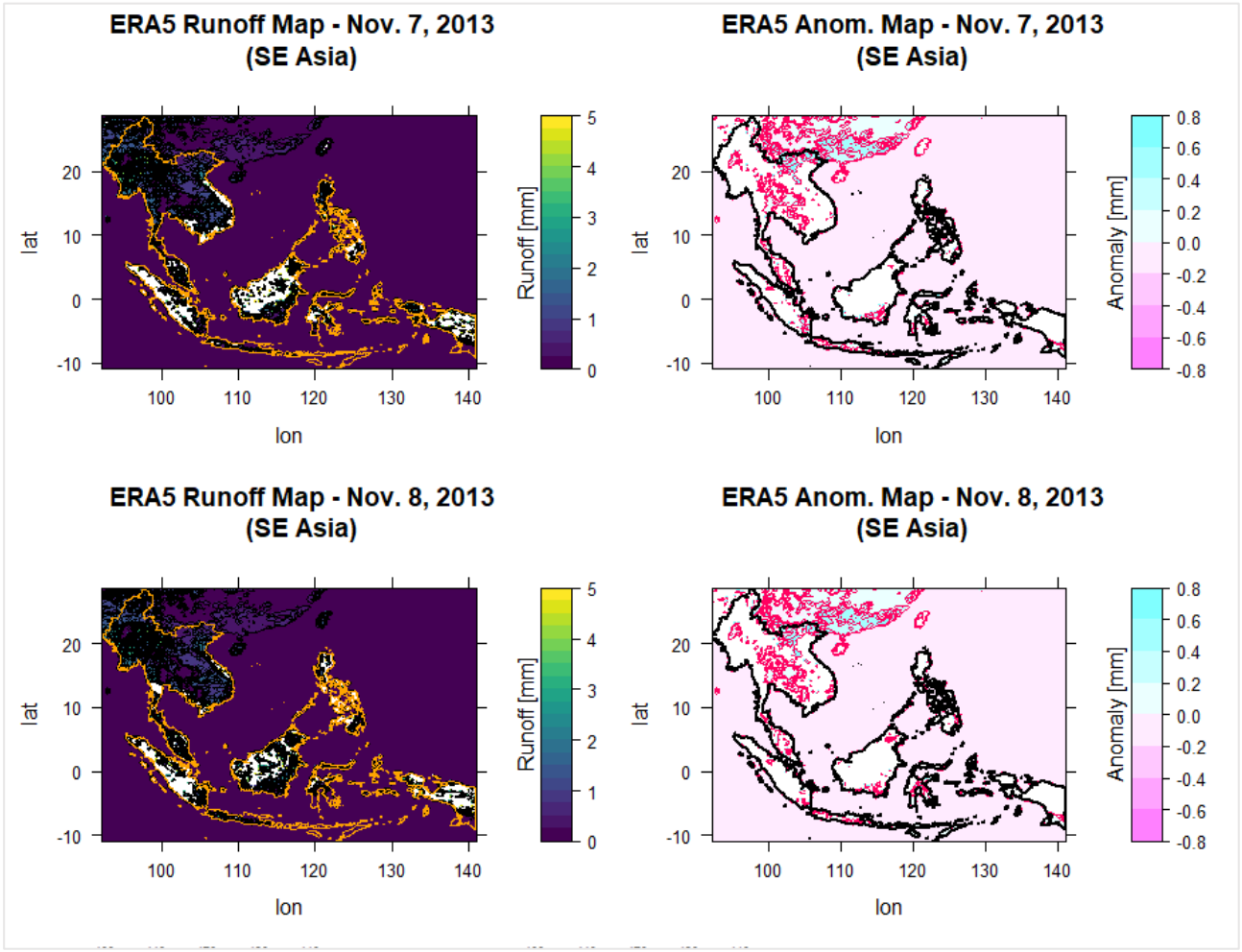

Figure 62. SE Asian Maps of Daily Mean Runoff (Absolute & Anomalies) for ERA5 on Nov. 7 & 8

Inspecting the rank and percentile of the absolute values for the two landfall days (Nov. 7 & 8, 2013) which also registered high anomalies, **Table 25** shows that November 7 and 8 ranked top, when comparing the same days across the 40 years. This is a clear indication that indeed, the typhoon occurrence has significantly affected the climate variables, most particularly with the windspeed and precipitation -- both in the Philippines and throughout the SE Asian region.

Table 25. Rank and Percentile of Nov. 7 and 8 2013 Absolute Values

Variable	SE ASIA				PHILIPPINES			
	Nov. 7		Nov. 8		Nov. 7		Nov. 8	
	Rank	*Percentile*	*Rank*	*Percentile*	*Rank*	*Percentile*	*Rank*	*Percentile*
Windspeed	2	0.975	**1**	**1**	3	0.95	**1**	**1**
Pressure	19	0.525	16	0.6	12	0.7	17	0.575
Precipitation								
GPCP	2	0.961	2	0.961	2	0.961	**1**	**1**
ERA5	9	0.8	14	0.675	3	0.95	2	0.975
Runoff	18	0.575	7	0.85	9	0.8	2	0.975

Previous studies identified connections between the impact of a typhoon in terms of precipitation and flooding, and its magnitude, which can be described through physical variables such as atmospheric pressure anomalies and wind speed. Therefore, to understand how the typhoon event in terms of windspeed and pressure has impacted the precipitation and runoff values, the daily precipitation and runoff values (response variables) for the whole month of November 2013 are regressed with wind speed and pressure (regressors) using different fitted models. For precipitation, the following models are regressed:

Fitted model 1 (fit1): $\text{Precip}=\beta_0 + \beta_1\text{Wind.Speed} + \beta_2\text{Pressure} + \epsilon$
Fitted model 2 (fit2): $\text{Precip}=\beta_0 + \beta_1\text{Wind.Speed} + \beta_2\text{Pressure} + \beta_3\text{Time} + \epsilon$
Fitted model 3 (fit3): $\text{Precip}=\beta_0 + \beta_1\text{Pressure} + \epsilon$
Fitted model 4 (fit5): $\text{Precip}=\beta_0 + \beta_1\text{Pressure} + \beta_2\text{Time} + \epsilon$
Fitted model 5 (fit4): $\text{Precip}=\beta_0 + \beta_1\text{Wind.Speed} + \epsilon$
Fitted model 6 (fit6): $\text{Precip}=\beta_0 + \beta_1\text{Wind.Speed} + \beta_2\text{Time} + \epsilon$

The values of R^2, adjusted R^2 and AIC as well as the mean of residuals and correlation between residuals and fitted values of the fitted models, are summarized in the following table.

Table 26. Summary of R^2, Adjusted R^2, and AIC for Precipitation Regression Models

Fitted Model	R^2	Adjusted R^2	AIC
Fit1	0.378	0.332	-269.12
Fit2	***0.385***	***0.314***	***-267.487***
Fit3	0.171	0.141	-262.495
Fit4	***0.178***	***0.117***	***-260.753***
Fit5	0.126	0.095	-260.941
Fit6	***0.214***	***0.155***	***-262.094***

LEGEND:

	Regressed with wind speed + pressure / ***[+ time in italics]***
	Regressed with pressure only / ***[+ time in italics]***
	Regressed with wind speed only / ***[+ time in italics]***

As shown, models 1 and 2 *[a) regressed by wind speed + pressure, and b) with time as additional regressor]* give the best R^2 among the fitted models. However, adding the time as a regressor did not result to a noticeable improvement in the adjusted R^2 and AIC.

Also investigating the mean and correlation of residuals, the two best models *[according to R^2, adjusted R^2 and AIC as above]* have zero mean and very low correlation. In addition, the plots of residuals vs. fitted values for these models do not show any visible pattern, thus providing further indication of a good fit. However, upon inspection of the summary of coefficients [**Table 27] ,** the p-value for time is not significant, hence, fit 1 [i.e., regressing with windspeed + pressure only without adding time] is the better model.

Since the values as shown in above table are short of 40% of variance, these are not very useful in getting relevant info of the typhoon event predictors, and the significance of the regression using p-values prevail.

Table 27. Summary of Coefficients and p-values for Precipitation Regression Models

Fitted Model	Summary of coefficients

Fit1	`> summary(fit1)$coefficients`
	`Estimate Std. Error t value Pr(>|t|)`
	`(Intercept) 1.395802e+00 4.227670e-01 3.301587 0.002709799`
	`pres_vec_long4 -1.381787e-05 4.183942e-06 -3.302595 0.002702898`
	`ws_vec_long2 1.327285e-03 4.425753e-04 2.999003 0.005759768`

Fit2	`> summary(fit2)$coefficients`
	`Estimate Std. Error t value Pr(>|t|)`
	`(Intercept) 1.822648e+00 8.676253e-01 2.100732 0.045511618`
	`pres_vec_long4 -1.266822e-05 4.699823e-06 -2.695468 0.012158640`
	`ws_vec_long2 1.328761e-03 4.482639e-04 2.964238 0.006418132`
	`t -3.923344e-10 6.935907e-10 -0.565657 0.576476612`

Fit3	`> summary(fit3)$coefficients`
	`Estimate Std. Error t value Pr(>|t|)`
	`(Intercept) 1.131266e+00 4.687836e-01 2.413195 0.02260622`
	`pres_vec_long4 -1.111623e-05 4.632489e-06 -2.399623 0.02330916`

Fit4	`> summary(fit4)$coefficients`
	`Estimate Std. Error t value Pr(>|t|)`
	`(Intercept) 1.544805e+00 9.790565e-01 1.5778504 0.1262458`
	`pres_vec_long4 -9.998742e-06 5.235803e-06 -1.9096866 0.0668518`
	`t -3.803654e-10 7.872645e-10 -0.4831481 0.6328854`

Fit5	`> summary(fit5)$coefficients`
	`Estimate Std. Error t value Pr(>|t|)`
	`(Intercept) -0.0003928761 0.0033973605 -0.1156416 0.90876200`
	`ws_vec_long2 0.0010125772 0.0005028763 2.0135711 0.05375607`

Fit6	`> summary(fit6)$coefficients`
	`Estimate Std. Error t value Pr(>|t|)`
	`(Intercept) 1.661583e+00 9.607607e-01 1.729445 0.09514831`
	`ws_vec_long2 1.097235e-03 4.883444e-04 2.246847 0.03302776`
	`t -1.200809e-09 6.941639e-10 -1.729864 0.09507224`

The mean runoff values for all November days are also regressed with the following models, adding precipitation as a regressor:

Fitted model 1 (fit1): Runoff=β_0 + β_1Wind.Speed + β_2Pressure +ϵ

Fitted model 2 (fit2): Runoff =β_0 + β_1Wind.Speed + β_2Pressure+ β_3Time +ϵ

Fitted model 3 (fit3): Runoff =β_0 + β_1Pressure + ϵ

Fitted model 4 (fit5): Runoff =β_0 + β_1Pressure + β_2Time + ϵ

Fitted model 5 (fit4): Runoff =β_0 + β_1Wind.Speed + ϵ

Fitted model 6 (fit6): Runoff=β_0 + β_1Wind.Speed + β_2Time + ϵ

Fitted model 7 (fit7): Runoff=β_0 + β_1Wind.Speed + β_2Pressure + β_3Precipitation + ϵ

Fitted model 8 (fit8): Runoff=β_0 + β_1Wind.Speed + β_2Pressure + β_3Precipitation +β_4Time + ϵ

The values of R^2, adjusted R^2 and AIC of the fitted models, are then summarized in the following table.

Table 28. Summary of R^2, Adjusted R^2, and AIC for Runoff Regression Models

Fitted Model	R^2	Adjusted R^2	AIC
Fit1	0.31	0.259	-424.632
Fit2	***0.311***	***0.231***	***-422.645***
Fit3	0.076	0.043	-417.86
Fit4	***0.076***	***0.56***	***-415.874***
Fit5	0.171	0.141	-421.107
Fit6	***0.192***	***0.132***	***-419.888***
Fit7	0.658	0.618	-443.635
Fit8	***0.664***	***0.611***	***-442.241***

LEGEND:

	Regressed with wind speed + pressure / ***[+ time in italics]***
	Regressed with pressure only / ***[+ time in italics]***
	Regressed with wind speed only / ***[+ time in italics]***
	Regressed with wind speed + pressure + precipitation / ***[+ time in italics]***

Based on above reflected values, models 7 and 8 *[a) runoff regressed by wind speed + pressure + precipitation, and b) with time as additional regressor]* gives the highest R^2 . However, adding the time again did not improve the adjusted R^2 value and the AIC. The mean of residuals and correlation for these models also indicate that this is a good fitting, with zero mean and negative correlation. Looking at the summary of coefficients, only fit 1 (regressed with windspeed + pressure) gave significant p-values among all the models, indicating that despite fit 7 and 8 having high R^2, adjusted R^2 and minimum AIC, the model may not be a good fit in assessing the response from the regressor.

This again demonstrates that, beyond statistical aspects (significance) the results are not supporting any useful connection in practical terms (with fit 1 just 30% of variance explained).

Table 29. Summary of Coefficients and p-values for Runoff Regression Models

Fitted Model	Summary of coefficients & p-values

Fit1	`> summary(fit1_2)$coefficients`
	`Estimate Std. Error t value Pr(>|t|)`
	`(Intercept) 7.378632e-02 3.165691e-02 2.330812 0.027478316`
	`pres_vec_long4 -7.320328e-07 3.132947e-07 -2.336563 0.027131198`
	`ws_vec_long2 1.003535e-04 3.314016e-05 3.028153 0.005361928`

Fit2	`> summary(fit2_2)$coefficients`
	`Estimate Std. Error t value Pr(>|t|)`
	`(Intercept) 6.775522e-02 6.535242e-02 1.0367668 0.309391347`
	`pres_vec_long4 -7.482767e-07 3.540062e-07 -2.1137387 0.044288394`
	`ws_vec_long2 1.003326e-04 3.376472e-05 2.9715218 0.006306051`
	`t 5.543474e-12 5.224355e-11 0.1061083 0.916310890`

Fit3	`> summary(fit3_2)$coefficients`
	`Estimate Std. Error t value Pr(>|t|)`
	`(Intercept) 5.378524e-02 3.518821e-02 1.528502 0.1376075`
	`pres_vec_long4 -5.277672e-07 3.477276e-07 -1.517760 0.1402858`

Fit4	`> summary(fit4_2)$coefficients`
	`Estimate Std. Error t value Pr(>|t|)`
	`(Intercept) 4.677572e-02 7.379160e-02 0.6338895 0.5314870`
	`pres_vec_long4 -5.467087e-07 3.946230e-07 -1.3853947 0.1772712`
	`t 6.447234e-12 5.933621e-11 0.1086560 0.9142788`

Fit5	`> summary(fit5_2)$coefficients`
	`Estimate Std. Error t value Pr(>|t|)`
	`(Intercept) -1.802919e-04 0.0002354072 -0.7658726 0.45016057`
	`ws_vec_long2 8.368112e-05 0.0000348449 2.4015310 0.02320916`

Fit6	`> summary(fit6_2)$coefficients`
	`Estimate Std. Error t value Pr(>|t|)`
	`(Intercept) 5.824156e-02 6.925778e-02 0.8409389 0.40776832`
	`ws_vec_long2 8.665701e-05 3.520299e-05 2.4616380 0.02050595`
	`t -4.221090e-11 5.003978e-11 -0.8435470 0.40633427`

Fit7	`> summary(fit7_2)$coefficients`
	`Estimate Std. Error t value Pr(>|t|)`
	`(Intercept) -3.751556e-04 2.693251e-02 -0.013929471 9.889926e-01`
	`pres_vec_long4 2.135115e-09 2.665627e-07 0.008009803 9.936703e-01`
	`ws_vec_long2 2.983245e-05 2.747614e-05 1.085758442 2.875505e-01`
	`prcp_vec_long3 5.313179e-02 1.034793e-02 5.134534965 2.357031e-05`

Fit8	`> summary(fit8_2)$coefficients`
	`Estimate Std. Error t value Pr(>|t|)`
	`(Intercept) -3.059403e-02 5.029235e-02 -0.6083237 5.484604e-01`
	`pres_vec_long4 -6.470536e-08 2.849170e-07 -0.2271025 8.221909e-01`
	`ws_vec_long2 2.863328e-05 2.778945e-05 1.0303653 3.127045e-01`
	`prcp_vec_long3 5.395954e-02 1.051089e-02 5.1336788 2.638213e-05`
	`t 2.671366e-11 3.740119e-11 0.7142461 4.816912e-01`

For the plot of individual regression between the variables ***(Figures 63 and 64),*** precipitation and runoff are positively correlated with windspeed, with significant p-values. This means that as windspeed increased, the precipitation and runoff likewise increased and vice versa. Regressing the two response variables (precipitation and runoff) against each other also gave significant p-value with a positive correlation, thereby indicating that precipitation and runoff both increases or decreases congruently. When regressed with pressure, runoff and precipitation are negatively correlated to this variable, but with less significance for precipitation having a p-value slightly higher than 0.05. For runoff, the relationship is not significant. This means that low pressure does not necessarily influence the precipitation and runoff values, as opposed to windspeed.

For the distribution of the regressors, the density plots in ***Figure 65*** reveal that the windspeed values are distributed more symmetrically (bell shaped) than pressure, which is skewed to the right.

Discussion

Based on the results, there are noteworthy changes to the observed variables especially in the Philippines due to the occurrence of Typhoon Haiyan, where very large precipitation anomalies are noted during the landfall days. These anomalies are likewise observed in the SE Asian region, albeit smaller compared to what is diagnosed for the Philippines. It can also be observed that there is an unusual dip in pressure anomaly and high positive runoff anomaly in the SE Asian region at the end of the typhoon period when Haiyan is about to dissipate. Analysis of the impacts of Haiyan on the main continent is beyond the scope of this thesis – which focused on the Philippines - but can be another topic of research in the future.

It was also observed in the timeseries plot for runoff, that there is an oddly high value on November 11, 2020. Upon quick investigation, the strongest Typhoon on record (Goni) occurred on this day, bringing torrential rains that caused flooding in many parts of the Philippines. This could have explained why this day is recorded having the highest daily spatial mean in the country. However, due to the fact the ERA5 are modeled values, there is still uncertainty with the estimates.

On the different highest precipitation day and coordinates recorded by ERA5 (07 November 2019) compared to GPCP, a quick investigation revealed that another typhoon occurred on this day [*International name Nakri (local name Quiel)]*, but with a weaker strength as shown in ***Figure 66***. Jiang, Halverson & Simpson (2008) compared the rainfall potential of two North Atlantic Hurricanes Lili and Isidore in 2002 and found that Isidore produced a much larger volume of total rainfall despite being a relatively weaker storm than Lili, during their landfall on the same area. However, Isidore had a history of producing large volume of rain over the gulf. A similar argument could explain why the grid point is recorded by ERA5 as having the highest absolute precipitation value, on the same day where Typhoon Nakri hit. The observational measurements of GPCP may have not recorded this event, due to their coarser resolution and limited (land-only) coverage compared to ERA5. On the other hand, GPCP data has directly recorded the Typhoon Haiyan precipitation during its landfall.

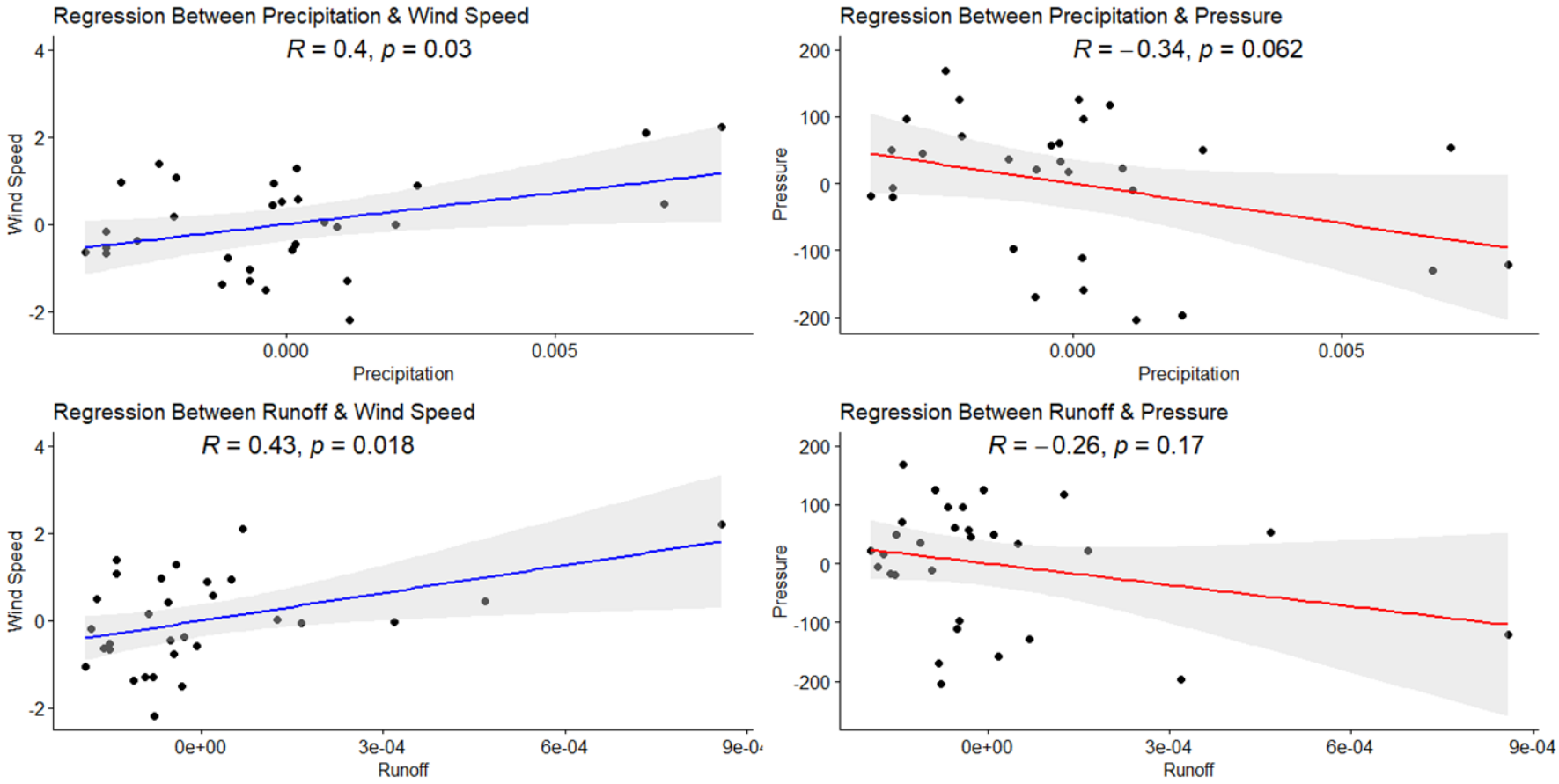

Figure 63. Regression Plots of Precipitation and Runoff against Windspeed and Pressure

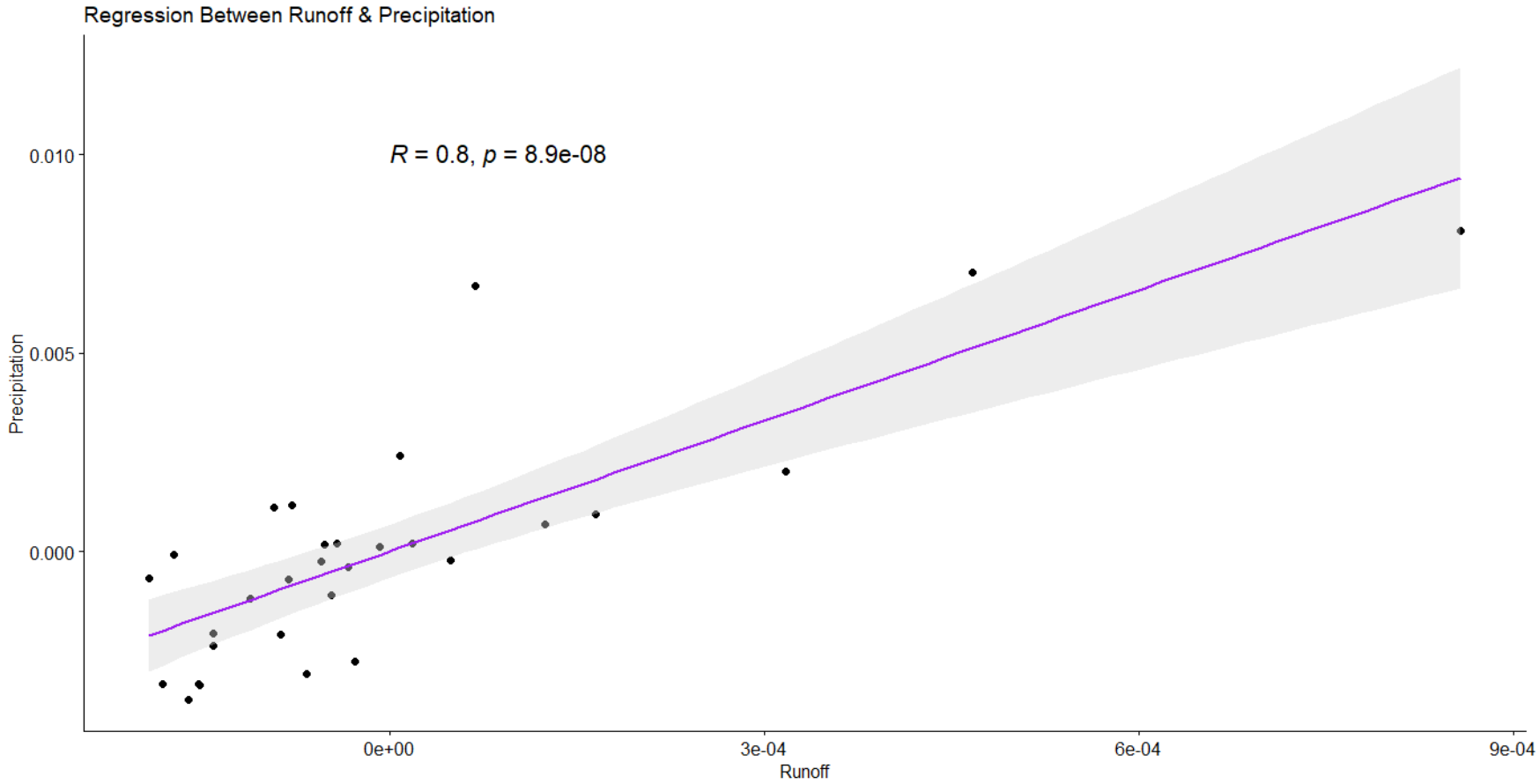

Figure 64. Regression Between Runoff and Precipitation

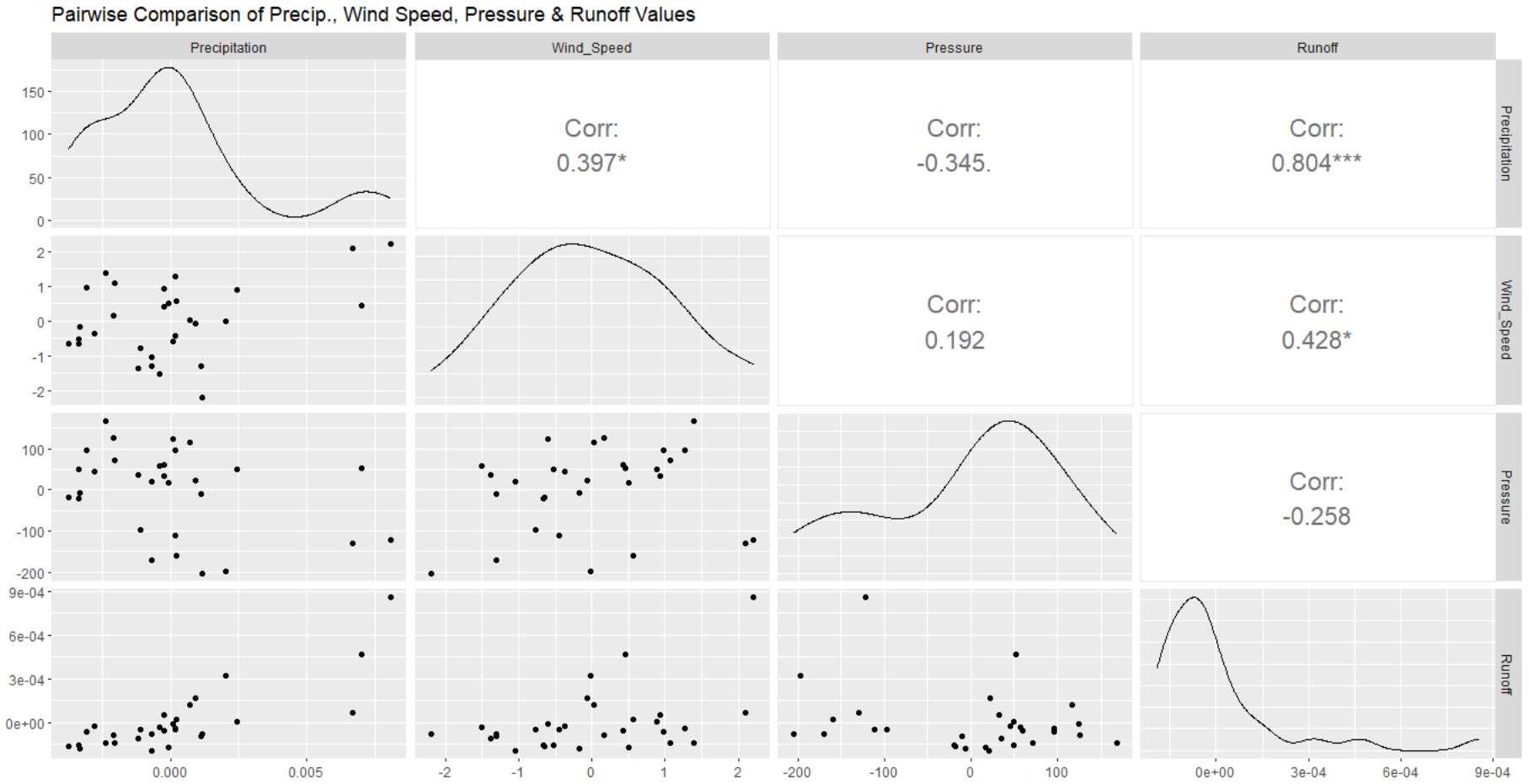

Figure 65. Density Plots, Scatterplots and Correlation of Precipitation and Runoff to Windspeed and Pressure

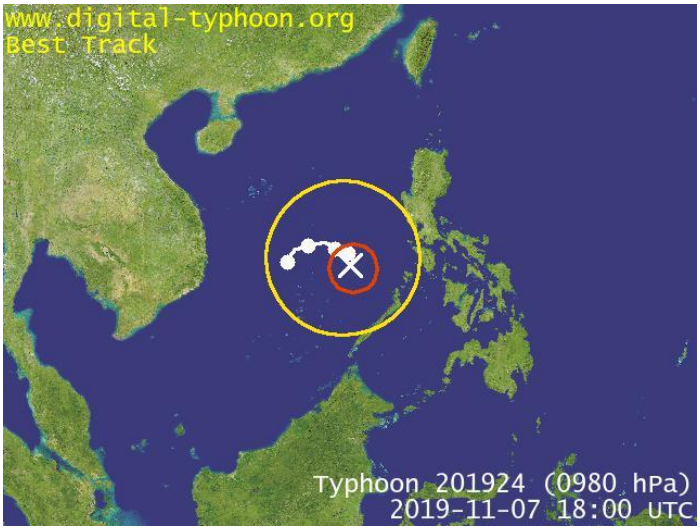

Figure 66. Track of Typhoon Nakri in November 2019[43]

For the regression analysis, it was seen that the best regression model for precipitation and runoff includes both windspeed and pressure as predictors. This model has the best R^2 and adjusted R^2 values among all fitted models, with low AIC. Although the values are not as high, the p-values that are significant for these models still demonstrate that it is the good model for predicting the response. From this multiple regression, the coefficients revealed that windspeed is positively related to precipitation while negatively related to pressure, as expected from fundamental dynamics of rainfall. This means that increase in wind speed during an extreme Typhoon event, together with decrease in pressure, result to increase in precipitation and runoff values. This is in accordance with the findings by Zhang, Chen & Li (2021), where the precipitation induced on land by Typhoon Hato (the strongest Typhoon that made landfall in China) is extremely high, lasting for six days from the formation until its dissipation. Wu & Alshdaifat (2019), however, stated that the accuracy of predicting precipitation induced by typhoons is still difficult because of the nonlinear relationship between the precipitation and the physical processes like the typhoon dynamics, heat, cloud, microphysics, and radiation.

The result also showed that adding time as a regressor has not improved the adjusted R^2 and AIC and does not result to a significant p-value. This confirms that trends do not capture the large variability induced during an extreme event such as a typhoon landfall.

[43] Map credits to Dr. Kitamoto of the National Institute of Informatics (NII) / Research Organization of Information and Systems (ROIS) (Japan). Source: http://agora.ex.nii.ac.jp/cgi-bin/dt/single2.pl?prefix=HMW819110718&id=201924&basin=wnp&lang=en

CHAPTER 4: CONCLUSION

From the results of the analysis, the spatio-temporal anomalies within the focal region (SE Asia) are evident in as far as the annual, seasonal, and monthly values are concerned. Comparing the non-typhoon and typhoon years, seasons, and months, Y2013, SON 2013 and November 2013 all revealed a wetter and hotter year/season/month, providing a background of the possible impacts of the typhoon Haiyan occurrence during these periods. However, it is with the annual mean that the precipitation and temperature anomalies are highest with respect to its ranking and percentile, compared to other years. The rank and percentile dropped when the analyses were narrowed down into seasonal and monthly. Between precipitation and temperature anomalies, the temperature is notoriously higher (that is apparently illustrated by the red-dominated anomaly maps), as compared to precipitation with blue and red colors distributed across different spots in the map. This is likewise confirmed by the ECDF plots and count, revealing high percentage of positive (warmer) values for temperature among all datasets.

Comparing the annual, seasonal, and monthly anomalies during the typhoon period, it is interesting to note that for precipitation, the percentage of positive anomalies are lowest on the monthly scale, whereas highest on the annual mean.

Investigating the anomalies and the values beyond local 5-95 range, the marked points in the map differ across all analyzed datasets, demonstrating that there are inconsistencies in as far as the analyzing these anomalies for its amplitude and geographical locations are considered. It can be noted that both GPCP and CRU data are constructed using rain gauge data and inhomogeneity with the recorded values can be a factor that affects the results. On the other hand, ERA5 is based on model results that also have its own estimation uncertainties.

Analysis of non-TC induced dynamics such as monsoonal phases and inter-annual ENSO variations also revealed that ENSO and monsoon significantly impacts the precipitation patterns in the region. However, ENSO does not significantly impact the temperature. Although it must be emphasized that Typhoon Haiyan occurred on an ENSO-Neutral year, therefore, it may have not necessarily influenced the variability of the studied variables.

Looking however at the relationship with Nino3.4 SST to the variables, it is shown that precipitation

and temperature are positively correlated with Nino3.4, indicating that precipitation and temperature increase (decrease) congruently with Nino3.4. This observation is only common for both CRU and ERA5 since GPCP demonstrated a contrasting result, again a manifestation of the differences among the datasets. Another evidence of differences are with the maxima/minima values where only two and not all three analyzed datasets share the common maximum (minimum) year, season or month. The significant differences are likewise confirmed by the result of the t-test comparing one dataset to another.

For the daily analysis, results revealed that during the typhoon period, the highest anomalies with respect to all variables (precipitation, runoff, windspeed and pressure) are recorded when typhoon Haiyan made landfall (November 7 & 8) predominantly in the Philippines where there is a large disparity of the calculated anomalies during these days, as compared to the rest of the days during the typhoon period. November 7 and 8 also topped the rank when compared with the same days of the non-typhoon years, especially with the windspeed and precipitation values.

Based on the result of the multiple linear regressions, it is revealed that regressing precipitation or runoff with windspeed + pressure, gives the best response, having significant p-values among all the fitted models. Although the R^2 , adjusted R^2 and AIC values for this model is not optimal, this does not reveal that the model is not a good fit but only an indication that the result cannot be very useful in explaining the event in practical terms. From the regression coefficients, it is shown that precipitation and runoff are positively correlated with windspeed, meaning, the Typhoon Haiyan event clearly increased the precipitation in as far as the Philippines is concerned. However, the negative relationship of these two variables with pressure is not significant.

Building from these results, it can be deduced that an extreme event such as Typhoon Haiyan can profoundly influence the climate variables surrounding its occurrence. In addition, non-TC-induced activities/events like ENSO and monsoon can further enhance the effects, especially on the precipitation patterns in the region.

From this study, further research can be conducted investigating the differences of the analyzed datasets. A deeper understanding on the effects of EN/LN can also be performed especially on years when maxima/minima values of the studied variables were recorded. Other extreme typhoon events can also be explored not just in the Philippines but in other countries of the region.

REFERENCES

Adler, R., Sapiano, M., Huffman, G., Wang, J.-J., Gu, G., Bolvin, D., Chiu, L., Schneider, U., Becker, A., Nelkin, E., Xie, P., Ferraro, R., & Shin, D.-B. (2018). The Global Precipitation Climatology Project (GPCP) Monthly Analysis (New Version 2.3) and a Review of 2017 Global Precipitation. *Atmosphere*, *9*(4), 138. https://doi.org/10.3390/atmos9040138

Asia Disaster Reduction Center (n.d.). *Information on Disaster Risk Reduction of the Member Countries [the Philippines].* Retrieved from https://www.adrc.asia/nationinformation.php?NationCode=608&Lang=en

Beirne, J., Renzhi, N., & Volz, U. (2021). Bracing for the Typhoon: Climate change and sovereign risk in Southeast Asia. *Sustainable Development, 29*(3), 537-551. https://doi.org/10.1002/sd.2199

Bhatia, K., Vecchi, G., Murakami, H., Underwood, S., & Kossin, J. (2018). Projected response of tropical cyclone intensity and intensification in a global climate model. *Journal of Climate, 31*(20), 8281-8303. https://doi.org/10.1175/JCLI-D-17-0898.1

Bhatia, K. T., Vecchi, G. A., Knutson, T. R., Murakami, H., Kossin, J., Dixon, K. W., & Whitlock, C. E. (2019). Recent increases in tropical cyclone intensification rates. *Nature communications*, *10*(1), 1-9. https://doi.org/10.1038/s41467-019-08471-z

Cartwright, D.E., Zetler, B.D., & Hamon, B.V. (1979). Pelagic tidal constants. *IAPSO Publication Scientifique No. 30*. 65pp.

Cartwright, D.E., & Zetler, B.D. (1985). Pelagic tidal constants - 2. *IAPSO Publication Scientifique No. 33.* 59pp.

Chen, J., Tam, C. Y., Cheung, K., Wang, Z., Murakami, H., Lau, N. C., ... & Wang, P. (2021). Changing impacts of tropical cyclones on East and Southeast Asian inland regions in the past and a globally warmed future climate. *Frontiers in Earth Science*, 1065. https://doi.org/10.3389/feart.2021.769005

Choi, K. S., Kim, D. W., & Byun, H. R. (2010). Statistical model for seasonal prediction of tropical cyclone frequency in the mid-latitudes of East Asia. *Theoretical and applied climatology, 102*(1), 105-114. https://doi.org/10.1007/s00704-009-0243-5

Chuan, G. K. (2005). The climate of southeast Asia. *The physical geography of Southeast Asia. Oxford university press, Oxford,* 80-93. Retrieved from https://books.google.it/books?hl=en&lr=&id=p64SDAAAQBAJ&oi=fnd&pg=PA80&dq=southeast+asia+climate&ots=Ooprwzth2W&sig=bCWHZmM6p64GHXSWluHBlfFRctU&redir_esc=y#v=onepage&q&f=false

Cinco, T. A., de Guzman, R. G., Ortiz, A. M. D., Delfino, R. J. P., Lasco, R. D., Hilario, F. D., ... & Ares, E. D. (2016). Observed trends and impacts of tropical cyclones in the Philippines. *International Journal of Climatology, 36*(14), 4638-4650. https://doi.org/10.1002/joc.4659

Climate Change Knowledge Portal (n.d.). Vulnerability - Natural Hazard Statistics (Country: Philippines). *World Bank Group*. Retrieved from https://climateknowledgeportal.worldbank.org/country/philippines/vulnerability

Comiso, J., Perez, G. J., & Stock, L. (2015). Enhanced Pacific Ocean sea surface temperature and its relation to Typhoon Haiyan. *Journal of Environmental Science and Management, 18*(1). https://ovcre.uplb.edu.ph/journals-uplb/index.php/JESAM/article/view/175

De Deckker, P. (2016). The Indo-Pacific Warm Pool: critical to world oceanography and world climate. *Geoscience Letters, 3*(1), 1-12. https://doi.org/10.1186/s40562-016-0054-3

del Rosario, E. D. (2014, April). FINAL REPORT- Effects of Typhoon YOLANDA (HAIYAN) [PDF FILE]. *NDRRMC.* Retrieved from https://ndrrmc.gov.ph/attachments/article/1329/FINAL_REPORT_re_Effects_of_Typhoon_YOLANDA_HAIYAN_06-09NOV2013.pdf

Deo, A., Chand, S. S., Ramsay, H., Holbrook, N. J., McGree, S., Magee, A., ... & Koshiba, S. (2021). Tropical cyclone contribution to extreme rainfall over southwest Pacific Island nations. *Climate Dynamics, 56*(11), 3967-3993. https://doi.org/10.1007/s00382-021-05680-5

Diffenbaugh, N. S., & Scherer, M. (2011). Observational and model evidence of global emergence of permanent, unprecedented heat in the 20th and 21st centuries: A letter. *Climatic Change*, *107*, 615-624. https://doi.org/10.1007/s10584-011-0112-y

Eckstein, D., Künzel, V., Schäfer, L., & Winges, M. (2019*). Global climate risk index 2020. Who suffers most from extreme weather events? Weather-related loss events in 2018 and 1999 to 2018* (Briefing Paper). Bonn, Germany: Germanwatch.

Frederick, W. H. and Leinbach, T. R. (2022, October 19). Southeast Asia. *Encyclopedia Britannica*. https://www.britannica.com/place/Southeast-Asia

Global Climate Observing System (n.d.). Essential Climate Variables. *WMO.* Retrieved from https://gcos.wmo.int/en/essential-climate-variables/table

Gottschalck, J. (2014, December 31). What is MJO, and why do we care? *NOAA, Climate.gov*. Retrieved from https://www.climate.gov/news-features/blogs/enso/what-mjo-and-why-do-we-care

Guzman, O., & Jiang, H. (2021). Global increase in tropical cyclone rain rate. *Nature communications, 12*(1), 1-8. https://doi.org/10.1038/s41467-021-25685-2

Hadley Centre for Climate Prediction and Research (2006): Met Office HadISST 1.1 - Global sea-Ice coverage and Sea Surface Temperature (1870-2015). NCAS British Atmospheric Data Centre, http://catalogue.ceda.ac.uk/uuid/facafa2ae494597166217a9121a62d3c

Harris, P. T., Macmillan-Lawler, M., Rupp, J., & Baker, E. K. (2014). Geomorphology of the oceans. *Marine Geology, 352*, 4-24. https://doi.org/10.1016/j.margeo.2014.01.011

Hawkins, E., & Sutton, R. (2012). Time of emergence of climate signals. *Geophysical Research Letters*, *39*(1). https://doi.org/10.1029/2011GL050087

He, H., Yang, J., Wu, L., Gong, D., Wang, B., & Gao, M. (2017). Unusual growth in intense typhoon occurrences over the Philippine Sea in September after the mid-2000s. *Climate Dynamics, 48*(5), 1893-1910. https://doi.org/10.1007/s00382-016-3181-9

Herring, S. C., Hoerling, M. P., Kossin, J. P., Peterson, T. C., & Stott, P. A. (2015). Explaining extreme events of 2014 from a climate perspective. *Bulletin of the American Meteorological Society*, *96*(12), S1-S172. https://doi.org/10.1175/BAMS-ExplainingExtremeEvents2014.1

Holden, W. N., & Marshall, S. J. (2018). Climate change and typhoons in the Philippines: Extreme weather events in the Anthropocene. *In Integrating disaster science and management* (pp. 407-421). Elsevier. https://doi.org/10.1016/B978-0-12-812056-9.00024-5

Intergovernmental Panel for Climate Change (2021). *Regional Fact Sheet-Asia, IPCC AR6, Working Group I: The Physical Science Basis* [PDF FILE] Retrieved from https://www.ipcc.ch/report/ar6/wg1/downloads/factsheets/IPCC_AR6_WGI_Regional_Fact

_Sheet_Asia.pdf

Jiang, H., Halverson, J. B., Simpson, J., & Zipser, E. J. (2008). Hurricane "rainfall potential" derived from satellite observations aids overland rainfall prediction. *Journal of Applied Meteorology and Climatology, 47*(4), 944-959. https://doi.org/10.1175/2007JAMC1619.1

Jiang, H., Halverson, J. B., & Simpson, J. (2008). On the differences in storm rainfall from Hurricanes Isidore and Lili. Part I: Satellite observations and rain potential. *Weather and Forecasting, 23*(1), 29-43. https://doi.org/10.1175/2007WAF2005096.1

Ji, C., Zhang, Y., Cheng, Q., & Tsou, J. Y. (2021). Investigating ocean surface responses to typhoons using reconstructed satellite data. *International Journal of Applied Earth Observation and Geoinformation, 103*, 102474. https://doi.org/10.1016/j.jag.2021.102474

Jin, C. S., Ho, C. H., Kim, J. H., Lee, D. K., Cha, D. H., & Yeh, S. W. (2013). Critical role of northern off-equatorial sea surface temperature forcing associated with central Pacific El Niño in more frequent tropical cyclone movements toward East Asia. *Journal of climate, 26*(8), 2534-2545. https://doi.org/10.1175/JCLI-D-12-00287.1

Kang, S. D., & Kimura, F. (2003). Effect of tropical SST on the northwest Pacific subtropical anticyclone. Part I: Linear Rossby wave propagation. *Journal of the Meteorological Society of Japan. Ser. II, 81*(5), 1225-1242. https://doi.org/10.2151/jmsj.81.1225

Kilic, C., & Raible, C. (2013). Investigating the sensitivity of hurricane intensity and trajectory to sea surface temperatures using the regional model WRF. *Meteorologische Zeitschrift, 22*(6), 685-698. http://dx.doi.org/10.1127/0941-2948/2013/0472

Kitamoto, A. (2019, November 7). *Typhoon Nakri Track.* National Institute of Informatics (NII) / Research Organization of Information and Systems (ROIS) (Japan). Retrieved from: http://agora.ex.nii.ac.jp/cgi-bin/dt/single2.pl?prefix=HMW819110718&id=201924&basin=wnp&lang=en

Knutson, T., Camargo, S. J., Chan, J. C., Emanuel, K., Ho, C. H., Kossin, J., ... & Wu, L. (2020). Tropical cyclones and climate change assessment: Part II: Projected response to anthropogenic warming. *Bulletin of the American Meteorological Society, 101*(3), E303-E322. https://doi.org/10.1175/BAMS-D-18-0194.1

Kumar, P., Rupa Kumar, K., Rajeevan, M., & Sahai, A. K. (2007). On the recent strengthening of the relationship between ENSO and northeast monsoon rainfall over South Asia. *Climate Dynamics*, *28*(6), 649-660. https://doi.org/10.1007/s00382-006-0210-0

Lagmay, A. M. F., Agaton, R. P., Bahala, M. A. C., Briones, J. B. L. T., Cabacaba, K. M. C., Caro, C. V. C., ... & Tablazon, J. P. (2015). Devastating storm surges of Typhoon Haiyan. *International journal of disaster risk reduction*, *11*, 1-12. https://doi.org/10.1016/j.ijdrr.2014.10.006

Lau, K. M., Zhou, Y. P., & Wu, H. T. (2008). Have tropical cyclones been feeding more extreme rainfall?. *Journal of Geophysical Research: Atmospheres, 113*(D23). https://doi.org/10.1029/2008JD009963

Lehner, F., Deser, C., & Sanderson, B. M. (2018). Future risk of record-breaking summer temperatures and its mitigation. *Climatic Change*, *146*, 363-375. https://doi.org/10.1007/s10584-016-1616-2

Luo, M., Leung, Y., Zhou, Y., & Zhang, W. (2015). Scaling behaviors of global sea surface temperature. *Journal of Climate*, *28*(8), 3122-3132. http://dx.doi.org/10.1175/JCLI-D-13-00743.1

Lyon, B., & Camargo, S. J. (2009). The seasonally-varying influence of ENSO on rainfall and tropical cyclone activity in the Philippines. *Climate Dynamics*, *32*(1), 125-141. https://doi.org/10.1007/s00382-008-0380-z

Mahlstein, I., Hegerl, G., & Solomon, S. (2012). Emerging local warming signals in observational data. *Geophysical Research Letters*, *39*(21). https://doi.org/10.1029/2012GL053952

Mei, W., Xie, S. P., Zhao, M., & Wang, Y. (2015). Forced and internal variability of tropical cyclone track density in the western North Pacific. *Journal of Climate, 28*(1), 143-167. https://doi.org/10.1175/JCLI-D-14-00164.1

Mei, W., & Xie, SP. (2016). Intensification of landfalling typhoons over the northwest Pacific since the late 1970s. *Nature Geosci 9*, 753–757. https://doi.org/10.1038/ngeo2792

Miller, S., Muir-Wood, R., & Boissonnade, A. (2008). An exploration of trends in normalized weather-related catastrophe losses. *Climate extremes and society, 12*, 225-247. Retrieved from https://www.academia.edu/82318708/An_exploration_of_trends_in_normalized_weather_related_catastrophe_losses?auto=citations&from=cover_page

Murakami, H., Delworth, T. L., Cooke, W. F., Zhao, M., Xiang, B., & Hsu, P. C. (2020). Detected climatic change in global distribution of tropical cyclones. *Proceedings of the National Academy of Sciences, 117*(20), 10706-10714. https://doi.org/10.1073/pnas.1922500117

National Centers for Environmental Information. NOAA. Annual 2013 Global Climate Report Retrieved from https://www.ncei.noaa.gov/access/monitoring/monthly-report/global/201313

National Centers for Environmental Information. NOAA. El Niño/Southern Oscillation (ENSO) Retrieved from https://www.ncei.noaa.gov/access/monitoring/enso/sst

National Oceanic and Atmospheric Administration (n.d.). *What is a Rosbby Wave?* Retrieved from https://oceanservice.noaa.gov/facts/rossby-wave.html#:~:text=Oceanic%20Rossby%20Waves&text=Unlike%20waves%20that%20break%20along,can%20change%20Earth's%20climate%20conditions.

National Oceanic and Atmospheric Administration (n.d.). *How Big Was Typhoon Haiyan?* [blog]. Retrieved from https://scijinks.gov/haiyan/

Nogueira, M. (2020). Inter-comparison of ERA-5, ERA-interim and GPCP rainfall over the last 40 years: Process-based analysis of systematic and random differences. *Journal of Hydrology, 583*, 124632. https://doi.org/10.1016/j.jhydrol.2020.124632

Oginni, T. E., Li, S., He, H., Yang, H., & Ling, Z. (2021). Ocean Response to Super-Typhoon Haiyan. *Water, 13*(20), 2841. https://doi.org/10.3390/w13202841

Pachauri, R. K., & Meyer, L. A. (2014). Climate Change 2014: Synthesis Report. Contribution of Working Groups I, II and III to the Fifth Assessment Report of the Intergovernmental Panel on Climate Change [PDF FILE]. *IPCC*. Retrieved from https://www.ipcc.ch/site/assets/uploads/2018/02/SYR_AR5_FINAL_full.pdf

Permanent Service for Mean Sea Level (n.d.). Oceanic Regions. *National Oceanography Centre.* Retrieved from https://psmsl.org/data/bottom_pressure/ocean_regions.php

Philippine Atmospheric Geophysical Astronomical Services Administration (n.d.). *About Tropical Cyclones*, Retrieved from https://www.pagasa.dost.gov.ph/information/about-tropical-cyclone

Rasmusson, E. M., & Carpenter, T. H. (1982). Variations in tropical sea surface temperature and surface wind fields associated with the Southern Oscillation/El Niño. *Monthly Weather Review*, *110*(5), 354-384. https://doi.org/10.1175/1520-0493(1982)110%3C0354:VITSST%3E2.0.CO;2

Rayner, N. A. A., Parker, D. E., Horton, E. B., Folland, C. K., Alexander, L. V., Rowell, D. P., ... & Kaplan, A. (2003). Global analyses of sea surface temperature, sea ice, and night marine air temperature since the late nineteenth century. *Journal of Geophysical Research: Atmospheres*, *108*(D14). https://doi.org/10.1029/2002JD002670

Santos, G. D. C. (2021). 2020 tropical cyclones in the Philippines: A review. *Tropical Cyclone Research and Review*, *10*(3), 191-199. https://doi.org/10.1016/j.tcrr.2021.09.003

Shean, M. (2014, June 19). Southeast Asia: Historical El Niño-Related Crop Yield Impact. Commodity Intelligence Report. Retrieved from https://www.fas.usda.gov/data/southeast-asia-historical-el-ni-o-related-crop-yield-impact

Smithson, M.J. (1992). Pelagic tidal constants - 3. *IAPSO Publication Scientifique No. 35*. 191pp.

Spalding, M. D., Fox, H. E., Allen, G. R., Davidson, N., Ferdaña, Z. A., Finlayson, M. A. X., ... & Robertson, J. (2007). Marine ecoregions of the world: a bioregionalization of coastal and shelf areas. *BioScience, 57*(7), 573-583. https://doi.org/10.1641/B570707

Thirumalai, K., DiNezio, P. N., Okumura, Y., & Deser, C. (2017). Extreme temperatures in Southeast Asia caused by El Niño and worsened by global warming. *Nature communications*, *8*(1), 15531. https://doi.org/10.1038/ncomms15531

Tran, T. L., Ritchie, E. A., & Perkins-Kirkpatrick, S. E. (2022). A 50-Year Tropical Cyclone Exposure Climatology in Southeast Asia. *Journal of Geophysical Research: Atmospheres*, *127*(4), e2021JD036301. https://doi.org/10.1029/2021JD036301

Trenberth, K. E., Cheng, L., Jacobs, P., Zhang, Y., & Fasullo, J. (2018). Hurricane Harvey links to ocean heat content and climate change adaptation. *Earth's Future*, *6*(5), 730-744. https://doi.org/10.1029/2018EF000825

Tu, J. Y., Chou, C., & Chu, P. S. (2009). The abrupt shift of typhoon activity in the vicinity of Taiwan and its association with western North Pacific–East Asian climate change. *Journal of Climate, 22*(13), 3617-3628. https://doi.org/10.1175/2009JCLI2411.1

University of Colorado-Boulder (2005, September 20). *Researchers Chart Hurricane Rita Through Gulf Of Mexico*. Retrieved from https://www.colorado.edu/today/2005/09/20/cu-boulder-researchers-chart-hurricane-rita-through-gulf-mexico

Uy, L. J. G., & Pilar, L. O. (2018, February 8). Natural disaster damage at P374B in 2006-2015. *Business World.* Retrieved from https://www.pressreader.com/philippines/business-world/20180206/281754154770834

Villarini, G., & Vecchi, G. A. (2012). Twenty-first-century projections of North Atlantic tropical storms from CMIP5 models. *Nature Climate Change, 2*(8), 604-607. http://www.nature.com/doifinder/10.1038/nclimate1530

Wang, G., Zhao, B., Qiao, F., & Zhao, C. (2018). Rapid intensification of Super Typhoon Haiyan: the important role of a warm-core ocean eddy. *Ocean Dynamics, 68*(12), 1649-1661. https://doi.org/10.1007/s10236-018-1217-x

Wang, C., & Wang, B. (2019). Tropical cyclone predictability shaped by western Pacific subtropical high: integration of trans-basin sea surface temperature effects. *Climate Dynamics, 53*(5),

2697-2714. https://doi.org/10.1007/s00382-019-04651-1

Wang, B., Luo, X., & Liu, J. (2020). How robust is the Asian precipitation–ENSO relationship during the industrial warming period (1901–2017)?. *Journal of Climate*, *33*(7), 2779-2792. https://doi.org/10.1175/JCLI-D-19-0630.1

Watters, D., & Battaglia, A. (2021). The NASA-JAXA Global Precipitation Measurement mission–part II: New frontiers in precipitation science. *Weather, 76*(2), 52-56. https://doi.org/10.1002/wea.3869

Weir, J. (2014, July 24). Reverberations of the Pacific Warm Pool. *NASA*. Retrieved from https://earthobservatory.nasa.gov/features/WarmPool

Wu, Z., & Alshdaifat, N. M. (2019). Simulation of marine weather during an extreme rainfall event: a case study of a tropical cyclone. *Hydrology*, *6*(2), 42. https://doi.org/10.3390/hydrology6020042

Yusuf, A. A., & Francisco, H. (2009). Climate change vulnerability mapping for Southeast Asia. http://hdl.handle.net/10625/46380

Zhang, J., Chen, Y., & Li, C. (2021). Typhoon Hato's precipitation characteristics based on PERSIANN. *Tropical Cyclone Research and Review*, *10*(2), 75-86. https://doi.org/10.1016/j.tcrr.2021.05.001

ANNEX 1. MAJOR OCEAN REGIONS

The Permanent Service for Mean Sea Level (PSML) website of the National Oceanography Centre defines the following regional oceanic groups associated with the five major global oceans. The oceans are further subdivided based on the categorization of pelagic tidal constants from established publications of the International Association for the Physical Sciences of the Oceans (IAPSO): Scientific Publication No. 30 (Cartwright, Zetler, & Hamon, 1979); Scientific Publication No. 33 (Cartwright & Zetler, 1985); and Scientific Publication No. 35 (Smithson, 1992).

1. ATLANTIC OCEAN

- ***Northeast Atlantic*** - north of 23° 30'N, east of 40°W, including the northern North Sea.
- ***Northwest Atlantic*** - north of 23° 30'N, west of 40°W, including the Gulf of Mexico, the Labrador Sea and Hudson Bay.
- ***Tropical Atlantic*** - between 23° 30'N and 23° 30'S, including the Caribbean Sea.
- ***South Atlantic*** - between 23° 30'S and 55°S, west of 20°E.

2. PACIFIC OCEAN

- ***Northeast Pacific*** - north of 23° 30'N, east of 180°W, including the Bering Sea and the Gulf of California.
- ***Northwest Pacific*** - north of 23° 30'N, west of 180°W, including the Seas of Okhotsk and Japan and the East China Sea.
- ***Tropical Pacific*** - between 23° 30'N and 23° 30'S, including the South China Sea.
- ***South Pacific*** - between 23° 30'S and 55°S, including the Tasman Sea.

3. INDIAN OCEAN

- ***East Indian*** - north of 55°S, between 80°E and 120°E, including the Bay of Bengal.
- ***West Indian*** - north of 55°S, between 20°E and 80°E, including the Arabian Sea and the Gulf of Aden.

4. SOUTHERN OCEAN

- ***East Southern*** - south of 55°S, from 20°E, eastwards to 160°W, including the Indian Ocean south of Australia (120°E to 150°E) and the Ross Sea.
- ***West Southern*** -south of 55°S, from 20°E, westwards to 160°W, including the Weddell Sea.

5. ARCTIC OCEAN

ANNEX 2. GLOBAL MAP OF NOVEMBER 2013 SIGNIFICANT CLIMATE EVENTS

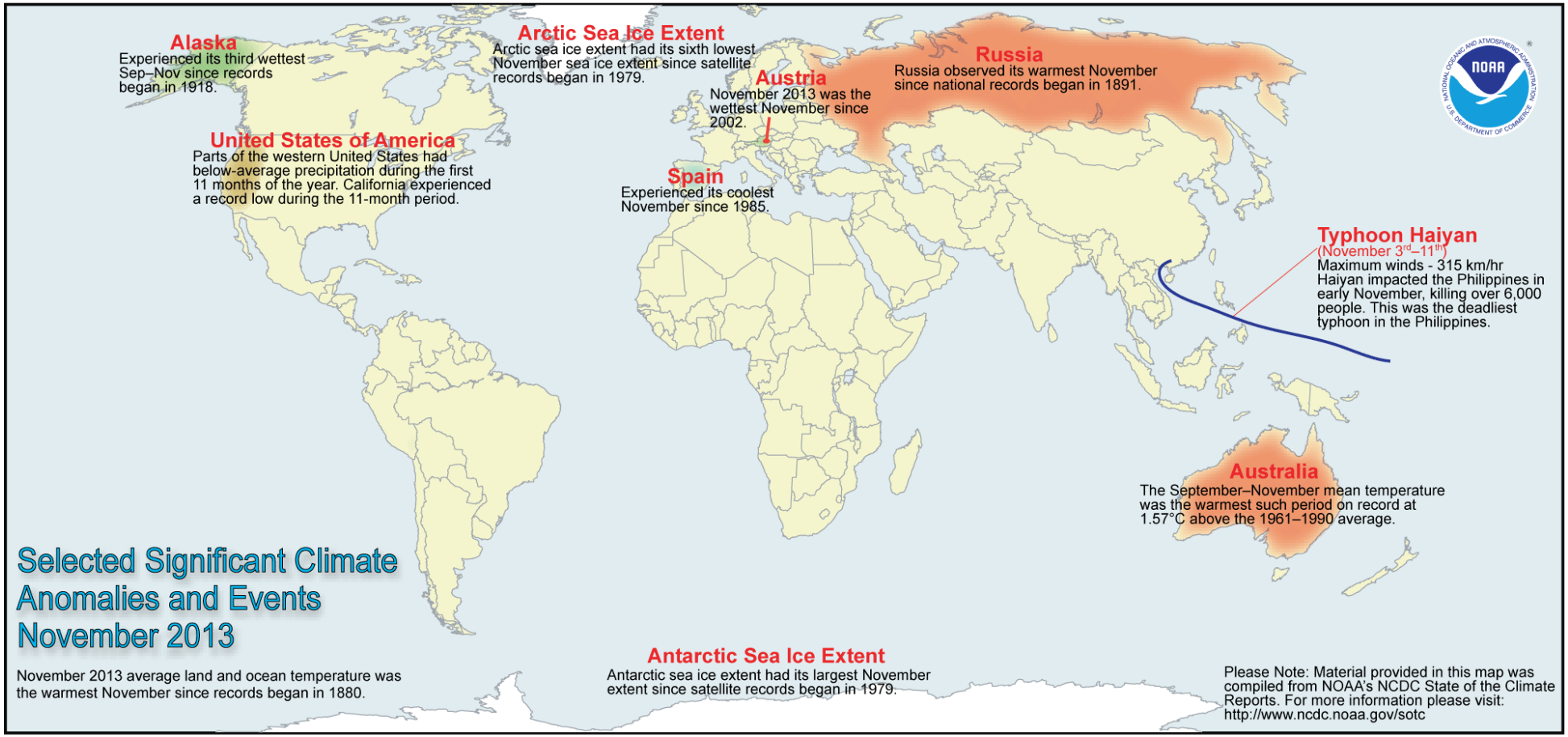

ANNEX 3. YEAR 2013 ABSOLUTE VALUES AND ANOMALIES

Maps of Annual Climatology, Absolute Values and Anomalies for Precipitation and Temperature for the Year 2013 showing the Global and Southeast Asian Region

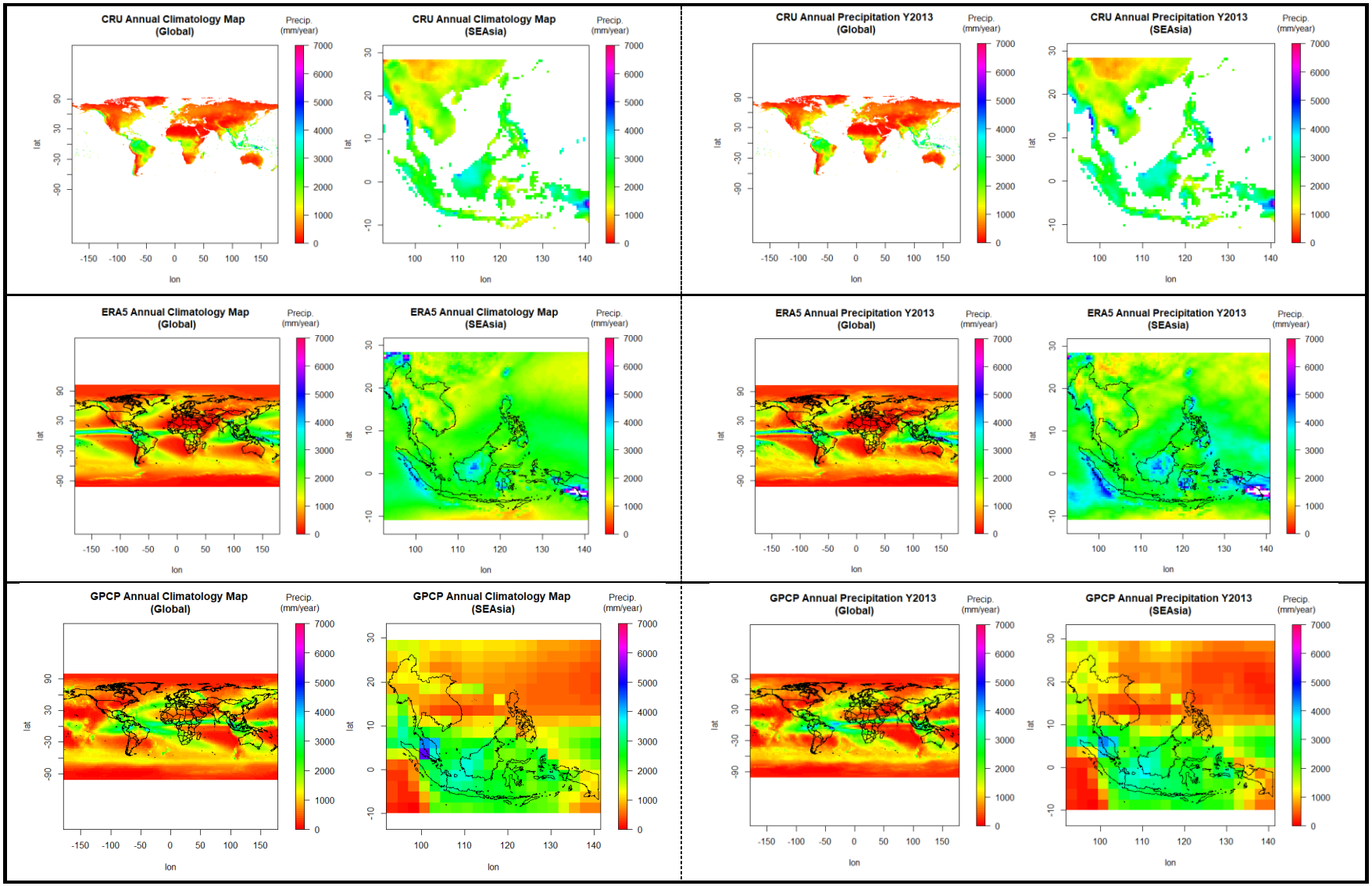

Maps of Annual Climatology [BP: 1981-2010] and Absolute Precipitation [Y2013] for Global and SE Asian Region

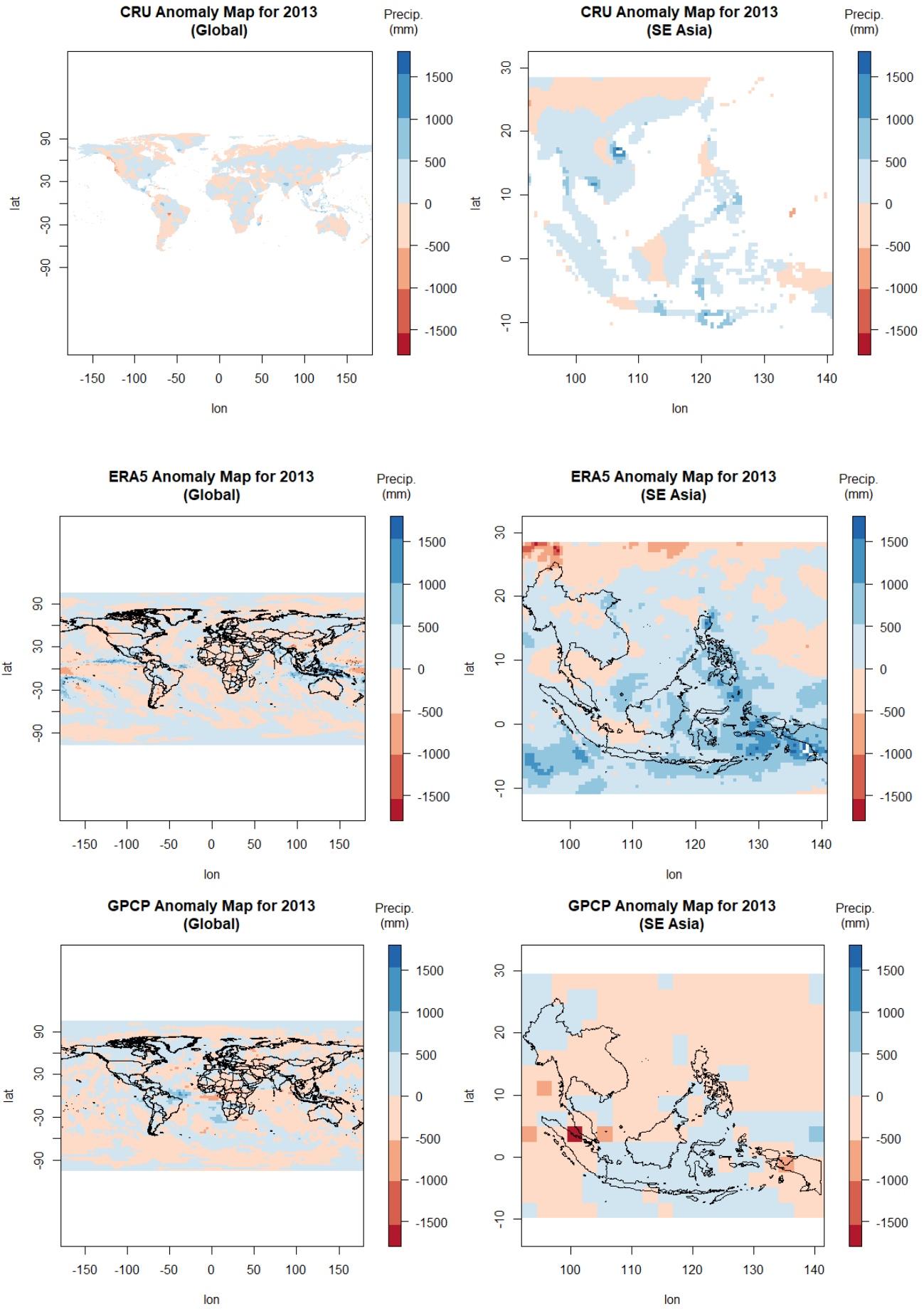

Maps of Y2013 Precipitation Anomalies for Global and SE Asian Region

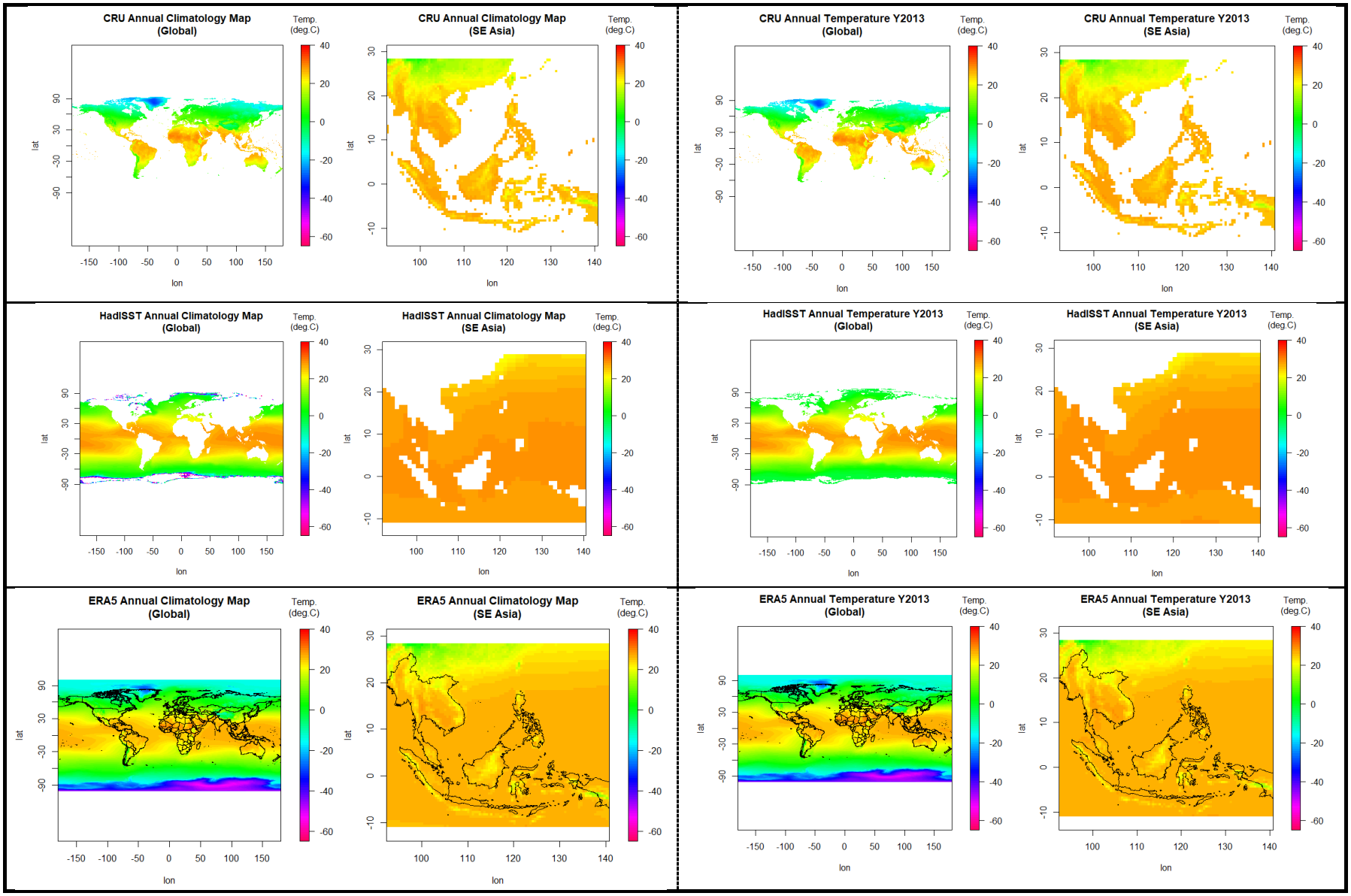

Maps of Annual Climatology [BP: 1981-2010] and Absolute Temperature [Y2013] for Global and SE Asian Region

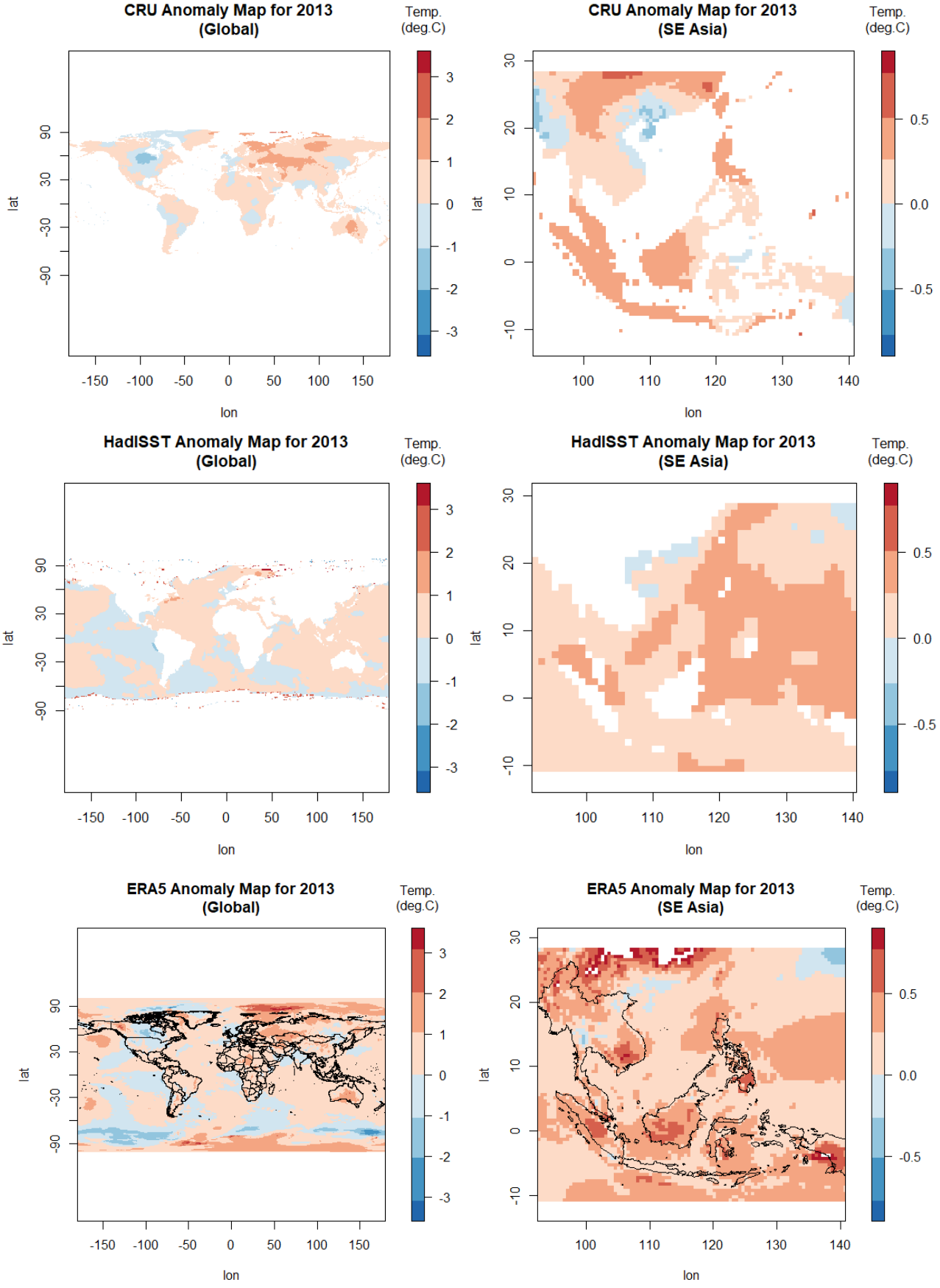

Maps of Y2013 Temperature Anomalies for Global and SE Asian Region

ANNEX 4. SON 2013 ABSOLUTE VALUES AND ANOMALIES

Maps of Seasonal Climatology, Absolute Values and Anomalies for Precipitation and Temperature for SON 2013 showing the Global and Southeast Asian Region

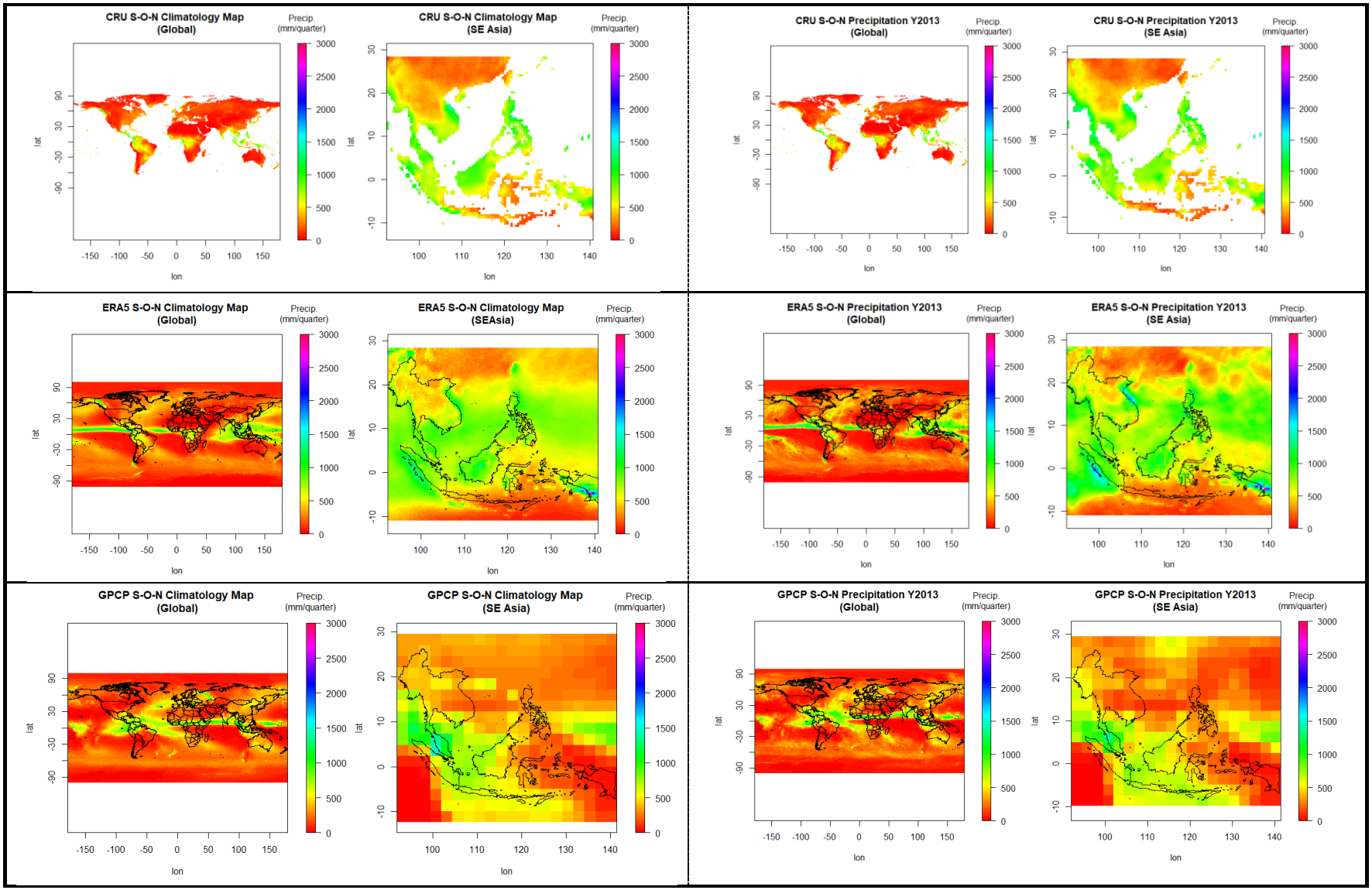

Maps of SON Climatology [BP: 1981-2010] and Absolute Precipitation [SON 2013] for Global and SE Asian Region

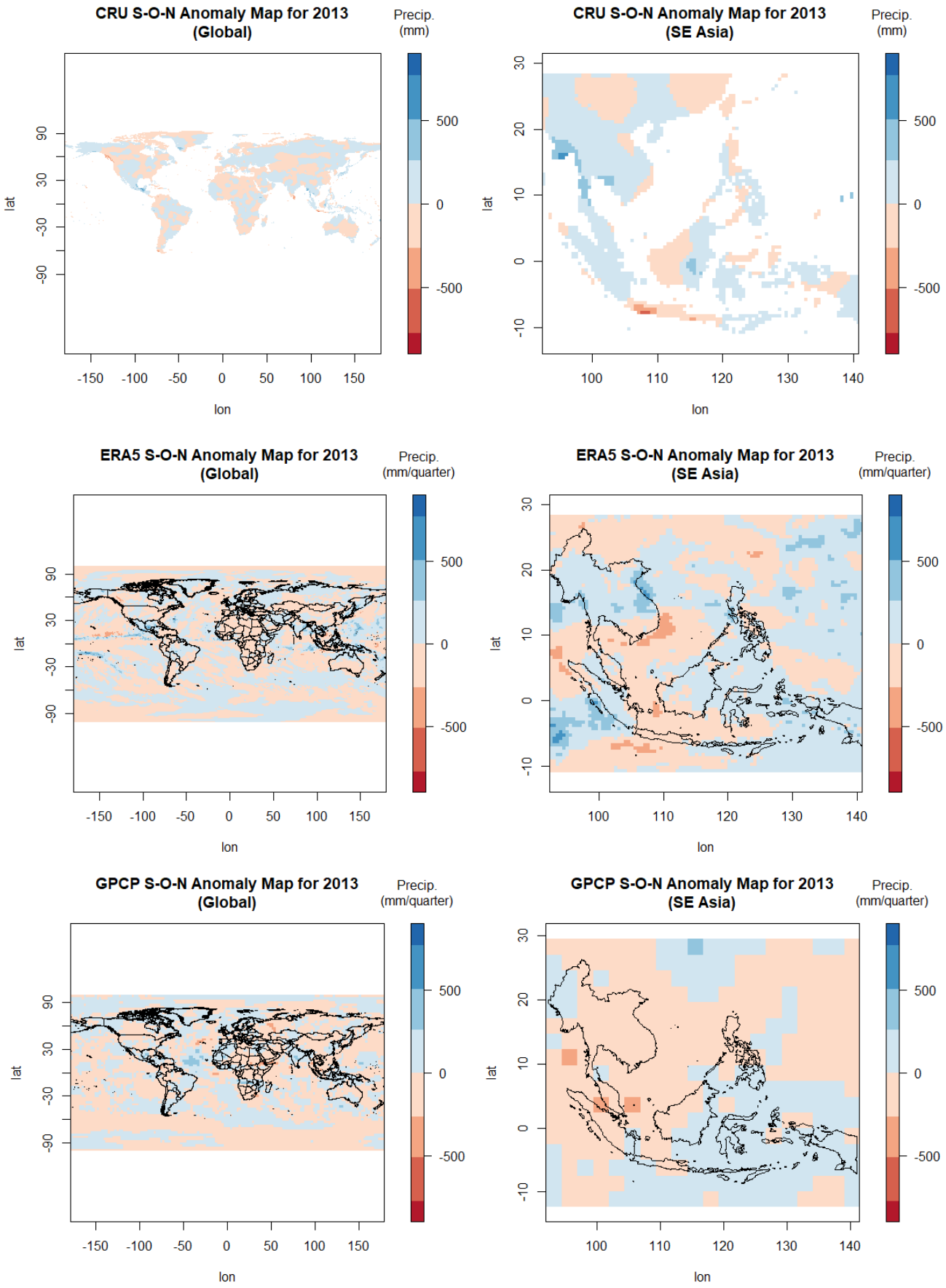

Maps of SON 2013 Precipitation Anomalies for Global and SE Asian Region

Asia]

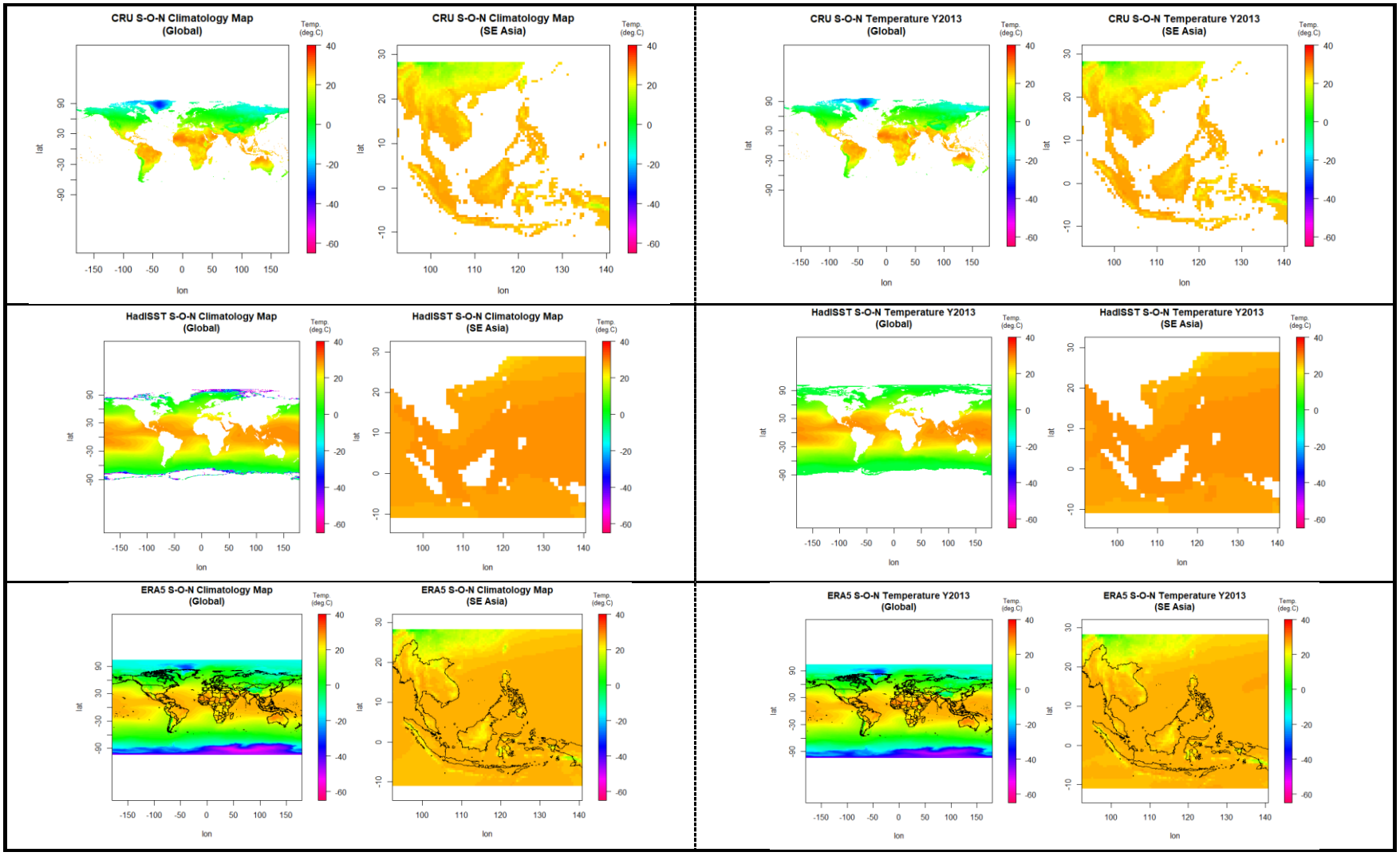

Maps of SON Climatology [BP: 1981-2010] and Absolute Temperature [SON 2013] for Global and SE Asian Region

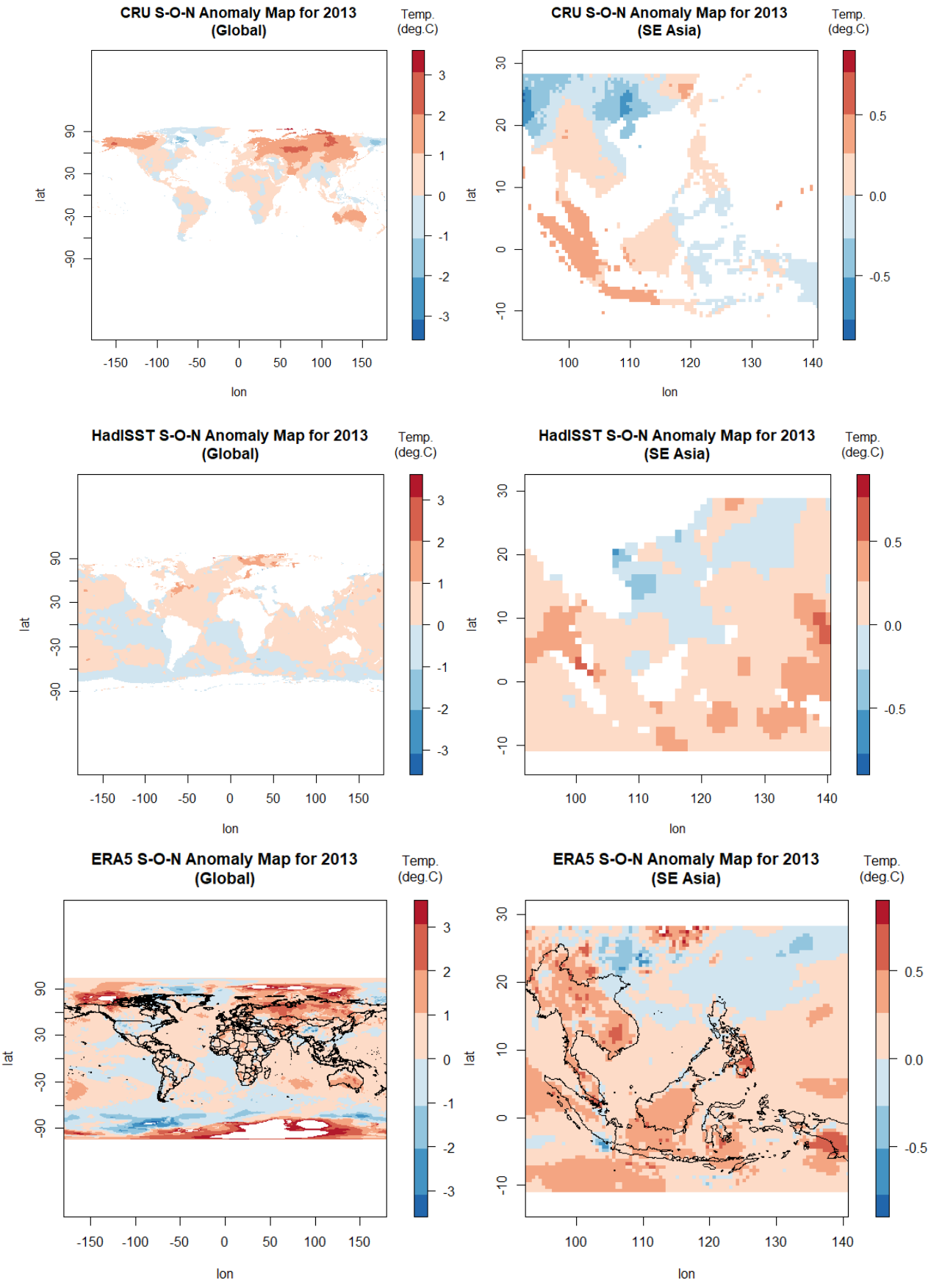

Maps of SON 2013 Temperature Anomalies for Global and SE Asian Region

ANNEX 5. NOVEMBER 2013 ABSOLUTE VALUES AND ANOMALIES

Maps of Monthly Climatology, Absolute Values and Anomalies for Precipitation and Temperature for November 2013 showing the Global and Southeast Asian Region

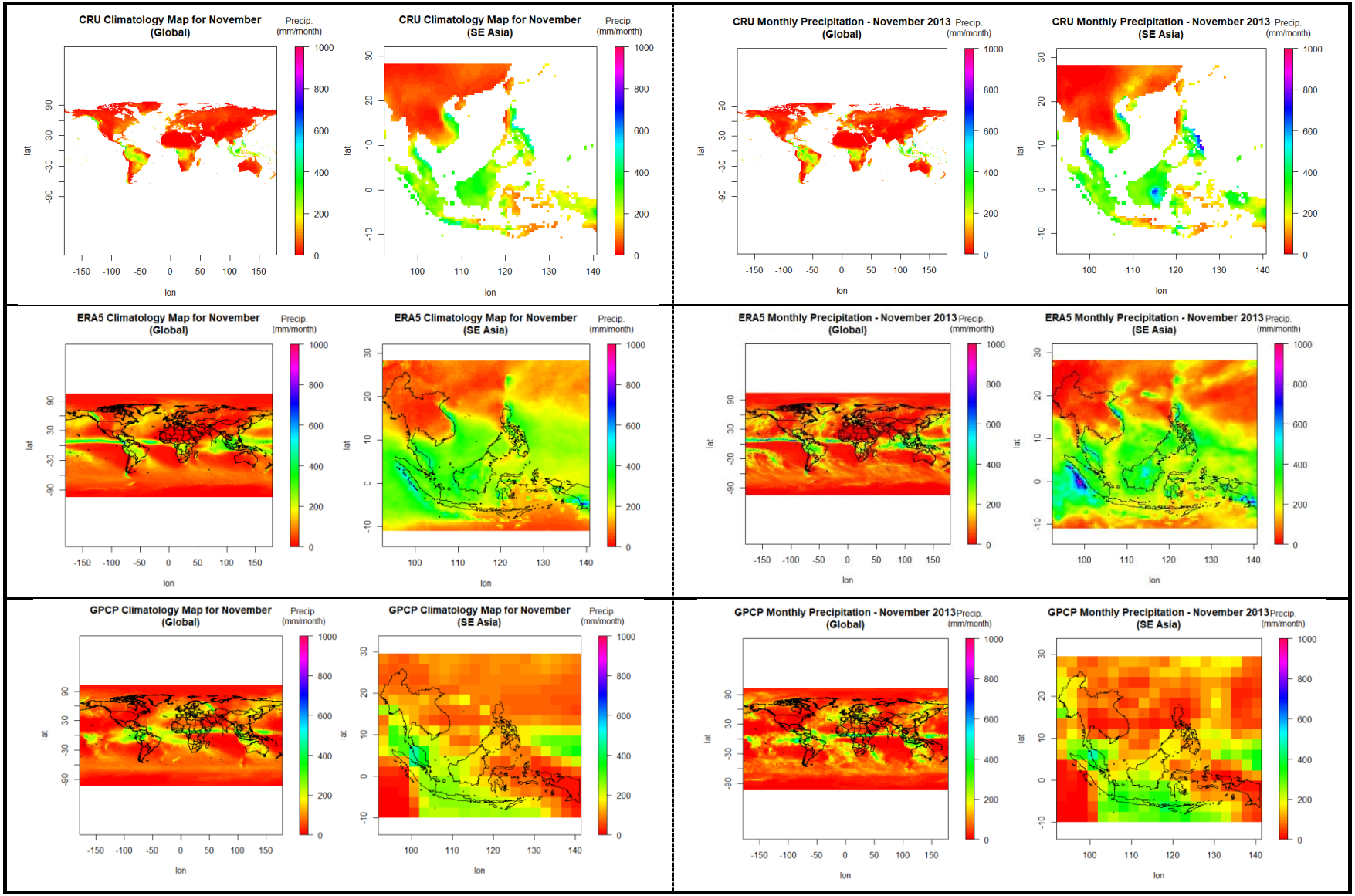

Maps of November Climatology [BP: 1981-2010] and Absolute Precipitation [Nov. 2013] for Global and SE Asian Region

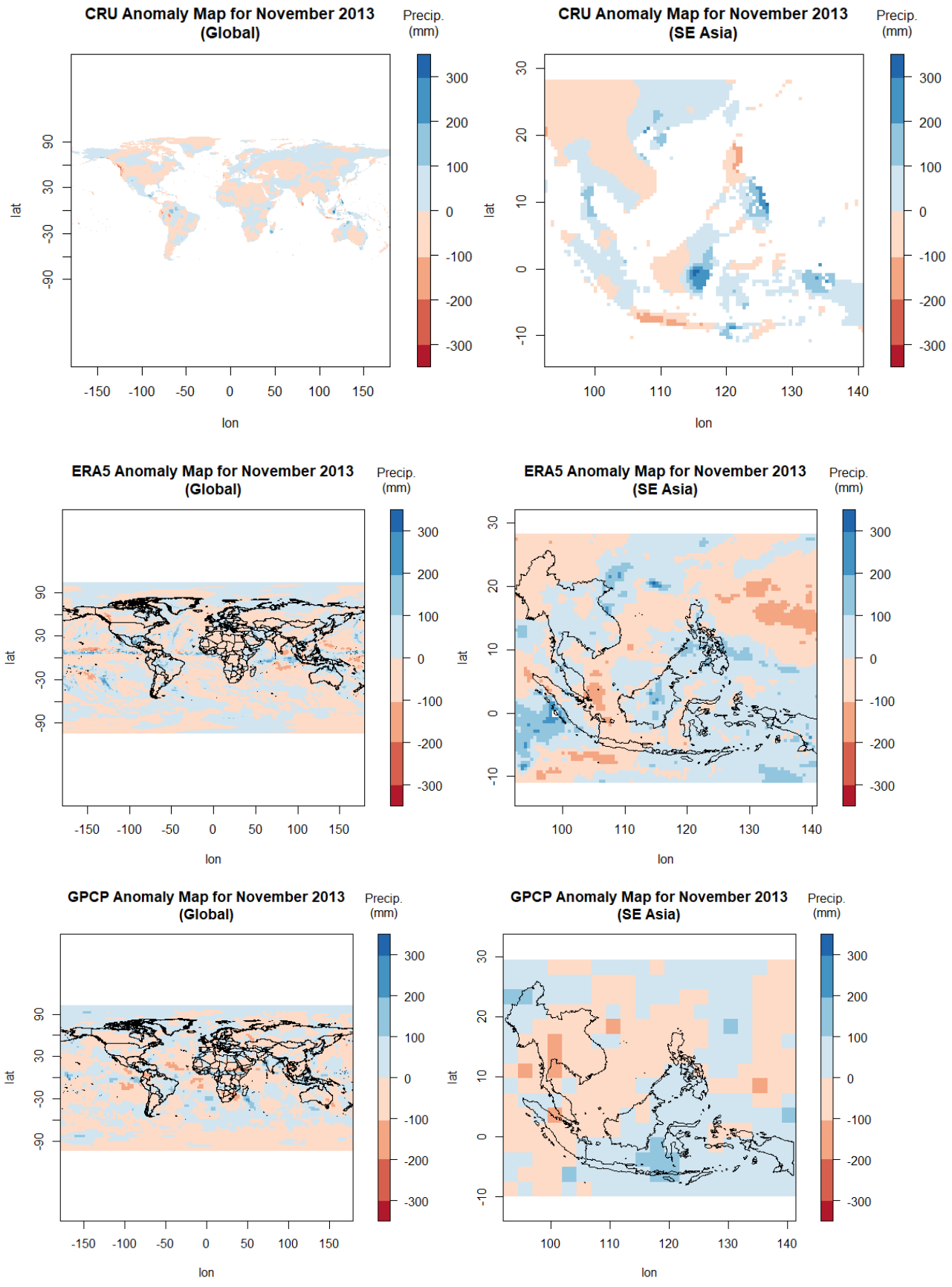

Maps of November 2013 Precipitation Anomalies for Global and SE Asian Region

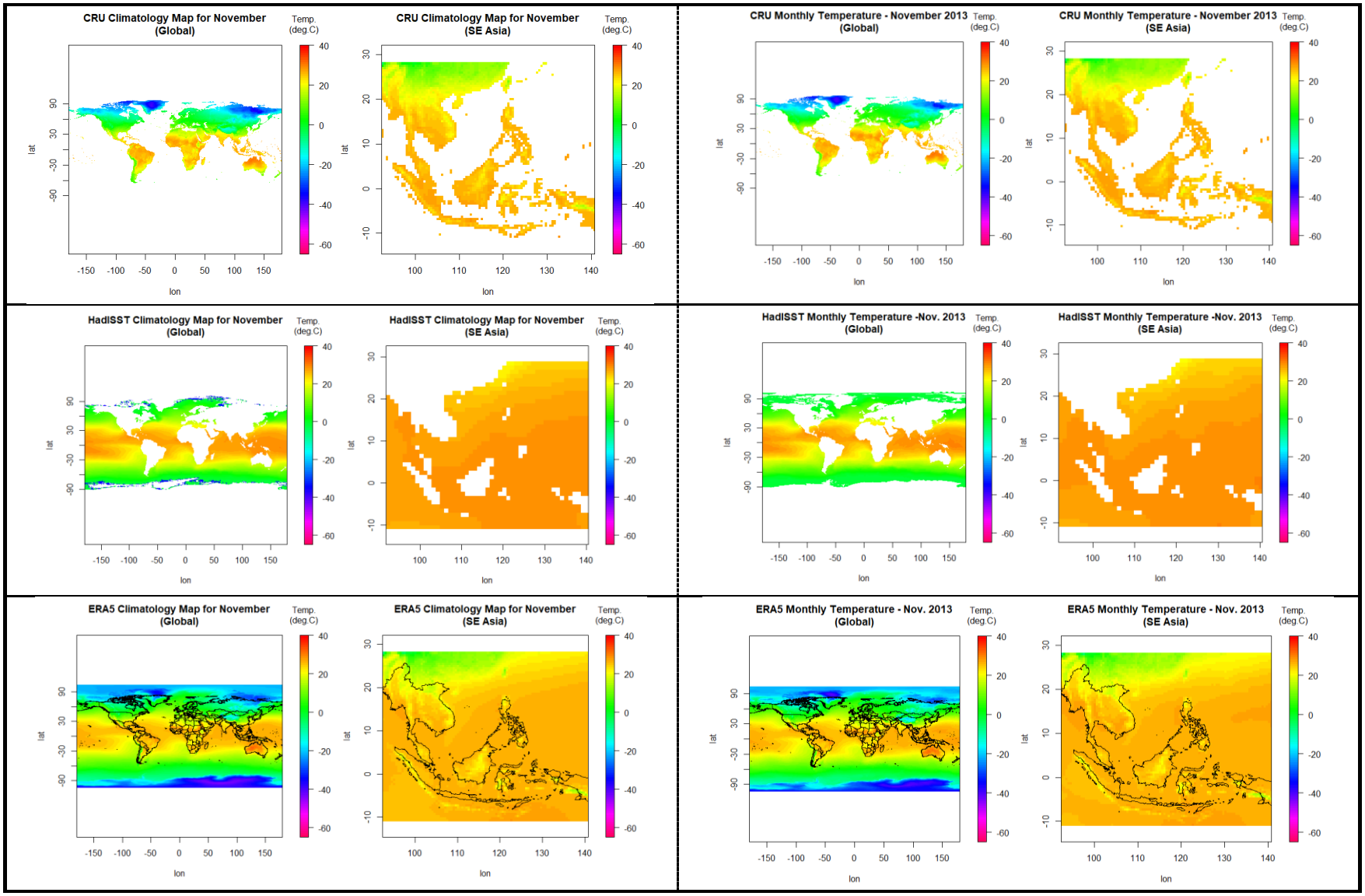

Maps of Nov Climatology [BP: 1981-2010] and Absolute Temperature [Nov. 2013] for Global and SE Asian Region

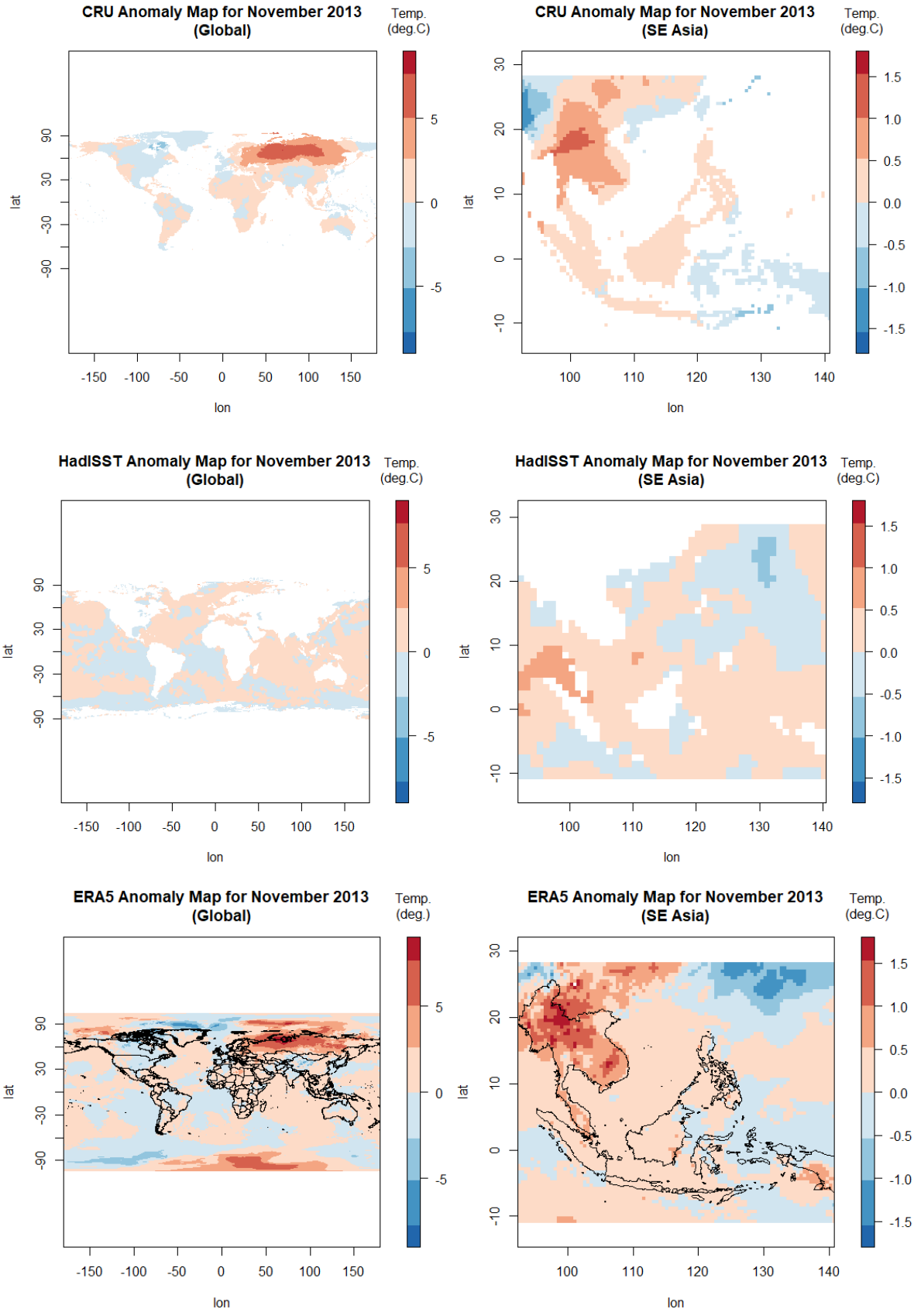

Maps of November 2013 Temperature Anomalies for Global and SE Asian Region